SPATIAL ORIENTATION OF ANGULAR MOMENTUM OF GALAXIES IN THE CLUSTERS AND SUPERCLUSTERS

A THESIS SUBMITTED TO THE

CENTRAL DEPARTMENT OF PHYSICS

INSTITUTE OF SCIENCE AND TECHNOLOGY

TRIBHUVAN UNIVERSITY

NEPAL

FOR THE AWARD OF

DOCTOR OF PHILOSOPHY

IN PHYSICS

By

SHIV NARAYAN YADAV

SEPTEMBER, 2016

SPATIAL ORIENTATION OF ANGULAR MOMENTUM OF GALAXIES IN THE CLUSTERS AND SUPERCLUSTERS

A THESIS SUBMITTED TO THE

CENTRAL DEPARTMENT OF PHYSICS

INSTITUTE OF SCIENCE AND TECHNOLOGY

TRIBHUVAN UNIVERSITY

NEPAL

FOR THE AWARD OF

DOCTOR OF PHILOSOPHY

IN PHYSICS

By

SHIV NARAYAN YADAV

SEPTEMBER, 2016

RECOMMENDATION

This is recommended that **Mr. Shiv Narayan Yadav** has carried out research entitled **"SPATIAL ORIENTATION OF ANGULAR MOMENTUM OF GALAXIES IN THE CLUSTERS AND SUPERCLUSTERS"** for the award of Doctor of Philosophy (Ph.D) in **Physics** under my supervision. To my Knowledge, this work has not submitted for any other degree.

He has fulfilled all the requirements laid down by the Institute of Science and Technology (IOST), Tribhuvan University, Kirtipur for the submission of the thesis for the award of Ph.D. degree.

. . . . . .

Prof. Dr. Binil Aryal

Supervisor

Central Department Of Physics

Tribhuvan University, Kirtipur

Kathmandu, Nepal

SEPTEMBER, 2016

LETTER OF APPROVAL

[Date:30/09/2016]

On the recommendation of Prof. Dr. Binil Aryal and Prof. Dr. Walter Saurer, this Ph. D. thesis submitted by "**Shiv Narayan Yadav**", entitled **"SPATIAL ORIENTATION OF ANGULAR MOMENTUM OF GALAXIES IN THE CLUSTERS AND SUPERCLUSTERS"** is forwarded by Central Department Research Committee (CDRC) to the Dean, IOST, T.U..

. . . . . .

Dr. Binil Aryal

Professor,

Head,

Central Department Of Physics

Tribhuvan University

Kirtipur, Kathmandu

Nepal

DECLARATION

Thesis entitled **"SPATIAL ORIENTATION OF ANGULAR MOMENTUM OF GALAXIES IN THE CLUSTERS AND SUPERCLUSTER"** which is being submitted to the Central Department of Physics, Institute of Science and Technology (IOST), Tribhuvan University, Nepal for the award of the degree of Doctor of Philosophy (Ph.D.), is a research work carried out by me under the supervision of Prof. Dr. Binil Aryal, Central Department of Physics Tribhuvan University, Kirtipur, Kathmandu, Nepal and co supervised by Prof. Dr. Walter Saurer, Innsbruck University, Austria.

This research is original and has not been submitted earlier in part or full in this or any other form to any university or institute, here or elsewhere, for the award of any degree.

Shiv Narayan Yadav

ACKNOWLEDGMENTS

I became able to know the fundamentals of research in physics and see the research world with third eye; this is only due to my supervisors. So, at first I would like to express my sincere gratitude to my supervisor Prof. Dr. Binil Aryal, HoD, CDP, TU, Kirtipur for the continuous scientific guidance, supports and parent-ship throughout my research work. I acknowledge to my Co-supervisor Prof. Dr. Walter Saurer, Innsbruck University, Austria for his critical suggestion particularly in the interpretation of the results. His contribution during the manuscript preparation is highly acknowledged. I remember his visit to Kathmandu during our holidays.

My sincere thank goes to Sloan Digitized Sky Survey (SDSS), Polar Sky Survey (POSS) team for providing data through our collaboration. I am thankful to Dr. Wolfgang Kausch of Innsbruck University, Austria for providing his masters thesis, and Mr. Rajesh Kumar Bachchan of Lund Observatory, Sweden for their help during the process of data access and processing. I heartedly remember Prof. Dr. Ranjeev Mishra's motivation to do extragalactic astrophysics during his visit to the department.

I would like to express my gratitude to Prof. Dr. Lok Narayan Jha, former HoD, CDP, TU, Kirtipur, Prof. Dr. Sita Ram Byhaut, Prof. Dr. Shekhar Gurung, Prof. Dr. Jeevan Jyoti Nakarmi, Prof. Dr. Narayan Prasad Adhikari for their support, help and encouragements during ups and downs of my journey of research work.

I would like to give thank to Prof. Dr. M. M. Aryal, Prof. Dr. U. R. Khanal, Prof. Dr. Raju Khanal, Dr. Bal Ram Ghimire, Dr. Sanju Shrestha and other faculty members of CDP for their constant support.

My special thanks go to Associate Prof. and my senior friend Ajay Kumar Jha and Associate Prof. Bhanu Bhakta Sapkota for the company. We learned a lot from each other.

Also, I am thankful to Librarian Mina Manandhar and other staffs of the CDP.

I would like to thank Department of Physics, Banaras Hindu University, Baranasi, India

and North Bengal University, Siliguri, India for helping to present my research work in the international conferences. I am thankful to the organizers of International Black Hole conference (2012 and 2014) for allowing me to present my results in the poster form.

I am thankful to Institute of Science and technology, TU, Kirtipur and Central Department of Physics for providing me study leave to carry out my research work.

It is my great pleasure to thanks University Grant Commission for Providing grants and Publishing paper in the Journal. I also thank SMBM Campus, TU, Rajbiraj, for giving permissions to carry out Ph.D. research.

Finally, I would like to thank my parent, family members for their constant support, patience and encouragements. Special thank goes to Sima, Nikita and Nischay who always makes me fresh and dynamic.

Shiv Narayan Yadav

September, 2016

ABSTRACT

Studying spatial orientation of angular momentum vectors of galaxies in the fields, groups, clusters and superclusters is one of the most effective ways of testing the galaxy formation scenarios. We have studied spatial orientation of 373 691 galaxies having redshift from 0.05 ($\sim 15\,000$ km s^{-1}) to 0.5 ($\sim 150\,000$ km s^{-1}) and the visible magnitude lies in the range 11 to 23. The 23 magnitude galaxy is about 10 000 times fainter than 11 magnitude galaxies in surface brightness. The database includes 5 987 blue shifted galaxies and 410 zone-of-avoidance galaxies. In addition, two superclusters were included. Therefore the database includes field (zone-of-avoidance galaxies), groups (low blue shifted galaxies), clusters (several Abell clusters of low and high redshift) and two superclusters SDSS S[239+016+0037] and SDSS S[223+022+0117]. The positions, position angles and inclination angles are used to covert two-dimensional observed parameters into three-dimensional angular momentum vectors of the galaxy. Astronomical data are often accompanied by several selection effects. These selection effects can be treated as noise in the data base. In this situation, even though all control parameters (independent variables) remain constant, the resultant outcomes (dependent variables) vary. The selections effects are removed from the database and the expected isotropic distribution curves are determined by running numerical simulations. The chi-square, autocorrelation and the Fourier tests are carried out in order to examine non-random effects in the expected isotropic distributions. We have presented our results in six sections, as follows: (1) low redshift galaxies ($0.05 \leq z \leq 0.10$), (2) high redshift galaxies ($0.40 \leq z \leq 0.50$), (3) blue shift galaxies (-3×10^{-4}) to (-1.1×10^{-6}), (4) Two SDSS superclusters, (5) zone-of-avoidance galaxies and (6) redshift dependence ($0.10 \leq z \leq 0.11$). For the low redshift galaxies, magnitude dependence is studied using infrared sensitive z-filter. The visible r-filter is used for the high redshift galaxies because of its low surface brightness. For the blue shifted galaxies, i- and u-filters are selected in order to check near infrared and ultraviolet activity in the galaxies that oppose Hubble flow. A redshift dependence in the preferred alignments of angular momentum of galaxies are studied using the database of visible r-filters. The alignments of galaxies in the

superclusters are studied using i, u, r and g-filters. The preferred alignments of zone-of avoidance galaxies are studied using three co-ordinate systems, namely, equatorial, galactic and supergalactic. Weak magnitude dependence is noticed in low as well as high redshift galaxies. However, no redshift dependence is found. In general a random orientation of angular momentum vectors of galaxies are found in the total sample of all six section of the result, supporting hierarchy model of galaxy formation. In hierarchical clustering scenario, galaxy clusters accrete mass through the aggregation of smaller systems. Thus, the velocity field of the in-fall regions of groups clusters or superclusters of galaxies contains significant random motion. In order to understand this random motion, global rotation of galaxies in the large scale structure is important. The global rotation theory predicts that the global rotation of the universe provides angular momentum to the large-scale structure. According to this model, galaxies form in a rotating universe, acquire angular momentum through global rotation. It is found that the vanishing angular momenta are preferred by the superclusters which are in dynamical equilibrium and have larger value of velocity dispersion.

TABLE OF CONTENTS

LIST OF TABLES

LIST OF FIGURES

LIST OF ACRONYMS AND ABBREVIATIONS

A&A	Astronomy and Astrophysics Journal
AJ	Astronomical Journal
ApJ	Astrophysical Journal
ApJS	Astrophysical Journal Suppliment
Ap&SS	Astrophysics and Space Science
APO	Apache Point Observatory
ASJ	Astronomical Society Japan
BM	Bautz Morgan system
CCDs	Charge Coupled Devices
CDM	Cold Dark Matter
CMB	Cosmic Microwave Background
CMBR	Cosmic Microwave Background Radiation
DEC	Declination
ECS	Equatorial Coordinate System
ESA	European Space Agency
ESO	European Space Observatory
HDM	Hot Dark Matter
HFI	High Frequency Instrument
HST	Hubble Space Telescope
LCRS	Las Companas Red Shift Survey
LFI	Low Frequency Instrument
LSC	Local Super Cluster
MNRAS	Monthly Notice of Royal Astronomical Society
NASA	National Aeronautical Space Administration
NED	NASA Extragalactic Database
OAJ	The Open Astronomy Journal
PANBG	Photometric Atlas of Northern Bright Galaxies
PASJ	Journal of Asia Pacific Society
PhRvD	Physical Review D (Particles and Fields)
POSS	Palomar Observatory Sky Survey

PSF	Point Spread Function
RA	Right Ascension
RAA	Research in Astronomy and Astrophysics
SDSS	Sloan Digital Sky Survey
VCC	Virgo cluster center
WMAP	Wilkinson Microwave Anisotripy Probe
2dFGRS	2degree Field Galaxy Redshift Survey
LSS	Large Scale Structure
BASI	Bulletin of Astronomical Society of India
FIRAS	Far Infrared Astronomical Satellite

CHAPTER 1

INTRODUCION

CHAPTER 1

INTRODUCTION

1.1 Introduction

It is well known that our Universe started with a big bang. But how well do we know about the Big Bang? As we know the big bang is not an explosion. The universe did not expand into space, as space did not exist before the universe. Instead, it is better to think of the big bang as the simultaneous appearance of space everywhere in the universe. The universe has not expanded from any one spot since the big bang - rather, space itself has been stretching, and carrying matter with it.

The universe started with the Big Bang about 14 000 million years ago. It started out very, very hot and has been expanding and cooling since then. For the first tiny fraction of a second, everything was so hot, that we cannot describe what it was like, but we can use our knowledge to give a good idea of what was happening from as little as 10^{-43} s after the beginning. The main stages can be described as follows: from the time of big bang to about 10^{-6} s particle physics dominates. Universe was so hot that none of the physics around us works and even forces like gravity act differently. Experiments in giant particle accelerators are helping us to understand these energetic processes in a better way. At about one second after the big bang some sub-atomic particles like protons and neutrons were created from even smaller particles like quarks. After 1 second, things have cooled down enough so that normal elements like hydrogen could exist in some form. The amount of hydrogen in the universe today is one of the important evidence for the big bang. At about 380 000 years after the big bang the universe is cool enough for normal atoms without any electrical charge to exist. This is when the Cosmic Microwave Background was formed - one of the most important pieces of evidence for

the Big Bang. Then dark-age began when universe became void of any radiation due to matter radiation decoupling.

The initial perturbations in matter density which is believed to be present in early universe, gradually kept on being enhanced with time as the universe expanded and thousands of millions of years after big bang. Later the large scale structures (e.g., galaxies, clusters, superclusters, hyperclusters, filaments and walls, etc) started getting formed. However, less dense regions did not grow, evolving into area of seemingly empty space called voids. Hereby, we see that our universe is ever evolving and expanding. Now a days, cosmologists and astronomers are trying to discover its final fate. The Lambda Cold Dark Matter (ΛCDM) model is the best model of our known universe about the origin of the large scale structures representing an improvement over the big bang theory (Blumenthal *et al.*, 1984).

These structures are one of the most mysterious discoveries, because their formation and evolution is not fully understandable yet. Thus, to know the origin of the expanding universe and large scale structures is one of the most fundamental question in the recent universe. One of the most accepted model on the evolution and expansion of the large scale structure is that it was the result of primordial fluctuations by gravitational instability. An additional factor complicating an understanding of galaxies is that their evolution is strongly affected by their environment. The gravitational effects of other galaxies can be important. Galaxies can sometimes interact and even merge.

To get deep insight to the evolution of these large scale structures, it is necessary to understand how and when they were formed and how their structures and constituents have been changing with time. According to Gamow (1952) and Wiezsacker (1951), the observed rotation of the galaxies are very important in order to understand the origin of the angular momentum of galaxies. It helps us to get right insight into the initial condition that triggered the formation of these structures. There are only few theories, which can describe the origin and evolution of these structures, each of them with their different strengths and weakness, assumptions and predictions, especially the theories about galaxy cluster formation. Concerning the spatial orientation of the spin vectors of the galaxies we have three models. These models are the 'pancake model', the 'hierarchy model', and the 'primordial vorticity theory'. The 'pancake model' (Doroshkevich,

1973; Doroshkevich & Shandarin, 1978) predicts that the angular momentum vectors of galaxies tend to lie within the cluster plane. According to the 'Hierarchy model' (Peeble, 1969), the directions of the angular momentum vectors should be distributed randomly. The 'primordial vorticity theory' (Ozernoy, 1971, 1978; Stein, 1974) predicts that the angular momentum vectors of galaxies are distributed primarily perpendicular to the cluster plane.

It's been a long time that modern observation facilities have revealed the existence of large scale structures (e.g., huge clusters and superclusters of galaxies) in the universe. These large scale structures are one of the mysterious discoveries whose formation and evolution is not fully understood yet. It has been computed that our observable universe is only 5% of the total universe. Fortunately, scientists have been paying a great effort in the extragalactic research so that the origin and evolution of these large scale structures and hence the whole universe could be understood.

The cosmological evolution of galaxies is a fascinating subject which has experienced explosive growth lately due to the incredible rate of new observational data and the development of new methods and codes in this observationally and computationally intensive research field. Galaxies, as the building blocks of the Universe, are also tracers of its large scale structure and of its evolution. Structure formation refers to a largely unsolved, but extensively researched problem in physical cosmology. Therefore, galaxy evolution is a part of the overall evolution in the Universe - from the largest spatial scales ruled by dark matter to the smallest ones taken over by dissipative baryons that can form stars and grow super massive black holes. In other words, the process of galaxy formation can be influenced strongly by a huge range of spatial scales.

The theoretical progress towards understanding the galaxy evolution has been attempted through numerical simulations assuming collision-less and dissipative processes in the Universe. Extragalactic astrophysics has acquired precious support from a large number of such virtual experiments. Because the dominant processes are so nonlinear, the synthesis of theoretical, observational and experimental components has contributed much of our current understanding of structure formation in the Universe on all spatial scales. If our goal is to be able to produce' realistic galaxies that can be directly compared with observations, we are well underway. The challenges in understanding galaxy

formation and evolution are amplified by the unknown physics of the dominant processes (e.g., star formation, mechanical and radiative physics, turbulence, etc), supplemented by often counter-intuitive nonlinear dynamics and by insufficient observational constraints.

The cornerstone of the current galaxy formation paradigm was established and refined during 1970-1990. It has been very successful in predicting and explaining disk galaxy properties. A two-stage process has been suggested, based on hierarchical clustering and dark matter halo formation in the first stage, and gas cooling and collapse into pre-existing potential wells in the second one (e.g., White & Rees, 1978; Fall & Efstathiou, 1980; Mo *et al*., 1998). Prior to gravitational collapse, the dark matter haloes acquire angular momentum (J) via gravitational torques, while baryons follow the dark matter and have the same specific angular momentum, $j = J/M$ (Liddle, 2003). In the next step, while the dark matter 'warms' up during virialization, the baryons can cool down and continue the collapse, with j, and hence its distribution, roughly constant. Finally, the low-j baryons accrete onto the inner regions and cause central starbursts, resulting in the formation of galactic bulges in disk galaxies and super massive black holes in their centers. Meanwhile high-j baryons form galactic disks with self-regulated star formation. In this framework, j determines the disk size, and the disk surface density fluxes.

The galaxy formation paradigm has received substantial support from both observations and high-resolution numerical simulations, although a long list of unresolved issue exists. The theoretical background for angular momentum distributions is still unclear. Current observations and mathematical models predict that the universe is arranged in a hierarchy of structures. These structures were already present in the early years of the universe's life. Deep sky observations of the universe at this early stage reveal important information regarding its fundamental construction and evolution right up to today.

The universe's biggest gravitationally cohesive structural units are galaxy clusters. Consequently, observations of clusters and their evolution are important tools for mapping the universe's large-scale structure. Galaxy groups and clusters are the largest known gravitationally bound objects to have arisen thus far in the process of cosmic structure formation. They form the densest part of the large structure of the universe. In models for the gravitationally formation structure with cold dark matter, the smallest structure

collapse first and eventually build the largest structures. The distribution of matter in the observed universe is inhomogeneous; most of matter is in various astronomical systems. The large-scale structure of the galaxy distribution is characterized by large voids and by a complex web of galaxy laments and clusters. superclusters are the largest components of the cosmic web. They are collections of galaxies and galaxy clusters, with typical sizes of 20-100 h^{-1} Mpc. They can contain up to hundreds of galaxy groups and several rich clusters. The first described supercluster is the Local supercluster, and many other superclusters have been found and studied. Astronomers have a long tradition of selecting galaxy clusters and groups from this web, but quantifying the overall web is a much more difficult task. Good recent examples are the application of the multiscale morphology filter and the bayesian inference for the density and the subsequent classification of the web elements by Jasche *et al*. (2010).

Aryal (2002) studied spatial orientation of angular momentum vectors (or spin vectors, hereafter SV) of galaxies in 42 clusters and found mixed results: a few clusters showed random orientation of their spin vectors and others preferred alignments supporting either pancake or primordial vorticity theory as mentioned above. During 2004 to till date, a large number of papers are published (for detail, section 2.7.3). We have critically reviewed their results in the literature review section. In the present work, we have planned to analyse spectroscopic database of galaxies having a wide range of redshift (0.05 to 0.50) available in the Sloan Digitized Sky Survey (SDSS). In addition, database of a few new superclusters will be studied. This thesis will be organized as follows: the literature review followed by the motivation and the objectives are given in the Chapter 2. In the Chapter 3, we discuss the methods, describing the process of random simulation as well as the statistics. We present our results with discussion in the Chapter 4. This chapter is further divided into six parts: In the first section of this chapter, results regarding the spatial orientation of low red-shifted galaxies will be presented. In the next section, database of high redshift galaxies will be studied. The third section of the Chapter 4 presents preferred alignments of angular momentum of blueshift galaxies. The fourth section describes preferred alignments of galaxies in newly discovered two SDSS superclusters. The fifth section included the preferred alignments of angular momentum of zone-of-avoidance galaxies. The last section deals a test of redshift dependence concerning galaxy alignments. In each section, a brief

description of the database is presented. The details about the database and the possible inhomogeniety in the database are given in the respective appendices. In all six sections, a result and discussion will be followed by the general discussion as well as a comparison with previous works.

CHAPTER 2

LITERATURE REVIEW

CHAPTER 2

LITERATURE REVIEW

2.1 Origin of Angular Momentum of Galaxies

Hoyle (1949) was apparently the first astrophysicist who discussed the source of galaxy rotation in the framework of a theory of gravitational instability (Fall, 1980). He explained that the galaxy acquired rotation from gravitational coupling with the surrounding matter. Weizsacker (1951) and Gamow (1952) were the pioneer who made it clear that the observed rotation of the galaxies is important for cosmology. According to them, the fact that the galaxies rotate may provide a clue to the physical conditions under which these systems formed. In the instability picture, one imagines that large irregularity like galaxies grew under the influence of gravity from small imperfections in the early Universe (Gamow & Teller, 1939; Peebles, 1965, 1967). In this picture one must abandon the idea that the angular momentum of the galaxies was given as the initial value, or developed in some sort of primeval turbulence(as was proposed by weizsaker, 1951 and Gamow, 1952), for otherwise the galaxies would have formed too soon (Peebles, 1967).

As we know that spirals and barred spiral galaxies are supported by rotation whereas elliptical galaxies are supported by random velocity dispersion. Therefore, elliptical galaxies are rotating less rapidly than spirals (Figure 1). The cause of galactic angular momentum can be recognized to the action of tidal torques between neighboring proto-galaxies. As long the proto-galaxies are not spherically symmetric, differential accelerations are induced by neighbors, and these result in the gaining of angular momentum (Peebles, 1965). As the proto-galaxy collapses, however, it spins more and more rapidly. Exactly how rapidly depends on whether a halo of inert dark matter is

Figure 1: An interacting spiral (NGC 5091) and elliptical galaxy (NGC 5090) in Centaurus (~ 150 million ly away). The spiral galaxies are believed to be supported by rotation whereas elliptical galaxies are supported by random velocity dispersion rather than by rotation. Here a tidal disruption of NGC 5091 by NGC 5090 can be seen. (source: `https://apod.nasa.gov/apod/ap971205.html`)

present. The dark halo acts as a support against which the gas can torque as it loses energy and falls towards the inner regions. After collapsing by about a factor of 10 in radius, the gas is supported centrifugally in the plane of rotation: perpendicular to this plane, the gas distribution flattens because there is no support. In this way, a rotating gas disk develops that now fragments into stars to form a spiral galaxy. In the absence of a dark halo, centrifugal forces do not become dominant; instead, stars form when the proto-galaxy has contracted to form a flattened spheroid. The flattening of an elliptical is due not to systematic rotation but to anisotropic random motions of the stars, the motions are somewhat smaller in the direction perpendicular to the symmetry plane. A merger of two disk galaxies also produces a spheroidal stellar system, much like an elliptical galaxy. Whether the usual elliptical galaxy formation mechanism is through loss of dark halo, followed by contraction of the gas cloud, or through mergers is not known, but both processes are likely to occur during the formation of galaxy groups and clusters. Let us consider the angular momentum of a galaxy in terms of a dimensionless

parameter λ, given by,

$$\lambda = \frac{\omega}{\omega_0} \tag{2.1}$$

where, ω and ω_0 represent the actual angular velocity and the hypothetical angular velocity needed to support the system against gravity, purely by rotation. We know that

$$M\omega_0^2 R = \frac{GM^2}{R^2} \tag{2.2}$$

while $\omega^2 = J^2/M^2R^4$ where, J is the actual angular momentum of the galaxy. Eliminating the radius in terms of the energy by $R = GM^2/|E|$, we get

$$\lambda = \frac{\omega}{\omega_0} = \frac{JE^{1/2}}{GM^{5/2}} \tag{2.3}$$

It follows that a self-gravitating system with appreciable rotational support has a λ comparable to unity. Observations suggest that disk galaxies have $\lambda \sim 0.4$ to 0.5 (Padmanabhan, 2006). It is important to understand how the galaxies got this angular momentum, parameterized by observed value of λ. We describe one possible way: during the initial collapse of the baryonic structures, tidal forces will be exerted on each proto-galaxy by its neighbours. The tidal torque can spin up the proto-galaxies providing some angular momentum to them. During the collapse of the gas due to cooling, the binding energy increases while mass and angular momentum remain unchanged. This can allow λ to increase as $\lambda \propto |E|^{1/2}$ and (possibly) reach observed values. Therefore, the proto-galaxies can acquire initial angular momentum because of tidal torquing due to other collapsing material around it. If the typical mass, comoving radius and density contrast are M, R and δ respectively then, the tidal acceleration of any one of a pair of blobs is,

$$\left(\frac{\delta GM}{a^3R^3}\right)(aR) = \left(\frac{\delta GM}{a^2R^2}\right). \tag{2.4}$$

Here we have considered the separation between the blobs to be of same order as the size of the blobs and used the expansion factor a to convert the co-moving radius to proper radius. If the masses involved are taken to be $M/2$ and the lever arm for the force is $aR/2$, then the net tidal torque is of the order of

$$T = \left(\frac{\delta GM}{a^2R^2}\right)\left(\frac{M}{2}\right)\left(\frac{aR}{2}\right) = \left(\frac{\delta GM^2}{4Ra}\right). \tag{2.5}$$

In a $\Omega_{NR} = 1$ universe, $\delta \propto a$ implying that the tidal torque is a constant and the angular momentum grows linearly with time: $J = Tt$. The total angular momentum acquired until the time of turn around t_{ta} can now be estimated for a spherical top hat model. Using the relation between energy and virial radius and the details of spherical top hat model, it is easy to show that the angular momentum parameter is about $\lambda \sim 0.025/v$ if the object has an over density which is v times fractional density contrast. Once again simple arguments lead to meaningful final results though several factors of order unity have been ignored in the analysis.

The dissipational collapse of the baryons will increase the value of λ, especially in the case of disks embedded in spherical halo. In the absence of dark matter halos (and assuming that a protogalaxy was just a self gravitating cloud of baryonic gas) it turns out that the idea is not viable. But the idea works in the presence of a massive halo. In the presence of a massive dark halo, the initial spin parameter of the system, before collapse of the gas, can be written as

$$\lambda_i = \frac{J|E|^{1/2}}{GM^{5/2}} \tag{2.6}$$

where the various quantities J, E and M refer to the combined dark matter-gas system, although the contribution from the gas is negligible compared to that of the dark matter. After the collapse, the gas becomes self-gravitating and the spin parameter of the resulting disk galaxy will be,

$$\lambda_d = \frac{J_d|E_d|^{1/2}}{GM_d^{5/2}} \tag{2.7}$$

where, the parameters now refer to the disc. So we find that

$$\frac{\lambda_d}{\lambda_i} = \left(\frac{J_d}{J}\right)\left(\frac{|E_d|}{|E|}\right)^{1/2}\left(\frac{M_d}{M}\right)^{-5/2} \tag{2.8}$$

The energy of the virialized dark matter-gas system, assuming that the gas has not yet collapsed, can be written as

$$|E| = k_1\left(\frac{GM^2}{R_c}\right) \tag{2.9}$$

While that of the disk is given by

$$|E_d| = K_2\left(\frac{GM_d^2}{r_c}\right) \tag{2.10}$$

Here, R_c and r_c are the characteristic radii associated with the combined system and the disk respectively, while k_1 and k_2 are constants of order unity which depend on the precise density profile and geometry of the two systems. The ratio of the binding energy of the collapsed disk to that of the combined system is then

$$\frac{|E_d|}{|E|} = \left(\frac{k_2}{k_1}\right)\left(\frac{M_d}{M}\right)^2\left(\frac{r_c}{R_c}\right)^{-1} \tag{2.11}$$

Further, the total angular momentum (per unit mass) acquired by the gas, destined to form the disc, should be the same as that of the dark matter. This is because all the material in the system experiences the same external torques before the gas separates out due to cooling. Assuming that the gas conserves its angular momentum during the collapse, we have

$$\frac{J_d}{M_d} = \frac{J}{M} \tag{2.12}$$

Hence,

$$\frac{\lambda_d}{\lambda_i} = \left(\frac{k_2}{k_1}\right)^{1/2}\left(\frac{R_c}{r_c}\right)^{1/2}\left(\frac{M}{M_d}\right)^{1/2} \tag{2.13}$$

where, we have used Eq. (2.11) to simplify Eq. (2.8). The gas originally occupied the same region as the halo before collapsing and so had a pre collapse radius of R_c. Hence the collapse factor for the gas is

$$\frac{R_c}{r_c} = \left(\frac{k_1}{k_2}\right)\left(\frac{M_d}{M}\right)\left(\frac{\lambda_d}{\lambda_i}\right)^2 \tag{2.14}$$

We see that the required collapse factor for the gas to attain rotational support has been reduced by a factor (M_d/M), from what would have been required in the absence of a dominant dark halo. For a typical galaxy with a halo which is ten times as massive as the disc, one needs a collapse by only a factor of about 40 or so before the gas can spin up sufficiently to attain rotational support. This is quite easy to achieve. (In the absence of dark matter halo, the factor $(M_d/M) \approx 10$ is replaced by unity and one requires collapse factors which are ten times larger.)

It is possible to extend these arguments and estimate the characteristic length scale, R_d, of an exponential disk profile $\exp(-R/R_d)$ if we assume that there is no exchange of angular momentum between the disk and halo as the disk forms. For an exponential disk, we can easily compute the angular momentum per unit mass and obtain: $J/M = 2R_d v_g$,

Obreschkow *et* al., 2015, where v_g is the constant rotational velocity of the stars and gas. Combining this with the virial theorem.

$$|E| = K = \left(\frac{3}{2}\right) M v_h^2 \tag{2.15}$$

where v_h^2 is the velocity dispersion of the halo, we can eliminate J and $|E|$ from

$$\lambda = \left(\frac{JE^{1/2}}{GM^{5/2}}\right) \tag{2.16}$$

in terms of$M$. Finally, expressing M in terms of the halo rotation velocity by $GM/R = v_h^2$ and assuming that the density was a factor f_c larger than the background density $\rho_{bg}(z) = (3\Omega_{NR}(z)H^2(z)/(8\pi G)$ at the time of the collapse redshift z, we get

$$R_d = \left(\frac{\lambda}{2v_g}\right)\left(\frac{3v_h^2}{2}\right)^{-1/2} (v_h)^3 \left[\frac{f_c}{2}\Omega_{NR}(z)H^2(z)\right]^{-1/2} \tag{2.17}$$

If we now use $f_c = 180$ and assume that when the disk settles down, $v_g \sim v_h$, we get

$$R_d = 6h^{-1} \text{ kpc} \left(\frac{v_g}{200 \text{ km s}^{-1}}\right)\left(\frac{H_0}{H(z_f)}\right) \tag{2.18}$$

which relates the scale length of the disk R_d to the formation redshift z_f of the disc. For reasonable scale lengths, disk could not have formed at redshift significantly higher than unity. For Milky Way, with $v_g \sim 220$ km s^{-1}, $R_d = 3.6$ kpc, we need $H_0/H(z_f) = 0.55$ corresponding to $z_f \sim 0.5$. The overall picture which arises from these considerations - that the spheroids and bulges form early on while the disks form at a somewhat later epoch - is consistent with the observations.

2.2 Galaxy Evolution Model

Most of the visible matter in the universe is concentrated in galaxies, which are the basic astronomical ecosystems in which stars born, evolve, and die. The gross structural properties of galaxies and their distribution in space are determined primarily by the processes of galaxy formation, while other properties such as the stellar and gas content of galaxies and their evolution with time depend mainly on the processes of star formation and stellar evolution. However, it can be difficult to separate the processes of galaxy formation from those of galactic evolution, and both must be considered in any effort to understand the origin of the observed properties of galaxies and the correlations among

them. The evolution of galaxies is driven strongly by dynamical processes including internal instabilities, tidal interactions and mergers. The cluster environment is a useful laboratory for studying these effects. Galactic clusters are gravitationally bound large-scale structures of multiple galaxies. The evolution of these aggregates is determined by time and manner of formation and the process of how their structures and constituents have been changing with time.

The theoretical models explaining galaxy evolution are the 'hierarchy', 'Li', 'Ostriker' and the 'primordial vorticity', 'pancake',. Their predictions are different from each other. A brief description of these theories are given in the next section.

2.2.1 Hierarchy Model

This model was introduced by Peebles in 1969. According to the hierarchy model, galaxies grow by subsequent merging of proto-galactic condensations or even by merging of already fully formed galaxies. Peeble (1969) assumed that the torque experienced by a young galaxy is the product of its quadrupole moment and the tidal field due to other galaxies. To find quadrupole moment of a young galaxy, a homogeneous ellipsoid of revolution model is taken into consideration. The quadrupole moment is given by (Peeble, 1969),

$$Q = \int \rho(3z^2 - r^2)d^3r = \frac{2}{5}M(a^2 - b^2) \tag{2.19}$$

where, a and b represent semi-axes of the ellipsoid along the axis of symmetry and in the perpendicular direction. The smaller value of semi-axes can be neglected in comparison to the larger in this equation.

Let us consider another neighbor galaxy having M, is at a distance r away in a direction θ relative to the z-axis. The magnitude of the torque exerted by the tidal field of this galaxy is given by,

$$\tau = \frac{3}{4}\frac{GMQ}{r^3}\sin 2\theta \tag{2.20}$$

Now ensemble average value is determined by considering point masses and two-point distribution function. The expression for the mean square torque takes this form,

$$\langle\tau^2\rangle = \left(\frac{3}{4}GMQ\right)^2 \int P(r)d^3r\frac{\sin^2 2\theta}{r^6} \tag{2.21}$$

Here, $P(r)$ is the two-point distribution function which gives the probability that a galaxy is at $r_0 + r$, given that a galaxy is at r_0. The radius of the volume belonging to each galaxy is found to be,

$$D \sim \left(\frac{3M}{4\pi\rho}\right)^{1/3} \tag{2.22}$$

Therefore, the ensemble average of torque is given by,

$$\langle\tau^2\rangle^{1/2} = \left(\frac{2\pi}{5}\right)^{1/2} \frac{GMQ}{D^{3/2}} \left(\frac{\rho}{M}\right)^{1/2} = \frac{1}{3}\left(\frac{2}{15}\right)^{1/2} \frac{Q}{t^2} \tag{2.23}$$

where, $t^2 = 2R^3/(9GM)$, A few globular clusters can be disrupted because of tidal interactions between merging fragments. In the hierarchical merger model, the disrupted systems would have led to the present distribution of halo stars throughout the spheroid. It can be expected that there is no net rotation of object in the halo because of many random mergers. In addition, this model predicts that a few proto-galactic fragments should still be out there. A significant number of small galaxies orbiting the Milky way and near by Andromeda are possibly the examples.

2.2.2 Li Model

According to the cosmological principal, in a homogeneous and isotropic Universe, matter not only expands in space but also rotates with respect to local gyroscopes. In 1998, Li Xin investigated the cosmic effects of the global rotation. He proposed a model, in which the global rotation of the Universe provide angular momentum to the celestial bodies during their formation, resulting in rotating systems. As a result, the celestial bodies are supported by rotation.

The very idea that as a consequence of the conservation of angular momentum in a rotating universe, the galaxies acquire its angular momentum during their formation, was already considered by Gamow (1946), Goedel (1949), and later by Collins and Hawking (1973). One of its drawbacks was that it predicted preferred alignments of angular momentum of galaxies, which was not confirmed observationally at that time. Li (1998) explored the issue of galaxy formation in a rotating universe by introducing a model of homogeneous, rotating and expanding universe, filled with ideal fluid, which additionally complies with the laws of energy and angular momentum conservation.

The relation between the mass of a cosmic structure and its angular momentum is usually expressed by the empirical relation $J \sim M^{5/3}$, which origin has been discussed for a long time. In the model of rotating universe the relation $J \sim M^{5/3}$ is a direct consequence of the law of angular momentum conservation. Actually the relation is of the form $J = kM^{5/3} - lM$, where k and l are constants dependent on the amount of the Universe's rotation, density of matter, size of a protostructure and the moment of its formation. Consequently, the relation $J(M)$ has the global minimum J_{min} for the mass M_{min}. It was also shown that M_{min} does not depend on the amount of rotation of the Universe, while depending on the size of forming proto-structure and the moment of its formation (redshift z_f), as well as on the value of parameter (it is presumed to be close to 1). Dark matter was ignored in the considerations, since it was assumed to be collisionless and non-interacting with the observable matter in any other way than by gravitational force.

From the observational point of view of interest is the absolute value of angular momentum $|J|$, since in general the direction of structures is not known, while one can quite readily identify the situation when angular momentum vanishes or is very small. The vanishing angular momentum $J = 0$ is obtained when the structure's mass is $M_0 = 2.15 \times M_{min}$. It should be remembered that Li model remains valid only provided rotation occurs on a sufficiently large scale.

2.2.3 Ostriker Model

The conventional models of galaxy formation usually assume that the primordial fluctuations are Gaussian in nature and scale invarient, and the Universe is dominated by either cold dark matter (CDM) or hot dark matter (HDM) or both. Such universe is either flat or open.

The theoretical scheme based on non-Gaussian processes is the explosion scenario for galaxy formation, initially proposed by Ostriker and Cowie (1981). They predicted that galaxies can originate because of a series of explosive events. They estimated that structures ($\sim$ 100 Mpc) could be created by this chain reaction of explosions. In the explosion scenario, the first objects to form are explosive seeds (stars or clusters of stars). These generate shocks which sweep up vast shells of gas; when the shells overlap, most of the gas gets compressed into thin sheets. The sheets then fragment either directly into

galaxies or into lower-mass systems, depending on the cooling mechanism. Although the explosion scenario was originally invoked to explain large-scale structure, this now seems to be incompatible with the upper limit Far Infrared Astronomical Satellite (FIRAS) data. However, one can still envisage this as a mechanism for amplifying the fraction of the gas going into stars - an idea applicable in models with or without nonbaryonic dark matter. Because of the fact that the mass of the seed object is lower than the mass of the final structure formed, Ostriker & Cowie (1981) refer to their explosive model as explosive amplification. Here, positive energy perturbations drive material away from "seeds", sweeping primordial gas into dense, expanding shells that cool and fragment into galaxies. A variety of physical mechanisms might generate such perturbations. Explosions of supermassive stars or supernovae from the earliest galaxies could act as seeds, perphps amplified by the supernova energy of later generations of galaxies born on the shells. In fact, the explosion scenario does not require energy at all-nonlinear, negative-density fluctuations grow by gravity alone into expanding voids that have structure similar to other cosmological blast waves.

The explosion scenario naturally accounts for the "bubbly" appearance of the galaxy distribution. Their "slice of the universe" and other galaxy redshift surveys suggest that shells of radius $(10 - 30)h^{-1}$ Mpc with a filling factor of order unity may be the dominant elements of large scale structure. Since, shells enclose an appreciable fraction of space, the dynamical interactions of shells play an important role in the development of clusters, Superclusters and voids.

Gravitational instabilities grow slowly on isolated shells, so shell interactions are essential to the formation of massive galaxy clusters. When two shells cross they interact in an overdense ring, which then accretes matter from the shells. The two voids act like negative masses in comoving coordinates, pushing matter into a circular wall where the shells overlap and from this wall into the ring. Rich clusters form when a third shell intersects this ring in two points, "knots" creating deep potential minima that accumulate the surrounding matter. The process is somewhat analogous to the formation of structure in the pancake scenario, Where the matter collapses to flat "sheets" then flows towards the lines of interaction "filaments", and along those to their points of interaction, the "knots".

2.2.4 Pancake Model

The pancake model was first introduced by Zel'dovich (1970) later extended by Doroshkevich (1973) and Doroshkevich & Shandarin (1978). According to them, the directions of the angular momentum vectors of galaxies tend to lie within the cluster plane. In this scenario, formation of clusters took place first and it was followed by their fragmentation into galaxies due to adiabatic fluctuations. According to the non-linear gravitational instability theory (Zeldovich, 1970; Zeldovich & Novikov, 1975; Doroshkevich *et al*., 1974; Doroshkevich *et al*., 1976), a growth of small inhomogeneities leads to the formation of thin, dense, and gaseous condensations that are called 'pancakes'. These condensations are compressed and heated to high temperatures by shock waves. These shock waves cause them to fragment into gas clouds. The clumping of these clouds seeds the formation of galaxies and their clusters. Thermal, hydrodynamic, and gravitational instabilities arise during the course of evolution. It leads to the fragmentation of gaseous proto-clusters and, subsequently, clustering of galaxies takes place. The pancake scheme follows three simultaneous processes: first, gas cools and new clouds of cold gas form; secondly, these clouds cluster to form galaxies; and thirdly, the forming galaxies and, to an extent, single clouds cluster together to form a cluster of galaxies.

2.2.5 Primordial Vorticity Theory

The primordial vorticity theory predicts that the angular momentum vectors of galaxies are distributed primarily perpendicular to the cluster plane. The primordial vorticity is called top-down scenario. Sometimes it is also called turbulence model. In the turbulence scenario, first flattened rotating proto-clusters formed due to cosmic vorticity in the early universe. Subsequent density and pressure fluctuations caused galaxies to form.

The idea that galaxy formation is initiated by primordial turbulence has a long history. Ozernoy (1971, 1978) proposes that galaxies form from high-density regions behind the shocks produced by turbulence. According to the primordial vorticity theory, the presence of large chaotic velocities generates turbulence, which,in turn, produces density and pressure fluctuations.

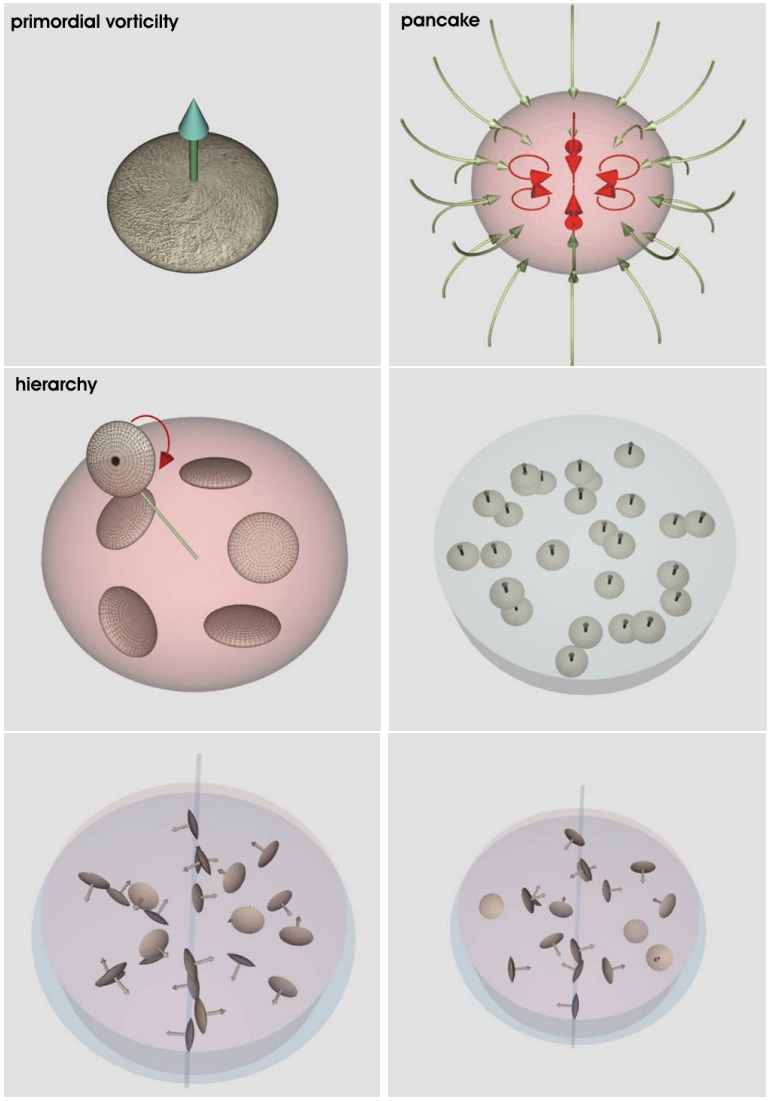

Figure 2: Explanation of the spatial orientations of angular momentum vectors of galaxies based on three existing models: primordial vorticity, pancake and hierarchy model. An arrow represents the preferred direction of the angular momentum vector of a galaxy in each model. The top and side view of these models are shown. (source: Kausch, 2004)

Density fluctuations on the scale of clusters of galaxies could be gravitationally bound, but galactic mass fluctuations are always unbound. Galaxies form when unbound galactic mass eddies, expanding faster than their bound cluster background. So forming galaxies collide with each other as clusters start to recollapse. These collisions produce shocks and high-density proto-galaxies at the eddy interfaces. As clusters recollapse, the system of galaxies undergoes a violent collective relaxation.

2.2.6 Galaxy Formation in Rotating & Expanding Universe

We assume spherically symmetric density fluctuation in the region containing the proto-galaxy (or matter) which will turn galaxy in future. The angular momentum relative to the gyroscopic frame is given by (Padmanabhan, 2006),

$$J_i = \frac{2}{5} M r_i^2 \omega_i \tag{2.24}$$

where M and r_i represent the mass and radius of the proto-galaxy. The angular velocity of the universe is represented by ω_i. Again, we define a local frame called galactic frame which correlate with the global rotation of universe and its origin is fixed at galactic center. This is the frame about which the measurement will be taken later. After the formation of the galaxy, it rotates relative to the galactic frames which is caused by the conservation of the angular momentum. After the galaxy has formed, its angular momentum relative to the gyroscopic frame is given by (Padmanabhan, 2006)

$$J_f = J + \beta M r_f^2 \omega_f \tag{2.25}$$

where ω_f is angular velocity of universe at present, β is the parameter that depends on the distribution of mass in galaxy, r_f radius of the galaxy at present and J is the angular momentum of the galaxy relative to the galactic frame. We know that,

$$\begin{aligned} \omega_i &= \omega_0 (1 + z_i)^2 \\ \rho_d &= \rho_{d0} (1 + z_i)^3 \\ M &= \frac{4}{3} \pi \rho_{di} r_i^3 \end{aligned} \tag{2.26}$$

From (2.24), (2.25), (2.26) and using law of conservation of angular momentum we get,

$$\begin{aligned} J_i &= J_f \\ \frac{2}{5} M r_i^2 \omega_i &= J + \beta M r_f^2 \omega_f \end{aligned}$$

Finally we get,

$$J = \frac{2}{5}\left(\frac{3}{4\pi\rho_{d0}}\right)^{2/3}\omega_0 M^{\frac{5}{3}} - \beta r_f^2(1+z_f)\omega_0 M \tag{2.27}$$

For $z_f < 1$, second term in (2.27) is sufficiently small compared to first term. Therefore,

$$J \simeq kM^{5/3}$$

$$\text{where} \quad k = \frac{2}{5}\left(\frac{3}{4\pi\rho_{d0}}\right)^{2/3}\omega_0$$

and this explains the observed empirical relation $J \propto M^{5/3}$. The limiting value of angular momentum can be calculated by minimizing (2.27) with respect to M, i.e.,

$$\begin{aligned}\left.\frac{dJ}{dM}\right|_{M_{min}} &= 0 \\ &= \left.\frac{d}{dM}\left(kM^{5/3} - lM\right)\right|_{M_{min}} \quad \text{where } l = \beta r_f^2(1+z_f)^2\omega_0 \\ &= k\frac{5}{3}M_{min}^{2/3} - l\end{aligned}$$

$$M_{min} = \left(\frac{3l}{5k}\right)^{3/2} = 1.95 r_f^3(1+z_f)^3\rho_{d0} \tag{2.28}$$

This is the mass corresponds to the minimum angular momentum. The condition for zero angular momentum can be obtained from (2.27), by putting $J = 0$, we get

$$kM^{5/3} = lM$$

Therefore

$$M = \left(\frac{l}{k}\right)^{3/2}$$

Hence, the mass corresponding to the zero angular momentum of galaxy is $M_0 \simeq 2.15 M_{min}$. It is observed that for less massive structures the angular momentum $\mid J \mid \neq 0$.

Therefore it can be concluded that the galaxy obtains its angular momentum due to the global rotation of the universe. One may expect that the angular momentum of galaxies should not distribute in the sky randomly. A dipole anisotropy can be expected and such kind of anisotropy lead the distribution of the angular momentum of galaxies to be different at different levels. Despite considering spherical symmetry the distribution of galaxy is found to be complicated. As the galaxy evolves the dissipation process inside it causes the components of angular velocity perpendicular to the angular momentum to vanish gradually, eventually the galaxy rotates about the direction of angular momentum.

2.3 Sloan Digital Sky Survey Photometry

Photometry is a technique of astronomy concerned with measuring the flux or intensity of an astronomical object's electromagnetic radiation emitted from astronomical objects. Usually, photometry refers to measurement over large wavelength bands of radiation; when not only the amount of radiation but also its spectral distribution are measured the term spectrometry is used. In astronomy, a photometric system is a set of well-defined passbands (or filters), with a known sensitivity to incident radiation. The sensitivity usually depends on the optical system, detectors and filters used. For each photometric system a set of primary standard stars is provided.

The first known standardized photometric system is the Johnson-Morgan or UBV photometric system (1953). At present, there are more than 200 photometric systems. Photometric systems are usually characterized according to the widths of their passbands:

- broadband (passbands wider than 30 nm, of which the most widely used is Johnson-Morgan UBV system),
- intermediate band (passbands between 10 and 30 nm wide) and
- narrow band (passbands less than 10 nm wide)

The methods used to perform photometry depend on the wavelength regime under study. At its most basic, photometry is conducted by gathering radiation in a telescope, perhaps passing it through specialized optical filters, and then capturing and recording the light energy with a photosensitive instrument. The set of passbands (filters) is called a photometric system.

Historically, photometry in the near infrared through long-wavelength ultra-voilet was done with a photoelectric photometer, an instrument that measured the light intensity of a single object by directing its light on to a photosensitive cell. These have largely been replaced with CCD (charge coupled device) cameras that can simultaneously image multiple objects, although photoelectric photometers are still used in special situations, such as where high time resolution is required. The Sloan Digital Sky Survey (SDSS) is one of the most ambitious and influential surveys in the history of astronomy.

In its first five years of operation, SDSS-I (2000 - 2005), the SDSS obtained five-band CCD imaging over 8 000 square degrees of the high Galactic latitude, Northern sky, detecting 217 million celestial objects. It obtained spectra of 675 000 galaxies, 90 000 quasars, and 215 000 stars, selected from 5 700 square degrees of this imaging (Abazajian *et al*., 2009). The data, fully calibrated and reduced, carefully checked for quality, and accessible through efficient data bases, have been publicly released in cumulative form, beginning with an early release of commissioning data and continuing with a series of annual data releases. The distance, magnitude and extinction relation is given (Karttunen *et al*., 2006)

$$m - M = 5 \log r' - 5 + 0.436 \alpha r' \tag{2.29}$$

Here m, M, r' and α represent apparent magnitude, absolute magnitude, distance and opacity of the medium. There are five different photometry (filters) in the SDSS telescope. There are u, g, r, z and i-filters. For SDSS u-filter,

$$u - M_u = 5 \log r' - 5 + 0.436 \alpha_u r' \tag{2.30}$$

Here, α_u represents opacity of UV light light emitted from the galaxy. Thus, the extinction is different for different filters. For r and g filters,

$$r - M_r = 5 \log r' - 5 + 0.436 \alpha_r r' \tag{2.31}$$

$$g - M_g = 5 \log r' - 5 + 0.436 \alpha_g r' \tag{2.32}$$

subtracting equation (2.31) from (2.32), we get,

$$r' = \frac{(r - g) - (M_r - M_g)}{0.436(\alpha_r - \alpha_g)} \tag{2.33}$$

and so on. This means the information of opacity is important to understand distance to the galaxy.

Thus, distance to the galaxy can be calculated if we know the database of extinction for given filters. SDSS database provides database of extinction as well as redshifts of almost all galaxies. SDSS uses a dedicated 2.5-m wide-angle optical telescope; from 2000-2009, it observed in both imaging and spectroscopic modes.

Figure 3 shows transmission curves of SDSS filters namely u, g, r, i and z. The peak wavelengths of these filters are 3551 A^o, 4686 A^o, 6166 A^o, 7480 A^o and 8932 A^o, with

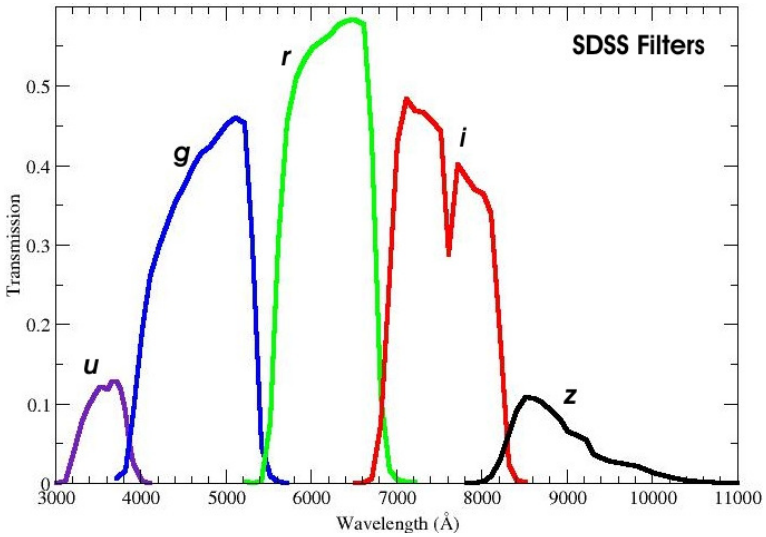

Figure 3: Standard photometric filter curves used by SDSS III telescope. (source: https://www.sdss3.org/instruments/camera.php)

95% completeness in typical seeing to magnitudes of 22.0, 22.2, 22.2, 21.3, as shown Figure 3 (Gunn, 1998). The response is the highest for r filter and the lowest for the z filter. Doi *et al*. (2010) studied the filter response and found that the u band has changed over time and appears to differ now from the curve estimated before.

2.4 Redshift

Redshift is a shift in the frequency of a photon towards lower energy, or longer wavelength. The redshift of any astronomical object is the displacement of its spectral features to longer wavelengths due to a combination of the gravitational redshift, Doppler motions and the general expansion of the Universe.

The redshift resulting from the relative motion of the light emitting object and the observer is attributed to the Doppler redshift. If the source of light is moving away from the observer then the wavelength of the light is stretched out, i.e., the light is shifted towards the red. The redshift may also caused by the expansion of the space. The wavelength of light increases as it traverses the expanding universe between its point of emission and its point of detection. Such process is termed as the cosmological redshift. The frequency of a photon may shift to lower energy as it climbs out of a gravitational field. This process by which electromagnetic radiation originating from a

source that is in gravitational field is reduced in frequency, or redshifted, when observed in a region of a weaker gravitational field is the gravitational redshift. So, the redshift of any astronomical object can be written as:

$$z_{total} = z_D + z_C + z_G \tag{2.34}$$

where z_D, z_C and z_G are the Doppler, cosmological and gravitational redshifts. A brief description of these redshift are given below.

2.4.1 Relativistic Doppler Redshift

The relativistic Doppler redshift is the change in frequency of light, caused by the relative motion of the source and the observer, when considering the special theory of relativity. Let the observer and the source are moving away from each other with a relative velocity v in the reference frame of the source. Let us suppose one wavefront arrives at the observer and the next wavefront is at a distance $\lambda = c/f_s$ away from him/her. Here λ is the wavelength, f_s is the frequency of the wave the source emitted, and c is the speed of light. Since the wavefront moves with velocity c and the observer escapes with velocity v, the time (measured in the reference frame of the source) between crest arrivals at the observer is (Karttunan *et al*., 2006) given by

$$t = \frac{\lambda}{c - v} = \frac{c}{(c - v)f_s} = \frac{1}{(1 - \beta)f_s} \tag{2.35}$$

where $\beta = v/c$. The observer will measure this time to be

$$t_\circ = t/\gamma \tag{2.36}$$

Therefore, the observed frequency becomes

$$f_\circ = \frac{1}{t_\circ} = \gamma\,(1 - \beta)\,f_s = \left(\frac{1 - \beta}{1 + \beta}\right)^{1/2} f_s \tag{2.37}$$

The ratio

$$\frac{f_s}{f_\circ} = \left(\frac{1 + \beta}{1 - \beta}\right)^{1/2} \tag{2.38}$$

is called the Doppler factor of the source relative to the observer. The corresponding wavelengths are related by

$$\frac{\lambda_\circ}{\lambda_s} = \frac{f_s}{f_\circ} = \left(\frac{1 + \beta}{1 - \beta}\right)^{1/2} \tag{2.39}$$

and the resulting redshift

$$z = \frac{\lambda_\circ - \lambda_s}{\lambda_s} = \frac{f_s - f_\circ}{f_\circ} \tag{2.40}$$

can be written as

$$z + 1 = \left(\frac{1+\beta}{1-\beta}\right)^{1/2} \tag{2.41}$$

In the non-relativistic limit (when $v \lll c$) this redshift can be approximated by

$$z \simeq \beta = \frac{v}{c} \tag{2.42}$$

corresponding to the classical Doppler effect.

When the light approaches at right angles to the direction of relative motion in the observer's frame, the relativistic redshift is known as the transverse redshift, given by,

$$z + 1 = [1 - v^2/c^2]^{-1/2}. \tag{2.43}$$

This redshuft can be measured even if the source is moving towards the observer.

2.4.2 Cosmological Redshift

The cosmological redshift is due to the expansion of space. The metric expansion of space is the increase of distance with time between distant parts of the universe. Metric expansion is a key feature of Big Bang cosmology and is modelled mathematically with the Friedmann − Robertson − Walker (FLRW) metric. The FLRW describes a homogeneous, isotropic, expanding or contracting universe. As a result of the metric expansion of space, photons propagating through the expanding space are stretched and hence increase their wavelength, creating the cosmological redshift. The redshift is related with the scale factor of now (a_{now}) and then (a_{then}) is given by (Padmanabhan, 2006),

$$z + 1 = \frac{a_{now}}{a_{then}} \tag{2.44}$$

In an expanding universe the scale factor is monotonically increasing as time passes, therefore, z is positive and distant galaxies appear redshifted according to the above relation.

2.4.3 Gravitational Redshift

The frequency of electromagnetic radiation originating from a source is reduced if it is in stronger gravitational field, and observed from a region of a weaker gravitational field. There is a corresponding reduction in energy when electromagnetic radiation is redshifted, as given by Planck's relation. There is a possibility of blueshift when electromagnetic radiation propagates from a region of a weaker gravitational field to the stronger gravitational field. The gravitational redshift of a photon can be calculated in the framework of general relativity using the Schwarzschild metric as (Padmanabhan, 2006),

$$z + 1 = [1 - r_s/R^*]^{-1/2} \tag{2.45}$$

with the Schwarzschild radius

$$r_s = \frac{2GM}{c^2} \tag{2.46}$$

where M and R^* represent the mass of the gravitating body and the distance between the center of mass of the gravitating body and the point at which the photon is emitted. In the Newtonian limit, i.e., when R^* is sufficiently large compared to the Schwarzschild radius r_s, the redshift becomes

$$z_{approx} = \frac{r_s}{2R^*} = \frac{GM}{c^2 R^*}. \tag{2.47}$$

2.5 Holmberg Equation

Erik Holmberg (1946) established a simple galaxy model which we have used to find the inclination angle of the galaxy. Holmberg equation is the relation between the axial ratio, b/a and the inclination angle i, the angle between the line-of-sight and normal to the galactic plane. Figure 4 shows the oblate spheroid aside. Holmberg (1946) assumes oblate spheroid which has light curve $\sim kr^{-3}$ and is seen from a distance, where the perspective distortion are negligible. The two major axes in the main plane are of equal size a, the polar axis is the smallest one representing the relative thickness of the ellipsoid. It has length $q\,a$, q being the so called flatness factor, a number $\in$ [0, 1] corresponding to the relative thickness of real spiral galaxies. The ellipse with an

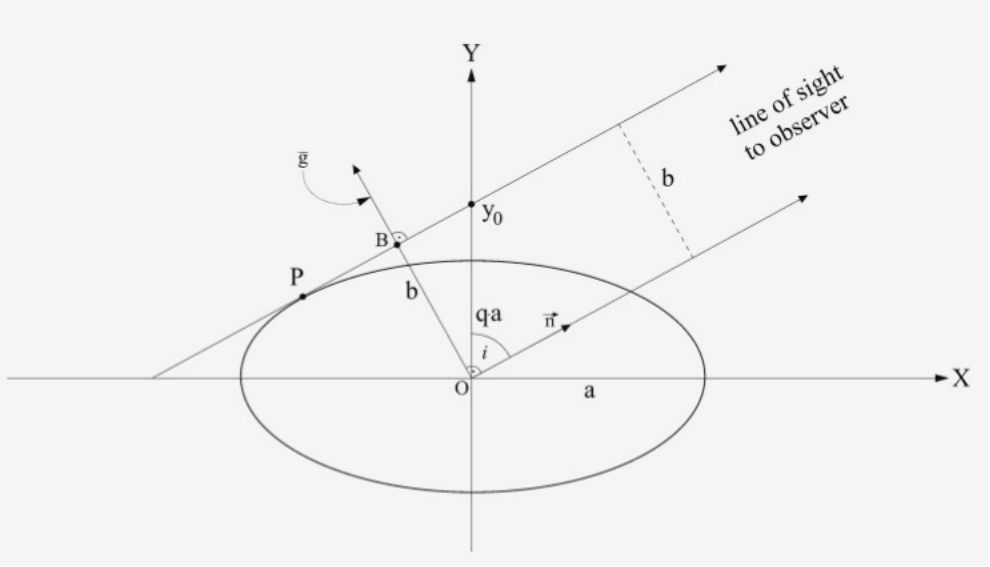

Figure 4: Derivation of Holmberg equation. (Kausch, 2004)

eccentricity of 0.2 is drawn. The celestial plane is perpendicular to the paper plane, intersection line is denoted by $\bar{g}$.

Figure 4 shows the line of sight to the observer, the inclination i is measured between this line and the Y-axis. This angle can be found between $\bar{g}$ and the X-direction.

The equation of the ellipse is (Kausch, 2004)

$$\begin{aligned} &\tfrac{x^2}{a^2} + \tfrac{y^2}{a^2 q^2} = 1 \\ &q^2 x^2 + y^2 = a^2 q^2 \end{aligned} \tag{2.48}$$

The oblate spheroid seems to be projected onto the celestial plane as an ellipse from the observers point of view. The length b is the semi minor axis of this ellipse. The semi major axis a is independent of the projection, because it is same as the one of oblate spheroid.

The equation of the tangent at point P is given by,

$$y = kx + y_0 \tag{2.49}$$

where $k = \cot i$ is the slope of the tangent and y_0 the intersection along Y-axis. The condition for contact to the ellipse in Figure 4 can be determined by applying the condition that (2.48) and (2.49) touches each other, i.e.,

$$a^2 k^2 + a^2 q^2 = y_0^2 \tag{2.50}$$

On substituting $k = \cot i$, we get,

$$y_0^2 = a^2 \cot^2 i + a^2 q^2 \tag{2.51}$$

From the figure, we have $b = y_0 \sin i$. Substituting this in (2.51) we get,

$$\sin^2 i = \frac{b^2/a^2 - 1}{q^2 - 1} \tag{2.52}$$

which leads to

$$\cos^2 i = \frac{b^2/a^2 - q^2}{1 - q^2} \tag{2.53}$$

(2.53) is called 'Holmberg Formula'. The Figure shows a plot between inclination angle

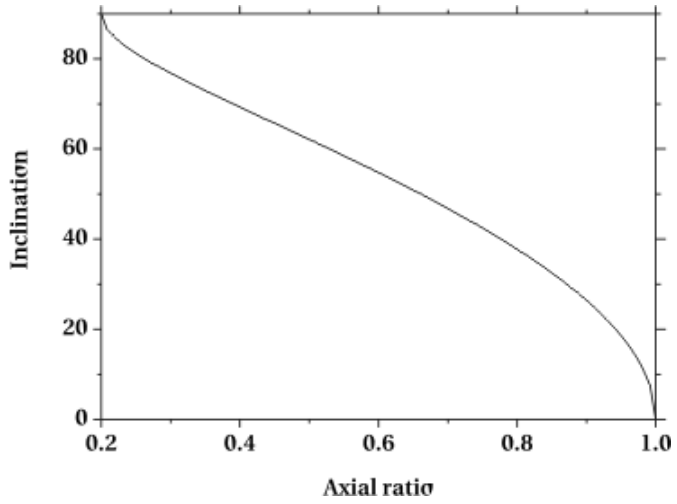

Figure 5: Axial ratio versus inclination angle plot. A strong nonlinearity at the lower and the upper end of the diameter ratio can be seen. Here flatness factor (q) is assumed to be 0.2 (source: Aryal, 2002)

(i) and the axial ratio (b/a). A strong nonlinearity can be seen at large diameter ratios. Therefore small error in the measurement of semi minor axes produce large deviations in the resulting inclination angle.

2.6 Spatial Orientations of Galaxies

The image of a galaxy that we obtain with the help of telescopes is simply a two dimensional projection of a real galaxy onto the celestial sphere. The major diameter, minor diameter, positions, position angle represent two dimensional observed data of

the three dimensional galaxy. On the basis of these optical data of a galaxy, Hawley and Peebles (1975) proposed a method to study the spatial orientation of galaxy. The method consists of analysis of the observed position angles (PA) or axial ratios b/a of galaxy images. This method was used in the early studies of galaxy orientation. It was merely a two dimensional analysis and deals only with the projection of galaxies in the celestial sphere. The projected shapes of galaxies look different depending on the line-of-sight of the observer. Since this method is based on the observed PA of the galactic image, it is very difficult to determine the PAs for galaxies seen face-on or nearly face-on. The PA yields information about the orientation of the galactic planes of edge-on galaxies.

In the late 70's Jaaniste and Saar (1978, JS hereafter) introduced the three dimensional method to analyze the galaxy orientation. The new method for galaxy orientation study analyzes the position angle and axial ratios b/a simultaneously. They analyzed not only the distributions of galaxy PAs, but also considered another important parameter - the galaxyŠs inclination with respect to the observerŠs line of sight, i.e., the inclination angle, as described by Holmberg (1946). These two angles helped to find the orientation of the nearly face-on and edge-on galaxies. By using JS approach face-on galaxies can be included in the analysis. These two angles allow us to find the orientations of two possible vectors normal to the galactic plane, one of them being assumed to be the galactic rotation axis or angular momentum vector of galaxy. Later, Flin & Godlowski (1986) studied the JS's approach and corrected a few inconsistencies and then proposed a model, called 'position angle - inclination angle' method which we describe below.

2.6.1 Flin-Godlowski Transformation

The position angle - inclination method is the transformation approach to obtain three-dimensional information of the angular momentum vector of galaxies with respect to an arbitrary coordinate system.

We derive the expressions for angular momentum vectors of the galaxies and its projections assuming their distribution in the equatorial co-ordinate system. An observer is situated at the origin of the E system. The X-Y plane represents the plane of the E system (i.e., equatorial plane) and the coordinates α and δ represent the equatorial longitude and latitude, respectively. The X-axis (EX) is directed towards the center of the equatorial

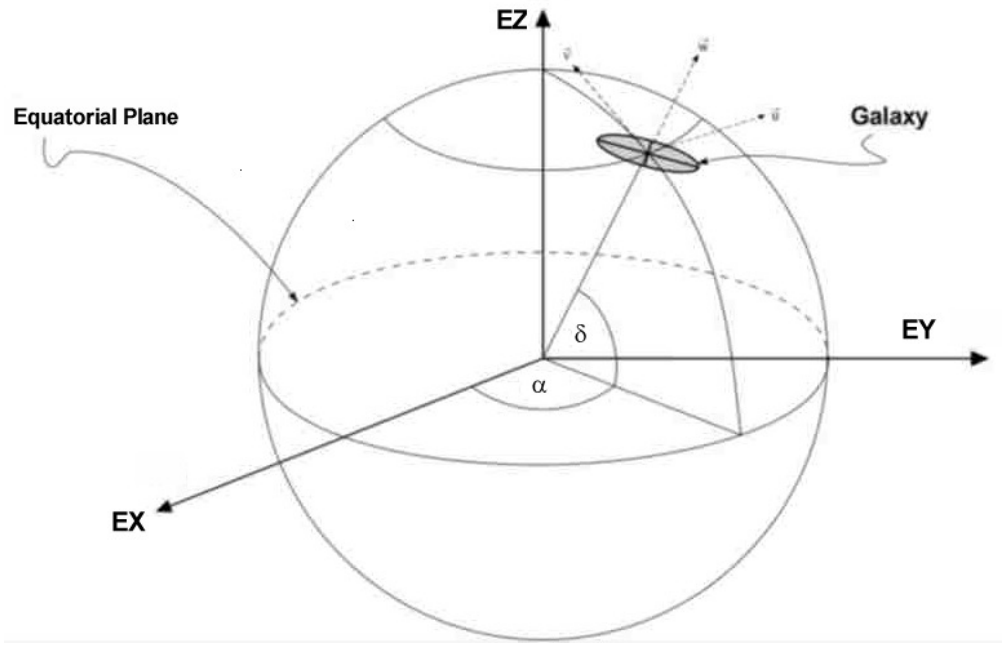

Figure 6: The coordinate system used for the derivation of the angular momentum vectors of the galaxy and its projection. Here α and δ represent right ascension and declination of the galaxy. (source: Kausch 2004)

plane ($\alpha = 0$, $\delta = 0$). The Y and Z-axis (EY and EZ) are directed towards the point $\alpha = \pi/2$, $\delta = 0$ and north equatorial pole ($\alpha = \pi/2$, $\delta = \pi/2$), respectively.

Let us assume another coordinate system. The origin of the this system is at the galaxy center. In this system, U and V-axes are perpendicular to each other and tangent to the celestial sphere. The U-axis is parallel to the equatorial latitude. The W-axis is perpendicular to both U and V-axes and is the extension of the connecting line between the centers of the cluster to the center of galaxy. This axis points out of the sphere. These can be seen in Figure 6. Figgure 7a shows the detailed view of the galaxy showing the vectors described above. The angle q is an angle between the U-axis and the projection of galaxy major axis a on the celestial sphere. The minor axis is denoted by b. The angle q is related to the equatorial position angle p, measured in the equatorial coordinate system is given by the expression: $q = p - \pi/2$ and is measured from $-\pi/2$ to $+\pi/2$.

Let us extend the normal to the galaxy plane passing through the origin of equatorial system. For an inclination angle, i, there will be two possible normals N_1 and N_2, and hence two possible positions of the galaxy rotation axis. The angular momentum vector is situated along one of these two normals. Let us consider N_1 and N_2 as the galaxy

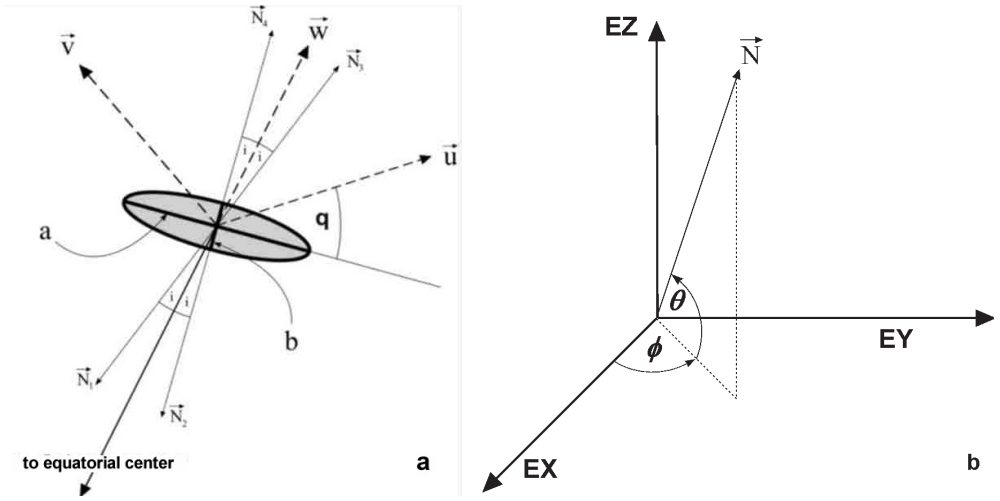

Figure 7: (a) Axial ratios and rotation axes of the galaxy: a and b are the major and the minor axes, $q = p - \pi/2$, N_1 and N_2 corresponds to the two possible rotation axes. (b) The polar and azimuthal angles (θ and ϕ) with respect to the equatorial coordinate system. (source: Kausch, 2004)

angular momentum vectors. It is seen from the Figure 7a that there are other two spin vectors N_3 and N_4 oriented just opposite to N_1 and N_2. N_1 and N_3 can be identified as one rotation axis whereas N_2 and N_4 as second rotation axis. So the ambiguity of four solutions for the spin vectors can be reduced to an ambiguity of two solutions. Therefore, just N_1 and N_2 are used for the statistical investigation.

The vectors N_1 and N_2 in the E system are

$$\begin{aligned} N_1 &= -W\cos i + \sin i(V\cos q + U\sin q) \\ N_2 &= -W\cos i - \sin i(V\cos q + U\sin q) \end{aligned} \tag{2.54}$$

Where, $\cos i$ is given by Holmberg's equation with the flatness factor $q*$ and is

$$\cos^2 i = \frac{[(b/a)^2 - (q*)^2]}{1 - (q*)^2} \tag{2.55}$$

and $(V\cos q + U\sin q)$ is the projection of the normals to the U-V plane. Now we apply the method of coordinate translation here. The galaxy related reference frame is translated to the center of the E system. This translation allows us to express the coordinates U, V and W in the E system. In the E system, these coordinates are the functions of right ascension (α) and declination (δ) only and they can be written as

follows:

$$\begin{aligned} U &= (-\sin\alpha\ \cos\alpha, 0) \\ V &= (-\sin\delta\cos\alpha, \cos\delta\sin\alpha, \cos\delta) \\ W &= (\cos\delta\cos\alpha, \cos\delta\sin\alpha, \sin\delta) \end{aligned} \tag{2.56}$$

here, $-\sin\alpha$, $\cos\alpha$ and 0 are the functions of the vector U along X, Y and Z axes, respectively. Similarly, $-\sin\delta\cos\alpha$, $-\sin\delta\sin\alpha$, $\cos\delta$ and $\cos\delta\cos\alpha$, $\cos\delta\sin\alpha$, $\sin\delta$ are the functions of the vectors V and W along X, Y and Z directions, respectively.

Substituting the values of U, V and W from equation (2.56) in (2.54) we get,

$$\begin{aligned} N_{ix} &= -\cos i\cos\delta\cos\alpha + \sin i(\mp\cos q\sin\delta\cos\alpha \mp \sin q\sin\alpha); \\ N_{iy} &= -\cos i\cos\delta\sin\alpha + \sin i(\mp\cos q\sin\delta\sin\alpha \pm \sin q\cos\alpha); \\ N_{iz} &= -\cos i\cos\delta \pm \sin i\cos q\cos\delta; \end{aligned} \tag{2.57}$$

where the upper and lower signs are for $i = 1$ and 2, respectively.

Now we introduce two angles: polar (θ) and azimuthal angle (ϕ) of galaxy rotation axis. The polar angle (θ), is the angle between the N_i vector and the galactic plane. The angle between the X-axis and the projection of the N_i vector on the galactic plane is termed as the azimuthal angle (ϕ). It should be noted that the reversal of the vectors N_1 and N_2 transforms the θ and ϕ values into $-\theta$ and $\phi + \pi$., respectively.

From Figure, we can write,

$$\begin{aligned} N_{ix} &= \cos\theta\cos\phi; \\ N_{iy} &= \cos\theta\sin\phi; \\ N_{iz} &= \sin\theta. \end{aligned} \tag{2.58}$$

Comparing the equations (2.57) and (2.58) gives,

$$\begin{aligned} \sin\theta &= -\cos i\sin\delta \pm \sin i\cos q\cos\delta; \\ \sin\phi &= \frac{-\cos i\cos\delta\sin\alpha + \sin i(\mp\cos q\sin\delta\sin\alpha \pm \sin q\cos\alpha)}{\cos\theta}; \\ \cos\phi &= \frac{-\cos i\cos b\cos\alpha + \sin i(\mp\cos q\sin\delta\cos\alpha \mp \sin q\sin\alpha)}{\cos\theta}. \end{aligned} \tag{2.59}$$

Substituting $q = p - \pi/2$ in equation (2.59),

$$\begin{aligned} \sin\theta &= -\cos i\sin\delta \pm \sin i\sin p\cos\delta; \\ \sin\phi &= \frac{-\cos i\cos\delta\sin\alpha + \sin i(\mp\sin p\sin\delta\sin\alpha \mp \cos p\cos\alpha)}{\cos\theta}; \\ \cos\phi &= \frac{-\cos i\cos\delta\cos\alpha + \sin i(\mp\sin p\sin\delta\cos\alpha \pm \cos p\sin\alpha)}{\cos\theta}. \end{aligned} \tag{2.60}$$

Using equation (2.59), the spin vector orientation of a galaxy can be derived. These equations (2.58) and (2.59) derived above are called 'Godlowski-Transformation' or 'Godlowskian Model'. In the equation (2.59) the position parameters are equatorial system parameters.

Expressions (2.59) and (2.60) give two solutions for both θ and ϕ for a given value of i. Hence, 4 solutions are obtained for the angular momentum vector of the galaxy. However, for a large sample of galaxies it is hardly possible to determine - for each galaxy - which one is the physical correct one. We count each of these possibilities independently for statistical analysis.

The expressions (2.59) and (2.60) give single solution for both θ and ϕ when a galaxy is seen exactly face-on ($i = 0°$). When seen edge-on ($i = 90°$), the two solutions for both and differ just in sign. In the case of θ, both solutions converge when approaching the equatorial pole or for galaxies with equatorial PA = 0°. In the case of ϕ, both solutions just differ in sign for $\alpha = 0°$. More interestingly, the characteristics of the solutions for and are also strongly influenced by the used coordinate system. This was already noted by Flin & Godlowski (1986). These authors suggested an analytical method to remove these selection effects due to positions.

2.7 Spatial Orientation of Galaxies: Literature Review

Hawley and Peeble (1975) proposed a method for studying the galaxy orientation. In their method, the observed position angles (hereafter PAs) and axial ratio distributions are analysed independently. They also introduced the Fourier method of analysing PA histograms. A second approach was proposed by Jaaniste and Saar (1978) in which another important parameter, the galactic plane inclination to the observer's line-of-sight, was also taken into the consideration.

Later, in 1986, Flin and Godlowski corrected the inconsistencies in the Jaaniste and Saar approach in the name of position angle - inclination method. In this method two dimensional information is used to generate the full three dimensional information about the galaxy orientation. In 2001, Aryal and Saurer developed a method to minimize the selection effect using numerical simulation. These days study of galaxy orientation is

based on position angle−inclination method along with numerical simulation.

2.7.1 Two Dimensional Study: Between 1975 - 1985

All the works in which two dimensional study of galaxies orientation has been carried out till date is listed in Table 1. First column lists the database. The next columns explain the general results followed by references.

The pancake theory was gaining popularity during 1970s. Authors were expecting to observe strong alignments in the clusters. Hawley & Peeble (1975) investigated position angle distributions in 5 559 galaxies in the direction of Virgo and Coma cluster. No significant alignment effects was noticed. Thompson (1976) published his study of the galaxy orientations in eight Abell clusters. The only cluster (Abell 2199) in which he found preferred alignment in the PA distribution. He also noticed a tendency for galaxies in Coma to point towards the cluster center. This result contradicts the result of Hawley & Peebles (1975). Macgillivary *et al*. (1982, 1985) investigated several groups and clusters and found a weak tendency of galaxies to be aligned with, or perpendicular to, their radius vectors to the cluster or group center. Their result for the Coma cluster was the same as the Thompson's result. Djorgovski (1983) analysed their data and observed very prominent alignment effects. He found that galaxies tend to align in the east-west direction with a high degree of significance. Strom and Strom (1978) studied the Perseus-Pisces Supercluster and noticed a distinct preference of the ellipticals to align with the main cluster chain. Gregory *et al*. (1981) noticed alignments and perpendicularity at a larger scale in the Perseus-Pisces Supercluster.

During this period, database come from the transparent plates obtained mostly from ground based optical telescopes. The interferometry and photometric techniques were commonly used. The resolution was up to 20 mag/arcmin. This resolution was not sufficient to resolve dwarf galaxies as well as late type spirals. The error in the photometric measurement was up to 30% (Storm & Storm, 1978). Therefore, the database was dominated by either normal spirals and bright elliptical. As we know that spirals are supported by rotation where as elliptical are supported by random velocity dispersion. In any case, the net angular momentum of an isolated system (groups, clusters and Superclusters of galaxies) should vanish according to cosmological principle. These

Table 1: A brief description of the two-dimensional study in the field of spatial orientation of galaxies published before 1986.

Sample/Database	Result & Conclusion	Reference
Several Clusters	• Couldn't find anything interesting	Hawley & Peebles, 1975
Eight Abell Clusters	• tendency for galaxies in Coma cluster to point toward the cluster center.	Thompson, 1976
Several groups & Clusters	• weak tendency to be aligned perpendicular to, their radius vectors cluster.	MacGillivary *et al*., 1979a, 1985b
6727 galaxies	• very prominent alignment effect.	Djorgovski, 1983
Perseus-Pisces Supercluster	• noticed a distinct perference of to align with the main cluster chain.	Storm & Storm, 1978
Perseus-Pisces Supercluster	• noticed perpendiculary alignments at a large scale.	Gregory *et al*., 1981
Local Supercluster (LSC)	• SVs of local Supercluster galaxies lie perpendicular to local Supercluster.	Reinhard & Roberts, 1972
Local Supercluster (LSC)	• tendency for galaxies to be parallel to Supercluster (LSC) plane with some secondary dependence on the Supergalactic latitude.	MacGillivary *et al*., 1982
Local Supercluster Spirals	• systematic alignment and winding direction of local Supercluster, effect be strongest for intermediate types.	MacGillivary *et al*., 1985a
Elliptical galaxies	• detected alignments in subsamples galaxies & of elliptical galaxies.	Dekel, 1985
Spiral pairs in Spiral	• mutual orientations of the spin vectors in pairs. • the spin vectors (SV) be antiparallel,	Helou, 1984

galaxies are formed because of merging and collision processes. These processes lead anisotropic in the distribution of angular momentum vectors (Peebles, 1969). Therefore most of authors have found anisotropic (non-vanishing angular momentum) result in the clusters. The database of Supercluster (LSC) galaxies was rich because of their low redshift (z <0.01). The position angle and axial ratio distribution were studied for spirals, ellipticals and irregulars. They (Helou, 1984; Dekel, 1985) found inconsistent result in spirals and ellipticals.

2.7.2 Three Dimensional Study: Between 1986-2003

All the works in which three dimensional study of galaxies orientation has been carried out between 1986-2003 are listed in Table 2. In the first column of the table, nature of the database is given. The next column explains the selection criteria imposed in the database. The last two columns gives the general results and the references.

The spectrometric techniques and the application of charge couple device (CCD) has been extensively used in the ground based optical telescope, after 1985. Therefore, the error in the magnitude and the redshift has been significantly decreased. However, resolution was not significantly increased. It means the quality of photometric database (axial ratio, position angle, etc.) was moderately improved. For the high redshift galaxies, the information regarding morphology and magnitude was rather poor. However, the population of galaxies has been significantly increased.

It can be seen in the Table 2 that the most of the results suggest anisotropy in the distribution of angular momentum vectors in the cluster. In other words, it is found that the net angular momentum of galaxies in the groups and clusters is non-vanishing, supporting either Pancake (Doroshkevich, 1973) or primordial vorticity theory (Ozernoy, 1978; Stein, 1974). For the local Supercluter galaxies, most of the author (see Table 2) found to support pancake model. Because of this result, pancake model was becoming popular even in cosmology. The major achievement of this period is the realization of a three-dimensional parameter, called inclination angle, the angle between line-of-sight and the normal to the galaxy. The technique for calculating inclination angle was investigated using landmark experimental work of Holmberg (1946). This method has been improved for different type of galaxies (Godlowski, 2003).

Table 2: A brief description of published studies 1986-2003.

Database	Selection criteria	Result & conclusion	Reference
1275 LSC galaxies (UGC)	• Radial Velocity (hereafter RV) <2600 km s^{-1}	• anisotropic distribution. • SVs of galaxies tend to lie parallelto the LSC plane. • anisotropy increases as axial ratio increases. • supports pancake model.	Flin & Godlowski, 1986
618 LSC galaxies (PANBG)	• RV<3000 km s^{-1} • $-3 \leq$ T (morphological type index) ≤ 10	• isotropy in most cases. • noticed bimodal near LSC plane SV parallel, • Virgo cluster show anisotropic and spin vectors tend to towards Virgo cluster center • supports pancake model.	Kashikawa & Okamura, 1992
2227 LSC galaxies (UGC, ESO, RCGR & TNGC)	• RV < 2600 km s^{-1}	• anisotropic distribution. • SVs of galaxies tend to lie parallel to the LSC plane. • projections of SVs tend to point towards Virgo center. • supports pancake model.	Godlowski, 1993
2227 LSC galaxies (UGC, ESO, RCGR & TNGC)	• RV < 2600 km s^{-1}	• anisotropic distribution. • azimuthal angle distribution strongly depends on supergalactic coordinates (L,B) and RV. • supports pancake model.	Godlowski, 1994
310 Virgo cluster galaxies (VCC, FGCP, UGC)	• RV<2700 km s^{-1}	• anisotropic. SVs projections of galaxies towards the Virgo center • morphological dependence. • SVs tend to perpendicular	Hu *et al*., 1995

Sample	Selection criteria	Result & conclusion	Reference
128 Coma cluster galaxies (CCG, CRCCG)	• 4500 ≤ RV ≤ 9900 km s^{-1} • $m_p \leq 15.6$ • R (radius from the cluster center) $\geq 3^0$	• anisotropic distribution. • morphologically dependent. • SVs of S0 lie parallel to cluster plane. • SVs of S lie parallel or • SVs projections of S point towards the cluster center.	Wu *et al*., 1997
302 Field galaxies (PANBG)	• RV < 3000 km s^{-1} • $-3 \leq T \leq 10$ • $R \geq 6^0$	• anisotropy in the azimuthal angle • projections of SVs point $\pm 30^0$ to Virgo center.	Yuan, *et al*. 1997
220 Bright isolated field galaxies (PANBG)	• RV < 2500 km s^{-1}	• anisotropic morphologically dependent. supports pancake for lenticulars	Hu *et al*., 1998
491 galaxies in field of the Abell 0754 (CUSSC)	• $b/a < 0.30$ (a & b: major and minor diameters,	• galaxy major planes be perpendicular to direction of PA of the cluster. • SVs parallel	Godlowski *et al*., 1998
18 subclusters of the LSC	• RV < 2800 km s^{-1}	• a strong systematic effect,	Godlowski & Ostrosky, 1999
557 galaxies of Coma Supercluster (CGCG,UGC, RC3, NED)	• 6000 ≤ RV ≤ 8000 km s^{-1} • $11^h.5 < \alpha < 13^h.5$, $18^0 < \delta < 32^0$	• anisotropic distribution. • SVs lie in plane of Supercluster. • projection of SVs towards the Supercluster	Flin, 2001
Cluster II Abell 14	Southern Sky Object Catalogue, 947 galaxies	evidence for non-random alignment in Abell and confirm subclustering	Baier *et al*., 2003

2.7.3 Numerical Simulation Method: 2004 to till date

Aryal & Saurer (2004-till date) carried out a systematic study by analyzing huge database of POSSII and ESO survey and found few important results. They have used a similar data reduction procedure and methods for different types of database. We summarize their results in a table here. During this period, a series of significant work was carried out by Godlowski *et al*. (2004-till date). We compare our result with their results later. Here, we list the nature of the database and the methods used by the authors.

Table 3: A brief descriptive published work during 2004 to till date. The first two columns briefly explain the database and the selection criteria. The third columns give the results obtained. References are listed in the last column.

Database	Selection	Results	Reference
Eight Abell Clusters: BM type I	POSSII & ESO Film: 1231 galaxies	• A42, A1775, A3558 and A3560 support Pancake • A401, A2199 and Abell 3556: supports Hierarchy	Aryal & Saurer, 2004
LSC Galaxies	UGC Catalog: 4073 morphologically identified galaxies with radial velocity < 3000 km s^{-1}	• LSC spiral galaxies : supports Pancake model • Barred & Irregulars: supports Hierarchy model • orientations of early-type and late-type are found different	Aryal & Saurer, 2005a
Seven Abell Clusters: BM type III	POSSII & ESO Film: 851 galaxies	• A1412, A2048 and Abell 4038: supports Pancake • A2061, A2065, A2151 and A2197: supports Primordial	Aryal & Saurer, 2005b
Galaxies in region $15^h48^m \leq\alpha(2000) \leq 19^h28^m$, $-68^0 \leq\delta(2000)\leq-62^0$	ESO Film: 1433 galaxies	• no morphological dependence • No preferred orientations for the spiral galaxies. • major diameters of < 47 arcsec galaxies: supports Primordial Vorticity model.	Aryal & Saurer, 2005c
Ten Abell Clusters: BM type II-III	POSSII & ESO Film: 1315 galaxies	• A1920, 2255 and 2256: bimodal orientation. • A168, 426, 1035, 1227, 1367 and 1904 : supports Pancake.	Aryal & Saurer, 2006
Shapley Supercluster	ESO Film: 323 galaxies	• No preferred alignments • low radial-velocity galaxies in A3558 showed anisotropy.	Aryal *et al.*, 2006

Database	Selection	Results	Reference
Seven Abell Clusters: BM type II-III	POSSII & ESO Film: 786 galaxies	• A1767, A1809, A2554, A2721: supports Pancake model. • systematic change in early-type (BM I) to late -type (BM III) clusters.	Aryal *et al*., 2007
Nearby LSC galaxies	2228 UGC, ESO galaxies: radial velocity 3000-5000 km s^{-1}	• noticed a preferred alignment and non-chiral property in leading and trailing arm barred galaxies. • predicts the progressive loss of chirality might have some connection with rotationally supported and randomized system	Aryal *et al*., 2008
Nearby LSC galaxies	5169 UGC, ESO galaxies: radial velocity 3000 - 5000 km s^{-1}	• spiral galaxies supports Pancake. • early-type barred spirals show random orientation. • a weak morphological dependence is noticed for barred spirals.	Aryal *et al*., 2008
LSC + nearby LSC galaxies	10562 galaxies: radial velocity $<$ 5000 km s^{-1}	• The galaxies of radial velocities 1500 to 2000 and 3000 to 3500 kms^{-1} show preferred alignments two- and three-dimensional analysis.	Aryal *et al*., 2008
Thirty Five Clusters	POSSII & ESO Films	• A dependence has been noticed between the optical search limit and the mean radial velocity of the cluster. • preferred position angle distribution of galaxies in the cluster has been found to be independent of the mean radial velocity of the cluster.	Aryal *et al*., 2010

Database	Selection Criteria	Results	Reference
Field galaxies	1621 field galaxies: radial velocity between 3000-5000 km s^{-1}	• random alignment in the PA-distribution of Z- and S- spirals. • a homogeneous distribution of S- and Z-shaped galaxies is found to be invariant global expansion.	Aryal *et al*.,
Three Merging Binary Cluster	merging binary clusters A1750, A3395 and A3528: SDSS database	• A3395 exhibits strongly distorted feature in maps of temperature and surface brightness showed a random orientation. • a relation between the stages of merging and non-random alignments of galaxies in the sub-structures of the binary clusters is expected.	Aryal *et al*., 2012
Zone-of-avoidance galaxies	POSSI prints: 410 galaxies	• spin vectors of galaxies lie in the equatorial plane whereas perpendicular to the Local Supercluster plane. • random alignment of spin vectors of galaxies is noticed with respect to the Galactic plane.	Aryal *et al*., 2012
Six rotating clusters	SDSS & 2dFGRS database: A954, A1139, A1399, A2366, A2162, A2169 and A2366	• a random orientation of SVs of galaxies are found in all six rotating clusters supporting Hierarchy model. • vanishing angular momentum is preferred by the rotating clusters which are in dynamical equilibrium .	Aryal *et al*., 2013

2.8 Motivation

The motivations to carry out the present work are as follows:

1. According to the cosmological principle, Universe is isotropic and homogeneous. In order to satisfy this principle, the curvature of space-time should be uniform. To make this, the total angular momentum of a group or cluster of galaxies should be zero. Though, a large number of study showed that the clusters of galaxies advocate non-vanishing angular momentum. Therefore a study of distribution of angular momentum vectors of galaxies is important for the better understanding of the cosmological principle. For a rotationally supported system (e.g., galaxies, stars, clouds, etc), the distribution of the angular momentum vectors can be an indicator of the initial conditions when these structures formed, provided the angular momentum of have not significantly changed since their formation (Wiezsacker, 1951 and Gamow, 1952). To gain an idea of the origin of angular momentum of galaxies it is very important to understand the evolution of large scale structures of the universe. Thus, a thorough study of the spatial orientations of angular momentum vectors of galaxies in the large scale structure is needed. Sloan Digitized Sky Survey (SDSS) data provides a very accurate spectroscopic and photometric data of large number of galaxies in the clusters and Superclusters. A systematic analysis of angular momentum of low- and high-redshift galaxies in the cluster and Superclusters would be important to understand evolution of galaxies in the clusters and Superclusters or vice versa.

2. There have been numerous galaxy orientation studies in the past, mostly to the end of verifying various galaxy cluster formation scenarios. The 'pancake model' (Doroshkevich, 1973; Shandarin, 1974) predicts that the angular momentum vectors of galaxies tend to lie within the cluster plane whereas the 'primordial vorticity model' (Ozernoy, 1978) says that the angular momentum vectors of galaxies tend to be oriented perpendicular to the cluster plane. According to the 'hierarchy model' (Peebles, 1969) the directions of the angular momentum vectors should be distributed randomly. Authors have drawn different conclusions regarding these scenarios: (1) no preferred alignment (Helou & Salpeter, 1982; Bukhari & Cram, 2003; Aryal & Saurer 2005c, Aryal *et al*., 2008, 2009, 2012, 2014a), (2) tend

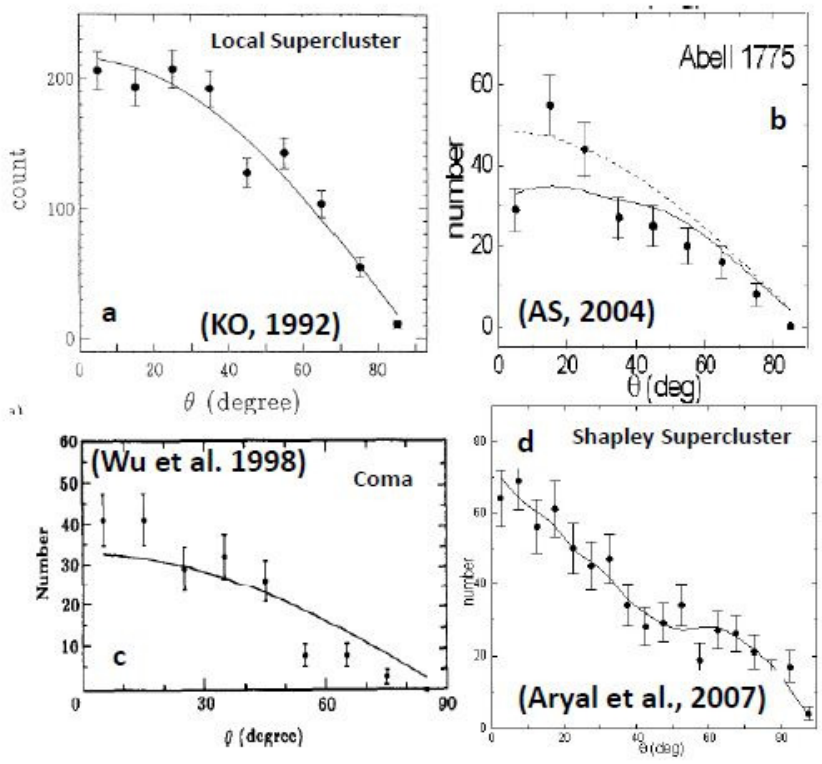

Figure 8: The distributions of angular momentum vectors of galaxies in past four works: (a) KO (1992) (b) AS (2004). (c) Wu *et al*. (1998) (d) Aryal *et al*. (2007).

to orient parallel (Jaaniste & Saar, 1978; Flin & Godlowski, 1986; Godlowski 1993, 1994; Godlowski, Baier & MacGillivray, 1998; Wu *et al*., 1998; Flin, 2001) or perpendicular (Rein- hardt & Roberts, 1972; Gregory, Thompson & Tift, 1981; MacGillivray *et al*., 1982; Baier *etal*., 2003) with respect to the cluster (or LSC) plane, (3) bimodal tendency (Kashikawa & Okamura, 1992) (3) local anisotropy (Flin, 1995; Djorgovski, 1983, Aryal & Saurer, 2004, 2005a, 2006a,b, 2013, 2014b), (4) global anisotropy (Parnovsky, Karachentsev & Karachentseva, 1994), etc. Godlowski & Ostrowski (1999) noticed a strong systematic effect, generated by the process of deprojection of a galactic axis from its optical image. Figure 8 shows anisotropic results of Kashikawa & Okamura (1992). (a) Aryal and Saurer (2004) and Wu *et al*. (1998). In these plots, significant humps or dips can be seen. Figure 8d shows a very good agreement between expected and observed distribution of angular momentum vectors. In isolated Abell clusters, only brightest galaxies are preferentially aligned (Trevese *et al*., 1992).

These results suggest different alignments of galaxies in clusters and Superclusters.

However, SDSS database was not available at that time and all of the above works have used photometric database (e.g., ESO, POSS, IC, MGC, etc). It is essential to find out the reason behind these differences. These differences might be correct or needs revision. We are interested work on the database of various type. The POSSI (Polomer Sky Survey I) and POSSII (Polomer Sky Survey II) compiled a photometric database but this database gives very accurate information regarding diameters and position angle. In addition to SDSS, we plan to use these database in order to check previous results.

3. The Local Supercluster (LSC hereafter) is the nearby Supercluster of galaxies that have mean radial velocity $\sim 3\,000$ km s^{-1}. The spatial orientation of angular momentum vectors of galaxies in the LSC has been a subject of many modern investigations. Godlowski *et al*. (1993) analysed the orientations of 2 227 LSC galaxies and concluded anisotropic distributions. This is the largest analysed database till 1993. Godlowski (1994) studied the dependence of galaxy alignment on radial velocity (RV) of 2 227 galaxies in the Local Supercluster (LSC) and found anisotropy for the galaxies that have RVs 1 000 km s^{-1} to 1 500 km s^{-1}. He concluded the dominance of Virgo cluster galaxies in this bin. In general, high RV clusters (A1920, 39 273 km s^{-1}) showed preferred alignments and low RV clusters (A0426, 5 366 km s^{-1}) showed random alignments. We intend to handle a huge all-sky database of the order of millions of galaxies. Fortunately SDSS provide such a rare opportunity these days.

4. Aryal & Saurer (2004-2006) and Aryal, Paudel & Saurer (2007) analysed the spatial orientations of galaxies in 32 Abell clusters of BM type I, II, II-III and III (Bautz & Morgan, 1970). They noticed a systematic change in the galaxy alignments from early-type (BM I) to late-type (BM III) clusters. This result suggests that the spiral-rich (late- type) clusters (BM II-III and BM III) show a preferred alignment than that of elliptical-rich (early-type) clusters. Liivamägi *et al*. (2012) compiled a set of Supercluster catalogues for the galaxies using SDSS survey main and luminous red galaxy (LRG) flux-limited samples. They calculated luminosity density fields using the B3-spline kernel of the radius of 8 Mpc/h for the main sample and 16 Mpc/h for the LRG sample and define regions with densities over a selected threshold as Superclusters.

5. Einasto *et al*. (2011) studies the morphology of a set of Superclusters drawn from the SDSS DR7. They calculated the luminosity density field to determine Superclusters from a flux- limited sample of galaxies from SDSS DR7, and select Superclusters with 300 and more galaxies. A study of a larger sample of Superclusters is needed to understand the alignments in their large-scale environment.

6. The redshift of galaxies comes either from the isotropic cosmic expansion or from the peculiar velocity due to gravitational attraction by their surroundings. In practice, determining the peculiar velocity of a galaxy requires knowledge of both its observable radial velocity relative to some reference system and the distance to the galaxy determined independently of the radial velocity. We live in the Local Supercluster, which is overdense part of the Universe. So there is possibly a local retardation of the cosmic expansion or a net infall within this region. The SDSS survey provides comple database of a huge number of blueshifted galaxies in the Local Supercluster. We intend to study preferred alignments of angular momentum vectors of these galaxies.

7. A complete photometric data gives valuable information regarding galaxy information. The SDSS survey uses near-ultraviolet to near-infrared CCD filters in almost all redshift limits. A strong emission through near-infrared filter suggests either the absorption of ultraviolet light by the dust emitted from the young stellar objects or because of the presence of older stellar population. In both the cases, the star formation activity can be assumed to be slower. Similarly, near-ultraviolet emission suggests the absence of dust in the interstellar medium and hence the older stellar population is rather low, advocating increasing star formation activity. It is believed that the slow star formation rate indicates the possibility of anisotropy (preferred orienting angle might be distorted due to collision or merging) and the rapid star formation rate slow down the angular momentum of the system, leading to a non-vanishing angular momentum. We intend to use a huge database of both low (< 0.1) and high (> 0.5) redshifted galaxies in both the ultraviolet and infrared filters in order to study above mentioned effects.

8. Selection effects may play an important role when galaxies are taken from an incomplete database. The SDSS database has this effect because it is a ground

based telescope located at northern hemisphere (New Mexico, USA) of our planet. These effects can lead to artificial structures (Aryal & Saurer, 2000). In most of the published works in galaxy orientation studies, selections of various kinds can be seen. These are mainly due to the face-on galaxies and inhomogeneity in positions. Only few authors have made an attempt to minimize these effects (Hu, *et al.*, 2005, Godlowski *et al.*, 2009). It is essential to remove such effects to avoid misinterpretations in the results. We intend to work on the removal of such effects by performing numerical simulation in all sort of database.

2.9 Objectives

Our major objectives are as follows:

1. We intend to work on spectroscopic database of millions of galaxies released by Sloan Dizitized Sky Survey (SDSS) data release 7 to 9, having different redshifts so that a comparison between the previous published works can be made.
2. The SDSS data release 7 and 9 provide a few thousands of galaxies with blueshift value.
3. We intend to study the distribution of angular momentum vectors of galaxies in a few SDSS Supercluster.
4. We are interested to study the relevance of equatorial, galactic and supergalactic co-ordinate system regarding galaxy orientation.
5. We intend to perform numerical simulation by generating 10^7 virtual galaxies to find the expected isotropic distribution of galaxies assuming cosmological principle. The expected distribution will be compared with the observed distribution with the help of suitable statistical methods.

CHAPTER 3

MATERIALS AND METHODS

CHAPTER 3

MATERIALS AND METHODS

3.1 Selection Effect in the Database

Aryal & Saurer (2000) studied the nature of database used by previous authors (Flin & Godlowski, 1986; Kashikawa & Okamura, 1992; Hu *et al*., 1999; Yuan *et al*., 1997; Wu *et al*., 1997) in the galaxy orientation study. They noticed a systematic effect in the database and realized that these effects should be removed from the database in order to find expected or theoretical distribution for polar and azimuthal angles of galaxies.

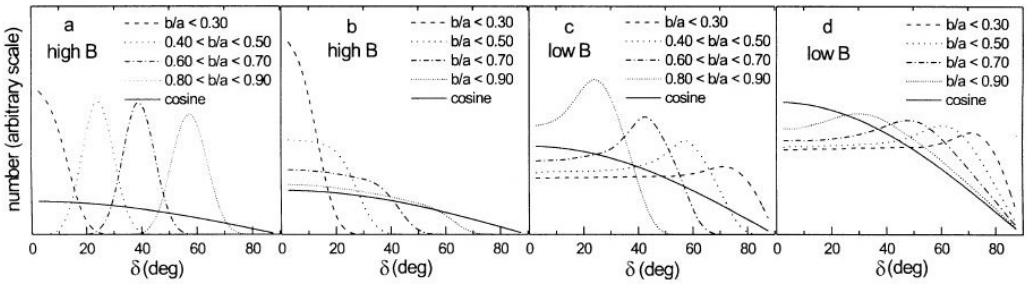

Figure 9: The expected isotropic distribution curves of the polar angle (here δ) for different selections on supergalactic latitude (B) and axial ratios (b/a) (Aryal & Saurer, 2000).

Aryal & Saurer (2000) found that selection effects concerning position and inclination angles of galaxies result a prominent change in the shape of the distributions of polar and azimuthal angles of galaxies in a cluster. The role of selection effects of this kind may be more significant when galaxies are taken from an incomplete dataset (e.g., from a limited region of sky). Due to these effects, artificial structures of the distributions are obtained which in turn lead to misinterpretation of results based upon them. In this paper Aryal

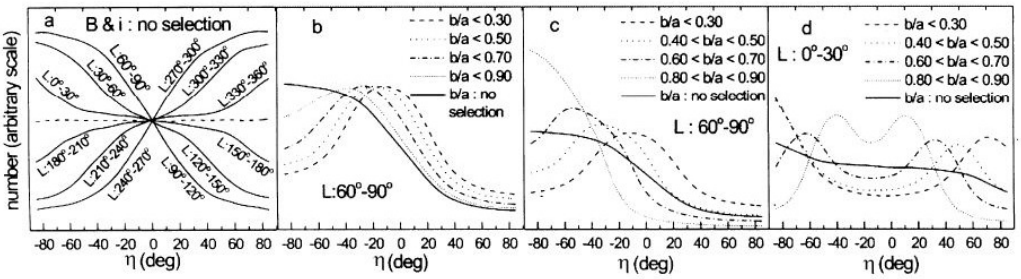

Figure 10: The expected isotropic distribution of azimuthal angle (here η) for different selections on supergalactic longitudes (L) and axial ratios (b/a) (Aryal & Saurer, 2000).

& Saurer (2000) discuss various possible effects due to the selection in the database. They have shown that nature of the expected isotropic curve changes severely when selection criteria are imposed on the dataset. They found that the isotropic distribution curve remains *cosine* for polar angle and a straight line for azimuthal angle(as previously adopted) only when there is no selection on L, B, P and i. The analytical method of Flin & Godlowski (1986) can be used only, when there is no selection in i. In the following points Aryal & Saurer (2000) summarize how selection effects change the shape of the isotropic distributions:

- The isotropic polar angle distribution is independent of L but changes with B when making selection on i.
- The isotropic distribution for polar angle is independent of B and L only when the range of i is full (i.e. no selections made); this distribution is independent of i, if there are no selection on positions.
- The azimuthal angle distribution is independent of the range of B, provided the range of i is full. It changes with L even when range of B and i is full.
- The isotropic polar angle distribution is different for edge on and face- on galaxies when making selection on B. However, the isotropic azimuthal angle distribution remains unchanged for face-on and edge-on galaxies when the range of L is full.

Here a list publications in which author's have used the method proposed by Aryal & Saurer (2000) is shown Table 4. In the present work, we have extensively used the numerical simulation method to find the expected isotropic distributions for both polar and azimuthal angles.

Table 4: Authors used numerical simulation method. The first column gives list of published papers in which authors have used the method proposed by Aryal & Saurer (2000). The second column gives the number of virtual galaxies created in the simulation. Third column represents selection effect that was noticed in their database.

S.N	Authors	No. of virtual galaxies	selection effect
1	Baier *et al*. (2003)	10^5	inclination
2	Aryal & Saurer (2004)	10^5	inclination
2	Aryal & Saurer (2005)	10^5	inclination & positions
3	Hu *et al*. (2005)	10^6	position angle
2	Aryal & Saurer (2006)	10^5	inclination & positions
4	Aryal *et al*. (2008)	10^6	inclination & positions
5	Aryal *et al*. (2012)	10^6	inclination
6	Godlowski *et al*. (2013)	N/A	inclination
5	Aryal *et al*. (2013)	10^6	inclination
7	Yadav *et al*. (2016)	10^7	inclination & positions

3.2 Numerical Simulation

Theoretically, the isotropic distribution curve for polar angle is *cosine* and that for azimuthal angle is the *average* distribution curve, with the restriction that the database is free from selection effect. Aryal & Saurer (2000) concluded that any selections imposed on the database may cause severe changes in the shapes of the expected isotropic distribution curves. In their method, a true spatial distribution of the galaxy rotation axis is assumed to be isotropic. Then, due to the projection effects, i can be distributed $\propto \sin i$, δ can be distributed $\propto \cos \delta$, the variables α and p can be distributed randomly, and the equation (2.60) can be used to calculate the corresponding values of polar angle (θ) and azimuthal angle (ϕ). We run simulations in order to define expected isotropic distribution curves for both the θ- and ϕ-distributions.

Here, we describe the procedure for the removal the selection effects to obtain the isotropic distributions for both θ and ϕ as given by Aryal & Saurer (2000). We present the process of numerical simulation for the sample $Z61$ (a sample described in the

Table 5: (a) Distributions of right ascension (α) (step size = 20°) and (b) declination (δ) (step size = 5°) of galaxies in sample Z61 (a sample described in the chapter 4.6.8). Here N and N' represent the observed (real) number and the corresponding virtual (created) number of galaxies in the sample. The total number of virtual galaxy is 10^7 in the simulation.

α	N	N'	δ	N	N'
10	4	20305	-12.5	1	5076
30	2	10152	-7.5	2	10152
110	3	15228	-2.5	8	40609
130	27	137056	2.5	25	126904
150	22	111675	7.5	18	91371
170	38	192893	12.5	13	65990
190	25	126904	17.5	20	101523
210	23	116751	22.5	17	86294
230	22	111675	27.5	18	91371
250	25	126904	32.5	20	101523
270	2	10152	37.5	11	55838
310	1	5076	42.5	13	65990
330	2	10152	47.5	5	25381
350	1	5076	52.5	9	45685
			57.5	9	45685
			62.5	8	40609

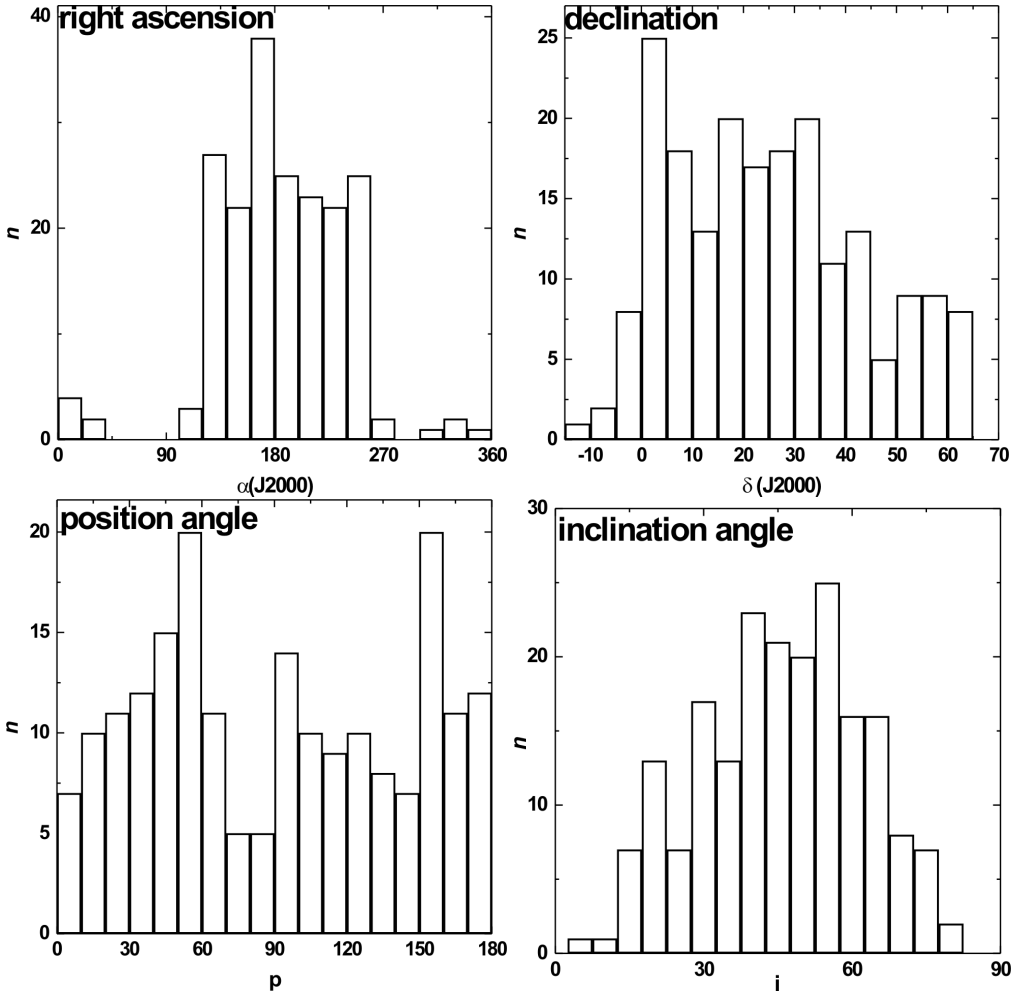

Figure 11: The distributions of right ascension (α), declination (δ), position angle (P) and inclination angle (i) of the galaxies in the sample Z61 (a sample described in the chapter 4.6.8). The Y-axes of histograms represent the number of observed galaxies.

chapter 4.6.8).

At first, we studied the distributions of right ascension (α), declination (δ), position angle (P) and inclination angle (i) for the galaxies in the sample $Z61$. Figure 11 shows the distributions of α, δ, P and i for the galaxies in the sample $Z61$. The histograms represent the number of observed galaxies.

Table 5 shows right ascension (α) and declination (δ) of galaxies in the sample Z61. The first two columns represent the value of α and the observed number of galaxies respectively. The last column shows the corresponding number of virtual galaxies created for the simulation. The total number of virtual galaxy is 10^7 in the simulation. We use these numbers to make input file for yje simulation.

Similarly, Table 6 shows the distributions of position angle (P) and inclination angle (i) for the galaxies in the sample $Z61$, respectively.

The right ascension is randomly distributed between 0° to 360° in 14 bins keeping the bin size 20°. The number of bin size has been fixed by using minimum standard error propagation method. The declination δ is randomly distributed in the range $-15°$ to 65° in 16 bins of size 5°. The distribution of the position angle P in the range 0° to 180° in 18 bins of bin size 10° is quite homogeneous. There is a inhomogeneous distribution of the inclination angle i in the range 0° to 90°, therefore distributed in 16 bins of size 5°.

3.2.1 Program and Input Files: An Example

Matlab 7.6.0 is used to write programme and input files for the simulation. As an example, we give program and input file for the galaxies of sample Z61 (a sample described in the chapter 4.6.8). The Program and Input Files is in Appendix G.

3.3 Statistical Tests

Galaxy clusters do not show an obvious alignment when looking at pictures. Therefore, statistical analysis is needed to check preferred alignments. In this work, we used the Fourier tests, auto-correlation and the chi-square. By applying statistical tests of the θ and ϕ-distributions resulting from the Godlowskian transformation, the investigation on alignments of the galaxies are made. The computer program used in these statistical computations were MICROSOFT EXCEL 2007 and ORIGIN5.0.

3.3.1 Fourier Test

Fourier series are infinite series of sines and cosines which are capable of representing almost any periodic function whether continuous or not. As an example, if the deviation from isotropy is only slowly varying with angles (in our case: θ and ϕ) the Fourier test can be applied.

Let N denote the total number of solutions for galaxies in the sample, N_k the number of solutions in the k^{th} bin, N_0 the mean number of solutions per bin, and N_{0k} the expected

Table 6: (a) Distributions of the position angle (P) (step size = 10°) and (b) the inclination angle (i) (step size = 5°) of galaxies in sample Z61 (a sample described in the chapter 4.6.8). Here N and N' represent the observed (real) number and the corresponding virtual (created) number of galaxies in the sample. The total number of virtual galaxy is 10^7 in the simulation.

P	N	N'	i	N	N'
5	7	35533	5	1	5076
15	10	50761	10	1	5076
25	11	55838	15	7	35533
35	12	60914	20	13	65990
45	15	76142	25	7	35533
55	20	101523	30	17	86294
65	11	55838	35	13	65990
75	5	25381	40	23	116751
85	5	25381	45	21	106599
95	14	71066	50	20	101523
105	10	50761	55	25	126904
115	9	45685	60	16	81218
125	10	50761	65	16	81218
135	8	40609	70	8	40609
145	7	35533	75	7	35533
155	20	101523	80	2	10152
165	11	55838			
175	12	60914			

number of solutions in the k^{th} bin. Then, the Fourier series is given by,

$$N_k = N_{ok}(1 + \Delta_{11}\cos 2\theta_k + \Delta_{21}\sin 2\theta_k + \Delta_{12}\cos 4\theta_k + \Delta_{22}\sin 4\theta_k) \tag{3.1}$$

Here, Δ_{ij} coefficients are parameters of the distribution and the angle θ_k represents the polar angle in the k^{th} bin. At first Hawley & Peebles (1975) used the Fourier Test. Flin & Godlowski (1986) used Fourier test to study the galaxies orientation and later Godlowski (1993, 1994) improved the method. If we take into account only the the first or second Fourier mode separately, then we obtain the following expressions for the Fourier coefficients (Godlowski, 1994),

$$\Delta_{11} = \sum_{k=1}^{n}(N_k - N_{0k})\cos 2\theta_k / \sum_{k=1}^{n} N_{0k}\cos^2 2\theta_k \tag{3.2}$$

$$\Delta_{21} = \sum_{k=1}^{n}(N_k - N_{0k})\sin 2\theta_k / \sum_{k=1}^{n} N_{0k}\sin^2 2\theta_k \tag{3.3}$$

where n is the number of bins. The standard deviations $\sigma(\Delta_{11})$ and $\sigma(\Delta_{21})$ can be obtained using the expressions,

$$\sigma(\Delta_{11}) = \left(\sum_{k=1}^{n} N_{0k}\cos^2 2\theta_k\right)^{-1/2} \tag{3.4}$$

$$\sigma(\Delta_{21}) = \left(\sum_{k=1}^{n} N_{0k}\sin^2 2\theta_k\right)^{-1/2} \tag{3.5}$$

The probability that the amplitude

$$\Delta_1 = (\Delta_{11}^2 + \Delta_{21}^2)^{1/2} \tag{3.6}$$

greater than a certain chosen value is given by,

$$P(> \Delta_1) = \exp(-nN_0\Delta_1^2/4) \tag{3.7}$$

with standard deviation

$$\sigma(\Delta_1) = (2/nN_0)^{1/2}. \tag{3.8}$$

This test was improved by Godlowski (1994) for the case when higher Fourier modes is taken into account:

$$N_k = N_{0k}\,(1 + \Delta_{11}\cos 2\theta_k + \Delta_{21}\sin 2\theta_k + \Delta_{12}\cos 4\theta_k + \Delta_{22}\sin 4\theta_k + \ldots\ldots) \tag{3.9}$$

So, the Δ_{ij} coefficients are:

$$\Delta_{1j} = \sum_{k=1}^{n}(N_k - N_{0k})\cos 2\,j\theta_k / \sum_{k=1}^{n}\cos^2 2\,j\theta_k \tag{3.10}$$

$$\Delta_{2j} = \sum_{k=1}^{n}(N_k - N_{0k})\sin 2\,j\theta_k / \sum_{k=1}^{n}\sin^2 2\,j\theta_k \tag{3.11}$$

where n is the number of bins. The standard deviation is given by,

$$\sigma(\Delta_{1j}) = \left(\sum_{k=1}^{n} N_{0k}\cos^2 2\,j\theta_k\right)^{-1/2} \tag{3.12}$$

$$\sigma(\Delta_{2j}) = \left(\sum_{k=1}^{n} N_{0k}\sin^2 2\,j\theta_k\right)^{-1/2}. \tag{3.13}$$

If we analyze Fourier modes separately, probablity that the amplitude

$$\Delta_j = \left(\Delta_{1j}^2 + \Delta_{2j}^2\right)^{\frac{1}{2}} \tag{3.14}$$

is greater than a certain chosen value is given by,

$$P(>\Delta_j) = exp\left(-\frac{n}{4}N_0\Delta_j^2\right) \tag{3.15}$$

where N_0 is the numbers per bin, with standard deviation

$$\sigma(\Delta_J) = (2/nN_0)^{1/2} \tag{3.16}$$

However, in this approximation, the theoretical probability function p_k is still symmetric with respect to the value θ that corresponds to the value $\delta = 0$. The expressions becomes,

$$\Delta_{11} = \frac{CK - UM}{AC - U^2}, \tag{3.17}$$

$$\Delta_{21} = \frac{DL - WN}{BD - W^2}, \tag{3.18}$$

$$\Delta_{12} = \frac{-UK + AM}{AC - U^2}, \tag{3.19}$$

$$\Delta_{22} = \frac{-WL + BN}{BD - W^2}, \tag{3.20}$$

where we have denoted

$$A = \sum N_{ok}\cos^2 2\theta_k\,, \qquad B = \sum N_{ok}\sin^2 2\theta_k\,, \tag{3.21}$$

$$C = \sum N_{ok}\cos^2 4\theta_k\,, \qquad D = \sum N_{ok}\sin^2 4\theta_k\,, \tag{3.22}$$

$$U = \sum N_{ok}\cos^2 2\theta\cos 4\theta_k\,, \qquad W = \sum N_{ok}\sin^2 2\theta\sin 4\theta_k, \tag{3.23}$$

$$K = \sum (N_k - N_{ok})\cos 2\theta_k\,, \qquad L = \sum (N_k - N_{ok})\sin 2\theta_k\,, \tag{3.24}$$

$$M = \sum (N_k - N_{ok})\cos 4\theta_k\,, \qquad N = \sum (N_k - N_{ok})\sin 4\theta_k\,, \tag{3.25}$$

The covariance matrix Cov = G^{-1} is

$$G^{-1}=\begin{pmatrix} C/(AC-U^2) & 0 & -U/(AC-U^2) & 0 \\ 0 & D/(BD-W^2) & 0 & -W/(BD-W^2) \\ -U/(AC-U^2) & 0 & A/(AC-U^2) & 0 \\ 0 & -W/(BD-W^2) & 0 & B/(BD-W^2) \end{pmatrix}$$

$$\Delta_{11} = \frac{\sum N_{ok}\cos^2 4\theta_k \sum(N_k - N_{ok})\cos 2\theta_k - \sum N_{ok}\cos^2 2\theta \cos 4\theta_k \sum(N_k - N_{ok})\cos 4\theta_k}{\sum N_{ok}\cos^2 2\theta_k \sum N_{ok}\cos^2 4\theta_k - (\sum N_{ok}\cos^2 2\theta|\cos 4\theta_k)^2} \tag{3.26}$$

$$\sigma^2(\triangle_{11}) = \left[\sum N_{ok}\cos^2 2\theta_k \sum N_{ok}\cos^2 4\theta_k - \left(\sum N_{ok}\cos^2 2\theta\cos 4\theta_k\right)^2\right]^{-1} \times \left(\sum N_{ok}\cos^2 4\theta_k\right) \tag{3.27}$$

$$\Delta_{22} = \frac{-\sum N_{ok}\sin^2 2\theta \sin 4\theta_k \sum(N_k - N_{ok})\sin 2\theta_k - \sum N_{ok}\sin^2 2\theta_k \sum(N_k - N_{ok})\sin 4\theta_k}{\sum N_{ok}\sin^2 2\theta_k \sum N_{ok}\sin^2 4\theta_k - (\sum N_{ok}\sin^2 2\theta \sin 4\theta_k)^2} \tag{3.28}$$

$$\sigma^2(\Delta_{22}) = \sum N_{ok}\sin^2 2\theta_k \sum N_{ok}\sin^2 4\theta_k - \left(\sum N_{ok}\sin^2 2\theta\sin 4\theta_k)^2\right) \times \left(\sum(N_k - N_{ok}\right)\sin 2\theta_k \tag{3.29}$$

It is important to understand whether the analysed distribution in the same as the theoretical one. We need the expression for the probability that the amplitude Δ(obtained from all Δ_{ij}) is greater than a certain chosen value. The formulae are given below.

$$\boldsymbol{I} = \begin{pmatrix} \Delta_{11} \\ \Delta_{21} \\ \Delta_{12} \\ \Delta_{22} \end{pmatrix}$$

Then the formula for probability is $P(\Delta) = (1+J/2)^2\exp(-J/2)$, where, $J = \sum\sum G_{ij}I_iI_j$. It should note that in the case when all probabilities p_k are equal (as an example, in the case of angle ϕ) the expressions (3.26) and (3.27) reduce to (3.10) and (3.12), respectively.

3.3.2 Chi-square Test

Chi-square test for goodness of fit, is a very popular for testing the significance of discrepancy between theoretical and expected values. It enables us to find if the deviation of the experiment from theory is just by chance or it is really due to inadequacy of the theory to fit the observed data. It tests whether a sample of data came from a population with a specific distribution. The chi-square test is always testing the null hypothesis, which states that there is no significant difference between the expected and observed results. For computation of chi-square test, the data are divided into 'n' bins (data classification). The chi-square value is given by,

$$\chi_v^2 = \frac{\chi^2}{v} \tag{3.30}$$

$$\chi^2 = \sum \frac{(N_{oi} - N_{ei})^2}{N_{ei}} \tag{3.31}$$

Where the summation is taken from one to n. Here n represents the number of bins (categories), N_{oi} and N_{ei} represent the observed and expected isotropic distributions.

The χ^2-distribution is a continuous probability distribution. The quantity χ_v^2 defined in Eq. (3.30) has the probability distribution given by

$$f(\chi^2) = \frac{1}{2^{v/2}\Gamma(v/2)}(\chi^2)^{v/2}e^{-\chi^2/2} \tag{3.32}$$

where $\Gamma(z)$ is the gamma function defined by

$$\Gamma(z) = \int_0^\infty u^{z-1}e^{-u}du; \quad z > 0 \tag{3.33}$$

The Eq. (3.31) is known as the χ^2 distribution with v degrees of freedom and is a positive integer.

For an isotropic distribution, the χ_v^2 value is expected to be nearly zero. The quantity $P(> \chi_v^2)$ gives the probability that the observed χ_v^2 value is realized by the isotropic distribution. The observed distribution is more consistent with the expected isotropic distribution when $P(> \chi_v^2)$ is larger. We set $P(> \chi_v^2) = 0.050$ as the critical value to discriminate isotropy from anisotropy, it corresponds to the deviation from the isotropy at 2σ level. The test is applied to all samples to examine the deviations of the observed θ and ϕ-distributions from the expected isotropic distributions.

3.3.3 Auto-correlation Test

In statistics, the auto-correlation of a random process describes the correlation between values of the process at different points as a function of time. Auto-correlation test is a mathematical tool for finding repeating patterns and measures the degree to which there is a linear relationship between two variables. If the function is well defined, its value must lie in the range $[-1, 1]$. In our case, it takes to account the correlation between the number of galaxies in adjoining angular bins. The correlation function is

$$C = \sum \frac{(N_k - N_{ok})(N_{k+1} - N_{ok+1})}{(N_{ok} N_{ok+1})^{1/2}} \tag{3.34}$$

with the standard deviation

$$\sigma(C) = (n)^{1/2} \tag{3.35}$$

In an isotropic distribution any correlation vanishes, so we expect to have $C \rightarrow 0$. The correlation function is important for theoretical models of physical cosmology because it provides a means of testing models which assume different things about the contents of the universe.

3.3.4 Summary

In the present work, the conditions for anisotropy are as follows:

- the chi-square probability $P(> \chi^2) < 0.050$
- the correlation coefficient $C/\sigma(C) > 1$
- the first order Fourier coefficient $\Delta_{11}/\sigma(\Delta_{11}) > 1.5$ and
- the first order Fourier probability $P(< \Delta_1) < 0.150$

as used by Godlowski (1993, 1994), Aryal & Saurer (2004-2006) and Aryal et al. (2007-2016).

CHAPTER 4

RESULTS AND DISCUSSION

CHAPTER 4

RESULTS AND DISCUSSION

4.1 Low Redshift Galaxies

These are nearby galaxies, receding from the Milky Way with radial or recessional velocity approximately greater than 15 000 km s^{-1} (or redshift > 0.05). We have chosen this limit because of the following two reason:

- The galaxies having radial velocity less than 15 000 km s^{-1} (or redshift < 0.05) have already studied by various authors in the past (Godlowski, 1994; Aryal *et al*., 2008, 2009, 2010 and 2013). They found inconsistent result and suggested to improve the quality of database as well as redshift limit.
- Availability of both spectroscopic and photometric database of about 242 902 galaxies that have radial velocity in the range 15 000 km s^{-1} to 30 000 km s^{-1} motivated us to study their spatial orientation.

4.1.1 Database

The selection criteria for the database of SDSS galaxies (Gunn *et al*., 2006) are as follows:

1. Photometric survey should be complete at 99% level of significance.
2. The position angle and diameters of the galaxies should be known in all passbands

The database used in this work consists of galaxies, located within the survey regions of SDSS (7^{th} data release) having redshift in the range 0.05 to 0.10. There are 242 902 galaxies in the region of interest. These galaxies have radial velocity in the range 15 000

km s^{-1} to 30 000 km s^{-1}. Among 242 902 galaxies; 5.44% galaxies were excluded due to the lack of the position angles. Thus, we have 229 675 galaxies in our sample, of which the positions, major and minor diameters, position angles in all SDSS passbands and magnitude are known. For low redshift galaxies we chose z-filter. We have planned to choose r-filter for the high and z for the low redshift galaxies. A sample page of database is given in Table A.1 of appendix A.

We classify samples on the basis of z-magnitude (m_z) of galaxies. For the sample classification, we have plotted bin size versus standard error using z-magnitude (m_z) of galaxies. The region of minimum fluctuations in the standard error propagation is considered as the stable bin size. This is found when setting bin size as 0.30 for m_z. Therefore, we have classified our database into 19 samples keeping $\Delta m_z = 0.30$.

4.1.2 Anisotropy in the Polar and Azimuthal Angle Distribution

We discuss distribution of polar (θ) and azimuthal (ϕ) angles of galaxy rotation axes in each sample. Later a general discussion of the result will be presented followed by a comparison with published works. Our aim is to study the non-random effects concerning z-magnitude dependence in the spatial orientation of spin vectors of galaxies. Any deviation from expected isotropic distribution will be tested using four statistical parameters, namely chi-square probability (P $>\chi^2$), auto-correlation coefficient (C/C(σ)), first order Fourier coefficient ($\Delta_{11}/\sigma(\Delta_{11})$) and first order Fourier probability (P $>\Delta_1$). For anisotropy, the limit of chi-square probability P($>\chi^2$) is < 0.050, the absolute value of auto-correlation coefficient (C/C(σ)) is > 1.0, the absolute value of first order Fourier coefficient ($\Delta_{11}/\sigma(\Delta_{11})$) is > 1.5 and Fourier probability P($>\Delta_1$) is < 0.150 respectively. These statistical limits were suggested by Godlowski (1993, 1994) in galaxy orientation studies.

The statistics for the polar angle (θ) and azimuthal angle (ϕ) distribution is given in Table 7 and Table 8 respectively. In the statistics of θ, a negative value of first order Fourier coefficient suggests that the spin vectors of galaxies tend to be oriented perpendicular with respect to the equatorial coordinate system. Similarly, a positive value of first order Fourier coefficient suggests that the spin vectors of galaxies tend to be oriented parallel with respect to the equatorial coordinate system. Whereas, in the statistics of ϕ, a positive

$\Delta_{11}/\sigma(\Delta_{11})$ with significant value suggests that the spin vector projections of galaxies tend to point radially towards the center of the equatorial coordinate system. Similarly, a significant negative value of $\Delta_{11}/\sigma(\Delta_{11})$ implies that the spin vector projection of galaxies tend to orient tangentially with respect to the equatorial coordinate system. In addition to the statistical tests, we also study the 'humps' (bins with more solutions than the expected) and 'dips' (bins with less solutions than the expected) in the polar and azimuthal angle distributions.

In the histogram of the θ-distribution (see Figure 12a as an example), solid curve represents the expected isotropic distribution whereas dashed curve is the cosine distribution. The solid circles with $\pm$ 1σ error bars represent the observed distribution. The shaded portion represents the range $0^\circ < \theta < 45^\circ$. A dip (or hump) at $\theta < 45^\circ$ suggests that the spin vectors of galaxies tend to orient perpendicular (or parallel) with respect to the equatorial coordinate system. Similarly, a hump (or dip) in the larger θ ($\theta > 45^\circ$) indicates that the spin vectors of galaxies tend to be oriented perpendicular with respect to the equatorial coordinate system.

In the histogram of the ϕ-distribution (see Figure 12b as an example), solid curve represents the expected isotropic distribution whereas dashed curve is the average distribution. The solid circles with $\pm$ 1σ error bars represent the observed distribution. The shaded portion represents the range $-45^\circ < \phi < +45^\circ$. The humps and dips in the histograms of ϕ-distribution are not so easy to interpret as compared to θ-distributions. It is because the range of ϕ is -90° to $+90^\circ$. In the histogram of the ϕ-distribution, $\phi = 0^\circ$ means spin vector projections tend to point radially towards the center of the equatorial coordinate system. A hump in the middle (central eight bins) of the histogram suggests that the spin vector projections of galaxies tend to point towards the center of the chosen co-ordinate system. Similarly, a hump at first four and last four bins indicates that the spin vectors projections of galaxies tend to be oriented tangentially with respect to the chosen reference co-ordinate system.

4.1.3 Sample z01 ($13.25 \leq m_z < 13.55$)

This sample contains a small number (51) of galaxies that have apparent magnitude in the range 13.25 to 13.55 when observed through z-filter. The smaller the value of magnitude

Table 7: Statistical values of the polar angle (θ) distribution of galaxies having redshift in the range 0.05 to 0.10. The first column represents the samples. In the table, $P(> \chi^2)$ (second column) and $C/C(\sigma)$ (third column) represent the chi-square probability and auto-correlation coefficient. The fourth and fifth columns give the first order Fourier coefficient $\Delta_{11}/\sigma(\Delta_{11})$ and first order Fourier probability $P(> \Delta_1)$. The last two columns shows the range of z-magnitude (Δm_z) for the corresponding samples and number (N) of galaxies in that sample.

sample	$P(> \chi^2)$	$C/C(\sigma)$	$\Delta_{11}/\sigma(\Delta_{11})$	$P(> \Delta_1)$	m_z	N
$z01$	0.458	-1.4	+0.5	0.849	13.25-13.55	51
$z02$	0.399	-0.3	-0.8	0.695	13.55-13.85	245
$z03$	0.071	+0.5	+0.6	0.365	13.85-14.15	761
$z04$	0.637	-1.1	-1.0	0.541	14.15-14.45	1878
$z05$	0.620	-1.6	-0.4	0.907	14.45-14.75	4136
$z06$	0.281	-1.8	+0.4	0.900	14.75-15.05	7406
$z07$	0.913	-1.1	+0.1	0.956	15.05-15.35	12238
$z08$	0.287	-1.0	-0.7	0.739	15.35-15.65	18268
$z09$	0.843	-0.4	-0.7	0.766	15.65-15.95	24341
$z10$	0.045	-1.2	-1.4	0.356	15.95-16.25	30541
$z11$	0.478	+0.2	-0.5	0.643	16.25-16.55	35463
$z12$	0.002	+5.6	-3.2	0.004	16.55-16.85	39548
$z13$	0.001	+4.8	-4.2	0.000	16.85-17.15	35635
$z14$	0.900	-0.4	+0.9	0.620	17.15-17.45	13967
$z15$	0.053	-2.5	-0.3	0.923	17.45-17.75	3089
$z16$	0.429	-1.2	+0.0	0.866	17.75-18.05	981
$z17$	0.954	+0.4	-0.2	0.941	18.05-18.35	534
$z18$	0.412	-1.3	+ 0.2	0.986	18.35-18.65	285
$z19$	0.347	+0.2	-0.4	0.658	18.65-18.95	110

Table 8: Statistics of the azimuthal angle (ϕ) distribution of galaxies having redshift in the range 0.05 to 0.10. The first column represents the sample. The next two columns give chi-square probability ($P(> \chi^2)$) and auto-correlation coefficient $C/C(\sigma)$. The last two columns give the first order Fourier coefficient $\Delta_{11}/\sigma(\Delta_{11})$ and first order Fourier probability $P(> \Delta_1)$.

sample	$P(> \chi^2)$	$C/C(\sigma)$	$Delta_{11}/\sigma(\Delta_{11})$	$P(> \Delta_1)$
$z01$	0.187	+0.0	+1.6	0.223
$z02$	0.619	-0.4	+0.5	0.756
$z03$	0.777	-0.3	+0.3	0.812
$z04$	0.327	+0.1	+1.5	0.173
$z05$	0.740	-0.7	-0.1	0.882
$z06$	0.729	-0.3	+1.5	0.319
$z07$	0.860	+0.2	+1.0	0.606
$z08$	0.137	+1.3	+2.5	0.027
$z09$	0.032	-0.1	+2.9	0.016
$z10$	0.549	-0.4	+1.6	0.233
$z11$	0.005	+ 2.9	+3.5	0.002
$z12$	0.099	+1.9	-2.7	0.001
$z13$	0.002	+5.8	-4.5	0.000
$z14$	0.006	+4.4	+2.2	0.009
$z15$	0.506	+0.2	+0.3	0.073
$z16$	0.255	-1.0	-1.1	0.518
$z17$	0.255	+0.2	+2.8	0.020
$z18$	0.752	-0.6	-0.7	0.684
$z19$	0.954	+ 0.0	-0.4	0.703

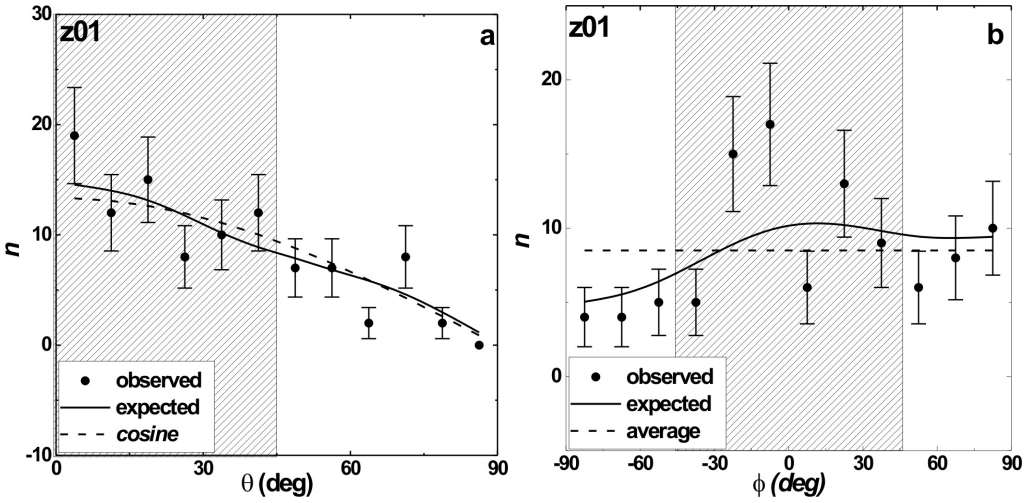

Figure 12: The polar (θ) and azimuthal angle (ϕ) distributions of galaxies that have z magnitude in the range 13.25 to 13.55. The solid line represents the expected isotropic distributions. The cosine and average distributions (dashed) are shown for the comparison. The solid circles with $\pm$ 1σ error bars represent the observed distribution. Here, σ represents $\sqrt{n}$ as suggested by Godlowski (1994).

brighter the object. Thus, these 51 galaxies are the brightest, sensitive towards the infrared. A significant infrared emission indicates the enhanced star formation activity and the relatively higher abundance of metal-rich elements in these galaxies. Thus, these are the brightest galaxies in the z-filter. Figure 12a shows the polar angle (θ) distribution of total galaxies of database in the sample $z01$. The statistics for the θ-distribution of galaxies of this sample is shown in the Table 7. The statistics for the polar angle distribution in this sample shows that the value of chi-square probability (P($>\chi^2$)) to be 0.458 i.e., 45.8% (greater than the significant level 0.050 i.e., 5.0%). The auto-correlation coefficient (C/C(σ)) is found to be -1.4 (greater than 1σ limit). The first order Fourier coefficient ($\Delta_{11}/\sigma(\Delta_{11})$) is found to be +0.5 (smaller than 1.5σ the limit). The first order Fourier probability (P $>(\Delta_1)$) is found to be 0.849 i.e., 84.9% (greater than 15% limit). Except auto-correlation coefficient, other statistical tests suggest isotropy. Anisotropy in the auto-correlation test suggests either binning effect or local anisotropy that should be seen in the humps/dips in the histogram. In Figure 12a the number of observed solutions that have $\theta < 45^\circ$ is found to be equal to the expected solutions i.e., 64. There is no any significant humps and dips in the lower angles($<45^\circ$) region. At bimodal region ($\theta \sim 45^\circ$), there are 2 more observed solutions than the expected in the

bimodal region. For the large angles (> 45°), the number of expected solutions is more by 2 than that of observed and there is a significant dip at 63.75° with > 2σ error limit in this region. Thus, we conclude no preferred alignment of spin vectors of galaxies that are brightest when observed through z-filter.

The statistics of the ϕ-distribution (Table 8) for the sample $z01$ are found as follows: P(>χ^2) = 0.187 i.e., 18.7% (greater than the 5.0% significant level), C/C(σ) = 0.0 (less than the limit 1σ), $\Delta_{11}/\sigma(\Delta_{11})$ = 1.6 (greater than the limit 1.5σ), P >(Δ_1) = 0.223 i.e., 22.3% (greater than 15% limit). The values of chi-square probability (P(> χ^2)), the auto-correlation coefficient C/C(σ) and the first order Fourier probability support strong isotropy. However first order Fourier coefficient suggests weak anisotropy.

In the azimuthal angle distribution as shown in Figure 12b, the observed solutions of central six bins (shaded region) are found to be 65, whereas the expected solutions are only 57. This shows that observed solutions exceeded the expected solutions by 8. In this region, one dip at an angle 7.5° is observed with ~1.5σ error limit and two humps are observed at −22.5° and −7.5° with ~ 1.5σ error limit. Since, there are no significant dips and humps outside the shaded part. Owing to the extremely poor statistics (i.e., the number of solutions per bin), we conclude no preferred alignments. The bright infrared galaxies that have redshift in the range 0.05 to 0.10 showed no preferred alignments in the spatial orientation of their spin vectors.

4.1.4 Sample $z02$ ($13.55 \leq m_z < 13.85$)

The polar angle (θ) distribution of galaxies in the sample $z02$ is shown in the Figure 13a. The number of observed solutions for $\theta < 45°$ is 305, which is less than the number of expected solutions by 4. There are no any significant humps and dips in this region. At bimodal region ($\theta \sim 45°$), the number of expected solutions are more by 11 than that of observed. For the large angles (> 45°), the number of observed solutions are more by 15 than that of expected and there is a hump at an angle 56.25° with ~1.5σ error limit. A preferred alignment is noticed in the θ-distribution of this sample. The spin vectors of galaxies tend to lie perpendicular with respect to the equatorial coordinate system. It is found that the second group of brightest galaxies support primordial vorticity theory.

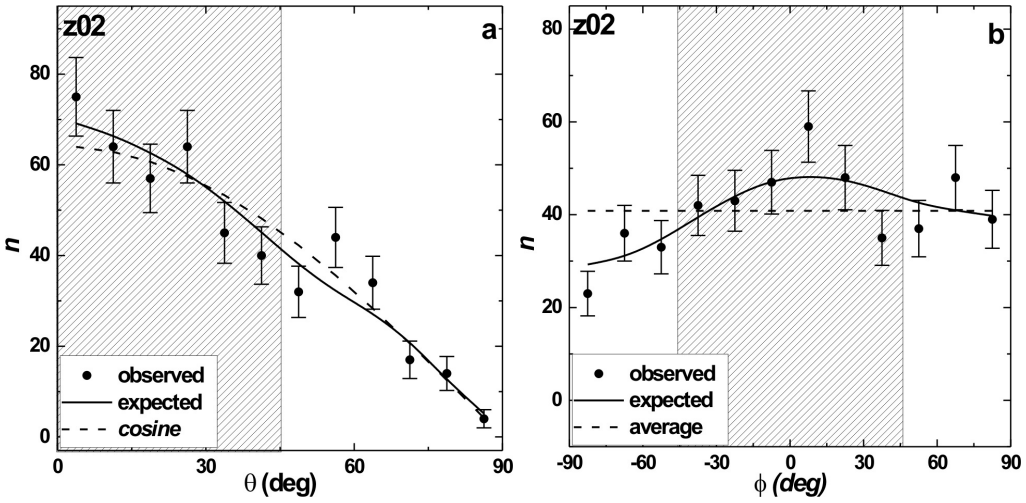

Figure 13: The polar (θ) and azimuthal angle (ϕ) distributions of galaxies that have z magnitude in the range 13.55 to 13.85. The solid line represents the expected isotropic distributions. The cosine and average distributions (dashed) are shown for the comparison. The solid circles with $\pm$ 1σ error bars represent the observed distribution. Here, σ = $\sqrt{n}$ as suggested by Godlowski (1994).

The statistics for the θ-distribution of galaxies of this sample are found as follows: P($>\chi^2$)= 0.399 i.e., 39.9% (greater than the 5.0% significant level), C/C(σ)= $-$0.3 (smaller than 1σ limit), $\Delta_{11}/\sigma(\Delta_{11})$= $-$0.8 (smaller than the limit 1.5σ) and P $>(\Delta_1)$= 0.695 greater than 15% limit. All these statistics suggest strong isotropy. The statistical results do not support primordial vorticity theory. This means that the local effect (i.e., gravitational tidal torque effect or shearing effect) should be studied in the future.

In the azimuthal angle (ϕ) distribution as shown in Figure 13b, the observed solutions of central six bins (shaded region) are found to be 274, whereas the expected solutions are only 272. This shows that observed solutions exceeded the expected solutions by 2. There is a dip at an angle 37.5° with $\sim$1.5σ error limit in this region. No any significant humps and dips are there outside the shaded part. Thus, no preferred alignment is noticed in this sample.

The statistics for the ϕ-distribution of galaxies of this sample are found as follows: P($>\chi^2$) = 0.619 i.e., 61.9% (greater than the 5.0% significant level), C/C(σ)= $-$0.4 (smaller than 1σ limit), $\Delta_{11}/\sigma(\Delta_{11})$= 0.5 (smaller than the limit 1.5σ) and P $>(\Delta_1)$= 0.756 i.e. 75.6% (greater than 15% limit). All these statistics suggest strong isotropy. Similar to the polar angle distribution we do not notice global effect here. This the

indication of primordial vorticity model is ruled out. The galaxies that have radial velocity in the range 0.05 to 0.10 and z-magnitude in the range 13.55 to 13.85 support hierarchy model, suggesting no preferred alignments of spin vectors of galaxies.

4.1.5 Sample $z03$ ($13.85 \leq m_z < 14.15$)

The statistics for the polar angle distribution in the sample $z03$ shows the value of chi-square probability, the auto-correlation coefficient (C/C(σ)), the first order Fourier coefficient, the first order Fourier probability are within the limit of isotropy (Table 7). Hence, all three statistics suggest strong isotropy. As shown in Figure 14a, in the sample

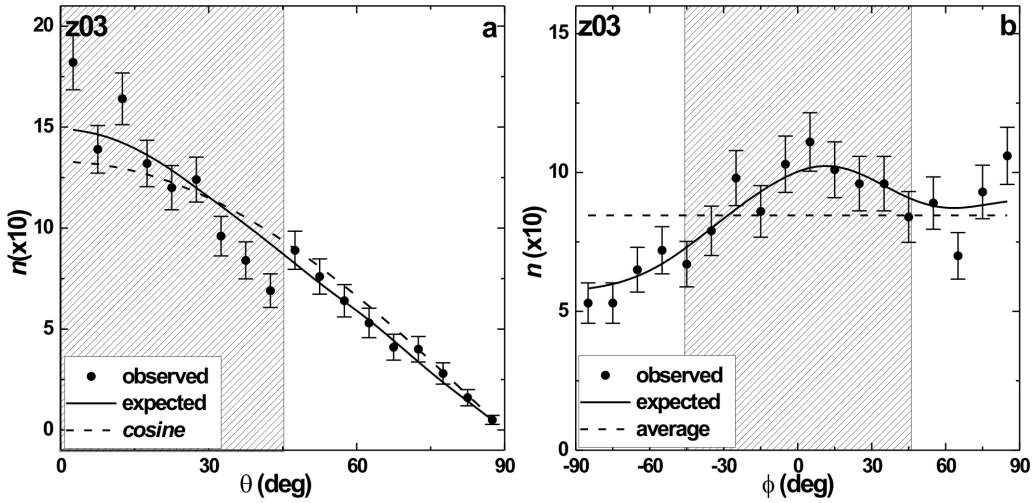

Figure 14: The polar (θ) and azimuthal angle (ϕ) distributions of galaxies that have z magnitude in the range 13.85 to 14.15. The solid line represents the expected isotropic distributions. The cosine and average distributions (dashed) are shown for the comparison. The solid circles with ± 1σ error bars represent the observed distribution. Here, σ = $\sqrt{n}$ as suggested by Godlowski (1994).

$z03$, the number of solutions for smaller angles ($\theta < 45°$) is found to be 1 041, whereas the expected solutions is also 1,036. Thus, number of observed solutions are more by 5 than that of the expected. There is one significant hump at an angle 2.5° with > 2σ error limit. There are two dips at angles 32.5° with ~ 2σ error limit and at 37.5° with ~ 1.5σ error limit. At bimodal region ($\theta \sim 45°$), there are 17 more expected solutions than the observed. For the large angles (> 45°), the number of observed solutions exceed the expected by 12 but there are no any significant humps and dips in this region. So, no

preferred alignment is noticed in the θ-distribution. All statistics of the ϕ-distribution (Table 8) for the sample $z03$ are found as follows suggest isotropy. That means no any preferred alignment is seen.

In the azimuthal angle distribution (Figure 14b), the observed number of central eight bins (shaded region) is found to be 770, whereas the expected value is only about 759. This shows that expected number lagged the observed number by 11. Though there is no any significant hump and dip in this region. One hump is observed at an angle 85° within $\sim 1.5\sigma$ error limit and one dip is seen at an angle 65° with $\sim 2\sigma$ error limit at outer region of shaded part. Thus, no preferred alignment is noticed in the ϕ-distribution of this sample.

Thus, a random orientation of spin vector and spin vector projection of galaxies is found in this sample.

4.1.6 Sample z04 (14.15 $\leq m_z <$ 14.45)

Figure 15a shows the polar angle (θ) distribution of galaxies of database in the sample $z04$. The statistics for the θ distribution of galaxies of this sample is shown in Table 7. All four statistical parameters advocate strong isotropy. In Figure 15a, the number of observed solutions for $\theta < 45°$ is is less than the number of expected solutions by 28. There are no any significant humps and dips in this region. At bimodal region ($\theta \sim 45°$), the number of observed solutions are more by 15 than that of expected. No any significant humps and dips are observed in this region. For the large angles ($> 45°$), the number of observed solutions are more by 15 than that of expected and also no any significant humps and dips are observed in this region. Thus, no any preferred alignment is noticed in the θ-distribution of this sample.

All the statistics of the ϕ-distribution (Table 8) for the sample $z04$ suggest isotropy in the azimuthal angle distribution of galaxies that have Z-magnitude in the range 14.15 to 14.45.

In the azimuthal angle distribution (Figure 15b), the observed number of solutions of central eight bins (shaded region) exceeds the expected solutions by 31. In this region, two humps at angles $-25°$ and 5° are observed $\sim 1.5\sigma$ error limit. Also, two dips are

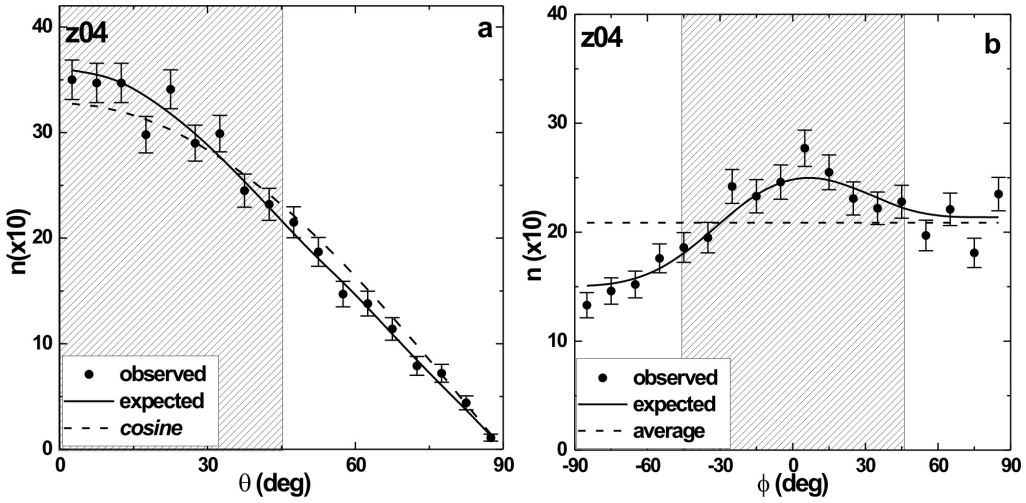

Figure 15: The polar (θ) and azimuthal angle (ϕ) distributions of galaxies that have z-magnitude in the range 14.15 to 14.45. The solid line represents the expected isotropic distributions. The cosine and average distributions (dashed) are shown for the comparison. The solid circles with $\pm$ 1σ error bars represent the observed distribution. Here, σ = $\sqrt{n}$ as suggested by Godlowski (1994).

observed at -85° with $\sim 1.5\sigma$ error limit and at 75° with $> 2\sigma$ error limit outside the shaded part. We conclude a random orientation of spin vector and spin vector projection of galaxies in this sample, supporting hierarchy model of galaxy formation as suggested by Peebles (1969).

4.1.7 Sample z05 (14.45 $\leq m_z <$ 14.75)

The statistics for the polar angle distribution in the sample z05 shows the value of chi-square probability (P($>\chi^2$)) to be 0.620 (greater than the 5.0% significant level). The auto-correlation coefficient (C/C(σ)) is found to be -1.6 (larger than 1σ). The first order Fourier coefficient ($\Delta_{11}/\sigma(\Delta_{11})$) is found to be -0.4 (smaller than 1.5σ). The first order Fourier probability (P $>(\Delta_1)$) greater than 15% limit). All these statistics except auto-correlation test suggest isotropy. Anisotropy in the auto-correlation test is because of the binning effect as well as local effect. As shown in Figure 16a, in the sample z05, the number of solutions that have $\theta < 45^\circ$ is found to be 5 679 which agrees with the expected solutions. There is no any significant hump and dip in this region. At bimodal region ($\theta \sim 45^\circ$), there are 11 more expected solutions than the observed. For the large

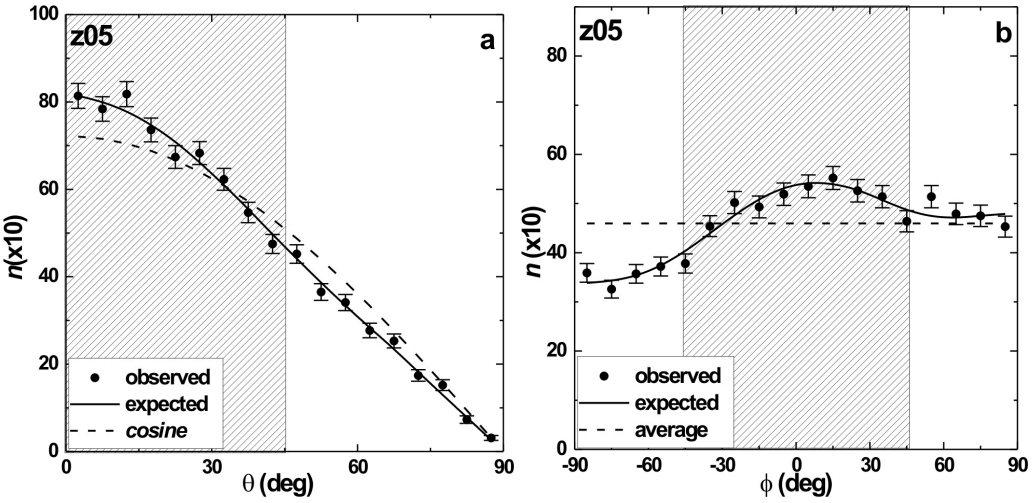

Figure 16: The polar (θ) and azimuthal angle (ϕ) distributions of galaxies that have z magnitude in the range 14.45 to 14.75. The solid line represents the expected isotropic distributions. The cosine and average distributions (dashed) are shown for the comparison. The solid circles with $\pm$ 1σ error bars represent the observed distribution. Here, σ = $\sqrt{n}$ as suggested by Godlowski (1994).

angles (> 45°), the number of observed solutions exceed the expected by 11 and there is one hump at an angle 77.5° with $\sim 2\sigma$ error limit. Hence, the spatial orientation of spin vectors of galaxies that have z-magnitude in the range $14.45 \leq m_z < 14.75$ seems to show a local effect, supporting primordial vorticity theory. This theory predicts that the spatial orientation of spin vectors of galaxies tend to be oriented perpendicular with respect to equatorial plane.

The statistics of the ϕ-distribution (Table 8) for the sample z05 are found as follows: P($>\chi^2$) = 0.740 i.e., 74.0% (smaller than the significant level 0.050 i.e., 5%), C/C(σ) = -0.7 (smaller than the limit 1σ), $\Delta_{11}/\sigma(\Delta_{11}) = -0.1$ (less than the limit 1.5σ), P >(Δ_1) = 0.882 i.e., 88.2% (greater than 15% limit). Hence, all the statistics advocate isotropy.

In the azimuthal angle distribution as shown in Figure 16b, the observed solutions of central eight bins (shaded region) are found that expected number lagged the observed number by 16. There are no any significant humps and dips in this region. One hump is observed at an angle 55° with $\sim 2\sigma$ error limit outside the shaded region. A preferred trend is noticed. The spin vector projections of galaxies tend to be oriented tangentially towards the center of the equatorial co-ordinate system.

In this sample, a weak local effect supporting primordial vorticity model is noticed. However, the general trend supports hierarchy model.

4.1.8 Sample z06 (14.75 $\leq m_z <$ 15.05)

Figure 17a shows the polar angle (θ) distribution of galaxies in the sample z06 . The number of observed solutions for $\theta < 45°$ is more than the number of expected solutions by 25. There is one hump at an angle 22.5° with $\sim 1.5\sigma$ error limit. At bimodal region ($\theta \sim 45°$), the number of expected solutions are more by 7 than that of observed. There is a dip at an angle 47.5 with $\sim 1.5\sigma$ error limit. For the large angles ($> 45°$), the number of expected solutions are more by 18 than that of observed and also there is no any significant hump and dip in this region. All the statistics for the θ-distribution

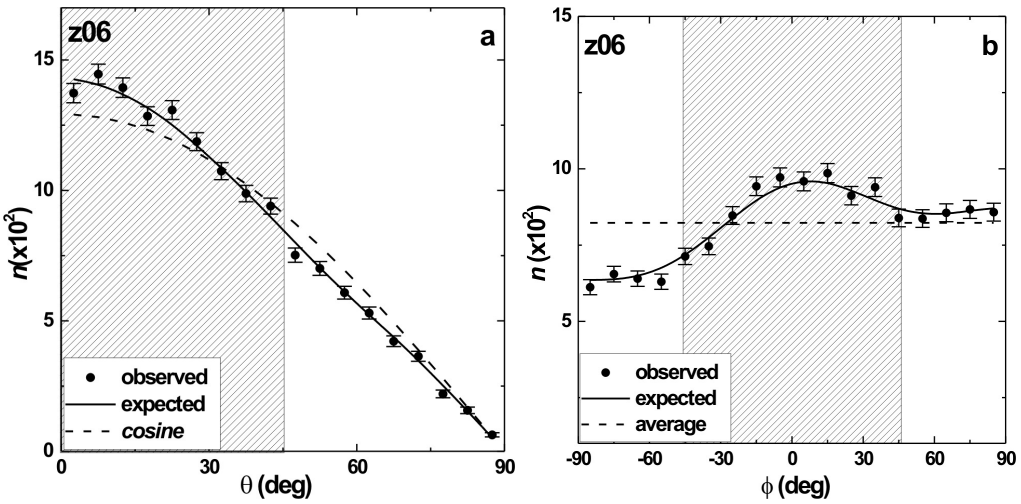

Figure 17: The polar (θ) and azimuthal angle (ϕ) distributions of galaxies that have z magnitude in the range 14.75 to 15.05. The solid line represents the expected isotropic distributions. The cosine and average distributions (dashed) are shown for the comparison. The solid circles with $\pm$ 1σ error bars represent the observed distribution. Here, $\sigma = \sqrt{n}$ as suggested by Godlowski (1994).

of galaxies of this sample (Table 7) suggest strong isotropy except auto-correlation test. Anisotropy in the auto-correlation test is because of the binning effect.

In the azimuthal angle distribution as shown in Figure 17b, the observed solutions of central eight bins (shaded region) exceed the expected solutions by 105. The number of solutions are very large and hence there is no any significance effect of the difference.

There is no any significant hump and dip in this region. No preferred alignment is noticed in this sample. All statistics for the ϕ-distribution of galaxies of this sample suggest isotropy. That means spin vectors of the galaxies are randomly oriented. As a whole no preference of alignment of spin vector and spin vector projections of galaxies can be concluded.

4.1.9 Sample $z07$ ($15.05 \leq m_z < 15.35$)

All statistics for the polar angle distribution in the sample $z07$ (Table 7) indicate isotropy of the θ distribution. A very good agreement between the expected and observed

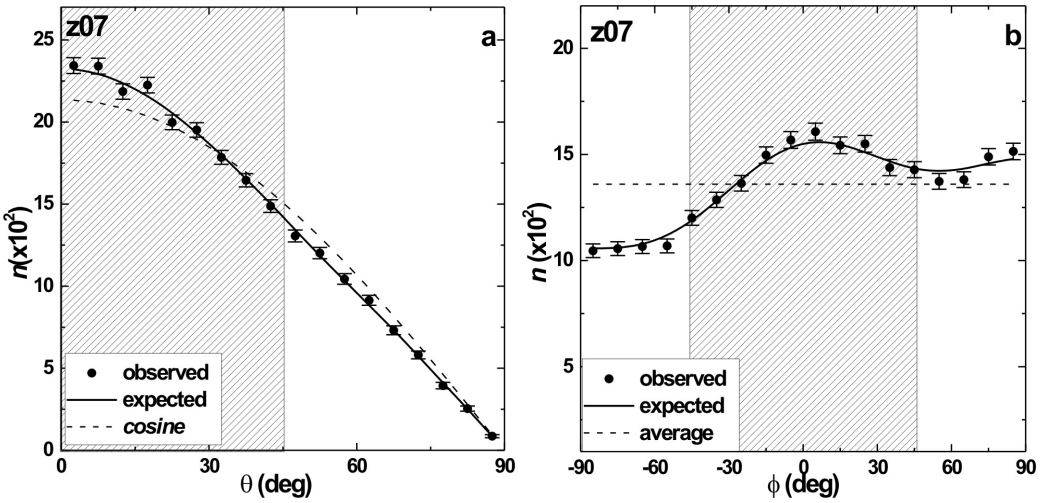

Figure 18: The polar (θ) and azimuthal angle (ϕ) distributions of galaxies that have z magnitude in the range 15.05 to 15.35. The solid line represents the expected isotropic distributions. The cosine and average distributions (dashed) are shown for the comparison. The solid circles with $\pm$ 1σ error bars represent the observed distribution. Here, σ = $\sqrt{n}$ as suggested by Godlowski (1994).

distribution is noticed. As shown in Figure 18a, in the sample $z07$, the number of observed solutions that have $\theta < 45^\circ$ are more by 5 than that of the expected. There is no any significant hump and dip in this region. At bimodal region ($\theta \sim 45^\circ$), there are 52 more expected solutions than the observed. For the large angles (> 45 °), the number of observed solutions exceed the expected by 47 and there is no any significant hump and dip in this region.There are very large number of solutions and hence there is no any significant meaning of such small differences. A random orientation of spin vectors of

galaxies is noticed.

All statistics of the ϕ-distribution (Table 8) for the sample $z07$ suggest isotropy. In the azimuthal angle distribution as shown in Figure 18b, the observed number of central eight bins (shaded region) is found to be 11 853, whereas the expected value is only about 11 768. This shows that expected number lagged the observed number by 85. There is no any significant hump and dip in this region. Also, no any significant humps and dips are noticed at outer region of shaded part. Thus, no preferred alignment is noticed in the ϕ-distribution of this sample.

We conclude a random orientation of spin vector and spin vector projection of galaxies in this sample,supports Hirrachy model as suggested by Peebles (1969).

4.1.10 Sample $z08$ ($15.35 \leq m_z < 15.65$)

The polar angle (θ) distribution of galaxies in the sample $z08$ is shown in the Figure 19a. The number of observed solutions for $\theta < 45^\circ$ are less than the number of expected solutions by 78. There is a significant hump at an angle 27.5 with $\sim 2\sigma$ error limit in this region. At bimodal region ($\theta \sim 45^\circ$), the number of expected solutions are less by 45 than that of observed. There is a hump at an angle 42.5 with $\sim 1.5\sigma$ error limit. For the large angles (>45°), the number of observed solutions are more by 33 than that of expected and also there is a dip at an angle 52.5° with $\sim 2\sigma$ error limit. No any preferred alignment is noticed in the θ-distribution of this sample. The statistics for the θ-distribution of galaxies of sample z08 suggest isotropy in the polar angle distribution.

In the azimuthal angle distribution as shown in Figure 19b, the observed solutions of central eight bins (shaded region) exceeds the expected solutions by 263. There are two significant humps at -25° with $\sim 2\sigma$ error limit and at -5° with $> 2\sigma$ error limit. Also, there are two significant dips at -65° and 65° with $> 2\sigma$ error limit outside the shaded part. Thus, no preferred alignment is noticed in this sample.

The statistics for the ϕ-distribution of galaxies of this sample are found as: P($>\chi^2$) = 0.137 (greater than the 5.0% significant level), C/C(σ) = 1.3 (greater than 1σ limit), $\Delta_{11}/\sigma(\Delta_{11})$ = 2.5 (greater than the limit 1.5σ) and P $>(\Delta_1)$ = 0.027 (smaller than 15% limit). The value of chi-square probability (P($> \chi^2$)) support isotropy while the auto-

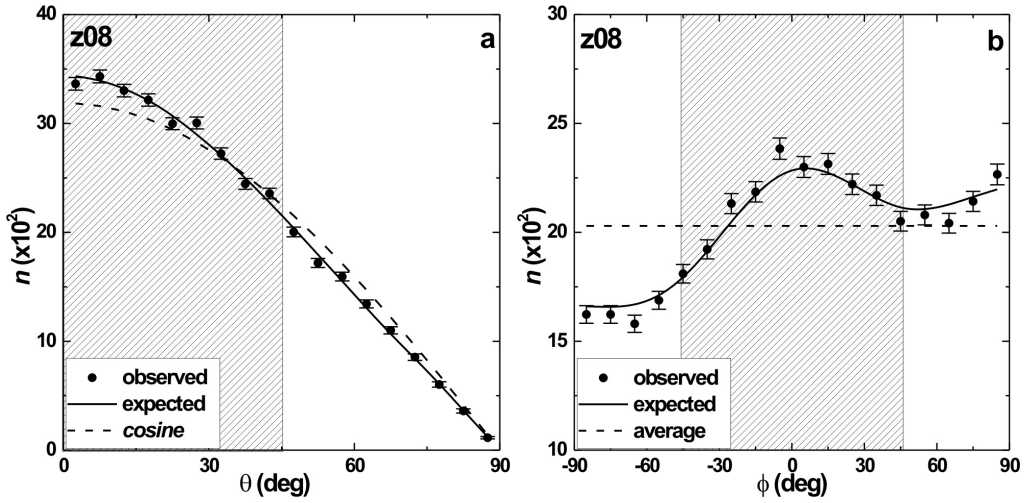

Figure 19: The polar (θ) and azimuthal angle (ϕ) distributions of galaxies that have z magnitude in the range 15.35 to 15.65. The solid line represents the expected isotropic distributions. The cosine and average distributions (dashed) are shown for the comparison. The solid circles with $\pm$ 1σ error bars represent the observed distribution. Here, σ = $\sqrt{n}$ as suggested by Godlowski (1994).

correlation coefficient C/C(σ), the first order Fourier coefficient ($\Delta_{11}/\sigma(\Delta_{11})$) and the Fourier probability (P($> \Delta_1$)) support anisotropy.

In this sample, polar angle distribution suggests isotropy whereas azimuthal angle distribution showed anisotropy. It indicates that the reference system is not appropriate for this sample. A physical reference co- ordinate system should be defined for this sample in the future. A need of physical reference system indicates formation of cluster and supercluster in the sample. However, isotropy in the spin vector distribution suggests hierarchy model.

4.1.11 Sample z09 (15.65 $\leq m_z <$ 15.95)

Figure 20a shows the polar angle (θ) distribution of total galaxies of database in the sample z09. The statistics for the θ-distribution of galaxies of this sample is shown in the Table 7. The statistics for the polar angle distribution in this sample shows strong isotropy, suggesting random orientation of spin vector of the galaxies in the sample. In Figure 20a, the number of observed solutions for $\theta < 45^\circ$ is less than the number of expected solutions by 140. There is one significant dip at an angle 27.5° within ~1.5σ

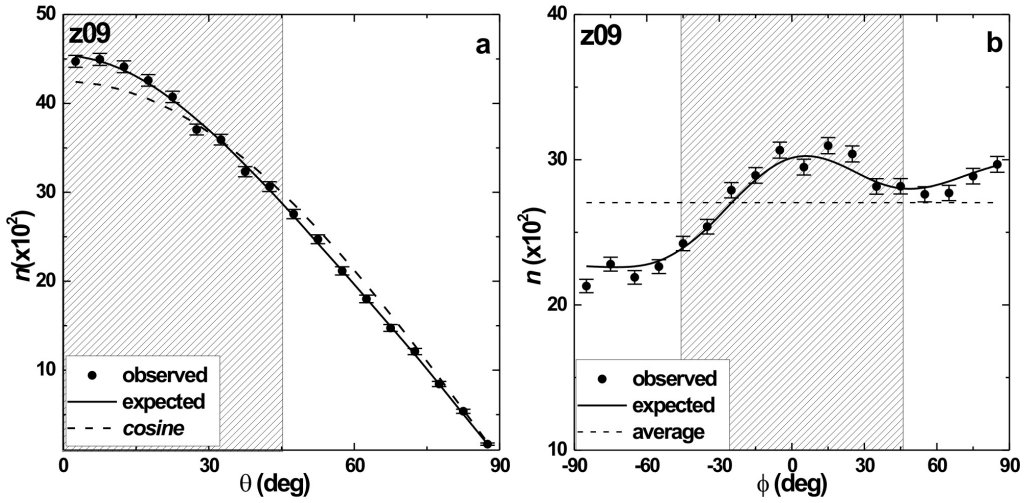

Figure 20: The polar (θ) and azimuthal angle (ϕ) distributions of galaxies that have z magnitude in the range 15.65 to 15.95. The solid line represents the expected isotropic distributions. The cosine and average distributions (dashed) are shown for the comparison. The solid circles with $\pm$ 1σ error bars represent the observed distribution. Here, σ = $\sqrt{n}$ as suggested by Godlowski (1994).

error limit in this region. At bimodal region ($\theta \sim 45°$), the number of observed solutions are more by 54 than that of expected. No any significant humps and dips are observed in this region. For the large angles ($> 45°$), the number of observed solutions are more by 86 than that of expected and also no any significant humps and dips are observed in this region. Thus, no any preferred alignment is noticed in the θ-distribution of this sample.

The statistics of the ϕ-distribution (Table 8) for the sample $z09$ are found as: P($>\chi^2$) = 0.032 (smaller than the 5.0% significant level), C/C(σ) =$-$0.1 (less than the limit 1σ), $\Delta_{11}/\sigma(\Delta_{11})$ = 2.9 (greater than the limit 1.5σ), P >(Δ_1) = 0.016 i.e., 1.6% (smaller than 15% limit). The values of chi-square probability (P($> \chi^2$)), the first order Fourier coefficient ($\Delta_{11}/\sigma(\Delta_{11})$) and the Fourier probability (P($> \Delta_1$)) support anisotropy. Where as auto correlation test suggest isotropy, we think this is due to binning effect.

In the azimuthal angle distribution as shown in Figure 20b, the observed solutions of central eight bins (shaded region) exceeds the expected solutions by 290. In this region, one humps at angles 15° are observed with $\sim$ 1.5σ error limit. Also, two dips are observed at $-$85° with $>$2σ error limit and at $-$65° with $\sim$ 1.5σ error limit outside the shaded part.

Similar to the z08, this sample showed a random orientation of spin vectors of galaxies, however, a suitable physical reference system for this sample should be discussed in detail in the future. A need of suitable reference system indicate either structure formation process (cluster or supercluster formation) or collision (cluster - cluster collision, Aryal et al., 2013 and Godloski et al., 2014.)

4.1.12 Sample $z10$ ($15.95 \leq m_z < 16.25$)

The polar angle (θ) distribution of galaxies in the sample $z10$ is shown in the Figure 21a. The number of observed solutions for $\theta < 45°$ is 39 879, which is less than the number of expected solutions by 349. There is a significant dip at 37.5° with $>2\sigma$ error limit in this region. At bimodal region ($\theta \sim 45°$), the number of expected solutions are less by 172 than that of observed. There is a hump at an angle 42.5° with 2σ error limit. For the large angles ($> 45°$), the number of observed solutions are more by 177 than that of expected and no any significant humps and dips are observed in this region. So, no any preferred alignment is noticed in the θ-distribution of this sample.

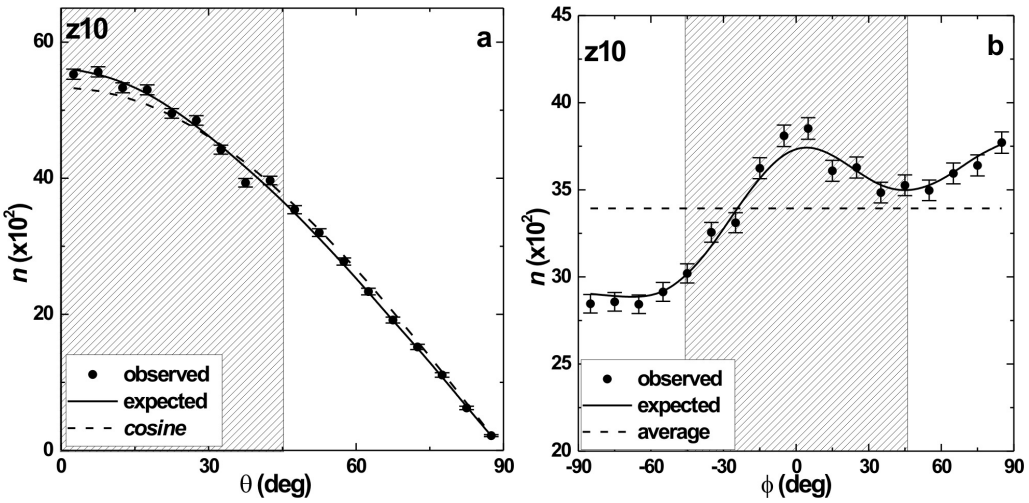

Figure 21: The polar (θ) and azimuthal angle (ϕ) distributions of galaxies that have z magnitude in the range 15.95 to 16.25. The solid line represents the expected isotropic distributions. The cosine and average distributions (dashed) are shown for the comparison. The solid circles with ± 1σ error bars represent the observed distribution. Here, $\sigma = \sqrt{n}$ as suggested by Godlowski (1994).

The statistics for the θ-distribution of galaxies of this sample are given in Table 7. The

value of chi-square probability (P($> \chi^2$)) support anisotropy while the auto-correlation coefficient C/C(σ), the first order Fourier coefficient ($\Delta_{11}/\sigma(\Delta_{11})$) and the Fourier probability (P($> \Delta_1$)) support isotropy.

In the azimuthal angle distribution as shown in Figure 21b, the observed solutions of central eight bins (shaded region) exceed the expected solutions by 145. There are three humps at angles $-35°$, $-5°$ and $5°$ with $\sim 1.5\sigma$ error limit in this region. No any dips and humps are observed outside the shaded part. Thus, a preferred alignment is noticed in this sample. Thus, we found that the spin vector projections of galaxies in this sample tend to be directed towards the equatorial center.

The statistics for the ϕ-distribution (Table 8) of galaxies of this sample are found as: P($>\chi^2$)= 0.549 (greater than the 5.0% significant level), C/C(σ)= -0.4 (smaller than 1σ limit), $\Delta_{11}/\sigma(\Delta_{11})$= 1.6 (greater than the limit 1.5σ) and P $>(\Delta_1)$= 0.233 (greater than 15% limit). The values of Chi-square probability (P($> \chi^2$)), the autocorrelation coefficient C/C(σ) and the Fourier probability (P($> \Delta_1$)) support isotropy.

We conclude local anisotropy in this sample. The spin vectors of galaxies tend to orient randomly in the equatorial plane whereas spin vector projections of galaxies tend to point towards the equatorial centre.

4.1.13 Sample z11 (16.25 $\leq m_z <$ 16.55)

All four statistics suggest strong isotropy in the θ distribution of galaxies having redshifts 0.05 to 0.10 and z-magnitudes 16.25 to 16.55. There are 35 463 galaxies in the sample. A huge database obviously suggests a possibility of super cluster, cluster and super cluster formation.

As shown in Figure 22a, in the sample z11, the number of observed solutions that have $\theta < 45°$ is less by 105 than that of the expected. There are no any significant humps and dips in this region. At bimodal region ($\theta \sim 45°$), there are 157 more observed solutions than the expected. For the large angles ($> 45°$), the number of expected solutions exceed the observed by 52 and also there are no any significant humps and dips. So, no preferred alignment is noticed in the θ-distribution.

The statistics of the ϕ-distribution (Table 8) for the sample z11 support strong anisotropy.

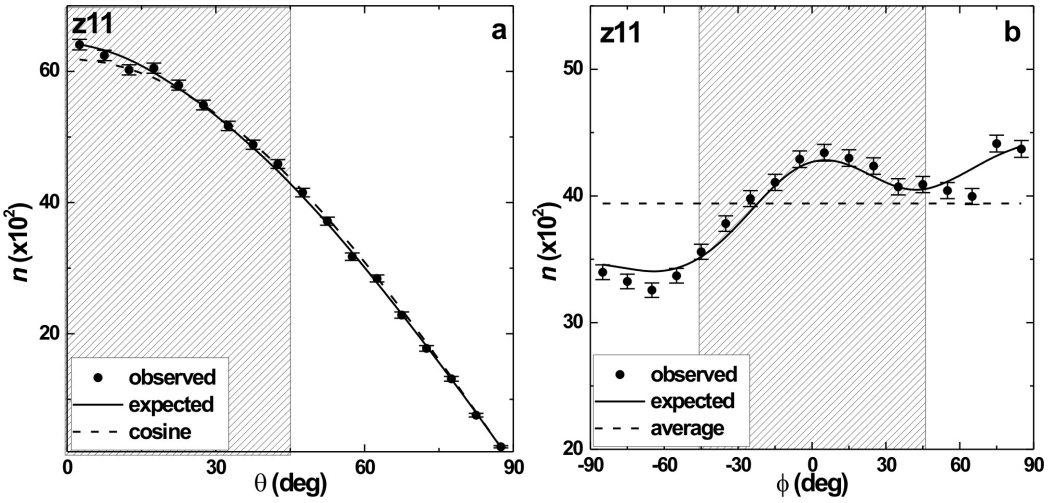

Figure 22: The polar (θ) and azimuthal angle (ϕ) distributions of galaxies that have z magnitude in the range 16.25 to 16.55. The solid line represents the expected isotropic distributions. The cosine and average distributions (dashed) are shown for the comparison. The solid circles with $\pm$ 1σ error bars represent the observed distribution. Here, σ = $\sqrt{n}$ as suggested by Godlowski (1994).

In the azimuthal angle distribution as shown in Figure 22b, the observed number of central eight bins (shaded region) is more than that of expected by 463. Two humps are observed at angles -35° and -25° with $\sim 1.5\sigma$ error limit. Three significant dips are observed at angles -75° with $\sim 1.5\sigma$ error limit and at -65° and 65° with $> 2\sigma$ error limit at outer region of shaded part. leads this sample to show anisotropy. These humps and dips So, no preferred alignment is noticed in the ϕ-distribution of this sample.

Therefore, we conclude random orientation of spin vector of galaxies whereas their projections showed a strong preference, suggesting a need of new reference coordinate system, because of on going large scale structure formation.

4.1.14 Sample z12 (16.55 $\leq m_z <$ 16.85)

Figure 23a shows the polar angle (θ) distribution of total galaxies of database in the sample z12. The statistics for the θ-distribution of galaxies of this sample is shown in the Table 7. The statistics for the polar angle distribution in this sample shows the value of chi-square probability (P($>\chi^2$)) to be 0.002(smaller than 5.0% significant level). The auto-correlation coefficient (C/C(σ)) is found to be 5.6 (greater than 1σ limit). The first

order Fourier coefficient ($\Delta_{11}/\sigma(\Delta_{11})$) is found to be -3.2 (greater than the limit 1.5σ). The first order Fourier probability (P $>(\Delta_1)$) is found to be 0.004, (smaller than 15% limit). Thus, all statistical tests strongly advocate anisotropy.

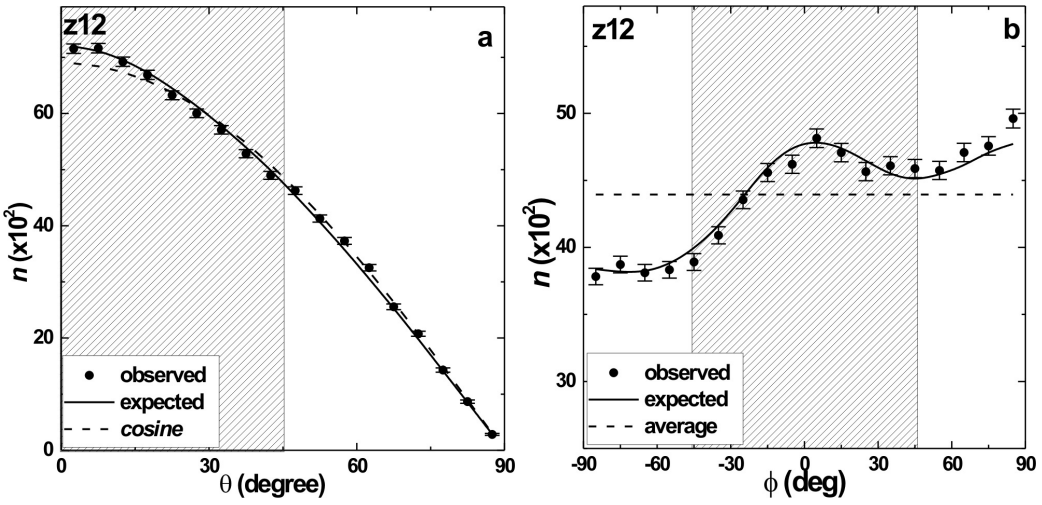

Figure 23: The polar (θ) and azimuthal angle (ϕ) distributions of galaxies that have z magnitude in the range 16.55 to 16.85. The solid line represents the expected isotropic distributions. The cosine and average distributions (dashed) are shown for the comparison. The solid circles with $\pm$ 1σ error bars represent the observed distribution. Here, σ = $\sqrt{n}$ as suggested by Godlowski (1994).

In Figure 23a, the number of observed solutions for $\theta < 45°$ is 51 249, which is less than the number of expected solutions by 539. Hence, a large number of galaxies are moved from shaded to unshaded part, supporting either hierarchy or primordial vorticity model. There are three dips at angles 22.5°, 27.5° and 37.5° with $\sim 1.5\sigma$ error limit in this region. At bimodal region ($\theta \sim 45°$), the number of observed solutions are less by 11 than that of expected. No any significant humps and dips are observed in this region. For the large angles ($> 45°$), the number of observed solutions are more by 550 than that of expected and there are three significant humps at angles 57.5°, 62.5° and 72.5° with $> 2\sigma$ error limit. Hence, the spatial orientation of spin vectors of galaxies that have z-magnitude in the range $16.55 \leq m_z < 16.85$ supports primordial vorticity theory. This theory predicts that the spatial orientation of spin vectors of galaxies tend to be oriented perpendicular with respect to equatorial plane. Thus formation of protocluster before the galaxy formation can not be ruled out (Shanderin,1974). The auto-correlation coefficient C/C(σ), the first order Fourier coefficient $\Delta_{11}/\sigma(\Delta_{11})$ and the first order

Fourier probability (P($> \Delta_1$)) support anisotropy.

In the ϕ distribution as shown in Figure 23b, the observed solutions of central eight bins (shaded region) are found to be 36 318, whereas the expected solutions are only 36 628. This shows that observed solutions lagged the expected solutions by 310. In this region, one dip at an angle $-5°$ is observed with $> 2\sigma$ error limit. Also, one significant hump is observed at 85° with $\sim 2\sigma$ error limit outside the shaded part. Thus, a preferred alignment is noticed in this sample. We found that the spin vector projections of galaxies in this sample tend to be directed towards the equatorial center.

We conclude strong anisotropy in this sample. The spin vectors of galaxies tend to be oriented perpendicular with respect to equatorial plane whereas spin vector projection of galaxies tend to point towards the equatorial centre. Thus, the infrared activity is found to be non-random indicating either star forming activity in these large number of galaxies or metalicity might be higher than the expected.

4.1.15 Sample z13 (16.85 $\leq m_z <$ 17.15)

All four statistical parameters suggest strong anisotropy. The result is similar to the sample z12 (Table 7) lists the values of statistical parameters.

As shown in Figure 24a, in the sample z13, the number of observed solutions that have $\theta < 45°$ are found to be 46 077 which is less than the number of expected solutions by 587. There are two dips at angles 2.5° with $\sim 1.5\sigma$ error limit and at 17.5° with $\sim 2\sigma$ error limit. At bimodal region ($\theta \sim 45°$), there are 144 more observed solutions than the expected. For the large angles ($> 45°$), the number of observed solutions exceed the expected by 443 and there are three humps at angles 62.5°, 67.5° and 72.5° with $> 2\sigma$ error limit. Hence, the spatial orientation of spin vectors of galaxies that have z-magnitude in the range $16.85 \leq m_z < 17.15$ supports primordial vorticity theory. This theory predicts that the spatial orientation of spin vectors of galaxies tend to be oriented perpendicular with respect to equatorial plane.

The statistics of the ϕ-distribution (Table 8) for the sample z13 are found as follows: P($>\chi^2$) = 0.002 (smaller than the 5% significant level), C/C(σ) = 5.8 (greater than the limit 1σ), $\Delta_{11}/\sigma(\Delta_{11}) = -4.5$ (larger than the limit 1.5σ), P $>(\Delta_1) = 0.000$ (smaller than

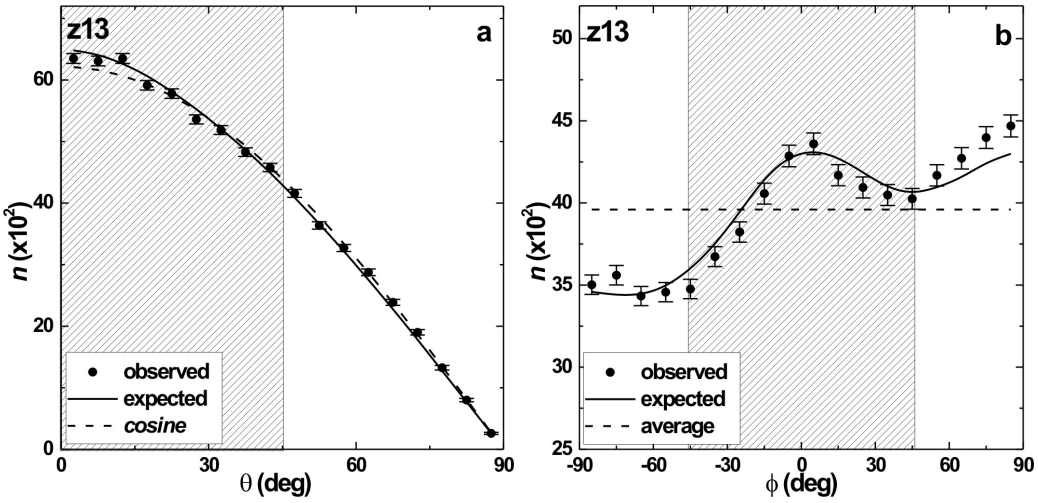

Figure 24: The polar (θ) and azimuthal angle (ϕ) distributions of galaxies that have z magnitude in the range 16.85 to 17.15. The solid line represents the expected isotropic distributions. The cosine and average distributions (dashed) are shown for the comparison. The solid circles with ± 1σ error bars represent the observed distribution. Here, σ = $\sqrt{n}$ as suggested by Godlowski (1994).

15% limit). Similar to the polar angle distribution, strong anisotropy is found in the azimuthal angle distribution.

In the azimuthal angle distribution as shown in Figure 24b, the observed solutions of central eight bins (shaded region) exceeds the observed solutions by 494. There are three dips at angles $-15°$ and $15°$ with $\sim 1.5\sigma$ error limit and at $-25°$ with $\sim 2\sigma$ error limit. There is one dip at an angle $-45°$ with $\sim 2\sigma$ error limit and four humps at angles $-75°$, $75°$ and $85°$ with $\sim 2\sigma$ error limit and at $65°$ with $\sim 1.5\sigma$ error limit outside the shaded region. Thus, the spin vector projections of galaxies tend to be oriented tangentially towards the center of the equatorial co-ordinate system.

Strong anisotropy is noticed in this sample. Thus, we conclude strong anisotropy in the polar as well as azimuthal angle distribution with spin vector and spin vector projection of galaxies supporting primordial vorticity theory. Thus the galaxies with a low luminosity (higher value of magnitude) showed a large scale structure formation without maintaining adiabatic equilibrium (Shandarin, 1974).

4.1.16 Sample $z14$ ($17.15 \leq m_z < 17.45$)

The polar angle (θ) distribution of galaxies in the sample $z14$ is shown in the Figure 25a. The number of observed solutions for $\theta < 45°$ is 18 081, which is more than the number of expected solutions by 84. There is one hump at an angle 7.5° with $\sim 1.5\sigma$ error limit. At bimodal region ($\theta \sim 45°$), the number of expected solutions are more by 14 than that of observed. For the large angles ($> 45°$), the number of expected solutions are more by 70 than that of observed and also there are no any significant humps and dips in this region.

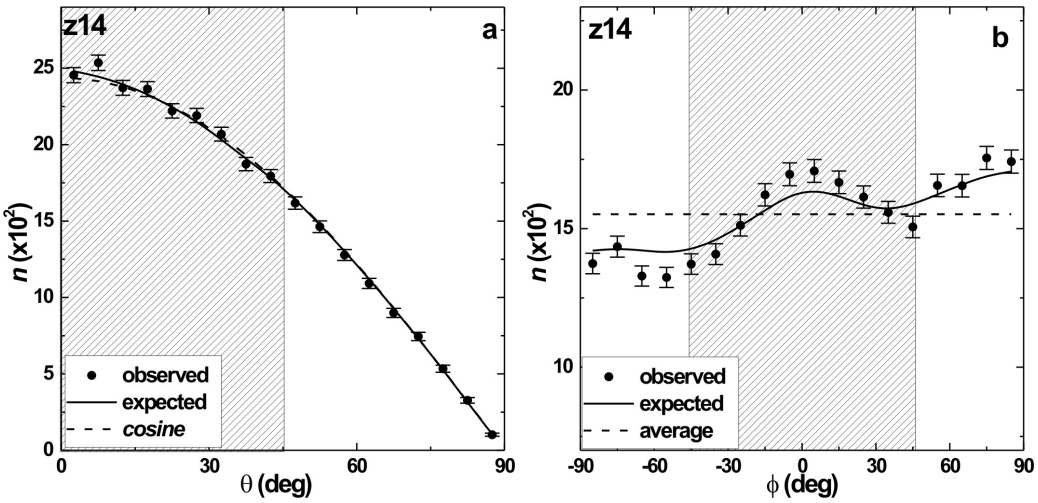

Figure 25: The polar (θ) and azimuthal angle (ϕ) distributions of galaxies that have z magnitude in the range 17.15 to 17.45. The solid line represents the expected isotropic distributions. The cosine and average distributions (dashed) are shown for the comparison. The solid circles with $\pm$ 1σ error bars represent the observed distribution. Here, $\sigma = \sqrt{n}$ as suggested by Godlowski (1994).

The statistics for the θ-distribution of galaxies of this sample are given in Table 7. All these statistics suggest a different result than above two samples z12 and z13. isotropy.

In the azimuthal angle distribution as shown in Figure 25b, the observed solutions of central eight bins (shaded region) are found to be 12 786, whereas the expected solutions are only 12 561. This shows that observed solutions exceeded the expected solutions by 225. There are two humps at angles $-5°$ and $5°$ with $\sim 1.5\sigma$ error limit. Also, there are three significant dips at $-65°$, $-55°$ and $45°$ with $\sim 2\sigma$ error limit outside the shaded part. Thus, no preferred alignment is noticed in this sample.

The statistics for the ϕ-distribution of galaxies of this sample are found as follows: P($>\chi^2$)= 0.006 (smaller than the 5.0% significant level), C/C(σ)= 4.4 (greater than 1σ), $\Delta_{11}/\sigma(\Delta_{11})$= 2.2 (greater than 1.5σ) and P >(Δ_1)= 0.009 (smaller than 15% limit). All these statistics suggest anisotropy.

Here, we conclude strong local anisotropy. Because of the hump at small angle, the spin vectors of galaxies tend to orient parallel with respect to equatorial plane whereas spin vector projections of galaxies tend to orient randomly in the equatorial plane. This effect can be seen in the statistical tests clearly.

4.1.17 Sample $z15$ ($17.45 \leq m_z < 17.75$)

All three statistics suggest strong isotropy except auto-correlation tests (Table 7). A strong binning effect (consecutive dips and humps) can be seen in Figure 26.

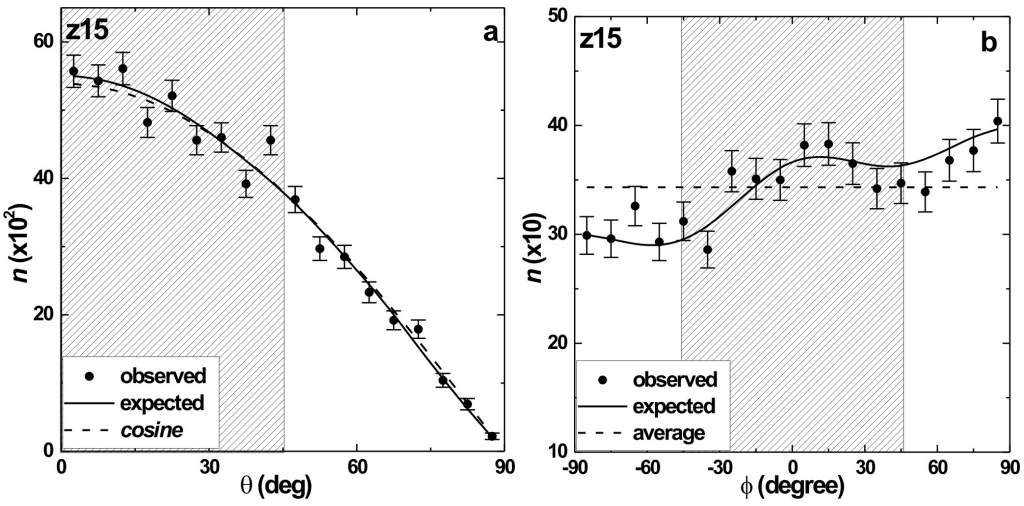

Figure 26: The polar (θ) and azimuthal angle (ϕ) distributions of galaxies that have z-magnitude in the range 17.45 to 17.75. The solid line represents the expected isotropic distributions. The cosine and average distributions (dashed) are shown for the comparison. The solid circles with $\pm$ 1σ error bars represent the observed distribution. Here, σ = $\sqrt{n}$ as suggested by Godlowski (1994).

As shown in the Figure 26a, in the sample $z15$, the number of observed solutions that have $\theta < 45°$ are found to be 3 972 whereas the expected solutions are 4 020. Thus, number of observed solutions are less by 48 than that of the expected. There is a dip at an angle 17.5° with ~2σ error limit. At bimodal region ($\theta \sim 45°$), there are 65 more

observed solutions than the expected. There is a significant hump at an angle 42.5° with $> 2\sigma$ error limit. For the large angles ($> 45°$), the number of observed solutions lagged the expected by 18 and there is a hump at an angle 72.5° with $\sim 2\sigma$ error limit. It seems that the isotropic orientation has been distorted but not at the significant level.

The statistics of the ϕ-distribution (Table 8) for the sample $z15$ suggests isotropy except the Fourier probability ($P(> \Delta_1)$). The anisotropy in the Fourier test is important because of its accountability of orientating angles.

The observed number of solutions in central eight bins (shaded region) lags the expected solutions by 5. There is a hump (Figure 26b) at an angle $-25°$ with $\sim 1.5\sigma$ error limit. Also, one hump at an angle $-65°$ with $\sim 2\sigma$ error limit and one dip at an angle 55° with $\sim 1.5\sigma$ error limit are noticed at outer region of shaded part. Thus, no preferred alignment is noticed in the ϕ-distribution.

We conclude a random orientation of spin vector and spin vector projection of galaxies, suggesting Hierarchy Model. Thus, merging and collisional consequence lead vanishing angular momentum of galaxies (Bardelli, 1989).

4.1.18 Sample $z16$ ($17.75 \leq m_z < 18.05$)

Figure 27a shows θ-distribution of galaxies in the sample Z16. The number of observed solutions for $\theta < 45°$ are less than the number of expected solutions by 3. There is a significant hump at an angle 2.5° with $\sim 2\sigma$ error limit. At bimodal region ($\theta \sim 45°$), the number of expected solutions are more by 9 than that of observed. For the large angles ($> 45°$), the number of observed solutions are more by 12 than that of expected and no any significant dips and humps are noticed there.

Except auto-correlation test, other three statistical parameters suggest isotropy (Table 7). Thus, no preferred alignment is found. Anisotropy in auto-correlation test is because of the binning effect.

In ϕ distribution (Figure 27b), the observed solutions of central eight bins (shaded region) the expected solutions by 28. There are no any significant humps and dips in this region. Also, there are two dips at $-65°$ with $\sim 2\sigma$ error limit and at 65° with $\sim 1.5\sigma$ error limit outside the shaded part. All statistics suggest strong isotropy. Thus, no preferred

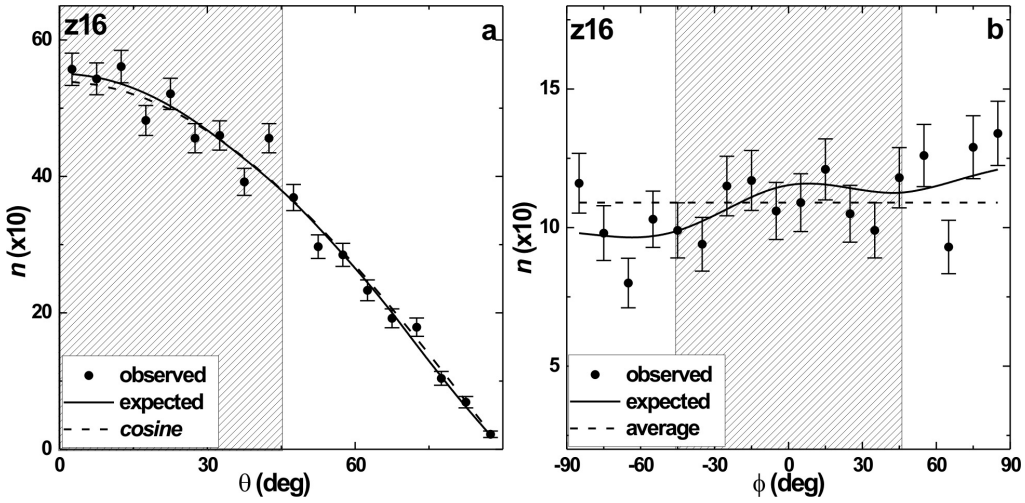

Figure 27: The polar (θ) and azimuthal angle (ϕ) distributions of galaxies that have z-magnitude in the range 17.75 to 18.05. The solid line represents the expected isotropic distributions. The cosine and average distributions (dashed) are shown for the comparison. The solid circles with $\pm$ 1σ error bars represent the observed distribution. Here, σ = $\sqrt{n}$ as suggested by Godlowski (1994).

alignment is noticed.

Hence, a random orientation of spin vectors of galaxies are observed in this sample, suggesting Hierarchy model as proposed by Peebles (1969).

4.1.19 Sample $z17$ ($18.05 \leq m_z < 18.35$)

Figure 28a shows the polar angle (θ) distribution of galaxies of database in the sample $z17$. The statistics for the θ-distribution of galaxies of this sample(Table 7) advocate strong isotropy.

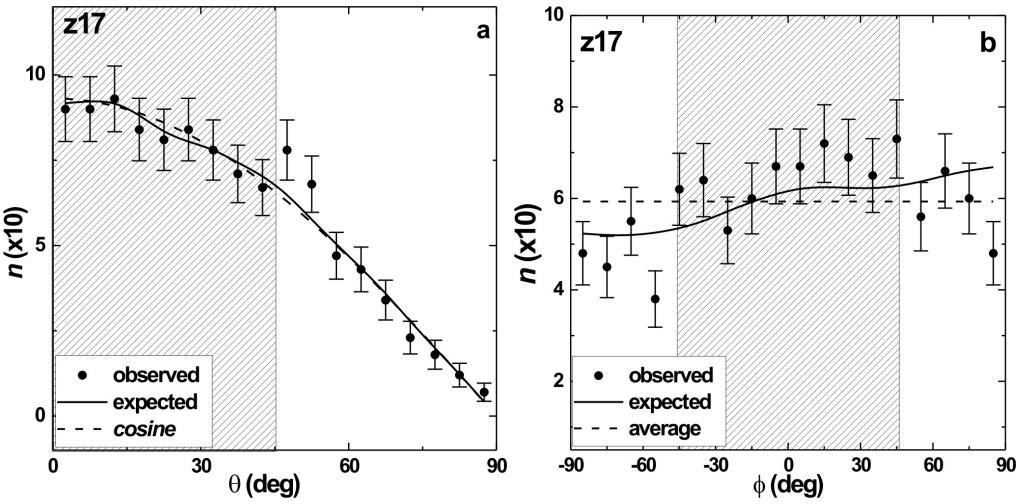

Figure 28: The polar (θ) and azimuthal angle (ϕ) distributions of galaxies that have z magnitude in the range 18.05 to 18.35. The solid line represents the expected isotropic distributions. The cosine and average distributions (dashed) are shown for the comparison. The solid circles with $\pm$ 1σ error bars represent the observed distribution. Here, σ = $\sqrt{n}$ as suggested by Godlowski (1994).

In Figure 28a, the number of observed solutions for $\theta < 45^\circ$ and ($> 45^\circ$), the number expected solutions are in good agreement and also no any significant humps and dips are observed in this region. Thus, no any preferred alignment is noticed in the θ-distribution of this sample.

The statistics of the ϕ-distribution (Table 8) for the sample $z17$ are found as follows: P($>\chi^2$) = 0.255 (greater than the 5.0% significant level), C/C(σ) = 0.2 (less than the limit 1σ), $\Delta_{11}/\sigma(\Delta_{11})$ = 2.8 (greater than the limit 1.5σ), P $>(\Delta_1)$ = 0.020 i.e., 2.0% (smaller than 15% limit). The first order Fourier coefficient ($\Delta_{11}/\sigma(\Delta_{11})$) and the Fourier probability (P($>\Delta_1$)) support anisotropy.

In the azimuthal angle distribution as shown in Figure 28b, the observed solutions of central eight bins (shaded region) exceeds the expected solutions by 35. In this region, no any significant humps and dips are noticed. Also, two dips are observed at -55° and

85° with > 2σ error limit outside the shaded part. Thus, no any preferred alignment is noticed in the ϕ-distribution of this sample.

We conclude a random orientation of spin vector and spin vector projection of galaxies in this sample.

4.1.20 Sample $z18$ (18.35 ≤ m_z < 18.65)

In (θ) distribution of galaxies in the sample $z18$ is shown in the Figure 29a. The number of observed solutions for θ < 45° is less than the number of expected solutions by 4. There is a significant hump at 18.75° with ~2σ error limit. At bimodal region (θ ~ 45°), the number of expected solutions are less by 8 than that of observed. For the large angles (> 45°), the number of observed solutions are less by 4 than that of expected and one dip at an angle 63.75°) with ~1.5σ error limit is noticed. That means, there is good agreement between observed and expected number of solution. Also, all statistical test except auto-correlation test (Table 7) suggest isotropy. An isotropy in auto-correlation test is due to binning effect.

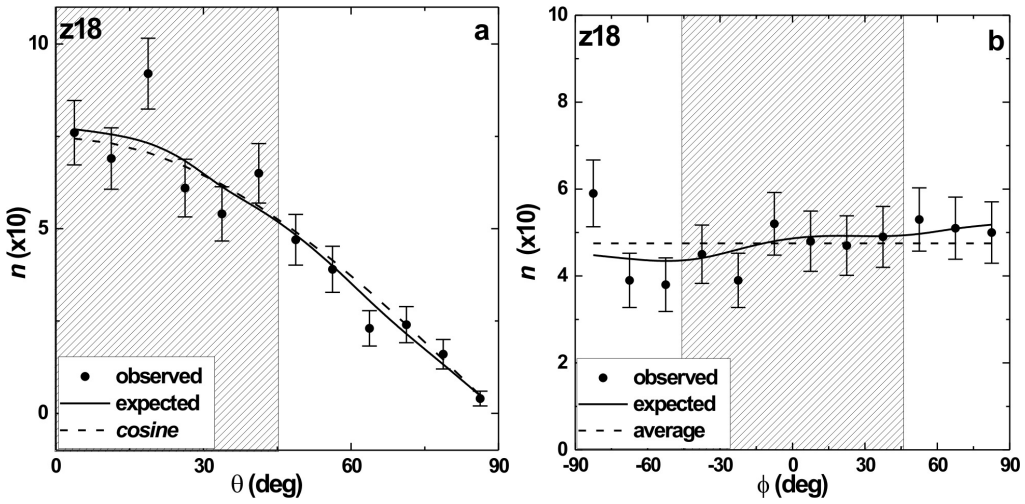

Figure 29: The polar (θ) and azimuthal angle (ϕ) distributions of galaxies that have z magnitude in the range 18.35 to 18.65. The solid line represents the expected isotropic distributions. The cosine and average distributions (dashed) are shown for the comparison. The solid circles with ± 1σ error bars represent the observed distribution. Here, σ = $\sqrt{n}$ as suggested by Godlowski (1994).

In the azimuthal angle distribution as shown in Figure 29a, the observed solutions of

central six bins (shaded region) are found to be 280, whereas the expected solutions are 286. This shows that observed solutions lagged the expected solutions by 6. No any dips and humps are observed there. There is a hump at -82.5° with $\sim 2\sigma$ error limit outside the shaded part. Thus, a preferred alignment is noticed in this sample. Thus, the spin vector projections of galaxies tend to be oriented tangentially towards the center of the equatorial co-ordinate system. The result is due less number of solution. The statistics for the ϕ-distribution of galaxies of this sample (Table 8) suggest isotropy. That means spin vectors of the galaxies are randomly oriented.

We conclude local anisotropy in this sample. The spin vectors of galaxies tend to lie in the equatorial plane whereas spin vector projections of galaxies tend to orient tangentially towards the center of the equatorial co-ordinate system. However, this effect is not strong and can not be seen in the statistical tests. It seems that the statistical tests might not be appropriate here. This sample should be tested by using multivariate tests e.g., K−S and Kuiper in the future.

4.1.21 Sample z19 (18.65 $\leq m_z <$ 18.95)

Figure 30a shows the polar angle (θ) distribution of total galaxies of database in the sample z19. The statistics for the θ-distribution of galaxies of this sample (Table 7) advocate strong isotropy.

In Figure 30a, the number of observed solutions and number of expected solutions have good agreement and also dips and humps suggest no any preferred alignment in the θ-distribution of sample. The statistics of the ϕ-distribution (Table 8) for the sample z19 suggest strong isotropy. Also number of observed and expected solution has good agreement. There are no any significant humps and dips in azimuthal angle distribution (Figure 30b) in any region. Thus, no any preferred alignment is noticed in the ϕ-distribution of this sample.

A random orientation of spin vector and its projection is found in this sample.

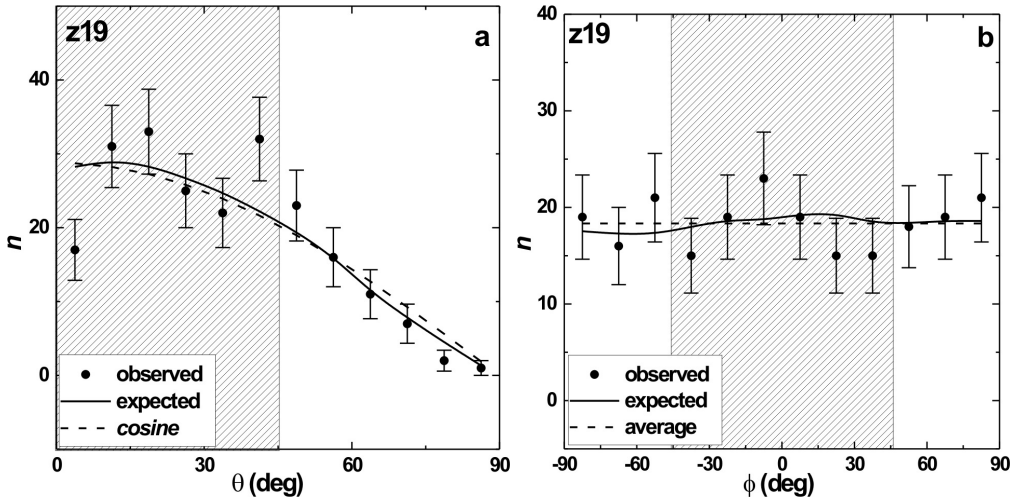

Figure 30: The polar (θ) and azimuthal angle (ϕ) distributions of galaxies that have z magnitude in the range 18.65 to 18.95. The solid line represents the expected isotropic distributions. The cosine and average distributions (dashed) are shown for the comparison. The solid circles with $\pm$ 1σ error bars represent the observed distribution. Here, σ = $\sqrt{n}$ as suggested by Godlowski (1994).

4.1.22 General Discussion

Scatter plot of z-magnitude versus $\Delta_{11}/\sigma(\Delta_{11})$ for polar angle and azimuthal angle distributions for the samples are shown in Figure 31a and Figure 31b. In the figure, grey shaded and dashed region represent the region of isotropy and week anisotropy for both the polar and azimuthal angles. The lower value of the z-magnitude represents the brighter galaxies. Thus, along the X-axis, the brightness profile of galaxies decreases. The distance magnitude relation: $m - M = 5\log r - 5 + 2.5\log_e \alpha r$. We know that, according to Hubble law, distance to the galaxy is proportional to its radial velocity or redshift. This suggest that the alignment of galaxies is independent of the value of z-magnitudes, supporting Hierarchy model of galaxy formation.

In Figure 31a, almost all points lie in the grey shaded region, i.e., the region of isotropy. Thus, we conclude that the spatial orientation of spin vectors of galaxies is random with respect to the equatorial coordinate system and is independent of z-magnitude of galaxies. The solid line represents the best fitted line. The slope of this line is very small.

In Figure 31b, seven samples $z08$, $z09$, $z11$, $z12$, $z13$, $z14$ and $z17$ can be seen outside

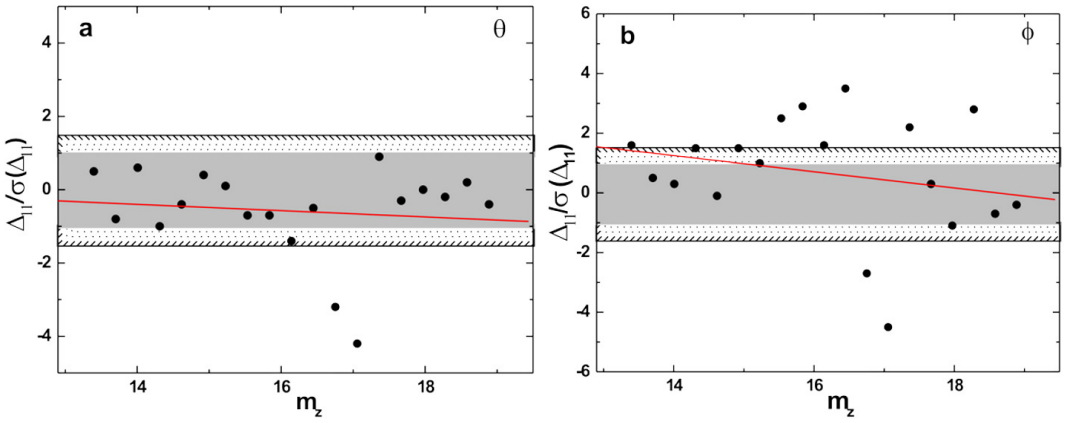

Figure 31: The scatter plot of z-magnitude (m_z) versus $\Delta_{11}/\sigma(\Delta_{11})$ for (a) polar angle and (b) azimuthal angle distributions for the samples. The solid lines represent best fitted line and the grey shaded region represents the region of strong isotropy. The dashed region is the region of weak anisotropy.

the region of isotropy, advocating anisotropy in the azimuthal angle distribution. The slope of best fitted line almost is flat, suggesting z-magnitude independence in the spatial orientation of spin vector projections of galaxies that have redshift in the region 0.05 and 0.10.

4.1.23 Comparison with Previous Works

The peak wavelength of SDSS z-filter is 913.4 nm, equivalent to infrared colour. The bandwidth covering this wavelength are mostly due to longer lines of Paschen and P-fund series of Hydrogen or Helium atoms and molecular lines due to rotational transitions. These lines are expected to be emitted from the hot region (T < 5000 K), probably from the warm interstellar medium of the galaxy, due to atomic and molecular transitions.

Aryal & Saurer (2005) studied spatial orientation of low redshifted galaxies (z<0.05) and found morphological dependence. Figure 32 shows polar angle distribution of galaxies in the low redshift spiral and barred spiral galaxies. A strong dip at 5 degree can be seen in the figure, suggesting preferred alignments for spirals whereas a good agreement between the expected and observed distribution can be seen for barred spirals. Though, we noticed no preferred alignments as well as no magnitude dependence.

Aryal & Saurer (2006) studied spatial orientation of galaxies in a few low redshifted

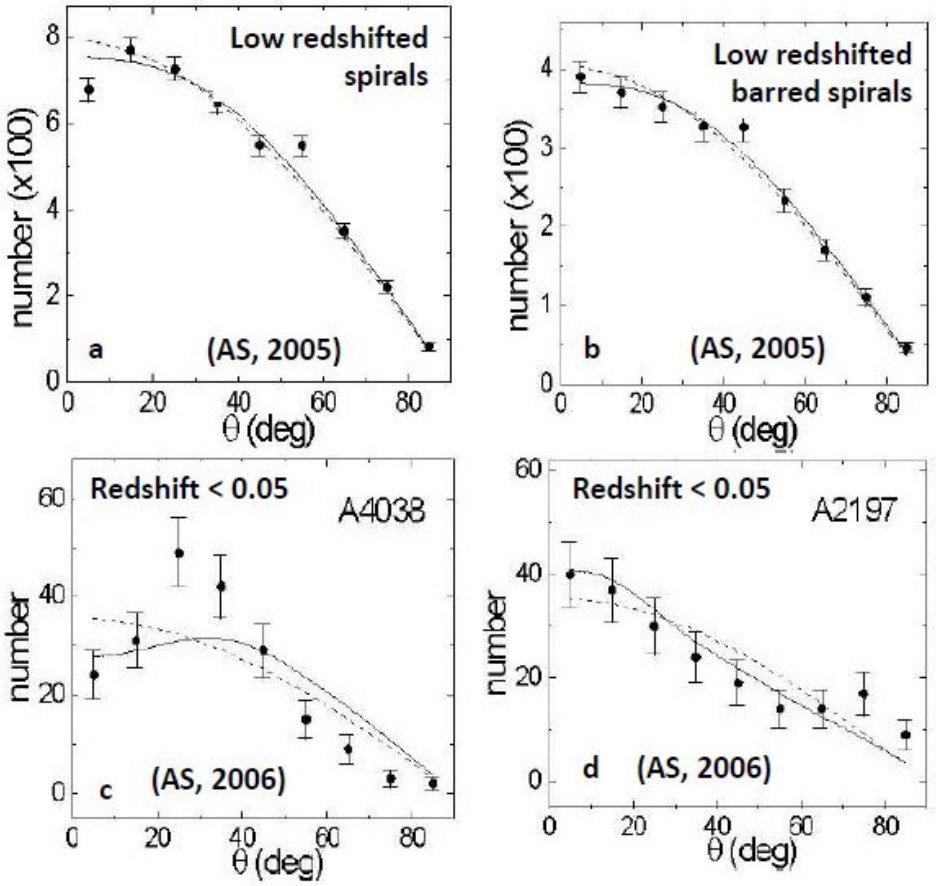

Figure 32: The distributions of angular momentum vectors of galaxies in past two works: (a) Aryal & Saurer (2005) studied nearby Local Supercluster galaxies and noticed a preference in the galaxy alignments of spirals. (b) Aryal & Saurer (2006) found strong anisotropy when studying low redshifted (z<0.01) Abell cluster A4038, whereas random orientation is noticed for another low redshifted cluster Abell 2197. Here, $\sigma = \sqrt{n}$ as suggested by Godlowski (1994).

Abell clusters. They found strong anisotropy when studying low redshifted ($z < 0.01$) Abell cluster A4038, whereas random orientation is noticed for another low redshifted cluster Abell A2197. In both works, database was not complete and they were taken from photometric rather than spectrometric. These inconsistencies is because of the incomplete database. In the present study, these inconsistency has been removed and hierarchy model of large scale structure formation is found to be true.

Godlowski *et al*. (2011) found that the cluster galaxies that are at less than 300 Mpc show a random alignments of angular momentum vectors of galaxies with respect to equatorial co-ordinate system. Their result is similar to that of our result. They concluded hierarchy

model for the galaxy evolution in the cluster. Our database contain cluster as well as supercluster of galaxies. That's why we noticed local anisotropy in few samples. Finally, it is found that the z-magnitude dependence concerning galaxy orientation is very weak.

Baral (2012) studied the spatial orientation of z-magnitude SDSS galaxies having redshift 0.10 to 0.11. He found that the spin vector orientations of galaxies is random, supporting hierarchy model. A local anisotropy was observed in samples $z04$, $z05$ and $z12$. We noticed a similar results in the redshift limit 0.05 to 0.10.

4.1.24 Publications

The result of the work has been published in national Journals and accepted in Research in Astronomy and Astrophysics.

4.2 High Redshift Galaxies

In the first section of the result and discussion we studied the evolution of galaxies having low redshifts. These galaxies are nearby galaxies having well known morphology. In general, we noticed that these galaxies are randomly distributed. In a few samples, where large structure formation are noticed, the preferred alignment (non-vanishing angular momentum) is found, supporting primordial vorticity theory. In this chapter, we study preferred alignments of distant or high redshifted galaxies. The morphology of these galaxies are mostly unidentified. Therefore, we choose red filter here for the sample classification.

4.2.1 Database

Observations of objects with very high redshifts play a central role in cosmology because they provide insight into the epochs and the mechanisms of galaxy formation, if one can reach redshifts that are high enough to correspond to the cosmic epochs when galaxies were forming their first populations of stars and began to shine light throughout space.

Because of their extreme distances, galaxies at high redshift necessarily appear to an observer as faint objects, even if their absolute luminosity is large. However, only a very small fraction of all the faint galaxies observed in a deep image of the sky are located at high redshifts. This is because galaxies have absolute luminosities that cover a wide range, extending over several orders of magnitude, and fainter galaxies are also much more abundant in space than brighter ones. Theoretical expectations of the mechanism of formation of the so-called spheroids, namely elliptical and bulges of spiral galaxies, provided a criterion to identify high redshift galaxies (Karttunen, 2006). The stars that constitute the spheroids are among the oldest observed in the local universe, and currently there is no appreciable ongoing activity of star formation in these systems. These facts indicate that the spheroids formed their stars during a very early cosmic epoch in a relatively short period of time. Since this epoch marked the first significant episodes of star formation during the cosmic evolution (note that about 1/2 of all the stars of the present-day universe are found within spheroids), it has been traditionally identified with the epoch of galaxy formation, and the nascent spheroids themselves

Table 9: Sample classification. First column represents samples. The second and third columns give the magnitude range and number of galaxies in corresponding samples.

samples	magnitude range	number of galaxies
$r01$	$18.10 \leq m_r < 18.32$	118
$r02$	$18.32 \leq m_r < 18.54$	432
$r03$	$18.54 \leq m_r < 18.76$	1526
$r04$	$18.76 \leq m_r < 18.98$	3786
$r05$	$18.98 \leq m_r < 19.20$	7192
$r06$	$19.20 \leq m_r < 19.42$	6685
$r07$	$19.42 \leq m_r < 19.65$	5302
$r08$	$19.65 \leq m_r < 19.87$	893
$r09$	$19.87 \leq m_r < 20.09$	357
$r10$	$20.09 \leq m_r < 20.31$	249
$r11$	$20.31 \leq m_r < 20.53$	155

have been identified with the primeval galaxies. The theoretical expectations predicted that the entire stellar content of a spheroid formed during the gravitational collapse of the proto-cloud of gas from which the structure originated. Simple physical arguments show that the duration of such a collapse is of the order of the time of free fall which, for a galaxy with the mass of the Milky Way, is about one hundred million years.

We have used SDSS DR7 database of galaxies that have redshift in the range 0.40 to 0.50 in order to study preferred alignments of spin vectors or angular momentum vectors of galaxies. We have compiled a homogeneous database of SDSS galaxies fulfilling the same selection criteria as mentioned in the section 4.1.2. There are 83 162 galaxies in the region of interest. A sample page of the database is given in Appendix B. In addition, distribution of positions, position angle, ratio of the diameters and magnitudes are shown in Appendix B.

Similar to the previous chapter, we use standard error propagation method for the sample classification. For this the database of red-filter magnitude (m_r) is used. After plotting bin size versus standard error, we obtained appropriate minimum fluctuation when setting

bin size as 0.22 (i.e., Δm_r = 0.22). The sample classification is shown in Table 9. At first, we discuss the distribution of polar (θ) and azimuthal (ϕ) angles of galaxy rotation axes in each sample. Later a general discussion of the result will be presented. Finally, a comparison will be made with the published works.

4.2.2 Anisotropy in the Polar and Azimuthal Angle Distribution

The descriptions regarding the statistical limits for isotropy and anisotropy, the dips and humps in the histograms and preferred alignments are the same as in section 4.1.3. Table 10 and Table 11 shows the statistics of polar and azimuthal angle distributions of samples. In the statistics of θ, a negative value of first order Fourier coefficient suggests that the spin vectors of galaxies tend to be oriented perpendicular with respect to the equatorial coordinate system suggesting primordial vorticity theory (Ozerney, 1971, 1978 and Stein, 1974). Similarly, a positive value of first order Fourier coefficient suggests that the spin vectors of galaxies tend to be oriented parallel with respect to the equatorial coordinate system Suggesting pancake model model (Doroshkevich, 1973; Doroshkevich & Shandarin, 1978). In the statistics of ϕ, a positive $\Delta_{11}/\sigma(\Delta_{11})$ with significant value suggests that the spin vector projections of galaxies tend to point radially towards the center of the equatorial coordinate system. Similarly, a significant negative value of $\Delta_{11}/\sigma(\Delta_{11})$ implies that the spin vector projection of galaxies tend to orient tangentially with respect to the equatorial coordinate system.

4.2.3 Sample r01 (18.10 $\leq m_r <$ 18.32)

This sample contains a small number (118) of galaxies that have apparent magnitude in the range 18.10 to 18.32 in the r-band (616.5 nm wavelength). Figure 33a shows the polar angle (θ) distribution of total galaxies of database in the sample r01. The statistics for the θ-distribution of galaxies of this sample is shown in the Table 10. The statistics for the polar angle distribution in this sample shows the value of chi-square probability (P($>\chi^2$)) to be 0.601 i.e., 60.1% (greater than the significant level 0.050 i.e., 5.0%). The auto-correlation coefficient (C/C(σ)) is found to be 1.13 (greater than 1σ limit). The first order Fourier coefficient ($\Delta_{11}/\sigma(\Delta_{11})$) is found to be 0.11 (smaller than the limit 1.5σ). The first order Fourier probability (P $>(\Delta_1)$) is found to be 0.806

Table 10: Statistics of the polar angle (θ) distribution of galaxies that have redshift in the range 0.40 to 0.50. The first column represents the samples. The chi-square probability and auto-correlation coefficients are represented by $P(> \chi^2)$ (second column) and $C/C(\sigma)$ (third column). The last two columns give the first order Fourier coefficient $\Delta_{11}/\sigma(\Delta_{11})$ and first order Fourier probability $P(> \Delta_1)$.

sample	$P(> \chi^2)$	$C/C(\sigma)$	$\Delta_{11}/\sigma(\Delta_{11})$	$P(> \Delta_1)$
$r01$	0.601	+1.1	+0.1	0.806
$r02$	0.426	+0.5	-0.2	0.931
$r03$	0.712	+1.2	-0.2	0.941
$r04$	0.208	-1.0	+0.0	0.999
$r05$	0.679	-2.6	-0.1	0.918
$r06$	0.529	+5.5	-2.0	0.119
$r07$	0.857	-0.2	+0.7	0.774
$r08$	0.654	-4.4	+0.2	0.977
$r09$	0.549	-7.4	+0.6	0.777
$r10$	0.431	-3.1	+0.0	0.994
$r11$	0.140	-10.3	-0.1	0.950

Table 11: Statistics of the azimuthal angle (ϕ) distribution of galaxies having redshift in the range 0.40 to 0.50. The columns as in table 10

subsample	$P(> \chi^2)$	$C/C(\sigma)$	$\Delta_{11}/\sigma(\Delta_{11})$	$P(> \Delta_1)$
$r01$	0.801	-3.2	-0.7	0.773
$r02$	0.346	+0.9	+2.2	0.086
$r03$	0.450	+0.4	+1.9	0.177
$r04$	0.207	+3.8	+2.0	0.066
$r05$	0.964	+0.3	+0.9	0.665
$r06$	0.480	-0.5	-1.1	0.543
$r07$	0.101	+6.9	+2.7	0.026
$r08$	0.725	+1.3	+2.3	0.061
$r09$	0.259	+6.4	+1.6	0.239
$r10$	0.344	-1.7	-0.1	0.991
$r11$	0.074	-9.4	-0.7	0.271
$r12$	0.554	-5.4	+0.7	0.767

i.e., 80.6% (greater than 15% limit). Except auto-correlation coefficient, other statistical tests suggest isotropy. Anisotropy in the auto-correlation test suggests either binning effect or local anisotropy that should be seen in the humps/dips in the histogram.

In Figure 33a, the number of observed and expected solutions that have $\theta < 45^\circ$ is found to be 155 and 156 respectively, which suggest a balance between observed and expected number. There is no any significant hump and dip in this region. At bimodal region ($\theta \sim 45^\circ$), there are 1 more observed solutions than the expected in the bimodal region. For the large angles ($> 45^\circ$), the number of observed solutions is more by 1 than that of expected and there is a significant dip at 32.5° with $> 2\sigma$ error limit and one significant hump at 77.5° with $> 1\sigma$ error limit in this region . Thus, we conclude no preferred alignment of spin vectors of galaxies that are brightest when observed through r-filter.

The statistics of the ϕ-distribution (Table 11) for the sample $r01$ are found as follows: P($>\chi^2$) = 0.801 i.e., 80.1% (much greater than the significant level 0.050 i.e. 5.0%), C/C(σ) = -3.16 (less than the limit 1σ), $\Delta_{11}/\sigma(\Delta_{11}) = -0.71$ (less than the limit 1.5σ), P $>(\Delta_1)$ = 0.773 i.e., 77.3% (greater than 15% limit). All these statistics suggest isotropy.

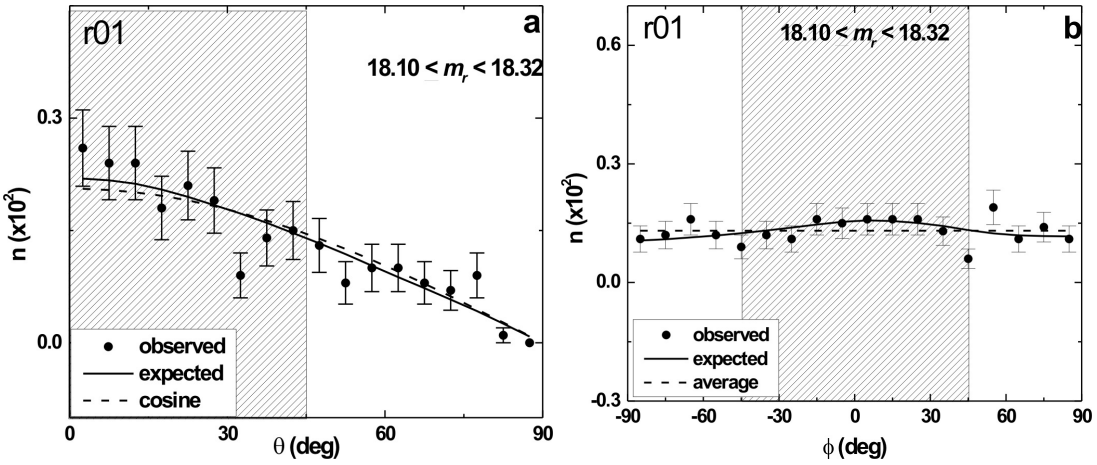

Figure 33: The polar (θ) and azimuthal angle (ϕ) distributions of galaxies that have r magnitude in the range 18.10 to 18.32. The solid line represents the expected isotropic distributions. The cosine and average distributions (dashed) are shown for the comparison. The solid circles with $\pm 1\sigma$ error bars represent the observed distribution. Here, $\sigma = \sqrt{n}$ as suggested by Godlowski (1994).

In the azimuthal angle distribution as shown in Figure 33b, the observed solutions of central eight bins (shaded region) are found to be 115, whereas the expected solutions are 118. This shows that expected solutions exceeded the observed solutions by 3. In this region, one dip at an angle 45° is observed with $\sim 1.5\sigma$ error limit. Outside the shaded part, two significant humps are observed at $-65°$ and 55° with $\sim 1\sigma$ error limit. Thus, no preferred alignments of spin vectors of galaxies in the low magnitude galaxies are found.

4.2.4 Sample r02 (18.32 $\leq m_r <$ 18.54)

The polar angle (θ) distribution of galaxies in the sample r02 is shown in the Figure 34a. The number of observed solutions for $\theta < 45°$ is less than the number of expected solutions by 5. There is one significant hump at $\sim$ 27.5°) and two significant dips at $\sim$ 32.5°) and $\sim$ 37.5°)in this region. At bimodal region ($\theta \sim 45°$), the observed and expected distribution agree within $\pm$ 1σ error limit. For the large angles (> 45°), the number of observed solutions are more by 7 than that of expected and there is a hump at an angle 67.5°, 72.5° with $\sim 1\sigma$ error limit.

The statistics for the θ-distribution of galaxies of this sample are found as follows:

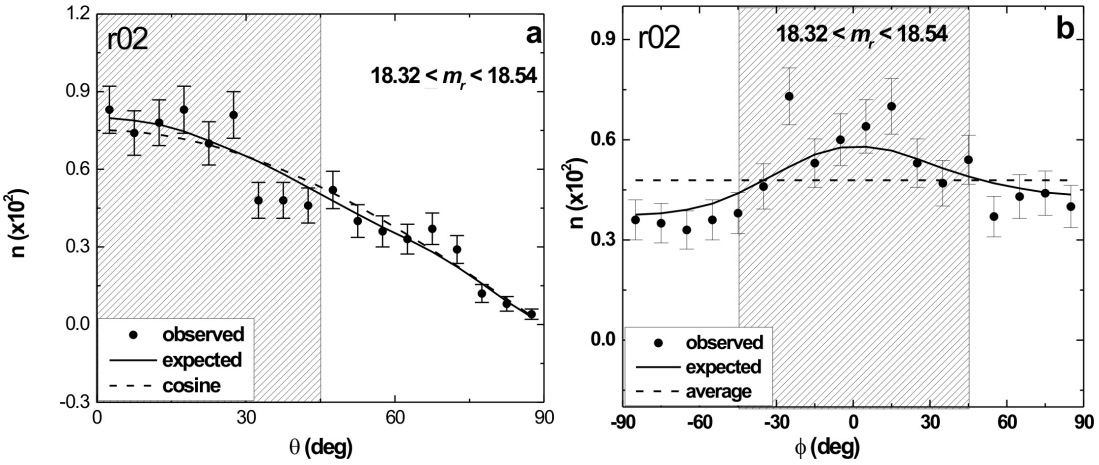

Figure 34: The polar (θ) and azimuthal angle (ϕ) distributions of galaxies that have r magnitude in the range 18.32 to 18.54. The solid line represents the expected isotropic distributions. The cosine and average distributions (dashed) are shown for the comparison. The solid circles with $\pm$ 1σ error bars represent the observed distribution. Here, σ = $\sqrt{n}$ as suggested by Godlowski (1994).

P($>\chi^2$) = 0.426 (greater than the 5.0% significant level), C/C(σ) = 0.51 (smaller than 1σ limit), $\Delta_{11}/\sigma(\Delta_{11}) = -0.18$ (smaller than the limit 1.5σ) and P $>(\Delta_1)$ = 0.931 (greater than 15% limit). All these statistics suggest isotropy. This suggest that the spin vector of galaxies are randomly oriented.

In the azimuthal angle (ϕ) distribution as shown in Figure 34b, the observed solutions of central eight bins (shaded region) are found to be 466, whereas the expected solutions are only 433. This shows that observed solutions exceeded the expected solutions by 33. There is a two significant hump at an angle -25° with $\sim 2\sigma$ error limit and 15° with $\sim 1.5\sigma$ error limit in this region. Outside the shaded part, there is one significant dip at 55° with $\sim 1.5\sigma$ error limit. Thus, no preferred alignment is noticed in this sample.

The statistics for the ϕ-distribution of galaxies of this sample are found as: P($>\chi^2$) = 0.346 (greater than the 5.0% significant level), C/C(σ) = 0.89 (smaller than 1σ limit), $\Delta_{11}/\sigma(\Delta_{11}) = 2.22$ (greater than the limit 1.5σ) and P $>(\Delta_1)$ = 0.086 i.e. 8.6% (less than 15% limit). Except first order fourier coefficient and first order fourier probability, all these statistics suggest isotropy. The anisotropy in first order Fourier coefficient suggest that the reference co-ordinate system is less reliable for this sample.

The galaxies that have radial velocity in the range 0.4 to 0.5 and r-magnitude in the

range 18.32 to 18.54 support hierarchy model, suggesting no preferred alignments of spin vectors of galaxies.

4.2.5 Sample $r03$ ($18.54 \leq m_r < 18.76$)

The statistics for the polar angle distribution in the sample $r03$ suggest strong isotropy (Table 10).

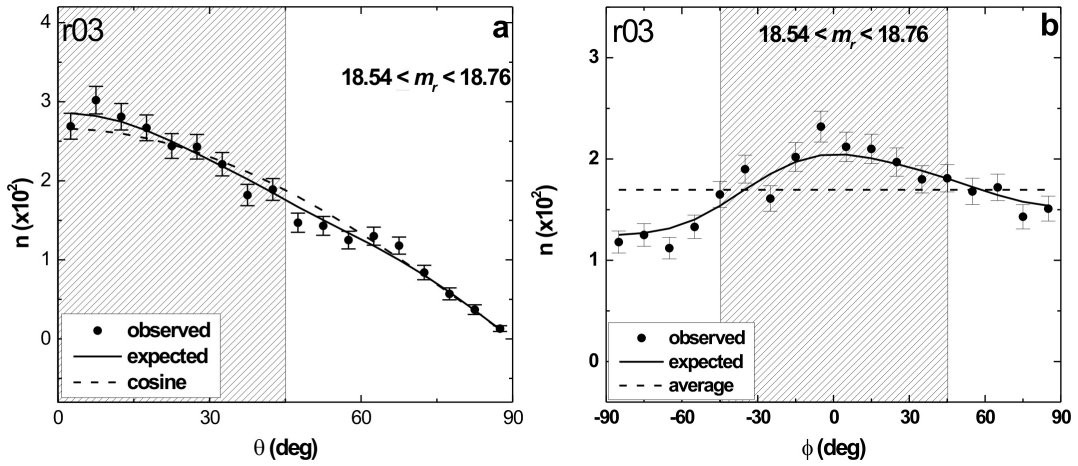

Figure 35: The polar (θ) and azimuthal angle (ϕ) distributions of galaxies in the sample $r03$.The solid line represents the expected isotropic distributions. The cosine and average distributions (dashed) are shown for the comparison. The solid circles with $\pm$ 1σ error bars represent the observed distribution. Here, $\sigma = \sqrt{n}$ as suggested by Godlowski (1994).

As shown in Figure 35a, in the sample $r03$, the number of observed solutions that have $\theta < 45°$ is less than expected solutions by 1. There are no any significant humps and dips in this region. At bimodal region ($\theta \sim 45°$), there are 4 more observed solutions than the expected. For the large angles ($> 45°$), the number of observed solutions exceed the expected by 17. There are two humps at an angles 62.5°, 67.5° with $> 1\sigma$ error limit. There is one significant dip at angle 47.5° with $\sim 1\sigma$ error limit. So, no preferred alignment is noticed in the θ-distribution. In the distribution of projections of spin vectors no such preference is noticed.

Except first order Fourier test, all values of the statistical parameters (Table 11) suggest isotropy in the ϕ-distribution of the sample $r03$. The anisotropy in first order Fourier coefficient suggest that the reference co-ordinate system is not appropriate.

In the azimuthal angle distribution as shown in Figure 35b, the observed number of central eight bins (shaded region) is lagged the observed number by 39. There are two significant hump at an angle -35° within $\sim 1\sigma$, -5° within $\sim 1.5\sigma$ error limit and one significant dip at an angle -25° within $\sim 1.5\sigma$ in this region. Two dip are observed at an angle -65° and 75° within $\sim 1\sigma$ error limit at outer region of shaded part. For last four bins 15 less observed solutions than expected is noticed whereas for first four bins 36 more expected solutions than the expected is found.

Thus, no preferred alignment of spin vector and spin vector projection of galaxies is found in this sample.

4.2.6 Sample r04 ($18.76 \leq m_r < 18.98$)

Figure 36a shows the polar angle (θ) distribution of galaxies of database in the sample r04. The statistics for the θ distribution of galaxies of this sample is shown in the Table 10. All these statistics advocate isotropy.

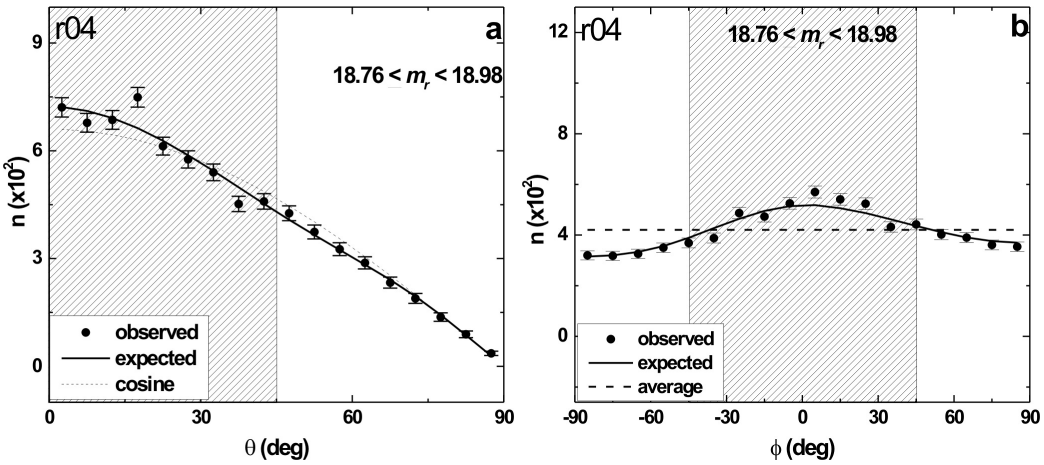

Figure 36: The polar (θ) and azimuthal angle (ϕ) distributions of galaxies in the sample r04. The solid line represents the expected isotropic distributions. The cosine and average distributions (dashed) are shown for the comparison. The solid circles with $\pm$ 1σ error bars represent the observed distribution. Here, $\sigma = \sqrt{n}$ as suggested by Godlowski (1994).

Figure 36a shows the θ-distribution of galaxies in the sample r04. A significant hump can be seen at 17.5° with (>2σ) error limit and one significant dip at 32.5° with (<1σ)

error limit at $\theta < 45°$. The observed solution is less than the expected solution by 30 in this region. At bimodal region ($\theta \sim 45°$), the observed solution is 7 more than that of the expected. For the θ greater than 45°, the observed solution is 6 more than the expected and there are no any significant hump and dip seen. The local anisotropy can not be observed, suggesting a random orientation of spin vectors of galaxies in the sample.

The statistics of the ϕ-distribution (Table 11) for the sample $r04$ are found as: P($>\chi^2$) = 0.207 i.e., 20.7% (much greater than the significant level 0.050 i.e., 5.0%), C/C(σ) = 3.85 (greater than the limit 1σ), $\Delta_{11}/\sigma(\Delta_{11})$ = 2.00 (greater than the limit 1.5σ), P >(Δ_1) = 0.066 i.e., 6.6% (less than 15% limit). Thus, all the statistical tests suggest anisotropy except chi-square probability.

For azimuthal angle distribution of galaxies, as shown in Figure 36b, a significant dips are noticed at an angle −35° and 35° with ($>1\sigma$), and two significant humps are noticed at an angle 5°, with ($>1.5\sigma$) and at 25°,−5° with ($>1\sigma$) error limit. Statistics shows 66 more observed solutions than the expected solutions in the center eight bins. For first four bins, the observed solution is less by 11 than expected solution whereas 41 less for last four bins.

We conclude a random orientation of spin vector and spin vector projection of galaxies in this sample, supporting hierarchy model of galaxy formation as suggested by Peebles (1969).

4.2.7 Sample $r05$ ($18.98 \leq m_r < 19.20$)

All statistics for the polar angle distribution in the sample $r05$ suggest strong isotropy (Table 10), that means spin vectors of the galaxies are randomly oriented with respect to equatorial plane.

As shown in Figure 37a, in the sample $r05$, the number of observed solutions that have $\theta < 45°$ is agrees with the expected solutions. There is no any significant hump and dip in this region. At bimodal region ($\theta \sim 45°$), there are 27 more observed solutions than the expected. For the large angles (> 45°), the number of expected solutions exceed the observed by 53 and there is one dip at an angle 52.5° with $\sim 1\sigma$ error limit.

The statistics of the ϕ-distribution for the sample $r05$ are as shown in Table 11. Hence,

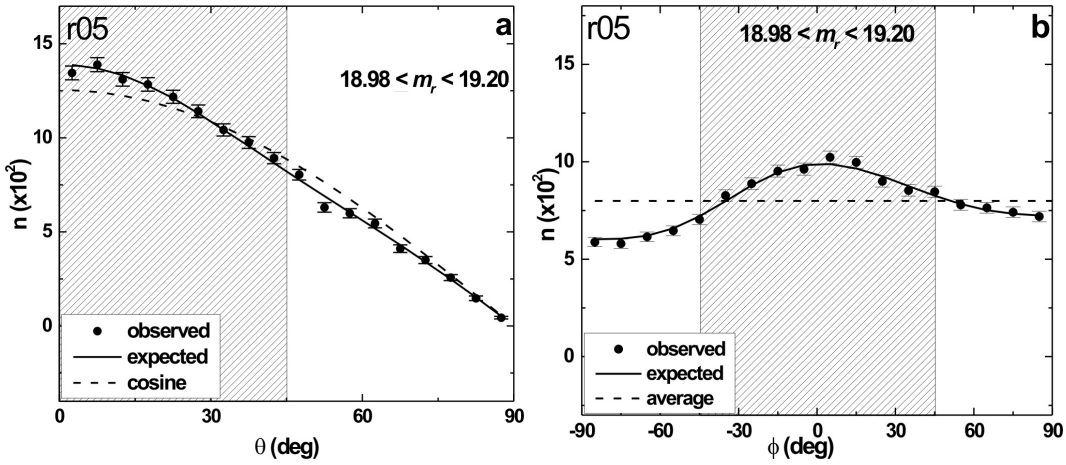

Figure 37: The polar (θ) and azimuthal angle (ϕ) distributions of galaxies in the sample $r05$.The solid line represents the expected isotropic distributions. The cosine and average distributions (dashed) are shown for the comparison. Here, $\sigma = \sqrt{n}$ as suggested by Godlowski (1994).

all the statistics advocate isotropy.

In the azimuthal angle distribution as shown in Figure 37b, the observed solutions of central eight bins (shaded region) lags the observed number by 43. There are no any significant humps and dips in this region. There is 57 less solutions for first four bins, observed than expected solution, whereas for last four bins, observed distribution is 11 more than the expected distribution. As a whole no preference of alignment of spin vector projections of galaxies can be concluded.

4.2.8 Sample $r06$ ($19.20 \leq m_r < 19.42$)

The polar angle (θ) distribution of galaxies in the sample $r06$ is shown in the Figure 38a. The number of observed solutions for $\theta < 45^\circ$ is less than the number of expected solutions by 111. There is one significant dip at an angle 2.5° with $\sim 1.5\sigma$ error limit. At bimodal region ($\theta \sim 45^\circ$), the number of expected solutions are more by 5 than that of observed. For the large angles ($> 45^\circ$), the number of observed solutions are more by 109 than that of expected and also there is no any significant hump and dip in this region. It seems that the galaxies in the - shaded region got distorted to get larger orienting angle, tending to lie perpendicular to the reference plane.

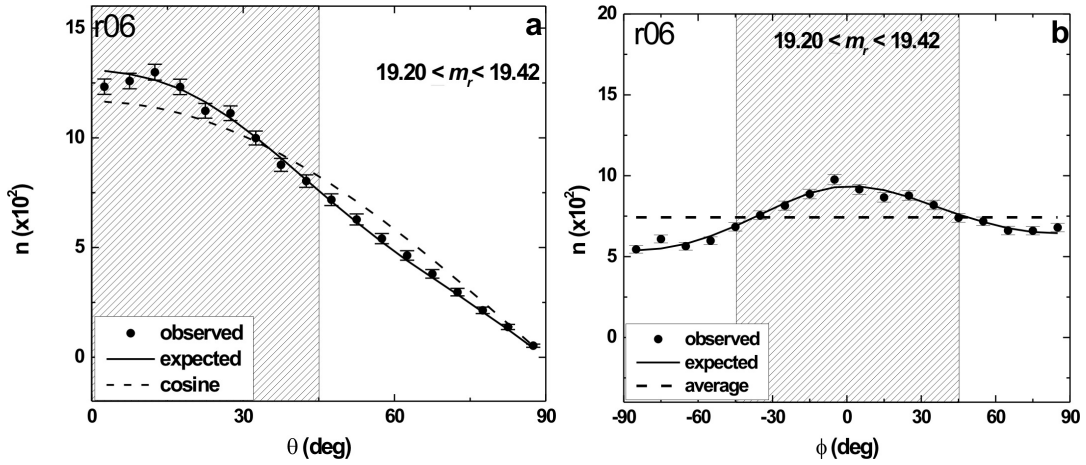

Figure 38: The polar (θ) and azimuthal angle (ϕ) distributions of galaxies in the sample $r06$. The solid line represents the expected isotropic distributions. The cosine and average distributions (dashed) are shown for the comparison. The solid circles with $\pm$ 1σ error bars represent the observed distribution. Here, $\sigma = \sqrt{n}$ as suggested by Godlowski (1994).

The statistics for the θ-distribution of galaxies of this sample are shown in Table 10. All these statistics except auto-correlation test and first order fourier probability suggest strong isotropy. Anisotropy in the auto-correlation test is because of the binning effect.

In the azimuthal angle distribution as shown in Figure 38b, the observed solutions of central eight bins (shaded region) exceeds the expected solutions 28. There is one significant hump at -5° with $\sim 1\sigma$ error limit in this region. Since, there is a one significant hump at -75° with $\sim 1\sigma$ error limit and no any significant dip outside the shaded part. In general, no preferred alignment is noticed in this sample.

All statistics for the ϕ-distribution of galaxies of this sample (Table 11) suggest strong isotropy.

As a whole no preference of alignment of spin vector and spin vector projections of galaxies can be concluded. The result suggest the galaxies are supported by rotation because of the global rotation of the Universe (Li, 1998).

4.2.9 Sample $r07$ ($19.42 \leq m_r < 19.65$)

All the statistics for the polar angle distribution in the sample $r07$ indicate isotropy (Table 10). The polar angle distribution of galaxies in the sample $r07$ is shown in Figure 39a.

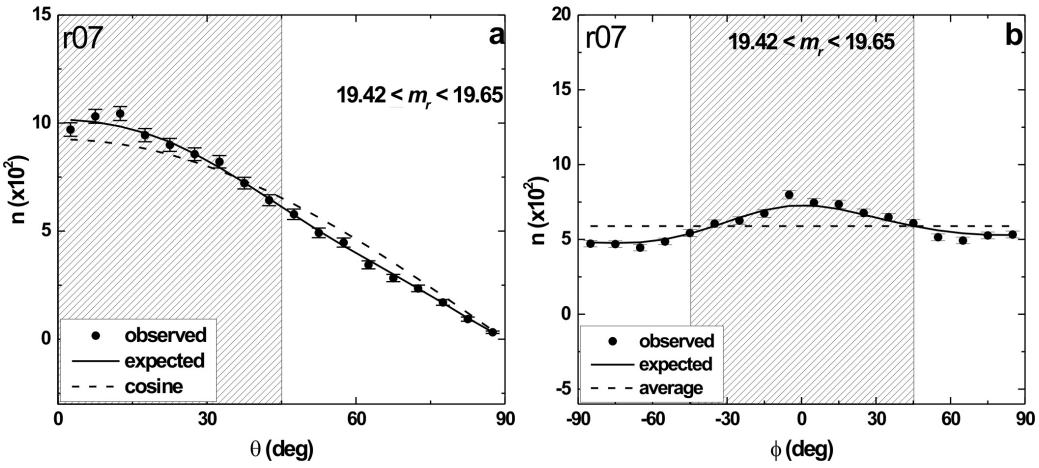

Figure 39: The polar (θ) and azimuthal angle (ϕ) distributions of galaxies in the sample $r07$. The solid line represents the expected isotropic distributions. The cosine and average distributions (dashed) are shown for the comparison. The solid circles with $\pm$ 1σ error bars represent the observed distribution. Here, $\sigma = \sqrt{n}$ as suggested by Godlowski (1994).

For $\theta < 45°$, the number of observed solution is more than the number of expected solutions by 41. There is a significant hump at an angle 12.5° (1.5σ), a significant dip and at angle 2.5° with (1σ) error limit. At bimodal region(θ~45°), the observed and expected distribution agree within $\pm$1σ error limit. There is no significant humps and dips can be seen at angles more than 45°. The observed distribution is 37 less than the expected distribution for $\theta > 45°$. A random orientation of spin vectors of galaxies is noticed.

The statistics of the ϕ-distribution (Table 11) for the sample $r07$ are found as follows: P($>\chi^2$) = 0.101 (greater than the significant level 0.050), C/C(σ) = 6.95 (greater than the limit 1σ), $\Delta_{11}/\sigma(\Delta_{11})$ = 2.70 (greater than the limit 1.5σ), P $>(\Delta_1)$ = 0.026 i.e., 2.6% (less than 15% limit). Here, mixed result are obtained. Auto-correlation and first order fourier coefficient suggest anisotropy where as chi-square probability and Fourier probability suggest isotropy.

As seen in Figure 39b, at angle −5°, a significant hump is seen. At an angle −65°, 55° and 65° there are three significant dips. There is 136 more solutions than the expected for center eight bins. The number of observed distributions is 66 less than the expected distributions in first four and 94 less in last four bins.

A week local anisotropy is found suggesting the spin vector projections of excess galaxies tend to point towards the equatorial centre.

4.2.10 Sample $r08$ ($19.65 \leq m_r < 19.87$)

The polar angle (θ) distribution of galaxies in the sample $r08$ is shown in the Figure 40a. The number of observed solutions for $\theta < 45°$ is less than the number of expected solutions by 4. There is a hump at an angle 2.5 with $\sim 1.5\sigma$ error limit and significant dip at an angle 12.5 with $<1\sigma$ error limit,22.5 with 1σ error limit,in this region. At bimodal region ($\theta \sim 45°$), the number of expected solutions are less by 3 than that of observed. For the large angles (>45°), the number of expected solutions are more by 8 than that of observed and also there is a dip at an angle 67.5° with $<1\sigma$ error limit. No any preferred alignment is noticed in the θ-distribution of this sample.

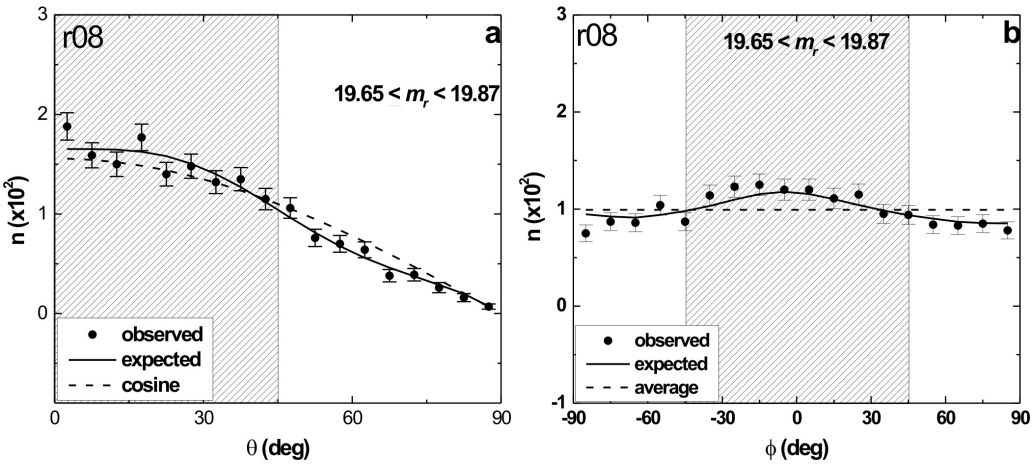

Figure 40: The polar (θ) and azimuthal angle (ϕ) distributions of galaxies in the sample $r08$. The solid line represents the expected isotropic distributions. The cosine and average distributions (dashed) are shown for the comparison. The solid circles with $\pm$ 1σ error bars represent the observed distribution. Here, $\sigma = \sqrt{n}$ as suggested by Godlowski (1994).

All statistics for the θ-distribution of galaxies of this sample suggest strong isotropy

(Table 10).

Figure 40b shows ϕ distribution of galaxies for sample $r08$. At angle $-85°$, a significance dip is seen with $> 2\sigma$ error limit. There are no any significant hump seen. For center eight bins, from the statistics, it is found that the number of expected solutions is 48 less than the observed solutions. Here, for first four bins number of observed solution is 20 less than expected and for last four bins number of observed solutions is 18 less than the expected solutions. Thus, no preferred alignment is noticed in this sample. All the statistics except chi-square probability suggest anisotropy. Since Chi-square test is not decessive test, we conclude no preferred alignments.

4.2.11 Sample $r09$ ($19.87 \leq m_r < 20.09$)

Figure 41a shows the polar angle (θ) distribution of total galaxies in the sample $r09$. The statistics for the θ-distribution of galaxies of this sample is shown in the Table 10. The statistics for the polar angle distribution in this sample advocate strong isotropy.

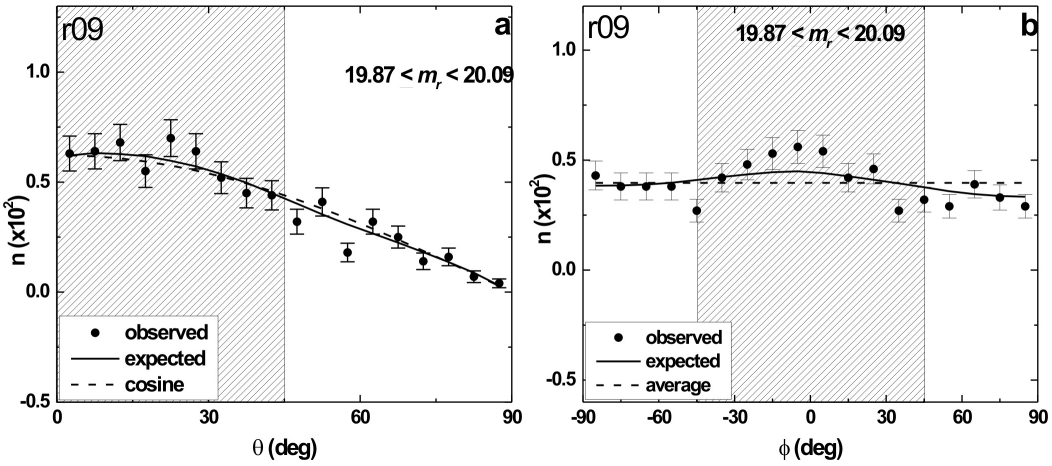

Figure 41: The polar (θ) and azimuthal angle (ϕ) distributions of galaxies in the sample $r09$. The solid line represents the expected isotropic distributions. The cosine and average distributions (dashed) are shown for the comparison. The solid circles with $\pm$ 1σ error bars represent the observed distribution. Here, $\sigma = \sqrt{n}$ as suggested by Godlowski (1994).

The θ distribution of galaxies for sample $r09$ is shown in Figure 41a. At angle 22.5° a significant hump is seen with (1σ) error limit. But, overall observed solutions is 11 more than the expected for $\theta < 45°$. At bimodal region ($\theta \sim 45°$), the observed and

expected distribution agree within $\pm 1\sigma$ error limit. For large angle ($> 45°$), there is no any significant hump seen but there are two significant dip at an angle 47.5° and 57.5° with (1.5σ) error limit. The number of observed solutions is 2 less than the expected solutions for $\theta > 45°$. Hence, overall balance in statistics strongly suggests the isotropy.

The statistics of the ϕ-distribution (Table 11) for the sample $r09$ are found as: P($>\chi^2$) = 0.259, (smaller than the 5.0% significant level), C/C(σ) = 6.39 (greater than the limit 1σ), $\Delta_{11}/\sigma(\Delta_{11})$ = 1.61 (greater than the limit 1.5σ), P $>(\Delta_1)$ = 0.239 i.e., 23.9% (greater than 15% limit). The values of chi-square probability (P($> \chi^2$)) and the Fourier probability (P($> \Delta_1$)) support the isotropy whereas the first order Fourier coefficient ($\Delta_{11}/\sigma(\Delta_{11})$) and auto-correlation test C/C(σ) support anisotropy.

In the azimuthal angle distribution as shown in Figure 41b, in the central eight bins (shaded region)the observed solutions exceeded the expected solutions by 26. In this region, two significant humps at angles $-5°$ and 5° are observed with $\sim 1.5\sigma$ error limit. Also, two dips are observed at $-45°$ with $>2\sigma$ error limit and at 35° with $\sim 2\sigma$ error limit.

Similar to the previous sample, this sample showed a random orientation of spin vectors of galaxies, however, a suitable physical reference system for this sample should be discussed in detail in the future.

4.2.12 Sample $r10$ ($20.09 \leq m_r < 20.31$)

The polar angle (θ) distribution of galaxies in the sample $r10$ is shown in the Figure 42a. The number of observed solutions for $\theta < 45°$ is less than the number of expected solutions by 4. There is a significant dip at 32.5° with $>1\sigma$ error limit and significant hump at an angle 12.5° with $>1\sigma$ error limit in this region. At bimodal region ($\theta \sim 45°$), the number of expected solutions are more by 6 than that of observed. For the large angles ($> 45°$), the number of observed solutions are more by 2 than that of expected and there are hump at an angle 47.5° with 1.5σ error limit and at 67.5° with 1.5σ error. So, no any preferred alignment is noticed in the θ-distribution of this sample.

The statistics for the θ-distribution of galaxies of this sample are shown in Table 10, suggests strong isotropy.

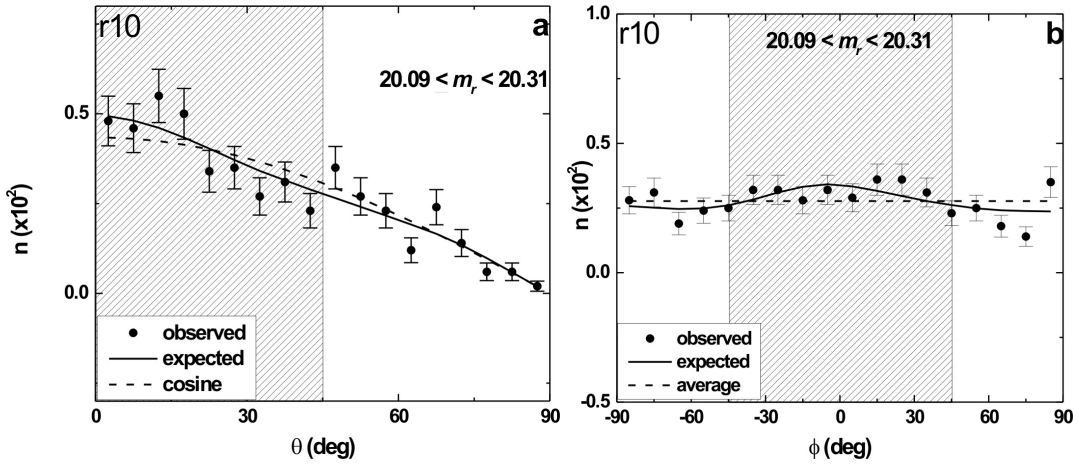

Figure 42: The polar (θ) and azimuthal angle (ϕ) distributions of galaxies in the sample $r10$. The solid line represents the expected isotropic distributions. The cosine and average distributions (dashed) are shown for the comparison. The solid circles with $\pm$ 1σ error bars represent the observed distribution. Here, $\sigma = \sqrt{n}$ as suggested by Godlowski (1994).

In the azimuthal angle distribution as shown in Figure 42b, At angle 12.5°, 47.5° and 67.5° significant humps are noticed with $< 1.5\sigma$ error limit and at an angle 32.5° and 62.5° significant dip are found with $> 1\sigma$ error limit The number of observed solutions is 7 more than the expected solutions in center eight bins. For last four bins 4 less observed solutions than expected is noticed whereas for first four bin 2 more observed solutions than the expected is found. Thus, a preferred alignment is noticed in this sample. Thus, we found that the spin vector projections of galaxies in this sample tend to be directed towards the equatorial center.

The statistics for the ϕ-distribution of galaxies of this sample advocates strong isotropy (Table 11).

4.2.13 Sample $r11$ ($20.31 \leq m_r < 20.53$)

All statistics for the polar angle distribution in the sample $r11$ suggest strong isotropy (Table 10). As shown in Figure 43a, in the sample $r11$, the number of observed solutions that have $\theta < 45°$ is less by 6 than that of the expected. There are three significant humps at an angle 17.5° (1σ), 22.5° (1.5σ), 42.5° (1σ) and two significant dips at an angle 12.5° (1.5σ), 27.5° (1.5σ). At bimodal region ($\theta \sim 45°$), there are 2 less observed solutions

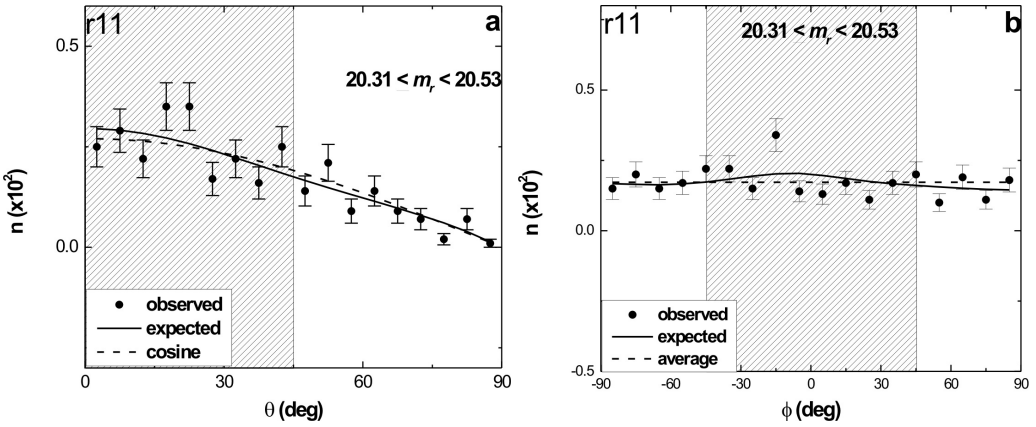

Figure 43: The polar (θ) and azimuthal angle (ϕ) distributions of galaxies in the sample $r11$. The solid line represents the expected isotropic distributions. The cosine and average distributions (dashed) are shown for the comparison. The solid circles with $\pm$ 1σ error bars represent the observed distribution. Here, $\sigma = \sqrt{n}$ as suggested by Godlowski (1994).

than the expected. For the large angles ($> 45°$), the number of observed solutions exceed the expected by 2 and also there are one significant hump at an angle 52.5° (1σ) and one significant dip at an angle 77.5° (1.5σ). So, no preferred alignment is noticed in the θ-distribution.

The statistics of the ϕ-distribution (Table 11) for the sample $r11$ support strong isotropy.

In the azimuthal angle distribution as shown in Figure 43b, the observed number of solution in central eight bins (shaded region) lags the expected number by 8. Three dips are observed at angles $-5°$, $5°$ with $\sim 1.5\sigma$ error limit and $25°$ with $\sim 1\sigma$ error limit and there is one hump at angle $-15° > 2\sigma$ in the shaded part. There is one significant dip at an angle 55° with $> 1\sigma$ error limit at outer region of shaded part. So, no preferred alignment is noticed in the ϕ-distribution of this sample.

Thus, we conclude random orientation of spin vector of galaxies whereas their projections showed a strong preference, suggesting a need of new reference coordinate system.

4.2.14 General Discussion

Figure 44a represents the scatter plot of r-magnitude versus $\Delta_{11}/\sigma(\Delta_{11})$ for (a) polar angle and (b) azimuthal angle distributions for the samples. As we know that the preferred orientation of galaxies can be studied by the parameter $\Delta_{11}/\sigma(\Delta_{11})$. The grey shaded and dashed region represent the region of isotropy and week anisotropy for both the polar and azimuthal angles. We know that magnitude is roughly proportional to the distance and distance is obviously proportional to redshift. This suggest that the alignment of galaxies is independent of the value of r-magnitudes, supporting hierarchy model of galaxy formation.

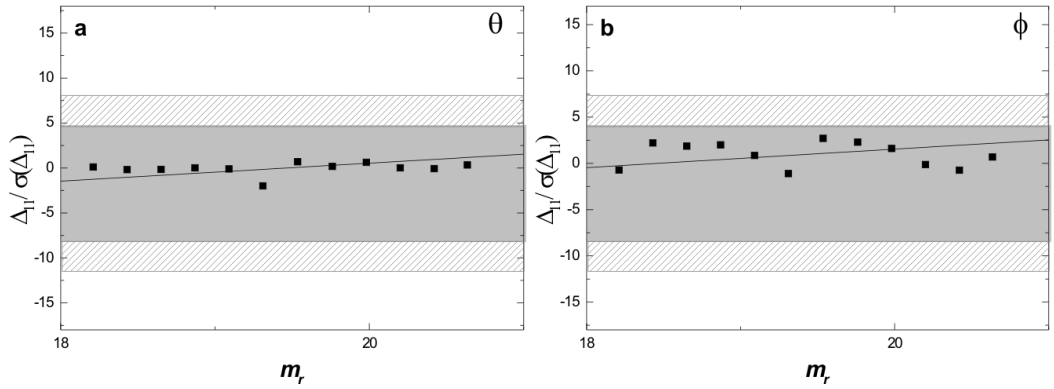

Figure 44: The scatter plot of r-magnitude versus $\Delta_{11}/\sigma(\Delta_{11})$ for (a) polar angle and (b) azimuthal angle distributions for the samples. The solid lines represent best fitted line and the grey shaded region represents the region of strong isotropy. The dashed region is the region of weak anisotropy.

In Figure 44b, all points lie in the grey shaded region, i.e., the region of isotropy. Thus, we conclude that the spatial orientation of spin vectors of galaxies is random with respect to the equatorial coordinate system and is independent of r-magnitudes of galaxies.

4.2.15 Comparison with Previous Works

The peak wavelength of SDSS r-filter is 616.5 nm, equivalent to yellow-orange color. The bandwidth covering this wavelength are mostly due to Balmer and Paschen lines of hydrogen atom. These lines are emitted from the hot region of the galaxy (e.g., extended HII region, etc) due to electronic transitions. We noticed no preferred alignments

suggesting a similar evolutionary stages of these galaxies. Since our database have a narrow range of redshift, we can assume that the formation and evolution process of our galaxies might be similar. These are at the same distance (Hubble law: $v = H_o d, i.e., d = v/H_o$). Considering average radial velocity of 22 500 km s^{-1} and Hubble constant (H_o) 73 km s^{-1}/Mpc, the distance becomes 308.2 Mpc. Godlowski *et al*. (2011) found that the cluster galaxies that is at > 300 Mpc show a random alignments of spin vectors of galaxies with respect to equatorial co-ordinate system. We also noticed the similar results. Our result contradicts the result obtained by Acharya (2012) and Dhamala (2012) but agrees well with the result obtained by Phuyal (2012). Acharya (2012) and Dhamala (2012) noticed a strong red-shift dependence in the similar database and concluded a preferred alignments, supporting Primordial Vorticity Theory (Ozerney 1971, 1978 and Stein, 1974). However, Phuyal (2012) observed a random alignments of spin vectors of galaxies with respect to equatorial co-ordinate system supporting Hierarchy model of structure formation (Peebles, 1969).

4.2.16 Publication

The results of this work has been submitted to the Journal Research in Astronomy & Astrophysics (RAA).

4.3 Blueshifted Galaxies

According to the conventional definition, the redshift of galaxies is the sum of two terms: the isotropic cosmic expansion velocity and the peculiar velocity owning to gravitational attraction by the surrounding matter. In practice, determining the peculiar velocity of a galaxy requires knowledge of both its observable radial velocity relative to some reference system and the distance to the galaxy determined independently of the radial velocity. According to the linear theory of gravitational instability, the peculiar velocities of galaxies are related to fluctuations in the mass (Peebles, 1993).

Burbidge & Demoulin (1969) first observed IC 3258, a small extragalactic object near the center of the Virgo Cluster, to have an emission-line with a blueshift of -490 km s^{-1}. They give three possible interpretations of their observations. First, IC 3258 is a member of the Virgo Cluster and has a very high velocity relative to the average for the cluster. Second, IC 3258 is a field galaxy closer to the Virgo Cluster and its large velocity is just a random motion. Third, IC 3258 has velocity because it has been ejected in an outburst involving one of the radio galaxies in the Virgo cluster. Several other blue-shifted galaxies appear in the direction of the Virgo cluster.

By measuring the distance d of a galaxy, we can obtain the peculiar velocity of a galaxy by following relation

$$V_{pec} = V_{obs} - H_o\, d$$

Here, $H_o\, d$ is Hubble expansion velocity, V_{obs} is observed velocity of the galaxy. Since the Hubble expansion velocity is small for nearby galaxies, the peculiar velocity could be negative. Negative peculiar velocities are seen all over the region around the Virgo Cluster and this have long been seen as a reflex of the pull of the cluster on us (Aaronson, *et al*., 1982). We live in the Local Supercluster, which is overdense part of the Universe. So there is possibly the a local retardation of the cosmic expansion or a net infall within this region. In another example, an observer living on the outskirts of a large concentration is also pulled towards the overdense part of the clusters.

When the radiation propagates inside the collapsing body it is blue-shifted. If this blueshift is greater than the redshift caused by the propagation of the radiation through expanding universe, distant observer can detect the gravitational blueshift from the

collapsing object. Also the AGNs have blue-shifted spectrum. Bian *et al* (2005) studied the radial velocity difference between the narrow emission-line components and of [O III] λ and Hβ in a sample of 150 SDSS narrow-line Seyfert 1 galaxies. They found seven 'blue outliers' with [O III] blueshifted by more than 250 km s^{-1}. They interpreted the blueshift as possible result of the outflowing gas from the nucleus and the obscuration of the receding part of the flow by an optically thick accretion disk and on the viewing angle.

4.3.1 Database

We obtained the data of 5 987 blue-shifted galaxy-like celestial objects from the Sloan Digital Sky Survey (SDSS) Data Release 7 . We have retained only those galaxies that have redshift ($-z$) data at 95% level of significance. This removed 569 galaxies form our original data. After this removal we have 4 595 galaxies left in our database. Then the remaining galaxies were separated into three bins based upon their redshift values. We binned the data by taking the bin size of 1×10^{-4}, this resulted in three bins with number of galaxies roughly in the ratio of $3 : 2 : 1$ in the largest, medium and the smallest bins respectively. In binning process, galaxies that have very low and high redshift values were also removed.

We have compiled the database of diameters and position angle of galaxies using the database of near infrared (i, 7 625) and ultraviolet (u, 3 543) filters. These filters provide extreme limits for the isophotes.

4.3.2 Anisotropy in the Polar and Azimuthal Angle Distribution

We have classified our database into six samples on the basis of their redshift values and u & i-magnitudes. Here we discuss the distribution of the polar (θ) and azimuthal (ϕ) angles of galaxy rotation axes in each samples. We study the spatial orientation of spin vectors of galaxies with respect to equatorial coordinate system. Any deviation from the expected isotropic distribution will be tested using four statistical parameters, namely the chi-square probability (P> χ^2), auto-correlation coefficient (C/C(σ)), first order Fourier coefficient ($\Delta_{11}/\sigma(\Delta_{11})$), and first order Fourier probability (P> Δ_1). Section

4.1.3 describes the descriptions regarding the limits of anisotropy in the distributions, humps and dips in the histograms and preferred alignments.

Table 12: Statistics of the polar angle (θ) distribution of blueshift galaxies. The first column lists the samples. The second to fifth column list the corresponding chi-square probability P($> \chi^2$), auto-correlation coefficient C/C(σ), the first order Fourier coefficient $\Delta_{11}/\sigma(\Delta_{11})$, the first order Fourier probability P($> \Delta_1$), and standard deviation of Fourier amplitude $\sigma(\Delta_1)$ respectively.

sample	P($> \chi^2$)	C/C(σ)	$\Delta_{11}/\sigma(\Delta_{11})$	P($> \Delta_1$)	$\sigma(\Delta_1)$
*i*01	0.781	−0.1	−0.4	0.939	0.023
*i*02	0.025	+1.9	−0.1	0.849	0.030
*i*03	0.023	−1.7	−0.7	0.773	0.042
*u*01	0.644	−1.0	+1.2	0.404	0.028
*u*02	0.896	−0.5	−0.2	0.931	0.035
*u*03	0.146	+1.8	−0.4	0.879	0.048

The statistics for the polar angle (θ) and azimuthal angle (ϕ) distribution is given in Table 12 and Table 13.

In the histogram of the θ-distribution (see Figure 45a as an example), solid curve represents the expected isotropic distribution whereas dashed curve is the cosine distribution. The solid circles with $\pm$ 1σ error bars represent the observed distribution. The shaded portion represents the range $0^\circ < \theta < 45^\circ$. A dip (or hump) at $\theta < 45^\circ$ suggests that the spin vectors of galaxies tend to orient perpendicular (or parallel) with respect to the equatorial coordinate system. Similarly, a hump (or dip) in the larger θ ($\theta > 45^\circ$) indicates that the spin vectors of galaxies tend to be oriented perpendicular with respect to the equatorial coordinate system.

In the histogram of the ϕ-distribution (see Figure 45b as an example), solid curve represents the expected isotropic distribution, whereas dashed curve is the average distribution. The solid circles with $\pm$ 1σ error bars represent the observed distribution. The shaded portion represents the range $-45^\circ < \phi < +45^\circ$. In the histogram of the ϕ-distribution, $\phi = 0^\circ$ means spin vector projections tend to point radially towards the center of the equatorial coordinate system. A hump in the middle of the histogram suggests that

Table 13: Statistics of the azimuthal angle (ϕ) distribution of blueshift galaxies. The first column lists the samples. The second, third, fourth, and fifth column list the corresponding chi-square probability P($> \chi^2$), auto-correlation coefficient C/C(σ), the first order Fourier coefficient $\Delta_{11}/\sigma(\Delta_{11})$, the first order Fourier probability P($> \Delta_1$), and standard deviation of Fourier amplitude $\sigma(\Delta_1)$ respectively.

sample	P($> \chi^2$)	C/C(σ)	$\Delta_{11}/\sigma(\Delta_{11})$	P($> \Delta_1$)	$\sigma(\Delta_1)$
*i*01	0.657	+0.1	−1.1	0.432	0.023
*i*02	0.107	−1.4	−2.1	0.090	0.030
*i*03	0.449	+1.5	−2.0	0.093	0.042
*u*01	0.039	+0.2	−2.2	0.098	0.028
*u*02	0.433	+0.5	−1.7	0.116	0.035
*u*03	0.860	+0.3	+0.1	0.747	0.048

the spin vector projections of galaxies tend to point towards the center of the chosen coordinate system. Similarly, a hump at first four and last four bins indicates that the spin vectors projections of galaxies tend to be oriented tangentially with respect to the chosen reference coordinate system.

In Figure 45a, the solid line being the expected distribution, the dots with $\pm 1\sigma$ statistical error bars being the observational distribution, and the dotted line being the cosine distribution. The statistics is given in the Table 12.

4.3.3 Sample *i*01

These galaxies are seen through i-filter, sensitive towards the infrared. The infrared activity in the blue shifted galaxies can be studied for the orientation. Therefore the role of star formation activity (fever infrared emission/ absorption)in the preferred alignment of blue shifted galaxies. All three statistical tests suggest isotropy in θ distribution for sample *i*01 (Table 12). The chi-square probability P($> \chi^2$) and first-order Fourier probability P($> \Delta$) are found to be 78 and 94 percent respectively. The correlation coefficient C/C(σ) and the first-order Fourier coefficient $\Delta_{11}/\sigma(\Delta_{11})$ are found to be within 1σ error limit. From Figure 45a, we can see that there are no significant humps or dips. Hence, there is no preferred alignment of angular momentum vectors of galaxies

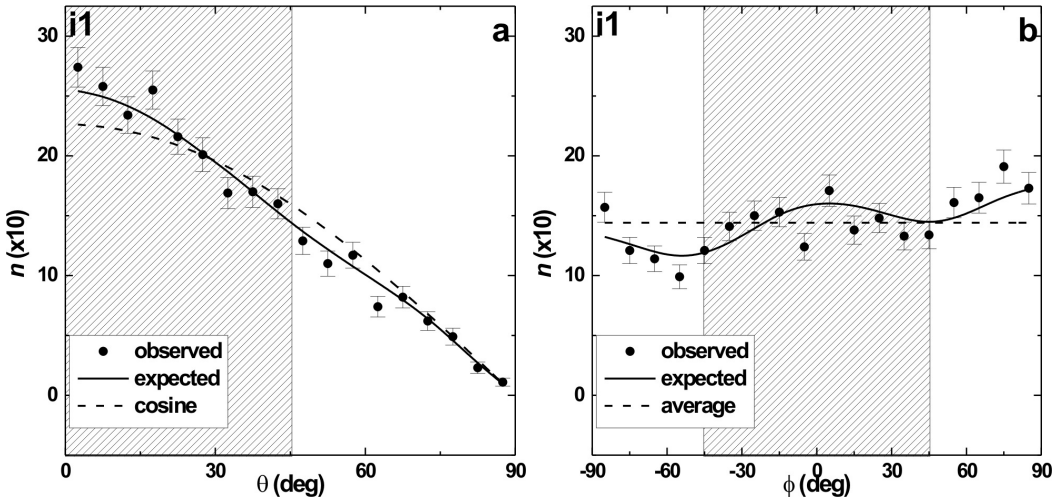

Figure 45: The polar (θ) and azimuthal angle (ϕ) distributions of blueshift galaxies in the sample $i01$. The solid line represents the expected isotropic distributions. The cosine and average distributions (dashed) are shown for the comparison. The solid circles with $\pm$ 1σ error bars represent the observed distribution. Here, $\sigma = \sqrt{n}$ as suggested by Godlowski (1994).

in sample $i01$ with respect to equatorial coordinate system.

All three statistics (Table 13) for sample $i01$ show isotropy in the azimuthal angle distribution. The chi-square probability P($> \chi^2$) and first-order Fourier probability P($> \Delta_1$) are found to be 66 and 43 percent respectively. The correlation coefficient C/C(σ) and the first-order Fourier coefficient $\Delta_{11}/\sigma(\Delta_{11})$ are $<1\sigma$ error limit. There are humps at $+65°$ and dips at $-5°$ and $-55°$ (Figure 45b). However, these humps and dips do not change the statistics of total sample. Also, the correlation coefficient shows strong isotropy. So, these are possibly the effect of binning. The random orientation for spin vector projections of galaxies is observed for sample $i01$.

Thus, we conclude random orientation of spin vectors of galaxies and spin vector projections of galaxies.

4.3.4 Sample $i02$

The chi-square probability and the correlation coefficient (Table 12) show the anisotropy in the θ distribution of galaxies in sample $i02$. However, the first order Fourier probability and the first order Fourier coefficient show isotropy. Since the observed distribution of

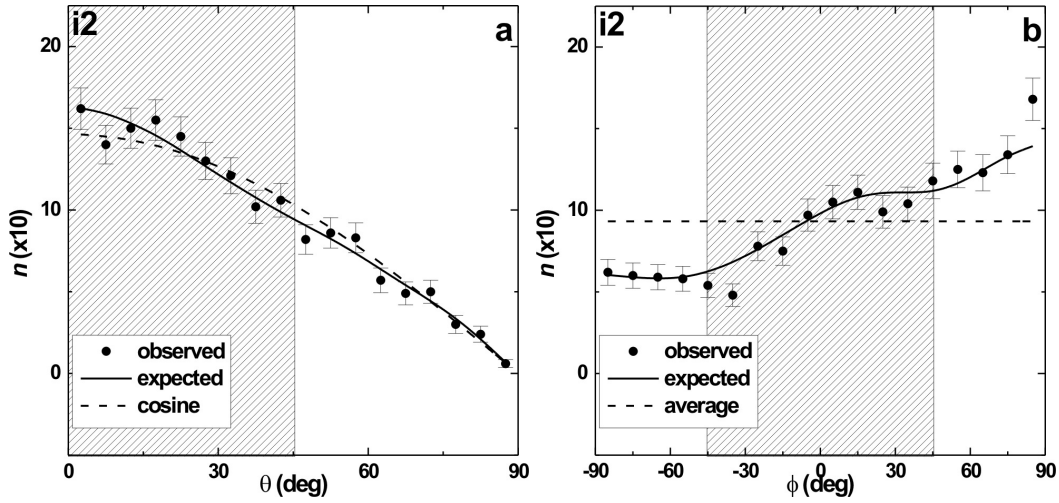

Figure 46: The polar (θ) and azimuthal angle (ϕ) distributions of blueshift galaxies in the sample $i02$. The solid line represents the expected isotropic distributions. The cosine and average distributions (dashed) are shown for the comparison. The solid circles with $\pm$ 1σ error bars represent the observed distribution. Here, $\sigma = \sqrt{n}$ as suggested by Godlowski (1994).

the θ closely follow the expected distribution, we regard the Fourier test as more reliable. Also we look correlation coefficient to examine the neighboring binning effect. The first-order Fourier probability P($> \Delta_1$) is found to be 85 percent and the first-order Fourier coefficient $\Delta_{11}/\sigma(\Delta_{11})$ are found to be within 1σ error limit. There are small dips at 0°, 60°, 65° and a hump at 15° (Figure 46a). Also the correlation coefficient is found to be 1.9. This suggests that there is no strong evidence for a departure of spin vectors from isotropy in sample $i02$.

All statistics except χ^2 suggest anisotropy in ϕ distribution for sample $i02$ (Table 13). We take the Fourier test and the correlation test as more reliable for interpretation of our results for the reason mentioned above. The chi-square probability P($> \chi^2$) and first-order Fourier probability P($> \Delta_1$) are found to be 10 and 9 percent respectively. The Correlation coefficient C/C(σ) and the first-order Fourier coefficient $\Delta_{11}/\sigma(\Delta_{11})$ are found to be $>1\sigma$ and $>1.5\sigma$ limit. The histograms for the azimuthal angle (ϕ) distribution for sample $i02$ is shown in Figure 46b. From figure we can see that there are humps at $-60°$, $+30°$ and $+90°$, and dips at $-50°$ to $+20°$. We observe anisotropy in spin vector projection of galaxies in sample $i02$ with respect to equatorial coordinate system.

In general, polar angle distribution shows isotropy, however correlation test shows the presence of local effects. On the other hand, spin vector projection of galaxies tend to point towards the equatorial centre.

4.3.5 Sample *i*03

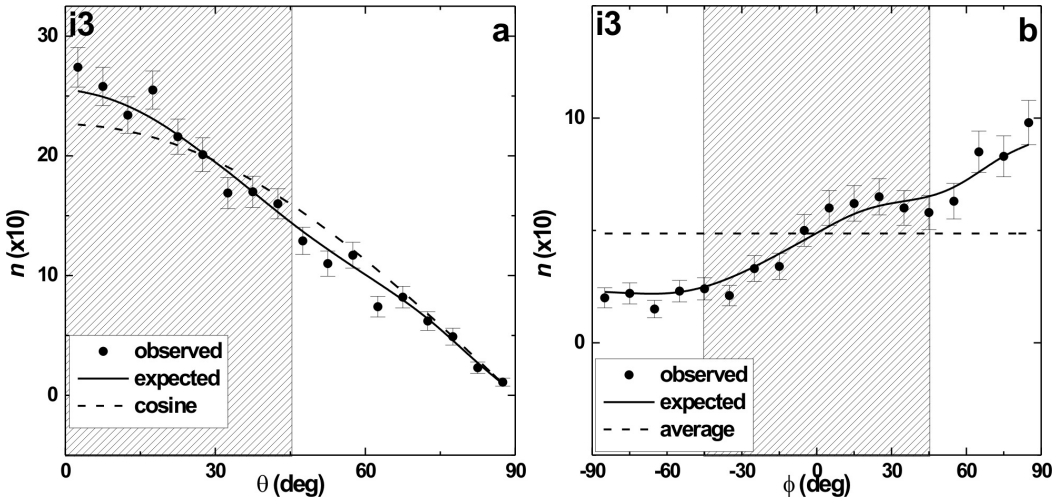

Figure 47: The polar (θ) and azimuthal angle (ϕ) distributions of blueshift galaxies in the sample *i*03. The solid line represents the expected isotropic distributions. The cosine and average distributions (dashed) are shown for the comparison. The solid circles with $\pm$ 1σ error bars represent the observed distribution. Here, $\sigma = \sqrt{n}$ as suggested by Godlowski (1994).

In sample *i*03, chi-square probability P($> \chi^2$) and correlation coefficient C/C(σ) show anisotropy, whereas first-order Fourier probability P($> \Delta_1$) and the first-order Fourier coefficient $\Delta_{11}/\sigma(\Delta_{11})$ show isotropy in the polar angle (θ) distribution (Table 12). Since our observed distribution follows closely with the theoretical distribution in θ-distribution, we regard the Fourier test as more reliable, and examine the local effects from the correlation test. There are humps at 0°, 45°, 60° and dips at 30°, 35°, 60° within $< 2\sigma$ limit (Figure 47a). Hence, we observe isotropy in θ distribution for sample *i*03, however correlation test shows the presence of local effect.

Figure 47b shows the distribution of the spin vector projections of galaxies in the sample *i*03. All three statistics except χ^2 (Table 13) show the anisotropy in the azimuthal angle (ϕ) distribution. There is a hump at +90° and dips at −10° and 0°. The statistics

advocates the strong anisotropy in ϕ distribution for sample $i03$ with respect to equatorial coordinate system.

Thus, polar angle distribution suggests the isotropy in general with local effects in the bimodal region for this sample. Anisotropy is observed in azimuthal angle distribution for this sample.

4.3.6 Sample $u01$

The galaxies are observed through u-filter, sensitive towards ultraviolet activities. Science UV activities is preferred for nearly born star and the region where hot gas flows. There activities lead interstellar medium to dilute interstellar gases. Therefore, the role of stellar evolution activity in the preferred alignment can be studied here.

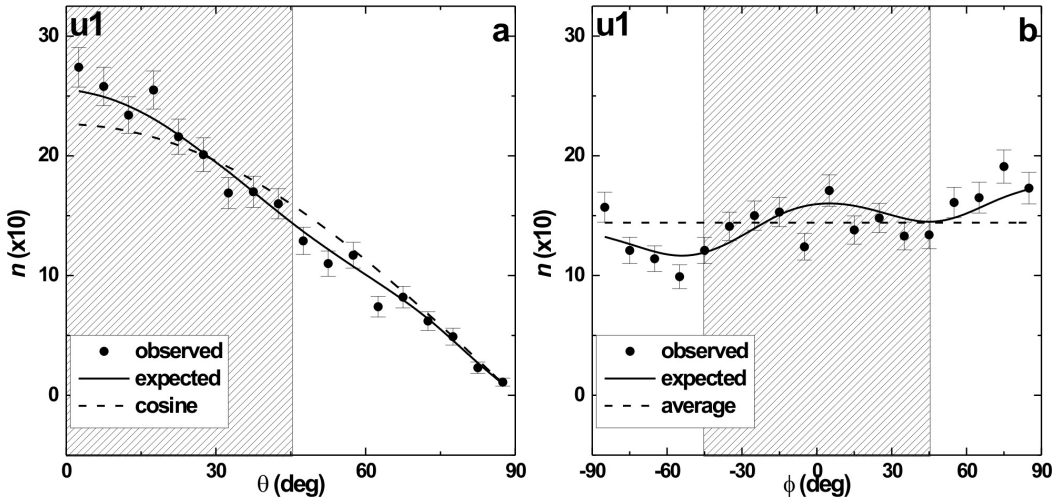

Figure 48: The polar (θ) and azimuthal angle (ϕ) distributions of blueshift galaxies in the sample $u01$. The solid line represents the expected isotropic distributions. The cosine and average distributions (dashed) are shown for the comparison. The solid circles with $\pm$ 1σ error bars represent the observed distribution. Here, $\sigma = \sqrt{n}$ as suggested by Godlowski (1994).

All three statistical tests suggest isotropy in θ distribution (Table 12). The chi-square probability P($> \chi^2$) and first-order Fourier probability P($> \Delta_1$) are found to be 64 and 40 percent respectively. The Correlation coefficient C/C(σ) and the first-order Fourier coefficient $\Delta_{11}/\sigma(\Delta_{11})$ are found to be within 1.5σ error limit. From Figure 48a, we can see that there are no significant humps or dips. We conclude that a small hump at 20°

and a dip at 60° are effects of binning because they do not change the overall statistics of the sample. Hence, we conclude there is no preferred alignment of angular momentum vectors of galaxies in sample *u*01 with respect to equatorial coordinate system.

All statistics, except the correlation coefficient C/C(σ), suggest anisotropy in ϕ distribution for sample *u*01. The chi-square probability P(> χ^2) and first-order Fourier probability P(> Δ_1) are found to be 4 and 10 percent respectively. The Correlation coefficient C/C(σ) is found to be +0.2, and the first-order Fourier coefficient $\Delta_{11}/\sigma(\Delta_{11})$ is found to be $>1.5\sigma$ limit. From Figure 48b, we can see that there are humps at $-90°$ and $+80°$, and dips in the region from $-50°$ to $+50°$. As before, we consider the Fourier test as more reliable. Anisotropy in azimuthal angle distribution of galaxies is found in sample *u*01 with respect to equatorial coordinate system.

Therefore, a random orientation of the spin vectors of blueshift galaxies is observed in this sample. However, the projections of spin vectors tend to lie towards the centre of the equatorial coordinate system.

4.3.7 Sample *u*02

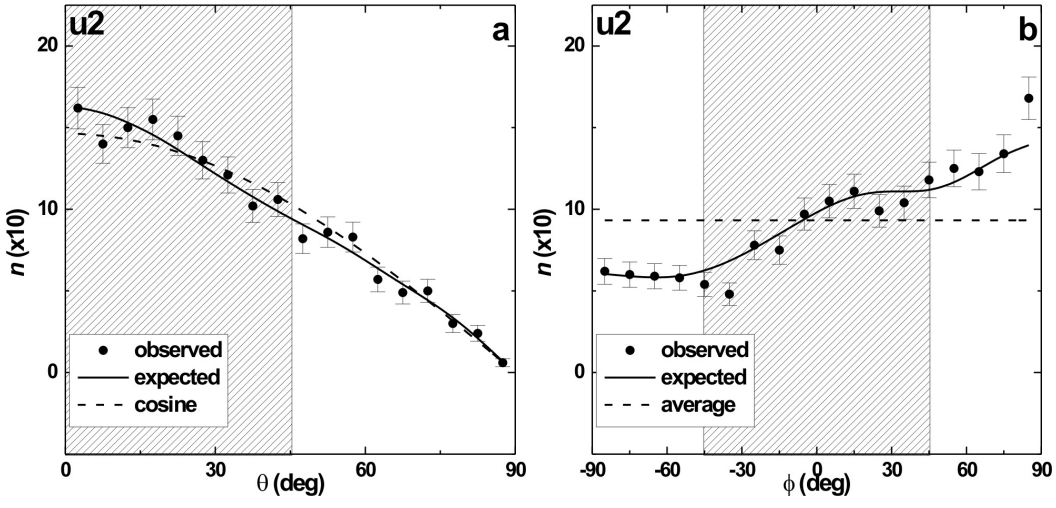

Figure 49: The polar (θ) and azimuthal angle (ϕ) distributions of blue shift galaxies in the sample *u*02. The solid line represents the expected isotropic distributions. The cosine and average distributions (dashed) are shown for the comparison. The solid circles with $\pm$ 1σ error bars represent the observed distribution. Here, $\sigma = \sqrt{n}$ as suggested by Godlowski (1994).

In sample $u02$, all three statistics (Table 12) show isotropy in polar angle (θ) distribution. From Figure 49a, we see that there is a small dip at 10°, but there are no humps. This dip do not change the overall statistics of the sample, hence we conclude this as an effect of binning. There is no preferred alignment of spin vector of galaxies in sample $u02$.

In the statistics of ϕ distribution for sample $u02$, chi-square probability and correlation coefficient show isotropy, whereas the first order Fourier coefficient and first order Fourier probability show anisotropy. P($> \chi^2$) and P($> \Delta_1$) are found to be 43 and 51 percent respectively. $\Delta_{11}/\sigma(\Delta_{11})$ and C/C(σ) are found to be -1.7 and 0.5. There are dips at $-40°$, $+20°$ and a hump at $+90°$ (Figure 49b). As the same reason mentioned above, we consider the Fourier test as more reliable. We observe weak anisotropy in the spin vector projection of galaxies for sample $u02$ with respect to equatorial coordinate system. Thus, we found a random orientation of spin vectors in this sample and weak anisotropy in its projections.

4.3.8 Sample $u03$

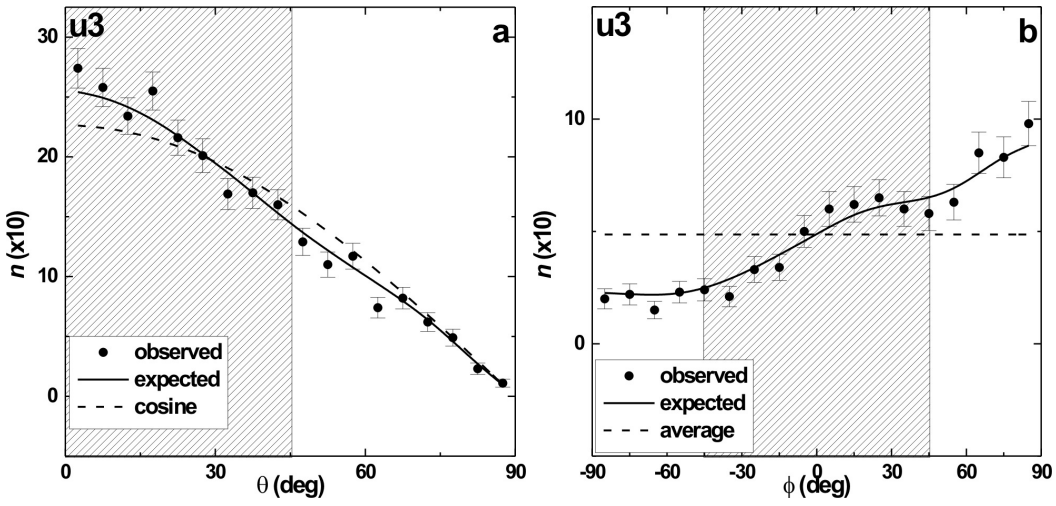

Figure 50: The polar (θ) and azimuthal angle (ϕ) distributions of blueshift galaxies in the sample $u03$. The solid line represents the expected isotropic distributions. The cosine and average distributions (dashed) are shown for the comparison. The solid circles with $\pm$ 1σ error bars represent the observed distribution. Here, $\sigma = \sqrt{n}$ as suggested by Godlowski (1994).

All statistics except correlation coefficient show the isotropy in the distribution of the

polar angle θ in sample $u03$ (Table 12). As before we regard the Fourier test as more reliable, and we examine the neighboring effect from correlation test. The correlation coefficient C/C(σ) is found to be 1.8 ($>1\sigma$ limit). From Figure 50a, we see there are humps at 10°, 45°, 55° and dips at 15°, 20°. Therefore, isotropy is observed in polar angle distribution with some local effect.

In the statistics of azimuthal angle distribution ϕ, all statistics show isotropy (Table 13). There are small dips at 70° and 40°, but there are no humps. Since these dips do not alter the total statistics of the sample, we conclude these dips as binning effect. There is a very good agreement between the observed and expected distributions (Figure 50b) suggesting a random orientation of spin vector projections of galaxies with respect to equatorial coordinate system.

Therefore the spin vector of galaxies and its projections show random orientation in this sample.

4.3.9 General Discussion

In general we found isotropic distribution of the spin vector of galaxies in all our six samples with respect to the equatorial coordinate system. There are humps and dips in the polar angle distributions, and these humps and dips alter the correlation test showing anisotropy in samples $i02$, $i03$, and $u03$. Hence, local effect was observed in these samples suggesting a local tidal connection between the rotation axes of galaxies. However, in the rest of the samples ($i01$, $u01$, and $u02$) small humps and dips do not alter the statistics of the total sample, so we suppose these as binning effects. In general, we observe that there is no preferred alignment of spin vectors of galaxies. Our results of θ distribution support the hierarchical clustering scenario (Peebles 1969), which predicts the random orientation of the directions of the spin vectors of galaxies.

On the other hand, we found interesting results for the ϕ distribution. As mentioned above, we have regarded the Fourier test as more reliable. Out of six samples only two samples ($i01$ and $u03$) show isotropy in all tests. Rest of the samples ($i02$, $i03$, $u01$, and $u02$) show anisotropic distribution of the spin vector projections of galaxies. Also, all samples (except $u03$) have negative value of the first order Fourier coefficient Δ_{11}.

Therefore, in general the spin vector projection of the galaxies tend to be orientated perpendicular to the equatorial plane. However, this problem needs to be examined by using other reference system such as Galactic or Supergalactic coordinate system.

4.3.10 Comparison with Previous Works

In the numerous past literatures authors have studied the spatial orientation of red-shifted galaxies in the field, clusters and superclusters and found mixed result:

- noticed anisotropy supporting either 'Pancake model' (Flin & Godlowski, 1986; Godlowski 1993, 1994; Godlowski *et al*., 1998; Flin, 2001) as suggested by Doroshkevich (1973) or 'Primordial Vorticity Model' (Baier *et al*., 2003) as proposed by Ozernoy (1978)
- found isotropy suggesting a random orientation of spin vectors og galaxies supporting 'Hierarchy model' (Bukhari & Cram, 2003; Aryal & Saurer, 2005a, Aryal *et al*., 2006, 2012, 2013) as recommended by by Peebles (1969). Interestingly, blue-shifted galaxies support hierarchy model. Thus, it can be concluded that the blue-shif is not different cosmological effect, it is because of the peculiar velocity as suggested by Aaronson *et al*. (1982).

No authors have studied the spatial orientation of blue shifted galaxies till date.

4.3.11 Publication

The result of this work has been accepted by the Journal Astrophysics and Space science (now available at arxiv: `https://arxiv.org/abs/1606.02881`).

4.4 SDSS Superclusters

4.4.1 Database

The database used in this work consists of galaxies within two superclusters S[223+022+0117] & S[239+016+0037] located within the survey regions of SDSS (7^{th} data release). The first supercluster has redshift limit in the range 0.111 to 0.122 whereas the second supercluster has the redshift limit in the range 0.029 to 0.049. We choose database of i, u, r filters for galaxies in supercluster S[223+022+0117] and i, u, g filters for galaxies in supercluster S[239+016+0037]. There are 1015 galaxies in the supercluster S[223+022+0117] and 1461 galaxies in the supercluster S[239+016+0037] in our region of interest. This database is compiled from Sloan Digital Sky Survey (SDSS) Data Release 7. A sample page of database is given in the AppendixD.

We have excluded number of galaxies in our database based on the value of intrinsic flatness factors $q^* = 0.2$ and $q^* = 0.15$. At first to find the inclination angle of galaxies, we used the value of intrinsic flatness factor $q^* = 0.2$ and again we used the intrinsic factor $q^* = 0.15$ to those edge-on galaxies. Finally we have excluded galaxies which do not give inclination angle for $q^* = 0.15$. Table 14 shows exact number of galaxies based on above explanation. We have selected three filters namely i, u & r for the supercluster S[223+022+0117]. They are S[223]i, S[223]u & S[223]r samples. Similar classification is done for supercluster S[239+016+0037].

4.4.2 Supercluster S[223+022+0117]: Anisotropy in the Polar & Azimuthal Angle

At first we describe the distribution of polar (θ) and azimuthal (ϕ) angles of galaxy rotation axes of superclusters S[223+022+0117] galaxies taking i, u, r-filters. Our aim is to study the non-random effect concerning magnitude dependence in the spatial orientation of spin vectors of supercluster galaxies with respect to equatorial coordinate system. Any deviation from expected isotropic distribution will be tested using four statistical parameters, namely chi-square probability (P $>\chi^2$), auto-correlation coefficient (C/C(σ)), first order Fourier coefficient ($\Delta_{11}/\sigma(\Delta_{11})$) and first order Fourier probability (P $>\Delta_1$). The statistical limits for anisotropy are the same as in previous chapters. The

Table 14: Number of galaxies for intrinsic flatness factor $q^* = 0.2$ and $q^* = 0.15$ in the superclusters S[223+022+0117] and S[223+022+0117].

Sample	Initial No. of Galaxies	No. of Galaxies excluded for $q^* = 0.2$	No. of galaxies included for $q^* = 0.15$	Final No. of Galaxies
S[223]i	1015	6	6	1015
S[223]u	1015	5	0	967
S[223]r	1015	44	4	1010
S[239]i	1461	38	36	1459
S[239]u	1461	67	0	1394
S[239]g	1461	41	37	1457

descriptions regarding humps and dips in the histograms and preferred alignments are described in the section 4.1.3.

4.4.2.1 Sample S[223]i ($14.42 \leq m_i < 22.64$)

This sample contains 1015 galaxies that have apparent magnitude in the range 14.42 to 22.64 in the i-band. The smaller the value of magnitude brighter the object. Significant infrared emission indicates the enhanced star formation activity and the relatively higher abundance of metal-rich elements in these galaxies. Thus, these are the brightest. Figure 51a shows the polar angle (θ) distribution of total galaxies of database in the sample S[223]i. The statistics for the θ-distribution of galaxies of this sample is shown in the Table 15. The statistics for the polar angle distribution in this sample shows the value of chi-square probability (P($>\chi^2$)) to be 0.033 i.e., 3.3% (smaller than the significant level 0.050 i.e., 5.0%). The auto-correlation coefficient (C/C(σ)) is found to be +3.8 (greater than 1σ limit). The first order Fourier coefficient ($\Delta_{11}/\sigma(\Delta_{11})$) is found to be +2.8 (larger than the limit 1.5σ). The first order Fourier probability (P $>(\Delta_1)$) is found to be 0.013 i.e., 1.3% (smaller than 15% limit). All statistical tests suggest anisotropy. In Figure 51a, the number of observed solutions that have $\theta < 45°$ is found to be 1347 and the expected solutions is found to be 1354 i.e expected solution exceeds observed solutions by 7. There is no any significant hump and dip in this region. At bimodal

Table 15: Statistics of the polar angle (θ) distribution of galaxies in the Superclusters S[223+022+0117] & S[239+016+0037]. The first column represents the different filters or samples. In the table, P($> \chi^2$) represents the chi-square probability (second column). Similarly, C/C(σ) represents the auto-correlation coefficient (third column). The last two columns give the first order Fourier coefficient $\Delta_{11}/\sigma(\Delta_{11})$ and first order Fourier probability P($> \Delta_1$).

Sample	P($> \chi^2$)	C/C(σ)	$\Delta_{11}/\sigma(\Delta_{11})$	P($> \Delta_1$)
S[223]i	0.575	−0.6	−0.5	0.850
S[223]u	0.583	−0.6	+0.1	0.975
S[223]r	0.534	−0.8	−0.4	0.903
S[239]i	0.968	−0.1	0.1	0.944
S[239]u	0.608	−1.6	0.27	0.880
S[239]g	0.999	+0.2	−0.6	0.782

region ($\theta \sim 45°$), there are 1 more expected solution than the observed in the bimodal region and there is dip at an angle 42.5° with $\sim 1.5\sigma$ error limit and hump at angle 47.5° with $\sim 1.5\sigma$ error limit. For the large angles ($> 45°$), the number of observed solutions is more by 8 than that of expected and there is no significant hump and dip in this region. The statistics of the θ-distribution (Table 16) for the sample S[223]i are found as follows: P($>\chi^2$) = 0.575, C/C(σ) = −0.6, $\Delta_{11}/\sigma(\Delta_{11})$ = −0.54, P $>(\Delta_1)$ = 0.85. All the statistical parameters suggest isotropy, supporting hierarchy model of random orientation.

The statistics of the ϕ-distribution (Table 16) for the sample S[223]i are found as follows: P($>\chi^2$) = 0.675 i.e., 67.5% (much greater than the significant level 0.050 i.e. 5.0%), C/C(σ) = −0.4 (less than the limit 1σ), $\Delta_{11}/\sigma(\Delta_{11})$ = 0.7 (smaller than the limit 1.5σ), P $>(\Delta_1)$ = 0.552 i.e., 55.2% (greater than 15% limit). All the parameters suggest isotropy.

In the azimuthal angle distribution as shown in Figure 51b, the observed solutions of central eight bins (shaded region) are found to be 1120, whereas the expected solutions are only 1105. This shows that observed solutions exceeded the expected solutions by 15. There are no significant hump and dip in the shaded and outside the shaded region. Owing to the statistics we conclude that the spin vector projections of galaxies in sample

Table 16: Statistics of the azimuthal angle (ϕ) distribution of galaxies in the Superclusters S[223+022+0117] & S[239+016+0037]. The first column represents the sample. In the Table 16, P(> χ^2) represents the chi-square probability (second column). Similarly, C/C(σ) represents the auto-correlation coefficient (third column). The last two columns give the first order Fourier coefficient $\Delta_{11}/\sigma(\Delta_{11})$ and first order Fourier probability P(> Δ_1).

Sample	P(> χ^2)	C/C(σ)	$\Delta_{11}/\sigma(\Delta_{11})$	P(> Δ_1)
S[223]i	0.675	−0.4	+0.7	0.552
S[223]u	0.091	+1.3	−0.5	0.727
S[223]r	0.606	−1.1	+0.6	0.748
S[239]i	0.394	+0.2	+0.3	0.716
S[239]u	0.279	−0.8	+0.8	0.744
S[239]g	0.675	−0.7	+0.7	0.746

S[223]i shows a random orientation.

4.4.2.2 Sample S[223]u (17.38 ≤ m_u < 28.82)

The polar angle (θ) distribution of galaxies in the sample S[223]u is shown in the Figure 52a. The number of observed solutions for $\theta < 45°$ is 1244, which is less than the number of expected solutions by 18. There is not significant dip and hump within the range. At bimodal region ($\theta \sim 45°$), the number of observed solutions are more by 7 than that of expected. For the large angles ($> 45°$), the number of observed solutions are more by 11 than that of expected and there is also no significant humps and dips. A preferred alignment is not noticed in the θ-distribution of this sample. The statistics for the θ-distribution of galaxies of this sample S[223]i are found as follows: P($>\chi^2$) = 0.583 i.e., 58.3% (greater than the significant level 0.050 i.e. 5.0%), C/C(σ) = −0.6 (smaller than 1σ limit), $\Delta_{11}/\sigma(\Delta_{11})$ = −0.1 (smaller than the limit 1.5σ) and P >(Δ_1) = 0.975 i.e., 97.5% (greater than 15% limit). All these statistics suggest strong isotropy.

In the azimuthal angle (ϕ) distribution as shown in Figure 52b, the observed solutions of central ten bins (shaded region) are found to be 1022, whereas the expected solutions are

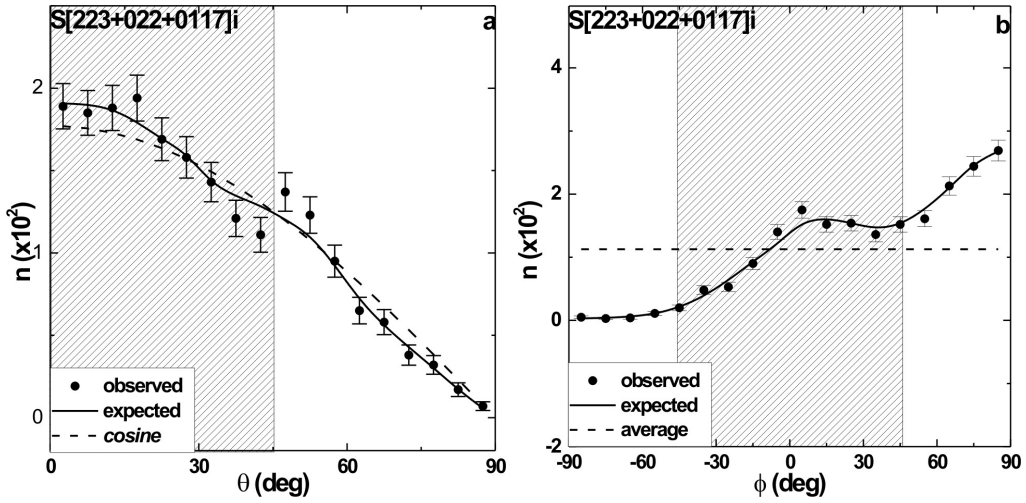

Figure 51: The polar (θ) and azimuthal angle (ϕ) distributions of galaxies in the Supercluster S[223+022+0117] having apparent magnitude in the range 14.42 to 22.64 in the i-band. The solid line represents the expected isotropic distributions. The cosine and average distributions (dashed) are shown for the comparison. The solid circles with $\pm$ 1σ error bars represent the observed distribution. Here, $\sigma = \sqrt{n}$ as suggested by Godlowski (1994).

only 1035. This shows that expected solutions exceeded the observed solutions by 13. There is a dip at an angle -25° with $\sim 1.5\sigma$ error limit and a hump at -5° with $\sim 1.5\sigma$ error limit in this region. There is no significant hump and dip outside the shaded region. Since more expected solutions than the observed in the central ten bins and negative value of first order fourier coefficient in sample S[223]u suggest that SV projections of galaxies tend to orient tangentially with respect to the center of equatorial co-ordinate system.

In the ϕ-distribution, all statistics suggest isotropy, suggesting no preferred alignments.

4.4.2.3 Sample S[223]r ($14.94 \leq m_r < 23.44$)

The statistics for the polar angle distribution in the sample S[223]r shows the value of chi-square probability (P($>\chi^2$))is 0.534, the auto-correlation coefficient (C/C(σ)) is -0.8, the first order Fourier coefficient ($\Delta_{11}/\sigma(\Delta_{11})$) is -0.4. The first order Fourier probability (P $>(\Delta_1)$) is found to be 0.903. Hence, all three statistics shows isotropy. As shown in Figure 53a, in the sample S[223]r, the number of observed solutions that have

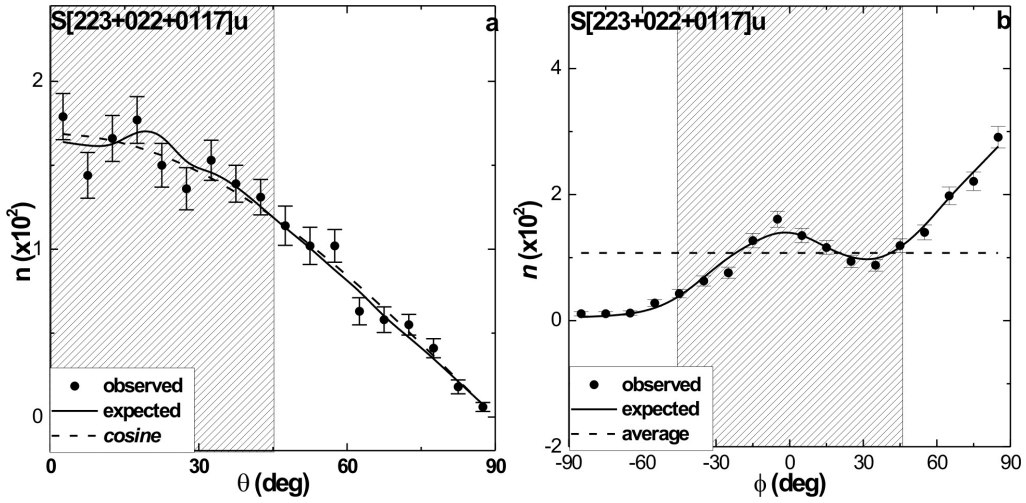

Figure 52: The polar (θ) and azimuthal angle (ϕ) distributions of galaxies in the Supercluster S[223+022+0117] having apparent magnitude in the range 17.38 to 28.82 in the u-band. The solid line represents the expected isotropic distributions. The cosine and average distributions (dashed) are shown for the comparison. The solid circles with $\pm$ 1σ error bars represent the observed distribution. Here, $\sigma = \sqrt{n}$ as suggested by Godlowski (1994).

$\theta < 45°$ is found to be 1,364, whereas the expected solutions is also 1,372. Thus, number of observed solutions are less by 8 than that of the expected. There is no significant humps and dips in the region $\theta < 45°$. At bimodal region ($\theta \sim 45°$), there are 15 more expected solutions than the observed and there is one significant dip at an angle 42.5° with $\sim 1.5\sigma$ error limit in the bimodal region. For the large angles ($> 45°$), the number of observed solutions exceed the expected by 23 and there is a hump at an angle at an angle 52.5° with $\sim 1.5\sigma$ error limit so, preferred alignment is noticed the θ-distribution. It is found that the , spin vectors of galaxies tend to be oriented perpendicular with respect to the equatorial coordinate system, supporting Primordial Vorticity theory (Ozernoy, 1978; Stein, 1974).

In ϕ- distribution except auto correlation, all four statistical parameters suggest isotropy (Table 16), indicating no preferred alignments. Anisotropy in the auto correlation is due to binning effect.

In the azimuthal angle distribution as shown in Figure 53b, the observed number solution more than the expected number of solution by 8. There is significant hump at an angle $-5°$ within $\sim 2\sigma$ error limit and a dip 35° within $\sim 1.5\sigma$ error limit in this region. There

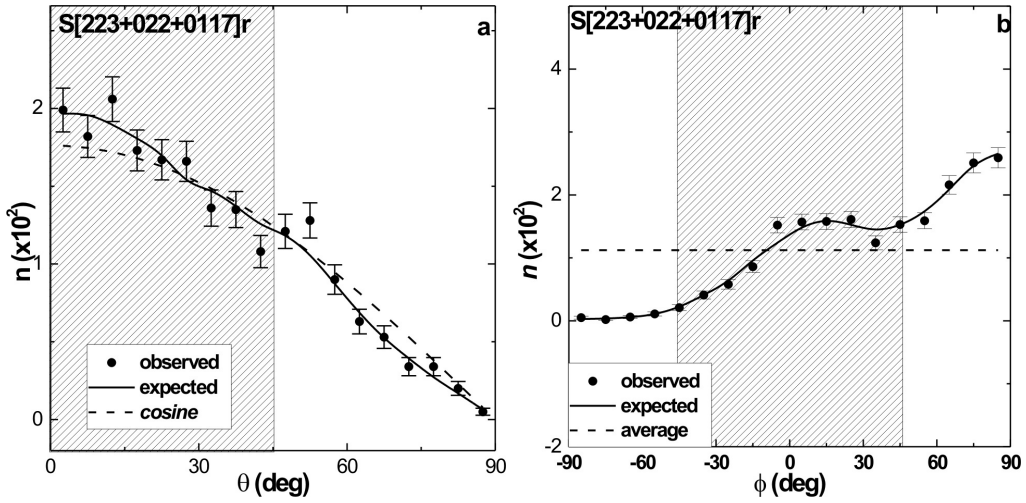

Figure 53: The polar (θ) and azimuthal angle (ϕ) distributions of galaxies in the Supercluster S[223+022+0117] having apparent magnitude in the range 14.94 to 23.44 in the r-band. The solid line represents the expected isotropic distributions. The cosine and average distributions (dashed) are shown for the comparison. The solid circles with $\pm$ 1σ error bars represent the observed distribution. Here, $\sigma = \sqrt{n}$ as suggested by Godlowski (1994).

is no significant hump and dip at outer region of shaded part. So we can conclude that the spin vector projections of galaxies in S[223]r shows a random distribution.

4.4.3 Supercluster S[239+016+0037]: Anisotropy in the Polar & Azimuthal Angle

We studied the distribution of polar (θ) and azimuthal (ϕ) angles of galaxy rotation axes in supercluster S[239+016+0037] considering i, u, g-filters.

4.4.3.1 Sample S[239]i (12.62 $\leq m_i <$ 29.45)

Figure 54a shows the polar angle (θ) distribution of total galaxies of database in the sample S[239]i. The statistics for the θ distribution of galaxies of this sample is shown in the Table 15. All these statistics advocate isotropy. In Figure 54a, the number of observed solutions for $\theta < 45°$ is 1 929, which is more than the number of expected solutions by 6. There are no any significant humps and dips in this region. At bimodal region ($\theta \sim 45°$), the number of observed solutions are more by 3 than that of expected.

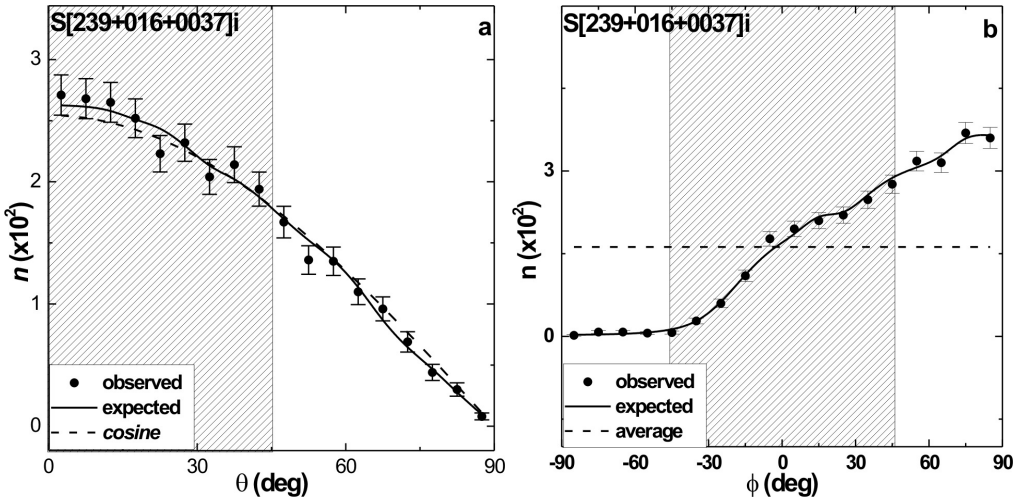

Figure 54: The polar (θ) and azimuthal angle (ϕ) distributions of galaxies in the Supercluster S[239+016+0037] having magnitude in the range 12.62 to 29.45 in i-band. The solid line represents the expected isotropic distributions. The cosine and average distributions (dashed) are shown for the comparison. The solid circles with $\pm$ 1σ error bars represent the observed distribution. Here, $\sigma = \sqrt{n}$ as suggested by Godlowski (1994).

No any significant humps and dips are observed in this region. For the large angles ($> 45^{\circ}$), the number of observed solutions are less by 9 than that of expected and also no any significant humps and dips are observed in this region. Thus, no any preferred alignment is noticed in the θ-distribution of this sample indicating random orientation of spin vector of galaxies in the sample S[239]i.

In the ϕ-distribution (Table 16) all the statistical tests suggest strong isotropy. In the azimuthal angle distribution as shown in Figure 54b, the observed solutions of central ten bins (shaded region) are found to be 1,531, whereas the expected solutions are only 1,540. This shows that expected solutions exceeded the observed solutions by 9. In this region and outside this region there are no significant humps and dips indicating SV projections of galaxies in the sample S[239]i shows a random orientation.

4.4.3.2 Sample S[239]u (15.70 $\leq m_z <$ 32.46)

The statistics for the polar angle distribution in the sample S[239]u (Table 15) shows the value of chi-square probability (P($>\chi^2$)) to be 0.608. The auto-correlation coefficient

(C/C(σ)) is found to be -1.6. The first order Fourier coefficient ($\Delta_{11}/\sigma(\Delta_{11})$) is found to be 0.27. The first order Fourier probability (P $>(\Delta_1)$) is found to be 0.888. All statistical test shows isotropy except auto-correlation test. As shown in Figure 55a, in the sample

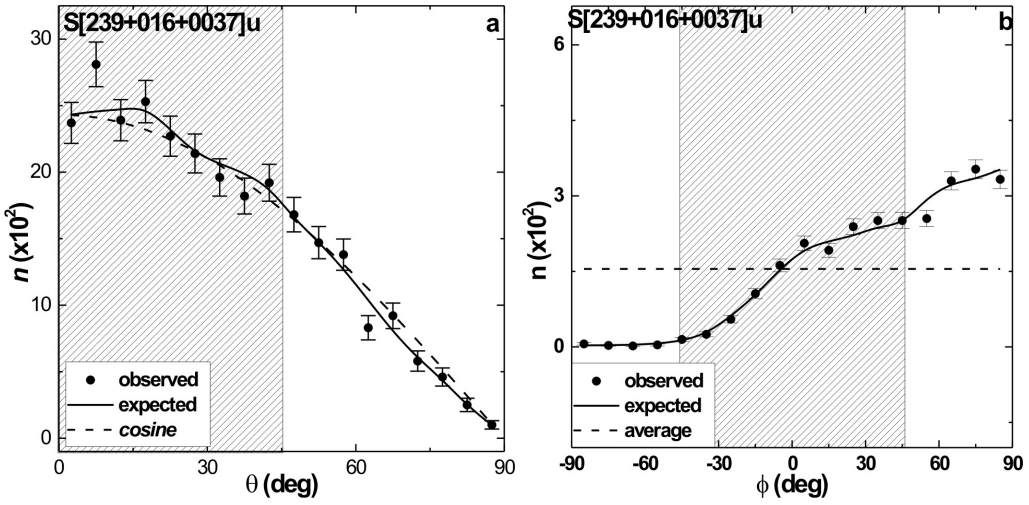

Figure 55: The polar (θ) and azimuthal angle (ϕ) distributions of galaxies in the supercluster S[239+016+0037] having magnitude in the range 15.70 to 32.46 in u-band. The solid line represents the expected isotropic distributions. The cosine and average distributions (dashed) are shown for the comparison. The solid circles with $\pm$ 1σ error bars represent the observed distribution. Here, $\sigma = \sqrt{n}$ as suggested by Godlowski (1994).

S[239]u, the number of observed solutions that have $\theta < 45°$ is found to be 8 less than expected solutions. There is significant hump at an angle 7.5° with $\sim 2\sigma$ error limit. At bimodal region ($\theta \sim 45°$), there are 6 more observed solutions than the expected. For the large angles ($> 45°$), the number of observed solutions exceed the expected by 2 and there is one dip at an angle 62.5° with $\sim 2\sigma$ error limit. These hump and dip make the value of Δ_{11} positive suggesting that SVs of galaxies in the sample S[239]u tend to lie perpendicular to the equatorial plane.

The statistics of the ϕ-distribution (Table 16) for the sample S[239]u suggests isotropy. Also humps and dips in different region and number of humps dips suggest isotropy.

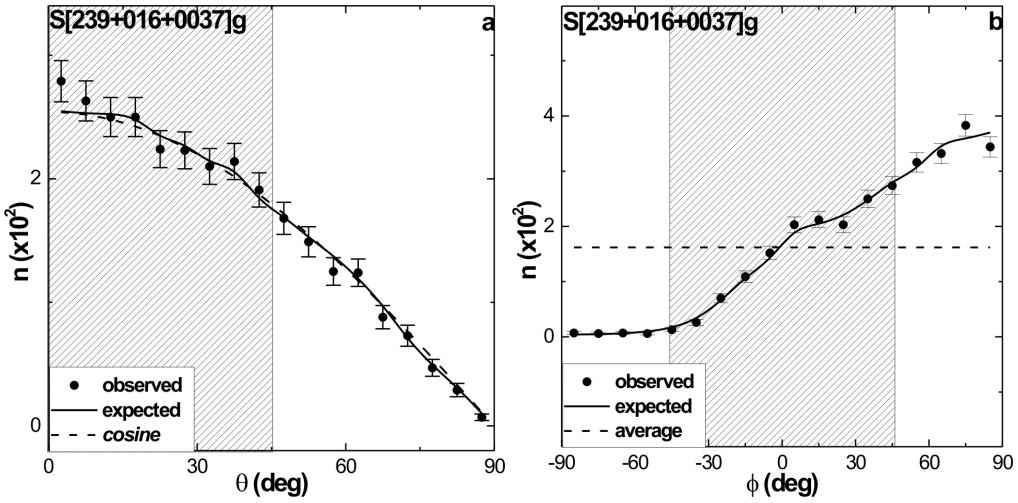

Figure 56: The polar (θ) and azimuthal angle (ϕ) distributions of galaxies in the Supercluster S[239+016+0037] having magnitude in the range 13.96 to 21.28 in g- band. The solid line represents the expected isotropic distributions. The cosine and average distributions (dashed) are shown for the comparison. The solid circles with $\pm$ 1σ error bars represent the observed distribution. Here, $\sigma = \sqrt{n}$ as suggested by Godlowski (1994).

4.4.3.3 Sample S[239]g ($13.96 \leq m_z < 21.28$)

The polar angle (θ) distribution of galaxies in the sample S[239]g is shown in the Figure 56a. The number of observed solutions for $\theta < 45°$ is 1913, which is more than the number of expected solutions by 19. There is one hump at an angle 2.5° with $\sim 1.5\sigma$ error limit. At bimodal region ($\theta \sim 45°$), the number of observed solutions are more by 8 than that of expected. For the large angles ($> 45°$), the number of expected solutions are more by 27 than that of observed and also there is no any significant hump and dip in this region. The hump at an angle 2.5° makes the first order fourier coefficient Δ_{11} negative suggesting spin vector of galaxies in in the sample S[239]g tend to lie parallel with respect to the equatorial plane.

All the statistics for the θ-distribution of galaxies of this sample suggest isotropy (Table 15).

In the azimuthal angle distribution as shown in Figure 56b, the observed solutions of central eight bins (shaded region) are exceeded the expected solutions by 6. There is no any significant hump and dip in this region and outside the region. Thus spin vector

projections of galaxies in the sample S[239]g shows a random orientation. All statistics for the ϕ-distribution of galaxies of this sample suggest isotropy (Table 16).

4.4.4 General Discussion

our results for two Superclusters S[223+022+0117] & S[239+016+0037] as follows:

(a) Supercluster S[223+022+0117]:

For sample S[223]i, distribution of galaxies shows isotropy in polar angle distribution suggesting spin vector of galaxies tend to be oriented randomly with respect of equatorial co-ordinate system. Thus galaxies in this sample supporting primordial vorticity model (Peebles, 1969). In case of azimuthal angle distribution statistical result shows isotropy i.e., spin vector projections of galaxies shows a random orientation.

Statistical result in sample S[223]u, in both azimuthal and polar angle distribution shows isotropy whereas small humps and dips are due local effects. this sample. Isotropic distribution in the *u*-filter indicates that either intergalactic medium is sufficiently hot or majority of galaxies are high energy emitter in the Supercluster.

In case of sample S[223]r, statistical result in both polar & azimuthal angle distribution shows isotropy and the galaxies in this sample supports hierarchy model. The *r*-filter is sensitive towards the all shorts of Balmer lines, i.e. capable of forming extended HII region in the galaxy but in our case we found anisotropy, this means the HII region is not capable of balancing heating & cooling process in the ISM cycle. The reason behind this should be known in the future.

We have seen some fluctuations in three different samples for Supercluster S[223+022+0117] but we a found very good agreement between expected and observed distributions for these samples. Thus we conclude that galaxies in the Supercluster S[223+022+0117] in general supports Hierarchy model (Peebles,1969).

(b) Supercluster S[239+016+0037]

In sample S[239]i, statistical test suggests isotropy in the polar angle distribution suggesting galaxies in this sample supports Hierarchy Model(Peebles, 1969). In the azimuthal angle distribution, statistical test suggests isotropy suggesting spin vector projections of

galaxies in this sample shows a random orientation. Anisotropy in *i*-magnitude shows that star formation activity in this sample is not normal similar to Sample S[223]i. In sample S[239]u, statistical result shows isotropy in the distribution of galaxies indicating abundance of stellar nursery (newly born stars, that emits UV radiation). The spin vector projection of galaxies tend to be oriented randomly. In sample S[239]g, the distribution of galaxies is isotropic supporting Hierarchy model. In this case hot HII region is very unstable, probably because of supernova activity. In this sample spin vector projections of galaxies shows a random orientation. Besides the fluctuations seen in three samples, we found very good agreement between expected and observed distributions so we can conclude that galaxies in the Supercluster S[239+016+0037] in general supports Hierarchy model.

4.4.5 Comparison with previous works

Aryal *et al*. (2008) studied core of the shapley concentration (Shapley Supercluter) and found anisotropy. Hu (2006) studied The spatial orientation of galaxy in the Local Supercluster and noticed anisotropy. Anisotropy is noticed by the Kitzbichler & Saurer (2003) while studying coma cluster. There are few works in which authors noticed isotropy (Aryal and Saurer, 2006) for the core of the Supercluster. Thus there is no consistancy in the result. It is because of the incomplete database and different morphology. Therefore, morphology of the galaxy should be understood very well. SDSS superclusters have well known morphology, classified based on the spectroscopeic database rather than photometer. We noticed mixed result; isotropy in few filter and anisotropy for others. No authors have studied SDSS superclusters. We noticed to work as SDSS supercluster in comming years in order to understand subcluster, cluster and group formation process in the superclusters and the preferred for the alignments.

4.4.6 Publication

The result of this work has been submitted to the Journal Monthly Notice of Royal Astronomical Society.

4.5 Zone-of-Avoidance Galaxies

The Zone of Avoidance (ZOA, hereafter) is the region of the sky that is obscured by the Galactic plane of the Milky Way. The dust and gas in the Milky Way cause extinction at optical wavelengths, and foreground stars can be confused with background galaxies, obstructing our view of around 20% of the extragalactic sky at visible wavelengths. Because of this, optical catalogues are usually incomplete close to the Galactic plane. In recent years, many projects (Weinberger*et al*., 1996; Huchtmeier et al., 1995; Seeberger & Saurer, 1998; Marchiotto *et al*., 1999; Marchiotto, 2000) have attempted to bridge the gap in our knowledge caused by the ZOA. The effect of extinction drops at longer wavelengths, such as the infrared, and the Milky Way is effectively transparent at radio wavelengths. Surveys in the infrared, such as the Infrared Astronomical Satellite (IRAS) survey and and Two Micron All Sky Survey (2MASS), have given us a more complete picture of the extragalactic sky. Two very large nearby galaxies, Maffei 1 and Maffei 2, were discovered in the ZOA by Paolo Maffei by their infrared emission in 1968 (Maffei, 1968). In spite of this, approximately 10% of the sky remains diffcult to survey as extragalactic objects can be confused with stars in the Milky Way. Projects to survey the ZOA at radio wavelengths, particularly using the 21-cm emission line of neutral atomic hydrogen, have detected many galaxies (e.g., Dwingeloo Galaxy 1 and Dwingeloo Galaxy 2) that could not be detected in the infrared (Ryan-Weber *et al*. 2002 and the references therein). Kerton & Brunt (2003) studied the association of CO emission with IRAS sources in the outer Galaxy using data from the FCRAO Outer Galaxy Survey (OGS). they found that of 25% of candidate ZOAGs are Galactic objects. They discovered two new far outer Galaxy star-forming regions, and six bright molecular clouds. Ryan-Weber *et al* (2002) presented 138 HIPASS BGC (Hi Parkes All-Sky Survey Bright Galaxy Catalog) galaxies that had no redshift measured prior to the Parkes multibeam Hi surveys. The majority (57) of the newly catalogued galaxies lie within 10° of the Galactic plane and are missing from optical surveys as a result of confusion with stars or dust extinction. Zone of Avoidance survey finds new Hi galaxies which lie hidden behind the Milky Way, and also provides redshifts for partially obscured galaxies known at other wavelengths. Donley *et al*. (2005) presented the results of the northern extension of the Hi Parkes Zone of Avoidance Survey, a blind Hi

survey utilizing the multibeam receiver on the Parkes 64 m telescope and detected 77 Hi galaxies, 20 of which have been previously detected in Hi. In addition, they found several filaments crossing the Galactic plane, one of which appears to be the continuation of a sine-wave-like feature that can be traced across the whole southern sky. Henning *et al*. (2010) observed two low-latitude precursor regions, totaling 138 deg2, with 72 HI galaxies.

4.5.1 Database

As the final part of the extensive Innsbruck ZOA galaxy project (e.g. Weinberger *et al*., 1995; Seeberger & Saurer, 1998; Marchiotto *et al*., 1999), Marchiotto (2000) presented the galaxy searches for the region $20^0 \leq l \leq 80^0$, $-10 \leq b \leq -5$ on first Palomar Observatory Sky Survey (hereafter POSS I). The POSS I (Reid *et al*., 1991) was carried out on the Oschin Schmidt Telescope in 1950-57 using 103aO and 103aF plates. POSS I continues to be one of the most frequently used astronomical resources; paper or glass copies of the plates are to be found in most of the world observatories and a digitized version is available on line from the Space Telescope Science Institute. Altogether 410 galaxy candidates are listed; about 5% have counterparts in the IRAS PSC. The position angle (PA) and diameters of the galaxies are available on-line1. A list of galaxies and about their distributions are given in Appendix E.

4.5.2 Anisotropy in the Polar and Azimuthal Angle Distribution

The statistics for the polar angle and azimuthal angle distribution is given in Table 17 and Table 18 respectively. In the statistics of θ, a negative value of first order Fourier coefficient suggests that the spin vectors of galaxies tend to be oriented perpendicular with respect to the equatorial coordinate system. Similarly, a positive value of first order Fourier coefficient suggests that the spin vectors of galaxies tend to be oriented parallel with respect to the equatorial coordinate system. Whereas, in the statistics of ϕ, a positive $\Delta_{11}/\sigma(\Delta_{11})$ with significant value suggests that the spin vector projections of galaxies tend to point radially with respect to the center of the equatorial coordinate system. Similarly, a significant negative value of $\Delta_{11}/\sigma(\Delta_{11})$ implies that the spin vector projection of galaxies tend to orient tangentially with respect to the equatorial coordinate

Table 17: Statistics of the polar angle (θ) of the Zone-of-Avoidance galaxies. Here ECS, GCS and SCS represent equatorial, galactic, and Supergalactic co-ordinate system, respectively. The first column represents the samples. In the table, P($> \chi^2$) represents the chi-square probability (second column). Similarly, C/C(σ) represents the auto-correlation coefficient (third column). The last two columns give the first order Fourier coefficient $\Delta_{11}/\sigma(\Delta_{11})$ and first order Fourier probability P($> \Delta_1$).

Abell	P($> \chi^2$)	C/C(σ)	$\Delta_{11}/\sigma(\Delta_{11})$	P($> \Delta_1$)
ECS	0.026	+2.886	+2.00	0.115
GCS	0.001	+4.268	+1.00	0.260
SCS	0.006	+4.470	−3.20	0.045

Table 18: Statistics of the azimuthal angle (ϕ) distribution of the Zone of Avoidance galaxies. The columns as in table 2.

Abell	P($> \chi^2$)	C/C(σ)	$\Delta_{11}/\sigma(\Delta_{11})$	P($> \Delta_1$)
ECS	0.000	−1.2	0.9	0.736
GCS	0.022	0.8	+2.4	0.150
SCS	0.001	−1.8	−1.6	0.136

system. In addition to the statistical tests, we also study the 'humps' (bins with more solutions than the expected) and 'dips' (bins with less solutions than the expected) in the polar and azimuthal angle distributions. The polar and azimuthal angle distributions of the total sample is shown in the Figure 57a and Figure 57b respectively.

4.5.3 Sample ECS

Here we discuss the polar and azimuthal angle distribution Zone of avoidance galaxies. In our database there are 410 galaxies of which diameters, right ascension, declination, position angle, galactic and super galactic longitude and latitude are known.

The statistics for the polar angle distribution of ZOA galaxies of database is given in the Table 17. All the statistics suggest weak anisotropy. The number of observed solutions

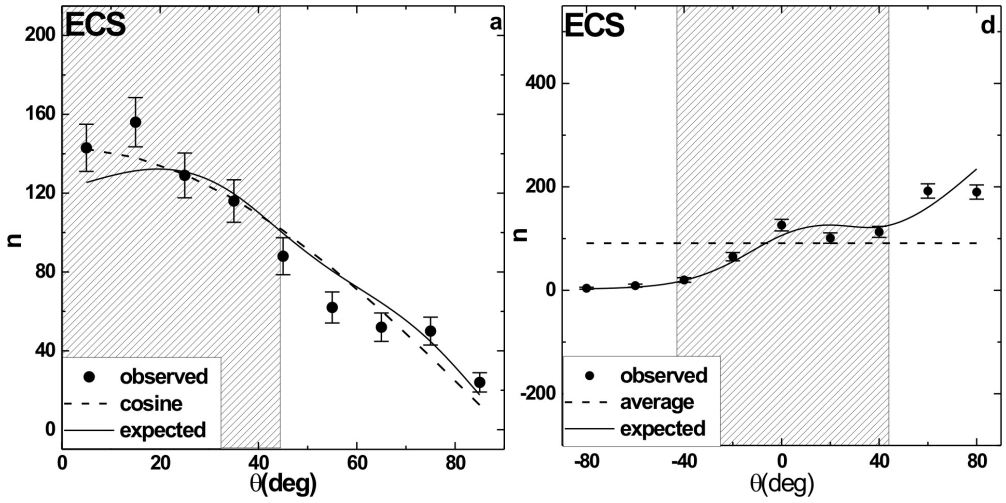

Figure 57: The polar angle (θ) and azimuthal angle (ϕ) distributions of the galaxies in the sample ECS. The solid line represents the expected isotropic distributions. The cosine and average distributions (dashed) are shown for the comparison. The solid circles with $\pm$ 1σ error bars represent the observed distribution. Here, $\sigma = \sqrt{n}$ as suggested by Godlowski (1994).

for $\theta < 45°$ is 632 and the number of expected solutions is 611. Thus number of observed galaxies is more by 21 than that of the expected. There are 11 more galaxies than the expected in the bimodal region ($\theta \sim 45°$) and the number of observed galaxies is less by 21 than that of the expected for large polar angles ($> 45°$). These observations support weak anisotropy with a alignment of spin vectors of galaxies parallel with respect to the equatorial coordinate system.

Figure 57a shows the θ distribution for the database with respect to equatorial coordinate system. There are two humps at 5° and 15° and two dips at angles 55° and 65° supports the results.

Table 18 shows the statistics for the ϕ distribution for the ECS sample. Here ,chi-square test shows anisotropy and also auto correlation test shows very weak anisotropy but Fourier test and Fourier probability suggest that the distribution is isotropy.

The ϕ distribution for the ECS sample is shown in the Figure57b. No significant humps and dips can be seen in Figure 57b.The weak anisotropy in same statistical test is due to polar statistics. Thus there is no preferred alignment of the spin vector projections of ZOA galaxies with respect to ECS is noticed.

4.5.4 Sample GCS

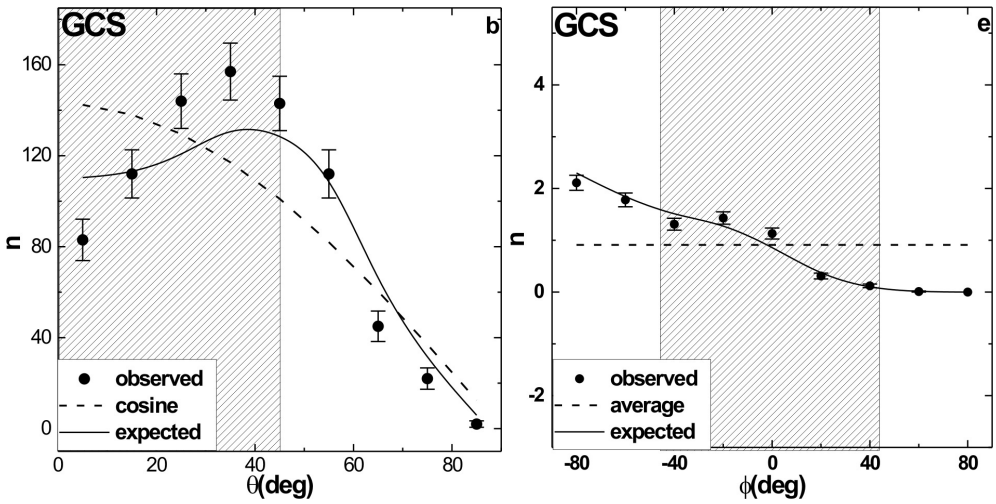

Figure 58: The polar angle (θ) and azimuthal angle (ϕ) distributions of galaxies in the sample GCS. The solid line represents the expected isotropic distributions. The cosine and average distributions (dashed) are shown for the comparison. The solid circles with $\pm$ 1σ error bars represent the observed distribution. Here, $\sigma = \sqrt{n}$ as suggested by Godlowski (1994).

Chi-square test and auto correlation test shows anisotropy of distribution with respect to GCS. But Fourier test and fourier probability suggested that the distribution is isotropy. The number of observed solutions for $\theta < 45°$ is 496 and the number of expected solutions is 476. Thus number of observed galaxies is more by 20 than that of the expected. There are 12 more galaxies than the expected in the bimodal region ($\theta \sim 45°$) and the number of observed galaxies is less by 32 than that of the expected for large polar angles ($> 45°$). These observations support isotropy no preferred alignment of spin vectors of galaxies with respect to the equatorial coordinate system. Figure 58a shows the θ distribution for the database with respect to equatorial coordinate system. In the figure humps at the middle (25°-45°) are seen These humps are compensated by dips at the smaller and larger angles,suggesting isotropy.

Table 18 shows the statistics for the ϕ distribution for the GCS sample. Here ,chi-square test shows anisotropy and also auto correlation test shows very weak isotropy but Fourier test and Fourier probability suggest that the distribution is anisotropy.

The ϕ distribution for the GCS sample is shown in the Figure 58b. Two humps at -20°

and at 0° at the middle of the histogram can be seen. Humps in the region -45° to +45° and dips at -90° -50° and 50° 90° turns the positive value of Δ_{11} in the ϕ distribution. The positive value of Δ_{11} suggest that the spin vector projection of galaxies tends to point to the galactic center.

4.5.5 Sample SCS

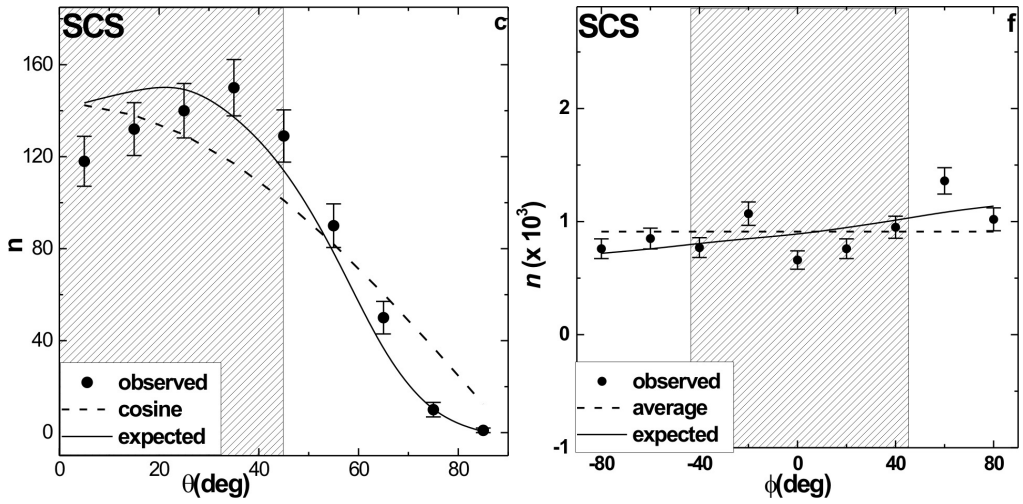

Figure 59: The polar angle (θ) and azimuthal angle (ϕ) distributions of all galaxies of the sample SCS. The solid line represents the expected isotropic distributions. The cosine and average distributions (dashed) are shown for the comparison. The solid circles with $\pm$ 1σ error bars represent the observed distribution.

Almost statistical all tests suggests that the θ distribution is anisotropy but Fourier probability suggest weak isotropy. The number of observed solutions for $\theta < 45°$ is 540 and the number of expected solutions is 583. Thus number of observed galaxies is less by 43 than that of the expected. There are 13 more galaxies than the expected in the bimodal region ($\theta \sim 45°$) and the number of observed galaxies is more by 43 than that of the expected for large polar angles ($> 45°$). These observations support anisotropy and preferred alignment of spin vectors of galaxies with respect to the super galactic coordinate system i.e, spin vectors of galaxies are perpendicular to the super galactic plane .

Figure 59a shows the θ distribution for the database with respect to galactic coordinate system . In the figure humps at larger angles (55°, 65° and 75°) can be seen (Figure 59a).

Because of these humps, the value of $\Delta_{11}/\sigma\Delta_{11}$ is found to be negative, suggesting that the SVs of galaxies tend to be oriented perpendicular to the Local Supercluster plane. Other statistical tests support this result. Thus, it is interesting that the SV orientation of ZOA galaxies support hierarchy model when analysing with respect to GCS whereas it supports pancake model (primordial vorticity model) when analyzing with respect to SCS (ECS). These inconsistencies in the preferred alignments strongly suggest the need of true physical reference system for ZOA galaxies.

Table 18 shows the statistics for the ϕ distribution for the GCS sample. In SCS, anisotropy is found in all three statistical tests. The Δ_{11} value is found to be > 1.5 error limit, suggesting a preferred alignment. SV projections of ZOA galaxies is found to be oriented perpendicular with respect to the LSC center. A significant hump at +60° supports this result (Figure 59b).

4.5.6 General Discussion

In general, we found isotropic with respect to galactic co-ordinate system and weak anisotropic with respect to equatorial and supergalactic co-ordinate system. We studied the spatial orientations of spin vector orientation of 410 Zone of Avoidance (ZOA) galaxies found in the region $20^0 \leq l \leq 80^0$, $-10^0 \leq b \leq -5^0$ on the first Palomar Observatory Sky Survey. We used the position angle - inclination method to find the three-dimensional rotation axes of galaxies. A spatially isotropic distribution is assumed to examine non-random effects. To check for anisotropy or isotropy we have carried out three statistical tests: Kolmogorov-Smirnov, Kuiper-V and the Fourier. Interestingly, all three possible scenarios (pancake-, primordial vorticity- and hierarchy model) are observed when we studied preferred alignments with respect to equatorial, Galactic and supergalactic systems. We noticed that the spin vectors orientation of ZOA galaxies tend to lie in the equatorial plane. These vectors are found to be oriented perpendicular to the Local Supercluster plane. A random alignment of spin vectors of galaxies is noticed with respect to the Galactic plane. The projections of showed a mixed picture: tend to point towards the Galactic centre and tend to be oriented perpendicular towards the LSC centre. This result clearly hints the need of suitable reference system for the ZOA galaxies. The supergalactic coordinate system is found to be most suitable among

three systems because we noticed anisotropy in both the spin vectors distributions and the distribution of spin vectors projections of galaxies. The issue of suitable physical reference system is critical while studying spatial orientation of galaxies

4.5.7 Comparison with Previous Works

No author have studied spatial orientation of Zone-of-avoidance galaxies. Through it is well known that the inter stellar extinction of this region is very high, because of this measuring true axil ratio of galaxy is a challenging task (Wenberger *et al*., 1995).

4.5.8 Publication

The result of this work has been published in the Journal Bulletin of Astronomical Society of India (BASI) in the year 2012.

4.6 Redshift Dependence

Because of the complete spectroscopic database of galaxies, we have considered redshift range 0.10 to 0.11 in order to study redshift dependence. This is the region where only a few cluster are identified in the Abell catalog. There is almost no supercluster observed in this region till date. Thus distribution of galaxies in this redshift limit (0.10 to 0.11) is homogeneous, satisfying cosmological principle. It is because of these reason, we selected this redshift limit to study the redshift dependence.

4.6.1 Database

The database used in this work consists galaxies located within the survey regions of Sloan Digital Sky Survey (SDSS) those have redshift in the range 0.10 to 0.11. Those database were searched and downloaded SDSS Data Release 7, which consists the table for the right ascension, declination, major diameter, minor diameter, position angle, five different magnitudes and redshift values of galaxies. There were 44 830 galaxies in the catalog. Among them, 81 galaxies were excluded due to the lack of the position angle. Finally we have 44 741 galaxies in our sample, of which the positions, major and minor diameters, position angles and redshifts are known.

4.6.2 Anisotropy in the Polar and Azimuthal Angle Distributions

In this section, we describe our results concerning the polar angle and azimuthal angle distributions of samples. Our whole database is divided into 200 samples. Here, we describe only 12 samples namely, Z2 ($0.10005 \leq z \leq 0.10010$), Z4 ($0.10020 \leq z \leq 0.10025$), Z10 ($0.1005 \leq z \leq 0.10055$), Z22A ($0.10110 \leq z \leq 0.10115$), Z36 ($0.10180 \leq z \leq 0.10185$), z61 ($0.10305 \leq z \leq 0.10310$), Z67 ($0.10335 \leq z \leq 0.10340$), Z72 ($0.10360 \leq z \leq 0.10365$), Z80 ($0.10400 \leq z \leq 0.10405$), Z91 ($0.10455 \leq z \leq 0.10460$), Z154 ($0.10770 \leq z \leq 0.10775$), Z175 ($0.10875 \leq z \leq 0.10880$. Result of all remaining samples are given in the appendix E. Any deviation from expected isotropic distribution will be tested using four statistical parameters, namely chi-square probability ($P > \chi^2$), autocorrelation coefficient ($C/C(\sigma)$), first order Fourier coefficient ($\Delta_{11}/\sigma(\Delta_{11})$) and first order Fourier probability ($P > \Delta_1$). For anisotropy, the limit of chi-square probability

Table 19: Statistics of the polar angle distribution of galaxies in the redshift range 0.10 to 0.11. The first column represents the sample. In the table, P(> χ^2) represents the chi-square probability (second column). Similarly, C/C(σ) represents the auto-correlation coefficient (third column). The last two columns give the first order Fourier coefficient $\Delta_{11}/\sigma(\Delta_{11})$ and first order Fourier probability P(> Δ_1).

sample	P(> χ^2)	C/C(σ)	$\Delta_{11}/\sigma(\Delta_{11})$	P(> Δ_1)
Z02	0.714	−0.8	−0.2	0.943
Z04	0.495	−0.4	0.2	0.937
Z10	0.643	−0.4	−0.1	0.954
Z22	0.416	0.4	0.4	0.915
Z36	0.145	1.5	2.3	0.052
Z61	0.927	−0.7	0.1	0.981
Z67	0.608	0.0	−0.0	0.963
Z72	0.566	0.3	−0.0	0.846
Z80	0.441	−1.5	0.7	0.753
Z91	0.013	1.0	0.2	0.788
Z154	0.674	0.5	−0.3	0.897
Z175	0.413	0.1	−0.2	0.984

P(> χ^2) is < 0.050, auto-correlation coefficient (C/C(σ)) is > 1.0, first order Fourier coefficient ($\Delta_{11}/\sigma(\Delta_{11})$) is > 1.5 and Fourier probability P(> Δ_1) is < 0.150 respectively.

The statistics for the polar angle and azimuthal angle distribution is given in Table 19 and Table 20. We have described statistical limits, interpretation about hump and dips and preferred alignments in the section 4.1.3.

4.6.3 Sample Z2 (0.10005 ≤ z < 0.10010)

Here we discuss the polar and azimuthal angle distribution galaxies of the redshift range 0.10005 to 0.10010. In the sample Z2 there are 454 galaxies of which diameters, position angle and position are known.

The statistics for the polar angle distribution of total galaxies of database is given in the

Table 20: Statistics of the azimuthal angle distribution of galaxies in the redshift range 0.10 to 0.11. The first column represents the sample/subsamples. In the table, P($> \chi^2$) represents the chi-square probability (second column). Similarly, C/C(σ) represents the auto-correlation coefficient (third column). The last two columns give the first order Fourier coefficient $\Delta_{11}/\sigma(\Delta_{11})$ and first order Fourier probability P($> \Delta_1$).

sample	P($> \chi^2$)	C/C(σ)	$\Delta_{11}/\sigma(\Delta_{11})$	P($> \Delta_1$)
Z02	0.268	0.4	0.9	0.507
Z04	0.574	1.2	2.0	0.053
Z10	0.960	−0.1	0.6	0.578
Z22	0.859	−0.1	−0.1	0.995
Z36	0.369	0.3	1.0	0.527
Z61	0.929	−0.2	0.7	0.609
Z67	0.396	−1.3	0.3	0.853
Z72	0.504	1.1	−1.9	0.121
Z80	0.677	0.4	1.9	0.126
Z91	0.882	0.1	1.7	0.250
Z154	0.998	−0.3	0.3	0.945
Z175	0.936	0.5	0.1	0.996

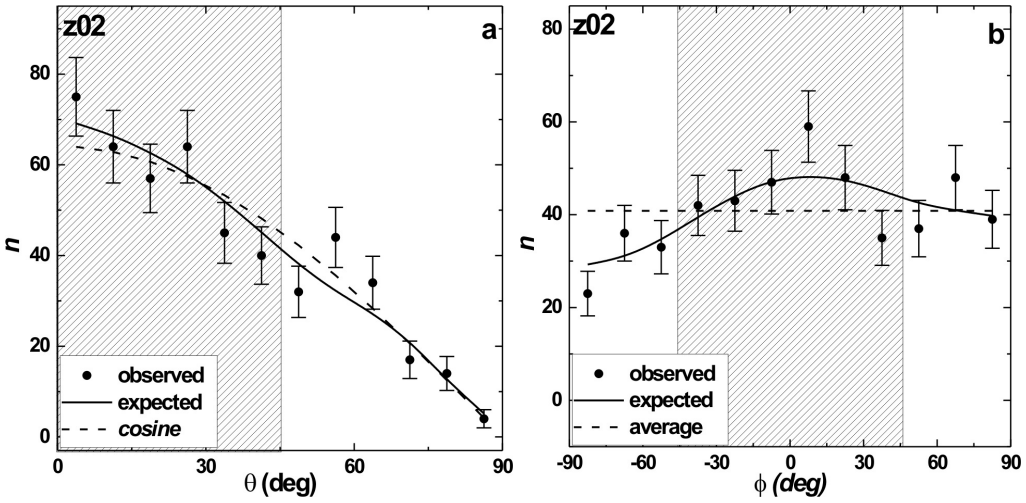

Figure 60: The polar angle (θ) and azimuthal angle (ϕ) distributions of redshift range 0.10005 to 0.10010. The solid line represents the expected isotropic distributions. The cosine and average distributions (dashed) are shown for the comparison. The solid circles with $\pm$ 1σ error bars represent the observed distribution.

Table 19. The statistics for the polar angle distribution in this sample shows the value of chi-square probability (P($>\chi^2$)) to be 0.7142, (greater than the 5.0% significant level). The auto-correlation coefficient (C/C(σ)) is found to be -0.8243 (less than 1.15σ limit). The first order Fourier coefficient ($\Delta_{11}/\sigma(\Delta_{11})$) is found to be -0.1982 (smaller than the limit 1.5σ). The first order Fourier probability (P $>(\Delta_1)$) is found to be 0.9434, (greater than 15% limit). All statistical tests suggest strong isotropy.

Figure 60a shows the θ distribution for the Z2 sample ($0.10005 \leq z \leq 0.10010$). The number of observed and expected solutions that have $\theta < 45°$ is found to be 316 and 317 respectively, which suggest a balance between observed and expected no. as a whole. There is no any significant hump and dip in this region. At bimodal region ($\theta \sim 45°$), there are 3 less observed solutions than the expected in the bimodal region. For the large angles ($> 45°$), the number of observed solutions is more by 5 than that of expected and there is a no any significant dip and hump in this region . Thus, we conclude no preferred alignment of spin vectors of galaxies.

The statistics of the ϕ-distribution for the sample Z2 are found as follows: P($>\chi^2$) = 0.2676 i.e., 26.76% (much greater than the significant level 0.050 i.e. 5.0%), C/C(σ) = -0.4240 (less than the limit 1.15σ), $\Delta_{11}/\sigma(\Delta_{11}) = -0.9131$ (less than the limit 1.5σ), P $>(\Delta_1)$ = 0.5069 i.e., 50.69% (greater than 15% limit). All these statistics suggest

isotropy.

In the azimuthal angle distribution as shown in Figure 60b, the observed solutions of central eight bins (shaded region) are found to be 291, whereas the expected solutions are 274. This shows that expected solutions exceeded the observed solutions by 7. In this region, one dip at an angle 35° is observed with $\sim 1\sigma$ error limit. But there is hump at 5° which balance the dip. Outside the shaded part, there is no any significant humps and dips. Here, for first four bins number of observed solution is 6 more than expected and for last four bins number of observed solutions is 7 more than the expected solutions. These deviation do not lead preferred alignments in the statistical tests. Thus, no preferred alignments of spin vectors of galaxies in the sample.

4.6.4 Sample Z4 ($0.10020 \leq z < 0.10025$)

Here, we discuss the polar and azimuthal angle distribution galaxies of the redshift range 0.10020 to 0.10025. In our database there are 478 galaxies in the sample of which diameter, position angle and position are known.

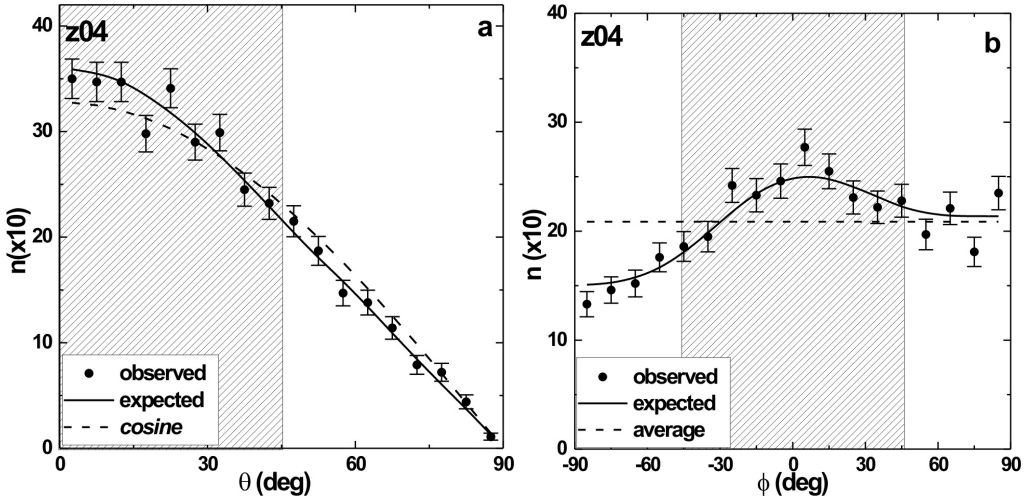

Figure 61: The polar angle (θ) and azimuthal angle (ϕ) distributions of galaxies having redshift range 0.10020 to 0.10025. The solid line represents the expected isotropic distributions. The cosine and average distributions (dashed) are shown for the comparison. The solid circles with $\pm\ 1\sigma$ error bars represent the observed distribution. Here, $\sigma = \sqrt{n}$ as suggested by Godlowski (1994).

The statistics for the polar angle distribution of total galaxies of database is given in the

Table 19. The statistics for the polar angle distribution in this sample shows the value of chi-square probability (P($>\chi^2$)) to be 0.495, (greater than the 5.0% significant level). The auto-correlation coefficient (C/C(σ)) is found to be -0.4 (less than 1.15σ limit). The first order Fourier coefficient ($\Delta_{11}/\sigma(\Delta_{11})$) is found to be -0.2 (smaller than the limit 1.5σ). The first order Fourier probability (P $>(\Delta_1)$) is found to be 0.943, (greater than 15% limit). All statistical tests suggest isotropy.

Figure 61a shows the θ distribution for the Z2 sample ($0.10005 \leq z \leq 0.10010$). The number of observed solution that have $\theta < 45^\circ$ is greater by 2 than expected which suggest a balance between observed and expected no. as a whole. There is no any significant hump and dip in this region. At bimodal region ($\theta \sim 45^\circ$), there are 2 less observed solutions than the expected . For the large angles ($> 45^\circ$), the number of observed solutions is less by 1 than that of expected and there is a no any significant dip and hump in this region. Thus, we conclude no preferred alignment of spin vectors of galaxies.

The statistics of the ϕ-distribution (Table 20) for the sample z2 are found as follows: P($>\chi^2$) = 0.574, (much greater than the 5.0% significant level), C/C(σ) = 1.2 (slightly greater than the limit 1.15σ), $\Delta_{11}/\sigma(\Delta_{11})$ = 2.0 (greater than the limit 1.5σ), P $>(\Delta_1)$ = 0.0532, (less than 15% limit). All these statistics suggest anisotropy except chi-square probability.

In the azimuthal angle distribution as shown in Figure 61b, the observed solutions of central eight bins (shaded region) are found to be 290, whereas the expected solutions are 270. This shows that expected solutions exceeded the observed solutions by 20. In this region, one dip at an angle 0° is observed with $\sim 1\sigma$ error limit. Outside the shaded part, there is also one dip at 75° is observed with $\sim 1\sigma$ error limit. Here, for first four bins number of observed solution is 15 less than expected and for last four bins number of observed solutions is 5 less than the expected solutions. Isotropy in polar angle distribution and anisotropy in azimuthal angle suggested that the reference equatorial co-ordinate system is not suitable for the sample.

4.6.5 Sample Z10 ($0.10050 \leq z < 0.10055$)

All the statistics for the θ-distribution of galaxies of this sample suggests isotropy (Table 19). The polar angle (θ) distribution of galaxies in the sample z10 is shown in the Figure 62a. The number of observed solutions for $\theta < 45°$ is less than the number of expected solutions by 2. There is no any significant hump and dip in this region. At bimodal region ($\theta \sim 45°$), the observed solution is more than expected by 5 and observed expected distribution agree within $\pm\ 1\sigma$ error limit. For the large angles ($> 45°$), the number of observed solutions are less by 3. Also there is no any significant hump and dip in the region. All statistical tests,number of observed and expected distribution and humps and dips shows that the distribution is strong isotropy. That means spin vector of galaxies are randomly distributed.

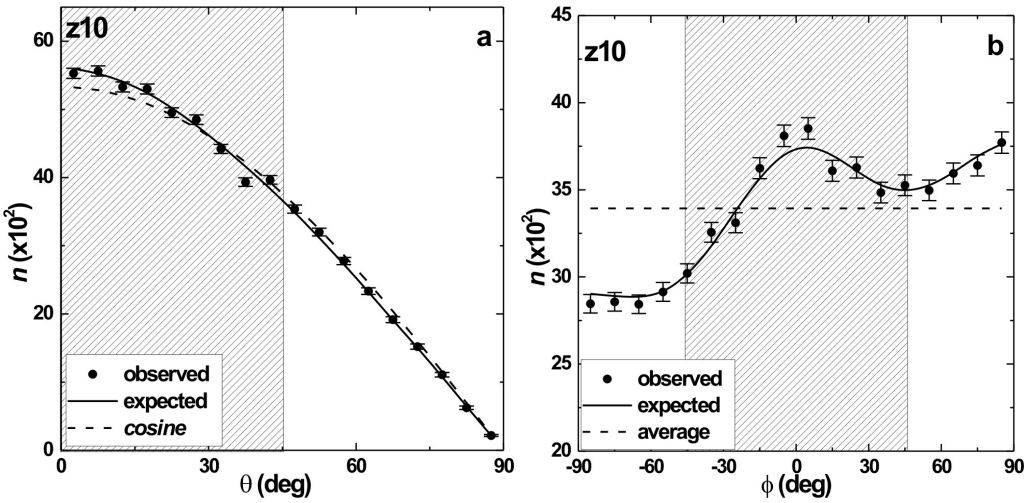

Figure 62: The polar angle (θ) and azimuthal angle (ϕ) distributions of galaxies that have redshift in the range 0.10050 and 0.10055. The solid line represents the expected isotropic distributions. The cosine and average distributions (dashed) are shown for the comparison. The solid circles with $\pm\ 1\sigma$ error bars represent the observed distribution. Here, $\sigma = \sqrt{n}$ as suggested by Godlowski (1994).

Similar to polar angle all statistics suggest strong isotropy in the ϕ distributions. In the azimuthal angle (ϕ) distribution as shown in Figure 62b, the observed solutions of central eight bins (shaded region) exceeded the expected solutions by 5. There is no any significant hump and dip in this region and also outside the shaded part. Thus, no preferred alignment is noticed in this sample.

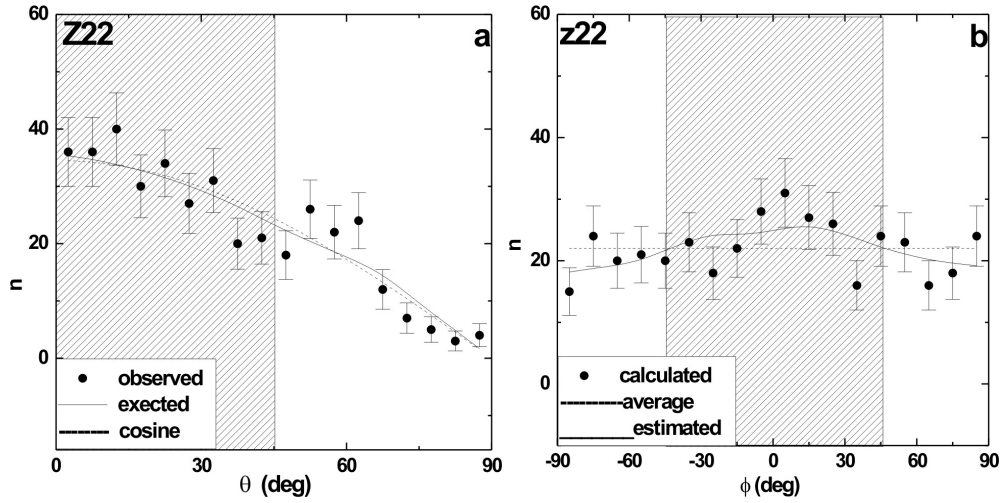

Figure 63: The polar angle (θ) and azimuthal angle (ϕ) distributions of galaxies that have redshift in the range 0.10110 and 0.10115. The solid line represents the expected isotropic distributions. The cosine and average distributions (dashed) are shown for the comparison. The solid circles with ± 1σ error bars represent the observed distribution. Here, $\sigma = \sqrt{n}$ as suggested by Godlowski (1994).

4.6.6 Sample Z22 (0.10110 ≤ z < 0.10115)

The statistics for the θ-distribution of galaxies of this sample are found as follows: P($>\chi^2$)= 0.4164 (greater than the 5.0% significant level), C/C(σ)= -0.3538 (smaller than 1.15σ limit), $\Delta_{11}/\sigma(\Delta_{11})$= −0.3800 (smaller than the limit 1.5σ) and P >(Δ_1)= 0.9153,(greater than 15% limit). All the statistics suggest isotropy.

The polar angle (θ) distribution of galaxies (Figure 63a) shows a very good agreement between observed and expected distributions. All statistic tests support strong isotropy in the ϕ-distributions as in the θ-distribution (Table 19). Therefore, no preference in the galaxy alignment is noticed.

There is a good agreement between the observed and expected distributions. No significant hump and dip is found, suggesting random alignment of spin vector of galaxies (Figure 63b)

4.6.7 Sample Z36 (0.10180 ≤ z < 0.10185)

The statistics for the θ-distribution of galaxies of this sample are found as follows: P($>\chi^2$) = 0.1454 i.e., 14.54% (slightly greater than the significant level 0.050 i.e. 5.0%), C/C(σ) = 1.4980 (larger than 1.15σ limit), $\Delta_{11}/\sigma(\Delta_{11})$ = 2.3427 (larger than the limit 1.5σ) and P >(Δ_1) = 0.0518 i.e., 5.18% (less than 15% limit).Except chi-square probability all statistical test suggest anisotropy.

The polar angle (θ) distribution of galaxies in the sample z36 is shown in Figure 64. The number of observed solutions for θ < 45° is more than the number of expected solutions by 35. A significant humps can be seen at 7.5° and 32.5° at > 1.5σ level in this region. For the large angles (> 45°), the number of observed solutions are less by 25. A significant dips can be seen at 72.5°, at 62.5° and 57.5.5° at > in this region. Almost all statistical tests, number of observed and expected distribution and humps and dips shows that the distribution is anisotropy and spin vector are parallel to the reference plane, supporting pancake model as suggested by Shandarin *et al*. (1978).

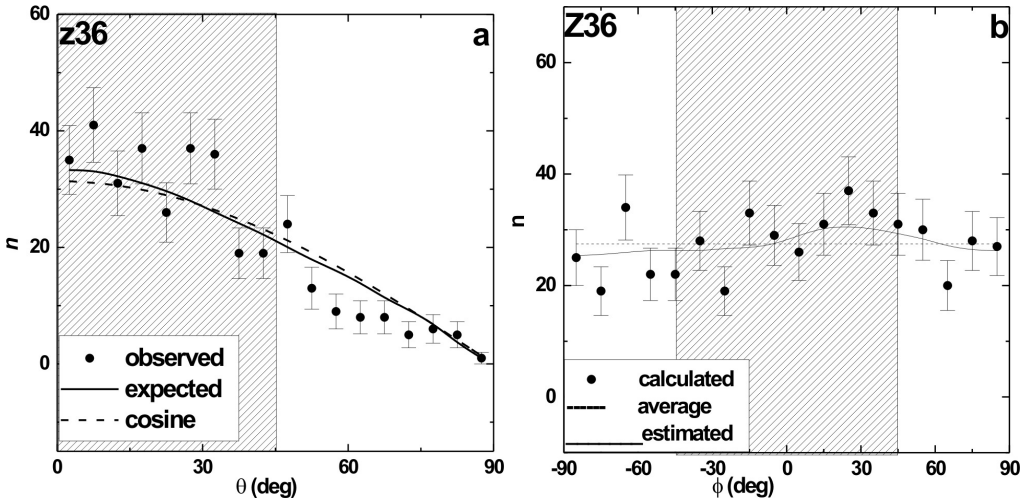

Figure 64: The polar angle (θ) and azimuthal angle (ϕ) distributions of galaxies that have redshift in the range 0.10180 and 0.10185. The solid line represents the expected isotropic distributions. The cosine and average distributions (dashed) are shown for the comparison. The solid circles with ± 1σ error bars represent the observed distribution. Here, $\sigma = \sqrt{n}$ as suggested by Godlowski (1994).

In the azimuthal angle (ϕ) distribution, all statistical tests show isotropy. This indicates the relevancy of equations Co- ordinate system for the distant galaxies.

In the azimuthal angle (ϕ) distribution, the observed solutions of central eight bins (shaded region) exceeded the expected solutions by 6. There is no any significant hump and dip in this region and also outside the shaded part. Thus, no preferred alignment is noticed in this sample.

4.6.8 Sample Z61 (0.10305 ≤ z < 0.10310)

In θ-distribution of galaxies of this sample all statistical test suggest that the distribution is isotropy, indicating a random alignments. The polar angle (θ) distribution of galaxies in the sample Z61 is shown in the Figure 65a. The number of observed solutions for $\theta <$ 45° is more than the number of expected solutions by 2. There is no any significant hump and dip in this region. For the large angles (> 45°), the number of observed solutions are less by 6. Also there is no any significant hump and dip in the region. Therefore, spin vector of galaxies of this sample are randomly distributed.

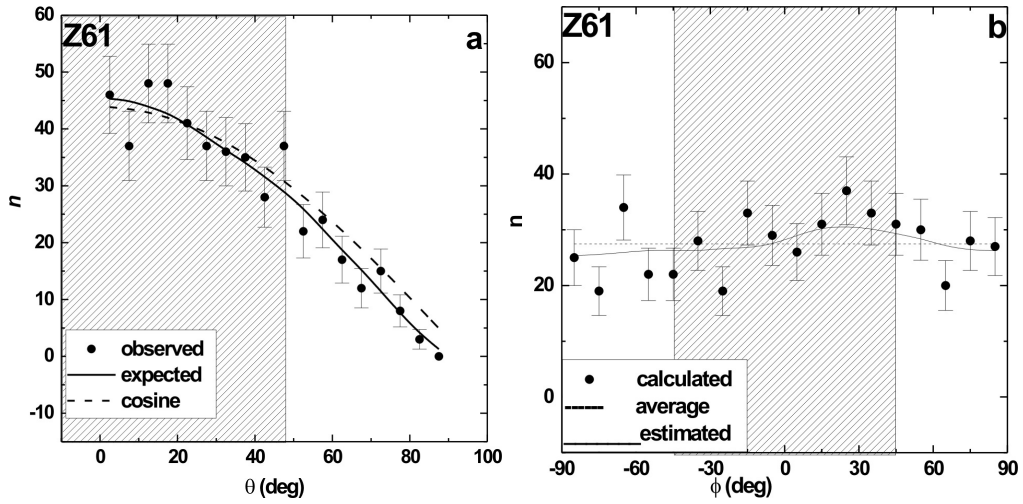

Figure 65: The polar angle (θ) and azimuthal angle (ϕ) distributions of galaxies that have redshift in the range 0.10305 and 0.10310. The solid line represents the expected isotropic distributions. The cosine and average distributions (dashed) are shown for the comparison. The solid circles with ± 1σ error bars represent the observed distribution. Here, $\sigma = \sqrt{n}$ as suggested by Godlowski (1994).

The statistics of the ϕ distribution for the sample similar to polar angle distribution suggest isotropy. In the azimuthal angle (ϕ) distribution as shown in Figure 65b, the observed solutions of central eight bins (shaded region) exceeded the expected solutions

by 6. There is no any significant hump and dip in this region and also outside the shaded part . Thus, no preferred alignment is noticed in this sample.

4.6.9 Sample Z67 ($0.10335 \leq z \leq 0.10340$)

All statistics for the θ-distribution of galaxies of the sample Z67 suggest that the distribution is isotropy (Table 19). Thus spin vectors are randomly distribution. The polar angle (θ) distribution of galaxies in the sample Z67 is shown in the Figure 66a. The number of observed and expected solutions for $\theta < 45^{\circ}$ same. That means spin vector of galaxies are randomly distributed. Therefore, vanishing angular momentum can be expected.

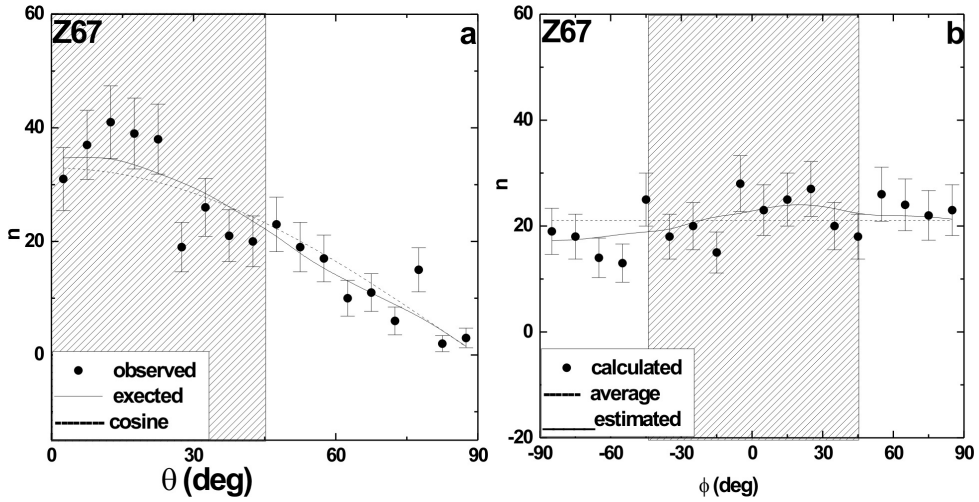

Figure 66: The polar angle (θ) and azimuthal angle (ϕ) distributions of galaxies that have redshift in the range 0.10335 and 0.10340 (Sample Z67). The solid line represents the expected isotropic distributions. The cosine and average distributions (dashed) are shown for the comparison. The solid circles with $\pm$ 1σ error bars represent the observed distribution. Here, $\sigma = \sqrt{n}$ as suggested by Godlowski (1994)

All statistical tests of the ϕ distribution for the sample suggest isotropy. In the azimuthal angle (ϕ) distribution as shown in Figure 66b, the observed solutions of central eight bins (shaded region) exceeded the expected solutions by 6. There is no any significant hump and dip in this region and also outside the shaded part. Thus, no preferred alignment is noticed in this sample.

4.6.10 Sample Z72 ($0.10360 \leq z < 0.10365$)

All the statistics for the $\theta-$distribution of galaxies of this sample suggests isotropy (Table 19). The polar angle (θ) distribution of galaxies in the sample Z72 is shown in the Figure 67a. The number of observed solutions and expected solution have good agreement in all region. Also there is no any significant hump and dip in the region. All statistical tests, number of observed and expected distribution and humps and dips shows that the distribution is strong isotropy. That means spin vector of galaxies are randomly distributed.

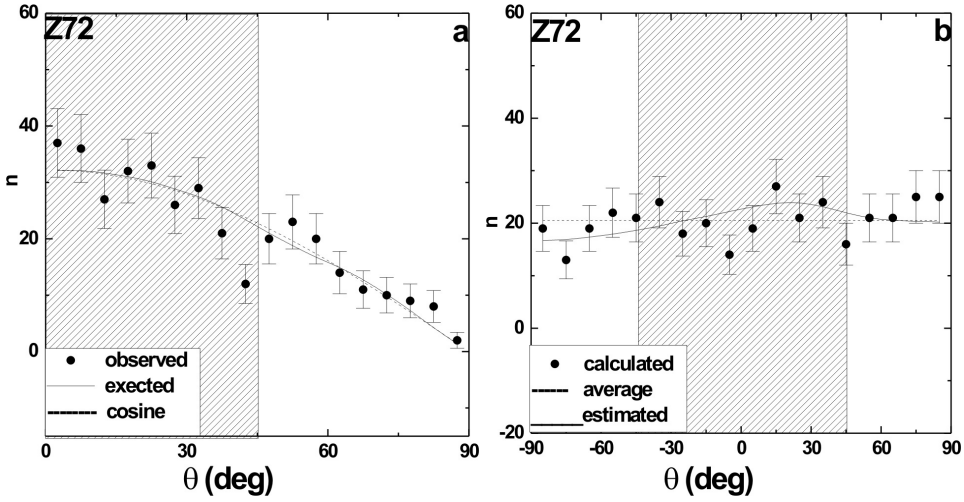

Figure 67: The polar angle (θ) and azimuthal angle (ϕ) distributions of galaxies in that have redshift in the range 0.10360 and 0.10365. The solid line represents the expected isotropic distributions. The cosine and average distributions (dashed) are shown for the comparison. The solid circles with $\pm$ 1σ error bars represent the observed distribution. Here, $\sigma = \sqrt{n}$ as suggested by Godlowski (1994).

The statistics of the ϕ distribution for the sample are found as: P($>\chi^2$) = 0.5044 (greater than the significant level 0.050), C/C(σ) = –1.0666 (slightly more than the limit 1σ), $\Delta_{11}/\sigma(\Delta_{11})$ =−1.9066 (less than the limit 1.5σ), P $>(\Delta_1)$ = 0.1207 (less than 0.15). Except chi-square test all statistical test suggest anisotropy in azimuthal angle distribution. The anisotropy in azimuthal angles distribution suggest less reliability of choosen reference co-ordinate system.

In the azimuthal angle (ϕ) distribution as shown in Figure 67b, the observed solutions of central eight bins (shaded region) exceeded the expected solutions by 6. Thus, no

preferred alignment is noticed in this sample.

4.6.11 Sample Z80 (0.10400 ≤ z < 0.10405)

The statistics for the θ-distribution of galaxies of this sample are found as follows: P($>\chi^2$)= 0.4408, (greater than the 5.0% significant level), C/C(σ) = -1.5 (smaller than 1.15σ limit), $\Delta_{11}/\sigma(\Delta_{11})$ = 0.7 (smaller than the limit 1.5σ) and P >(Δ_1) = 0.7527 (greater than 15% limit). Accept auto-correlation test all statistical test suggest that polar angle distribution is isotropy. An isotropy in polar angle suggest binning effect.

The polar angle (θ) distribution of galaxies in the sample Z80 is shown in the Figure 68a. The number of observed solutions for $\theta < 45°$ is more than the number of expected solutions by 1. There is no any significant hump and dip in this region. For the large angles (> 45°), the number of observed solutions are more by 5. Also there is no any significant hump and dip in the region. All these result suggest the distribution is isotropy. This suggest that spin vector of galaxies are randomly distributed.

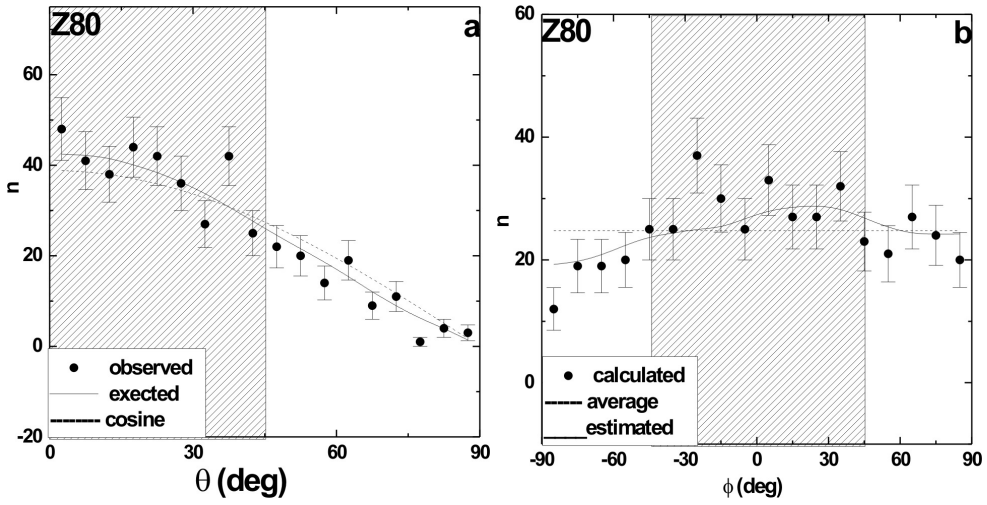

Figure 68: The polar (θ) and azimuthal angle (ϕ) distributions of galaxies that have redshift in the range 0.10400 and 0.10405. The solid line represents the expected isotropic distributions. The cosine and average distributions (dashed) are shown for the comparison. The solid circles with ± 1σ error bars represent the observed distribution. Here, $\sigma = \sqrt{n}$ as suggested by Godlowski (1994).

The statistics of the ϕ distribution for the sample are found as: P($>\chi^2$) = 0.6768 (greater than the significant level 0.050), C/C(σ) = 0.3813 (less than the limit 1σ), $\Delta_{11}/\sigma(\Delta_{11})$

= 1.8551 (less than the limit 1.5σ), P $>(\Delta_1)$ = 0.1257 (less than 15 % limit). There is mixed result in the statistical test. The chi-square test and auto-correlation test suggest isotropy while first order Fourier coefficient and Fourier probability suggest anisotropy.

In the azimuthal angle (ϕ) distribution as shown in Figure 68b, the observed solutions of central eight bins (shaded region) exceeded the expected solutions by 6. There is no any significant hump and dip in this region and also outside the shaded part . Thus, no preferred alignment is noticed in this sample.

4.6.12 Sample Z91 ($0.10455 \leq z < 0.10460$)

The polar angle distribution of galaxies in the sample z91 is shown in Figure 69a and the statistical tests in the table 19. All the statistical tests suggest the polar angle is isotropy. Thus , spin vectors are randomly oriented with respect to equatorial co-ordinate system.

The number of observed solutions and the expected solutions have good agreement. Also no significant dips can be seen at any angles. This strongly support the statistical results.

The statistics of the ϕ distribution for the sample Z91 are found as: P($>\chi^2$) = 0.882 (greater than the significant level 0.050), C/C(σ) = 0.1 (less than the limit 1σ), $\Delta_{11}/\sigma(\Delta_{11})$ = 1.7 (greater than the limit 1.5σ), P $>(\Delta_1)$ = 0.250 i.e. 16.5% (greater than 15 % limit). The Chi-square probability (P($>\chi^2$)), Auto-correlation Coefficient C/C(σ) and the Fourier probability (P($>\Delta_1$)) supports isotropy. But, the value of $\Delta_{11}/\sigma(\Delta_{11})$ put forward the idea of local anisotropy.

Figure 69b shows azimuthal angle distribution of galaxies in the sample Z91. Several humps and dips are seen. Two humps are seen at angles -75° and $+25^\circ$. In addition, two dips are observed at angles -65° and -35°. Thus, a random orientation of spin vector projection of galaxies with respect to the equatorial coordinate system is found in the sample.

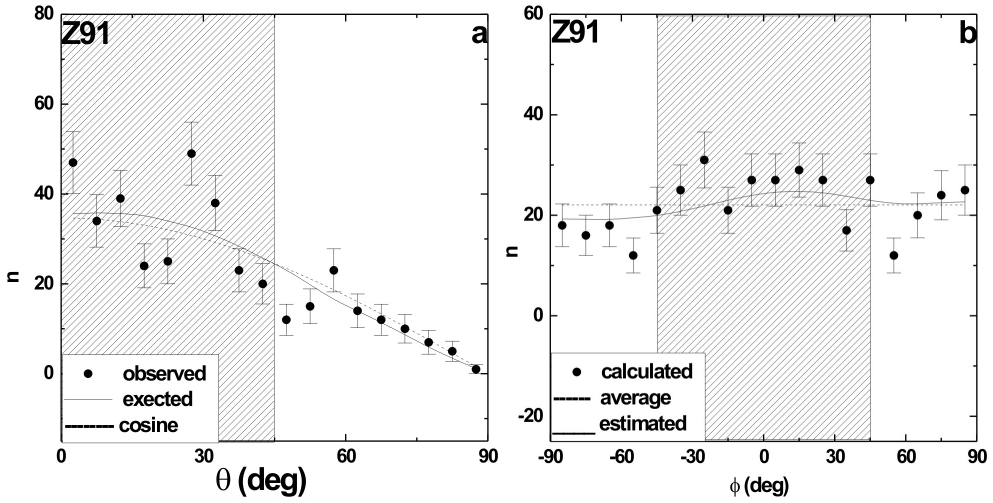

Figure 69: The polar (θ) and azimuthal angle (ϕ) distributions of galaxies that have redshift in the range 0.10455 and 0.10460. The solid line represents the expected isotropic distributions. The cosine and average distributions (dashed) are shown for the comparison. The solid circles with $\pm$ 1σ error bars represent the observed distribution. Here, $\sigma = \sqrt{n}$ as suggested by Godlowski (1994).

4.6.13 Sample Z154 (0.10770 $\leq$ z $<$ 0.10775)

The statistics for the θ distribution of galaxies of this sample is shown in the Table 19. All statistics for the polar angle distribution in this sample shows isotropy in polar angle distribution. Thus spin vectors of galaxies are randomly oriented.

In the polar angle distribution of galaxies of this sample (Figure 70a), no any significant humps are seen for smaller angles ($\theta > 45°$) and larger angles ($\theta > 45°$). Also these is very good agreement between expected number of solutions and observed number of solution. Thus, we conclude that the spin vectors of galaxies in this sample randomly oriented with respect to the equatorial coordinate system.

In the azimuthal angle distribution of the galaxies of this sample (Figure 70b), there are no significant dips in all the first four and last four bins. Also, no significant humps/ dips are seen in almost all the central eight bins. These observations suggests that the projections of the galaxies tend to be oriented randomly.

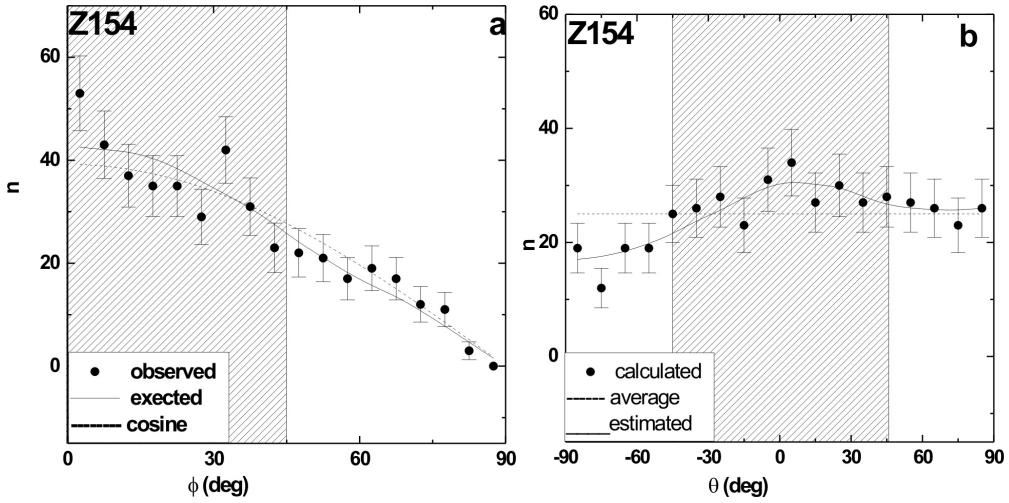

Figure 70: The polar (θ) and azimuthal angle (ϕ) distributions of galaxies that have redshift in the range 0.10770 and 0.10775. The solid line represents the expected isotropic distributions. The cosine and average distributions (dashed) are shown for the comparison. The solid circles with $\pm$ 1σ error bars represent the observed distribution. Here, $\sigma = \sqrt{n}$ as suggested by Godlowski (1994).

4.6.14 Sample Z175 (0.10875 $\leq$ z $<$ 0.10880)

The statistics for the θ distribution of galaxies of this sample is shown in the Table 19. All the statistics suggest isotropy. Thus,spin vectors of the galaxies are randomly oriented.

In the polar angle distribution of galaxies of this sample (Figure 71a),only one significant hump is seen at angles 17.5° with $>$ 1.5σ error limit for the smaller angle range ($\theta <$ 45°).In these bins the number of observed solutions are less by 6 than that of expected. Also, for the large angles ($\theta >$ 45°) the number of observed solutions is greater than the expected by 5. There is no any significant humps and dips in this range. Thus, we conclude that the spin vectors of galaxies in this sample randomly oriented.

In the azimuthal angle distribution of the galaxies of this sample (Figure 71b), there are no significant dips in all the first four and last four bins. Also, no significant humps are seen in almost all the central eight bins. Observations suggests that the projections of the galaxies randomly oriented with respect to equatorial co-ordinate system.

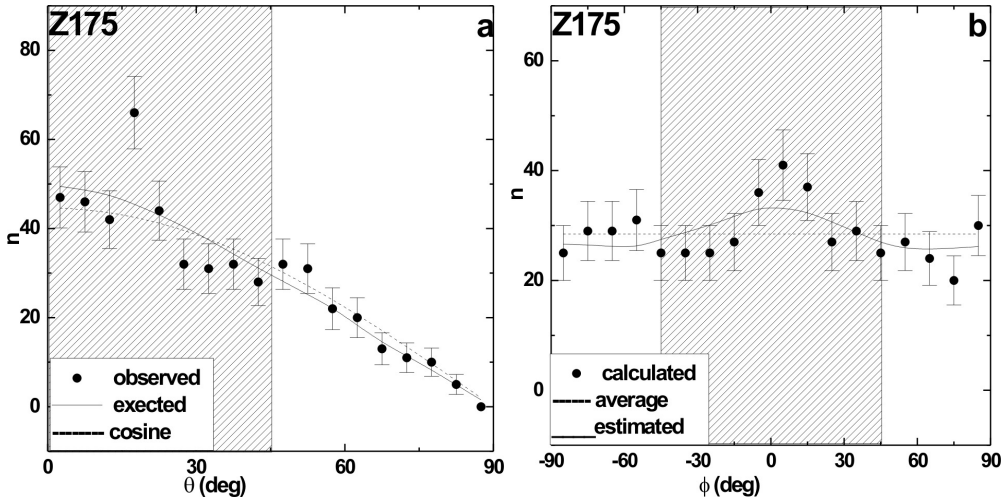

Figure 71: The polar (θ) and azimuthal angle (ϕ) distributions of galaxies in that have redshift in the range 0.10875 and 0.10880. The solid line represents the expected isotropic distributions. The cosine and average distributions (dashed) are shown for the comparison. The solid circles with $\pm$ 1σ error bars represent the observed distribution. Here, $\sigma = \sqrt{n}$ as suggested by Godlowski (1994).

4.6.15 General Discussion

There was 200 sample of which only one sample Z36 shows weak anisotropy in the Fourier test for θ distributions. Remaining all samples shows isotropy, suggesting vanishing angular momentum. Therefore, hierarchy model is most preferred. In one sample (Z36) pancake model is noticed. This might be because of the presence of clusters or Superclusters in the region. Figure 72 represents the scatter plot of redshift (z) versus $\Delta_{11}/\sigma(\Delta_{11})$ for (a) polar angle and (b) azimuthal angle distributions for the samples. As we know that the preferred orientation of galaxies can be studied by the parameter $\Delta_{11}/\sigma(\Delta_{11})$. In the figure, grey shaded and dashed region represent the region of isotropy and week anisotropy in both the polar and azimuthal angle distributions. This suggest that the alignment of galaxies is independent of the value of redshift z, supporting hierarchy model of galaxy formation.

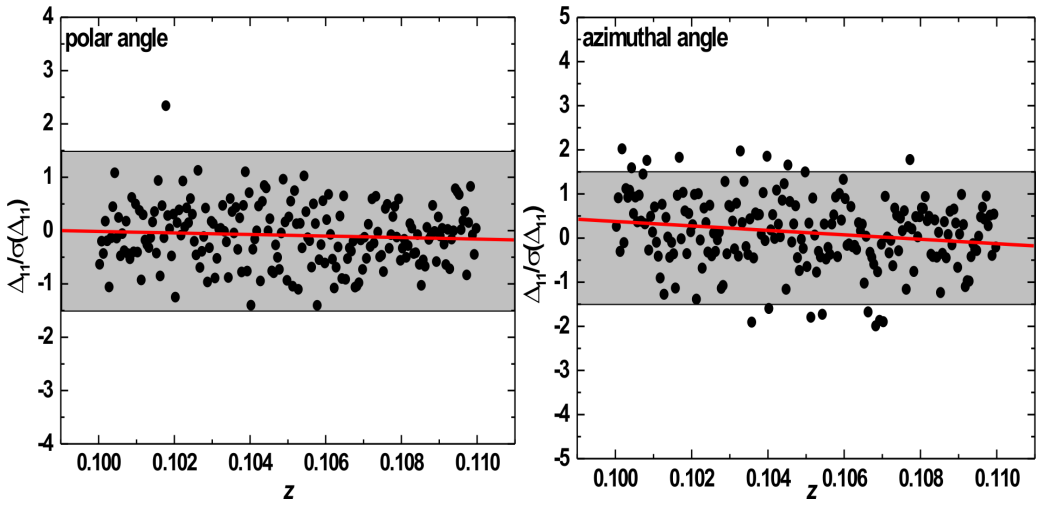

Figure 72: The scatter plot of redshift (z) versus $\Delta_{11}/\sigma(\Delta_{11})$ for (a) polar angle and (b) azimuthal angle distributions for the samples. The solid lines represent best fitted line and the grey shaded region represents the region of strong isotropy. The dashed region is the region of weak anisotropy.

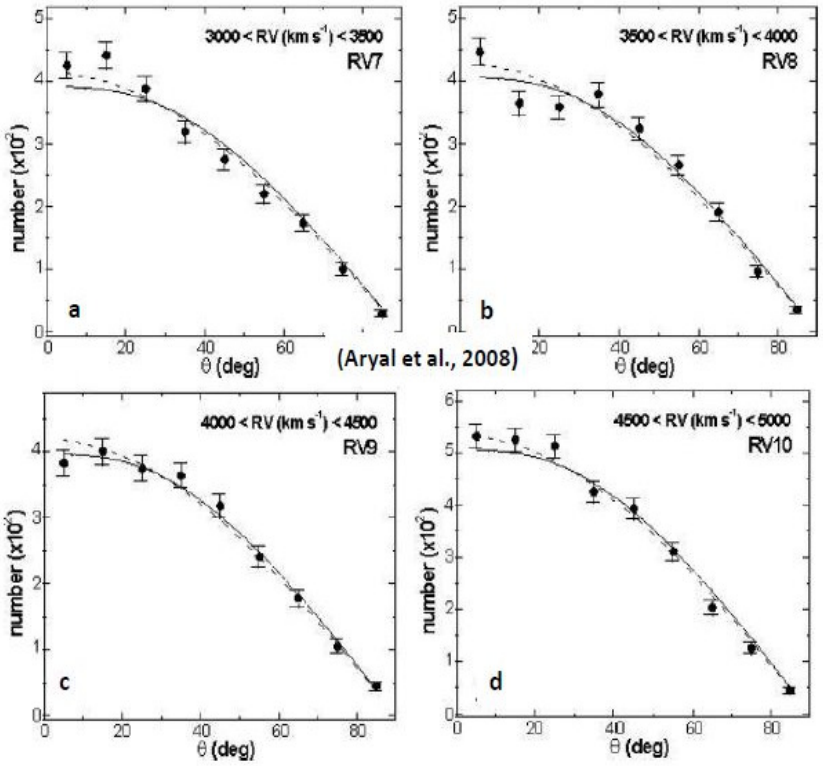

Figure 73: The distributions of angular momentum vectors of galaxies in Aryal *et al*. (2008). A week redshift dependance was noticed for the galaxies having radial velocity in the range 3 000 to 4 000 km s^{-1}.

4.6.16 Comparison with Previous Works

Aryal & Saurer (2008) studied redshift dependence in the Local Supercluster and nearby Local Supercluster galaxies. Figure 73 shows polar angle distribution of galaxies having radial velocity between 3 000 to 4 000 km s^{-1}. A hump at small angle suggests a preference, supporting Pancake model of galaxy formation. No preferred alignments can be seen in other two plots.

In this study, database was very good and they were taken from 30 different catalogs and corrected for a fixed isophot-level. In the present study, our results support hierarchy model rather than pancake.

4.6.17 Publication

The partial result of the work has been published in the Journal of University Grand commission, Nepal and Pragyan Journal, Nepal. A complete result of this chapter is in the process of publication in BASI.

CHAPTER 5

CONCLUSIONS AND RECOMMENDATIONS

CHAPTER 5

CONCLUSIONS AND RECOMMENDATIONS

5.1 Conclusion

We have studied spatial orientation angular momentum vectors of 373 691 galaxies having redshift from 0.05 ($\sim$ 15 000 km s^{-1}) to 0.5 ($\sim$ 150 000 km s^{-1}). In addition to redshift galaxies 5 987 blue shifted galaxies are added in the database. The database of these galaxies is taken from Sloan Digitized Sky Survey (Gunn *et al*., 2006). In addition to SDSS, Polomor Observatory Sky Survey (Reid *et al*., 1991) is used in order to compile database of zone-of-avoidance galaxies. The visible magnitude (r-filter) of galaxies in our database lies in the range 11 to 23. The 23 magnitude galaxy is 10 000 times fainter than 11 magnitude galaxies in surface brightness. In addition, two Superclusters were included. Therefore, the database includes field (zone-of-avoidance galaxies), groups (low blue shifted galaxies), clusters (several Abell clusters of low and high redshift) and two SDSS Superclusters S[239+016+0037] and S[223+022+0117].

Astronomical data are affected by several selection effects depending on the nature of the techniques used in the telescope as well as the region of interest. These selection effects can be treated as noise in the data base. These noises show a systematic pattern and can be propagated in a way. In the case of galaxies, even though all control parameters (independent variables, e.g., positions and inclination) remain constant, the resultant outcomes (dependent variables, e.g., position and polar angles) vary. The selections effects should be removed from the database and the expected isotropic distribution curves are determined by performing numerical simulations. We used the method proposed by Flin & Godlowski (1986) in order to compute two-dimensional data to three dimensional galaxy rotation axes (polar & azimuthal angles). We have carried out

random simulation by creating 10^7 virtual galaxies and adopting the method proposed by Aryal & Saurer (2000) in order to find theoretical distribution of galaxy rotation axes. We have compared the differences between theoretical distributions and observed distributions using three statistics, namely chi-square, auto-correlation and the Fourier. We have presented our results in six sections as follows:

Low Redshift Galaxies ($0.05 \leq z \leq 0.10$):

We have used the database taken from near infrared sensitive z-filter for low redshift galaxies. The peak wavelength of SDSS z-filter is 913.4 nm. These emission lines at this wavelength are expected to be emitted from the hot region (T < 5000 K), mostly from the interstellar medium of the galaxy, star forming region, the extended HII region. All samples show isotropy in the polar angle distribution for low redshift galaxies suggesting that the spatial orientation of angular momentum vectors of galaxies is random with respect to the equatorial coordinate system, supporting hierarchy model as suggested by Peebles (1969). Godlowski *et al*. (2011) found that the cluster galaxies that are at less than 300 Mpc show a random alignments of angular momentum vectors of galaxies with respect to equatorial co-ordinate system. Their result is similar to that of our result. They concluded hierarchy model for the galaxy evolution in the cluster. Aryal & Saurer (2006) studied spatial orientation of galaxies in a few low redshift Abell clusters (z<0.01). They found strong anisotropy for Abell cluster A4038, whereas random orientation is noticed for another low redshifted cluster Abell A2197. Aryal & Saurer (2006) concluded that the gravitational shearing effect might be the region for the anisotropy, it is supported by the X-ray emission from that cluster.

High Redshift Galaxies ($0.40 \leq z \leq 0.50$):

The visible *r*-filter is used for the high redshift galaxies because of its low surface brightness. The peak wavelength of SDSS *r*-filter is 616.5 nm, equivalent to yellow-orange color. The bandwidth covering this wavelength is mostly due to Balmer and Peschen lines of hydrogen atom. These lines are emitted from the hot region of the galaxy, mostly from the stars, HII region, planetary nebula, etc. A very good agreement between the observed and expected distribution is noticed in both the polar and azimuthal angle distributions of high redshift galaxies. This suggest that the alignment of galaxies is independent of the value of *r*-magnitudes, supporting hierarchy model of galaxy

formation. No authors have studied the angular momentum distribution of galaxies having redshift greater than 0.30 till date. This redshift limit is recommended by the special theory of relativity (Peebles, 1969). Our result is important in the sense that the speed of quasars is relativistic which provides the information when redshift was 1 to 7. The preferred alignments of quasars should be studied in the future as well as high redshifted galaxies should be studied in infrared band to understand the star formation activity in the distant object.

Blueshift Galaxies (-6×10^{-3} to -2×10^{-7}):

These galaxies are coming towards us with a very small speed. We found isotropic distribution of the angular momentum vectors of galaxies in all samples. Though a fluctuations (humps and dips) in few samples is found. Therefore, local effects e.g., tidal connection between the rotation axes of galaxies might be the reason. In addition, gravitational shearing effect leads galaxies to be oriented in a systematic pattern, perturbing the hierarchy scenario. An interesting result is noticed in the azimuthal angle distributions of blueshift galaxies. We found that the projections of angular momentum vectors of the blueshift galaxies tend to be orientated perpendicular to the equatorial plane. However, this problem needs to be examined by using other reference system such as galactic or Supergalactic coordinate system.

SDSS Superclusters:

We have studied the orientation of galaxies in two Superclusters namely S[223+022+0117] & S[239+016+0037] located within the survey regions of SDSS (7th data release). The first Supercluster has redshift limit in the range 0.111 to 0.122 whereas the second supercluster has the redshift limit in the range 0.029 to 0.049. We choose database of i, u, r filters for galaxies in the Supercluster S[223+022+0117] and i, u, g filters for galaxies in Supercluster S[239+016+0037]. In the Supercluster S[223+022+0117] preferred alignment is noticed. The distribution of angular momentum vectors of galaxies tend to be oriented perpendicular with respect of equatorial co-ordinate system, supporting primordial vorticity model as suggested by Ozernoy (1978). In this Supercluster anisotropy in i-magnitude shows that the star formation activity in this sample is not uniform, suggesting unknown interplay between matter (visual as well as dark matter) and dark energy (vacuum, etc). In the Supercluster S[239+016+0037], anisotropy is

found in the polar angle distribution suggesting that the galaxies in this sample supports Pancake model (Doroshkevich, 1973; Doroshkevitch & Shandarin, 1978). Anisotropy in i-magnitude shows that star formation activity in this Supercluster is not uniform, similar to the Supercluster S[223+022+0117]. These results suggest that the Supercluster should have hidden feature regarding their formation and evolutions. No authors have studied SDSS Superclusters till date. We intend to extend this work by studying hundreds of Superclusters in all filters in the future. Our preliminarily result hints that the galaxy evolution model need a revision.

Zone-of-avoidance Galaxies:

The zone-of-avoidance is the region of the sky that is obscured by the Galactic plane of the Milky Way. The dust and gas in the Milky Way cause extinction at optical wavelengths, and foreground stars can be confused with background galaxies, obstructing our view of around 20% of the extragalactic sky at visible wavelengths. Because of this, optical catalogues are usually incomplete close to the Galactic plane. We studied a database of only 410 galaxies in this region. Interestingly, all three possible scenarios (pancake, primordial vorticity and hierarchy model) are observed when we studied preferred alignments with respect to equatorial, galactic and Supergalactic systems. The 'pancake model' predicts that the angular momentum vectors of galaxies tend to lie within the reference plane. According to the 'hierarchy model' the directions of the angular momentum vectors should be distributed randomly. The 'primordial vorticity theory' advocates that the angular momentum vectors of galaxies are distributed primarily perpendicular to the reference plane. We noticed that the angular momentum vectors of zone-of-avoidance galaxies tend to lie in the equatorial plane. These vectors are found to be oriented perpendicular to the Local Supercluster plane. A random alignment of angular momentum vectors of galaxies is noticed with respect to the Galactic plane. The projections of angular momentum vectors showed a mixed picture: tend to point towards the Galactic centre and tend to be oriented perpendicular towards the LSC centre. This result clearly hints the need of suitable reference system for the zone-of-avoidance galaxies. The Supergalactic coordinate system is found to be most suitable among three systems because we noticed anisotropy in both the angular momentum vectors and its projections. The issue of suitable physical reference system is critical while studying spatial orientation of galaxies in a cluster or Supercluster. We intend to work on this

issue using the Sloan Digital Sky Survey (seventh data release) and Galaxy Zoo project data in the future.

Redshift Dependence ($0.10 \leq z \leq 0.11$).

There was 200 samples of which only one sample Z36 (redshift lie in the range 0.10305 to 0.10310) showed weak anisotropy. The angular momentum vectors of galaxies in this sample tend to be oriented parallel with respect to the equatorial coordinate system, supporting pancake model. Other 199 samples support hierarchy model. Therefore, no redshift and visual magnitude dependence is found. Aryal & Saurer (2008) studied redshift dependence in the Local Supercluster and nearby Local Supercluster galaxies. The galaxies having radial velocity between 3 000 to 4 000 km found to support Pancake model of galaxy formation. No preferred alignments can be seen in other two plots. In their study, database was very good and they were taken from 30 different catalogs and corrrected for a fixed isophot-level. In the present study, our results support hierachy model rather than pancake.

5.2 Recommendation

1. Sloan Digitized Sky Survey (SDSS) provide a huge database for the astronomers of all disciplines at all redshift with a very high precision level. We intend to study the preferred alignments of the angular momentum vectors of galaxies (several millions) of the SDSS database. In specific, the database of SDSS Superclusters (Einasto *et al*., 2014) should be studied in order to understand the role of intergalactic medium in the orientation. In addition, distribution of angular momentum of galaxies in the merging binary clusters, rotating clusters, irregular clusters provide information regarding origin of angular momentum in the large scale structure.

2. We have studied the galaxy orientation with respect to the equatorial coordinate system. We wish to define a local reference system within the galaxies and study the preferred alignments of galaxies with respect to it. Though, the importance of galactic and Supergalactic coordinate system cannot be denied.

3. The result of the statistical analysis has been noticed to have a strong dependence on

the sample/subsample classification criteria. Finding out a straight mathematical computation method instead of statistical method is essential and interesting in the future.

CHAPTER 6

SUMMARY

CHAPTER 6

SUMMARY

In the present thesis, we have studied spatial orientation of 373 691 galaxies having redshift from 0.05 ($\sim$ 15 000 km s^{-1}) to 0.5 ($\sim$ 150 000 km s^{-1}) and the visible magnitude lies in the range 11 to 23. The database includes 5 987 blue shifted galaxies and 410 zone-of-avoidance galaxies. In addition, two superclusters were included. Therefore the database includes field (zone-of-avoidance galaxies), groups (low blue shifted galaxies), clusters (several Abell clusters of low and high redshift) and two superclusters SDSS S[239+016+0037] and SDSS S[223+022+0117]. The positions, position angles and inclination angles are used to covert two-dimensional observed parameters into three-dimensional angular momentum vectors of the galaxy by Glodlowskian transformation. Astronomical data are often accompanied by several selection effects. The selections effects are removed from the database and the expected isotropic distribution curves are determined by running numerical simulations. The chi-square, autocorrelation and the Fourier tests are carried out in order to examine non-random effects in the expected isotropic distributions. We have presented our results in six sections, as follows: (1) low redshift galaxies ($0.05 \leq z \leq 0.10$), (2) high redshift galaxies ($0.40 \leq z \leq 0.50$), (3) blue shift galaxies (-3×10^{-4}) to (-1.1×10^{-6}), (4) Two SDSS Superclusters, (5) zone-of-avoidance galaxies and (6) redshift dependence ($0.10 \leq z \leq 0.11$). We summarize our results as follows:

1. The database of high redshift galaxies, located within the survey regions of SDSS (7^{th} data release, 2008 October) having redshift in the range 0.05 to 0.10. We choose database through filter z for the study. The peak wavelength of SDSS z-filter is 913.4 nm, equivalent to infrared colour. There are 229 675 galaxies in the region of interest with all required information. These galaxies have radial

velocity in the range 15 000 km s^{-1} to 30 000 km s^{-1}. They are divided in to 19 bins with bin size 0.30 magnitude. We conclude that the spatial orientation of spin vectors of galaxies is random with respect to the equatorial coordinate system and is independent of z-magnitude of galaxies. Seven samples $z08$, $z09$, $z11$, $z12$, $z13$, $z14$ and $z17$ advocating weak anisotropy in the azimuthal angle distribution.

2. In the second chapter of result and discussion, we have used SDSS, DR7 database of galaxies that have redshift in the range 0.40 to 0.50 in order to study preferred alignments of spin vectors of galaxies. For the sample classification, we choose database of magnitude through r-filter . There are 83 162 galaxies in the region of interest. We conclude that the spatial orientation of spin vectors of galaxies is random with respect to the equatorial coordinate system and is independent of r-magnitude of galaxies. We noticed no preferred alignments in general suggesting a similar evolutionary stages of these galaxies. This suggest that the alignment of galaxies is independent of the value of r-magnitudes, supporting Hierarchy model of galaxy formation. Only in $r06$ sample we observed weak anisotropy result for polar angle distribution but for azimuthal angle six samples $r02$, $r03$, $r04$, $r07$, $r08$, $r09$ shows weak in isotropy.

3. We obtained the data of 5 987 blue-shifted galaxies from The Sloan Digital Sky Survey(SDSS) Data Release 7 (DR7). We have retained only those galaxies that have redshift ($-z$) data at 95% level of significance. In binning process, galaxies that have very low and high redshift values were also removed. We have compiled the database of diameters and position angle of galaxies using the database of near infrared (i, 7 625 A°) and ultraviolet (u, 3 543 A°) filters. These filters provide extreme limits for the isophotes. In general, we found isotropic distribution of the spin vector of galaxies in all our six samples with respect to the equatorial coordinate system. There are humps and dips in the polar angle distributions, and these humps and dips alter the correlation test showing anisotropy in samples $i02$, $i03$, and $u03$. Hence, local effect was observed in these samples suggesting a local tidal connection between the rotation axes of galaxies. However, in the rest of the samples ($i01$, $u01$, and $u02$) small humps and dips do not alter the statistics of the samples, so we suppose these as binning effects.

4. The database used in this work consists of two superclusters S[223+022+0117] & S[239+016+0037] located within the survey regions of SDSS (7^{th} data release). The first supercluster has redshift limit in the range 0.111 to 0.122 whereas the second supercluster has the redshift limit in the range 0.029 to 0.049. We choose database of i, u, r filters for galaxies in supercluster S[223+022+0117] and i, u, g filters for galaxies in supercluster S[239+016+0037]. For sample S[223]i, distribution of galaxies shows isotropy in polar angle distribution suggesting spin vector of galaxies tend to be oriented randomly with respect of equatorial co-ordinate system. In case of sample S[223]r, statistical result in both polar & azimuthal angle distribution shows isotropy and the galaxies in this sample supports hierarchy model. In sample S[239]u, statistical result shows isotropy in the distribution of galaxies indicating abundance of stellar nursery (newly born stars, that emits UV radiation). In sample S[239]g, the distribution of galaxies is isotropic supporting hierarchy model. Besides the fluctuations seen in three samples, we found very good agreement between expected and observed distributions so we can conclude that galaxies in the supercluster S[239+016+0037] in general supports hierarchy model.

5. The Zone-of-avoidance is the region of the sky that is obscured by the Galactic plane of the Milky Way. The dust and gas in the Milky Way cause extinction at optical wavelengths, and foreground stars can be confused with background galaxies, obstructing our view of around 20% of the extragalactic sky at visible wavelengths. We studied the spatial orientations of spin vector orientation of 410 Zone of Avoidance (ZOA) galaxies found in the region $20^0 \leq l \leq 80^0$, $-10^0 \leq b \leq -5^0$ on the first Palomar Observatory Sky Survey. Interestingly, all three possible scenarios (pancake, primordial vorticity and hierarchy model) are observed when we studied preferred alignments with respect to equatorial, Galactic and supergalactic systems. We noticed that the spin vectors orientation of ZOA galaxies tend to lie in the equatorial plane. These vectors are found to be oriented perpendicular to the Local supercluster plane. A random alignment of spin vectors of galaxies is noticed with respect to the Galactic plane. The projections of showed a mixed picture: tend to point towards the Galactic centre and tend to be oriented perpendicular towards the LSC centre. This result clearly hints the need of suitable

reference system for the ZOA galaxies.

6. The database used in this work consists galaxies located within the survey regions of Sloan Digital Sky Survey (SDSS) those have redshift in the range 0.10 to 0.11. There are 44 741 galaxies with right ascension, declination, major diameter, minor diameter, position angle,five different magnitude and redshift. There are 200 sample of which only one sample Z36 shows weak anisotropy in the Fourier tests for θ distributions. Remaining all samples shows isotropy, Suggesting non - vanishing angular momentum. Therefore, Hierarchy model is most preferred suggesting that in these samples no redshift dependence. In only one sample (Z36) Pancake model is noticed. This might be because of the presence of clusters or superclusters.

REFERENCES

Aaronson, M., Huchra, J., Mould, J., Schechter, P. L. & Tully, R.B. (1982). The velocity field in the Local Supercluster. *The Astrophysical Journal*, **258**, 64-76.

Abazajian, Kevork N., Adelman-McCarthy, Jennifer K., et al., (2009). The Seventh Data Release of the Sloan Digital Sky Survey. *ApJS,* (The Astrophysical Journal Supplement) **182**, Issue 2, 543-558.

Acharya, B. & Dhamala, S. (2012). *A Study of spin vector orientation of incomplete search limit SDSS galaxies having redshift 0.10 < z < 0.11*. M.Sc. (Physics) Dissertation, Central Department of Physics, Institute of Science and Technology, Tribhuvan University, Kathmandu, Nepal.

Adams, M., Strom, K., & Strom, S. (1980), Linear clusters of galaxies. *The Astrophysical Journal*, **238**, 445-457.

Andrew, Liddle. (2003). *An Introduction to Modern Cosmology* (2nd ed.). Wiley.

Aryal, B. (2002). *Spatial Orientation of Spin Vectors of galaxies in 42 Abell clusrers*. Ph.D. Thesis, Institute of Astro- and Particle physics, Innsbruck University, Technikstrasse **25/8**, A-6020 Innsbruck, Austria.

Aryal, B. (2011). Winding sense of galaxies around the local supercluster. *Research in Astron. Astrophys.*, **11**, 293-304.

Aryal, B. & Saurer, W. (2000). Comments on the expected isotropic distribution curves in galaxy orientation studies. *Astronomy & Astrophysics Journal*, **364**, L97-111.

Aryal, B. & Saurer, W. (2001). The Influence of Selection Effects on the Isotropic Distribution Curve in Galaxy Orientation Studies. *ASP Conference Series*, **230**, A145-154.

Aryal, B. & Saurer, W. (2004). Spin vector orientations of galaxies in eight Abell clusters of BM type I. *Astronomy & Astrophysics Journal*, **425**, 871-879.

Aryal, B. & Saurer, W. (2005a). Spin vector orientations of galaxies in seven Abell clusters of BM type III. *Astronomy & Astrophysics Journal*, **432**, 841-831.

Aryal, B. & Saurer, W. (2005b). Morphological dependence in the spatial orientations of Local Supercluster galaxies. *Astronomy & Astrophysics Journal*, **432**, 431-439.

Aryal, B. & Saurer, W.(2005c). Spin vector orientation of galaxies in the region $15^h48^m <= \alpha(2000) <= 19^h28^m$, $-68^o <= \delta(2000) <= -62^o$. *Monthly Notices of the Royal Astronomical Society*, **360**, 125-135.

Aryal, B. & Saurer, W. (2006). Spatial orientations of galaxies in 10 Abell clusters of BM type II-III., *Monthly Notices of the Royal Astronomical Society*, **366**, 438-449.

Aryal, B., Kandel, S. & Saurer, W. (2006). Spatial orientation of galaxies in the core of the Shapley concentration - the cluster Abell. *Astronomy & Astrophysics Journal*, **458**, 357-367.

Aryal, B., Paudel, S. & Saurer, W. (2007). Spatial orientations of galaxies in seven Abell clusters of BM type II, *Monthly Notices of the Royal Astronomical Society*, **379**, 1011-1021.

Aryal, B., Kafle, P. R. & Saurer, W. (2008). Radial velocity dependence in the spatial orientations of galaxies in and around the local supercluster. *Monthly Notices of the Royal Astronomical Society*, **389**, 741-749.

Aryal, B., Neupane, D. & Saurer, W. (2008). Morphological dependence in the spatial orientations of galaxies around the Local Supercluster. *Astrophysics & Space Science* , **314**, 177-186.

Aryal, B., Paudel, S., & Saurer, W. (2008). Coexistence of chiral symmetry restoration and random orientation of galaxies. *Astronomy & Astrophysics Journal*, **479**, 397-407.

Aryal, B., Bachchan, R. K., & Saurer, W. (2010). Optical search limit and preferred position angles of galaxies in 35 clusters. *Bull. Astr. Soc. India,* **38**, 165-176.

Aryal, B., Paudel, R., & Saurer, W.(2012). Spatial orientation of angular momentum vector of galaxies in three merging binary clusters. *Astrophysics & Space Science*, **337**, 313-324.

Aryal, B., Yadav, S. N. & Saurer, W. (2012). Spatial orientation of galaxies in the Zone of Avoidance. *Bull. Astr. Soc. India,* **40**, 65-76.

Aryal, B., Bhattarai, H., Dhakal, S., Rajbahak, C. & Saurer, W. (2013). Spatial orientation of angular momentum vectors of galaxies in six rotating clusters. *Monthly Notices of the Royal Astronomical Society*, **434**, 1939-1951.

Baier, F. W., Godowski, W., & MacGillivray, H. T. (2003). Substructures and galaxy orientations in clusters II. Cluster Abell 14. *Astronomy & Astrophysics Journal*, **403**, 847-856.

Baral, N.(2012). *A Study of z-Magnitude Dependence in the Spatial Orientation of SDSS Galaxies*. M.Sc. (Physics) Dissertation, Central Department of Physics, Institute of Science and Technology, Tribhuvan University, Kathmandu, Nepal.

Bautz, L. P., & Morgan, W. W. (1970). On the Classification of the Forms of Clusters of Galaxies. *The Astrophysical Journal*, **162**, 149-155.

Bian, W., Yuan, Q. & Zhao, Y. (2005). The blueshift of the [OIII] emission line in narrow-line Seyfert 1 galaxies. *Monthly Notices of the Royal Astronomical Society*, **364**, 187-194.

Blumenthal, G. R., Faber, S. M., Primack, J. R. & Rees, M. J.,(1984). Formation of galaxies and large-scale structure with cold dark matter. *Nature*, **311**, 517-525.

Bukhari, F.A. & Cram, L.E. (2003). Orientation of Galaxies in Clusters. *Astrophysics and Space Science*, **283**, 173-181.

Burbidge, E. M. & Demoulin, M. H., (1969). IC 3258, a Small Extragalactic Object with a Blueshift. *Astrophys.*, **157**, 155-166.

Collins, C. B. & Hawking, S. W. (1973). The rotation and distortion of the Universe. *Monthly Notices of the Royal Astronomical Society*, **162**, 307-320.

Dekel, A. (1985). A search for galaxy-pancake alignments. *The Astrophysical Journal*, **298**, 461-472.

Djorgovski, S., (1983). Alignment of galaxies in the Coma Cluster. *The Astrophysical Journal*, **274**, L7-11.

Donley, J. L., Staveley-Smith, L., Kraan-Korteweg, R. C., Islas-Islas, J. M., Schröder, A., Henning, P. A., Koribalski, B., Mader, S. & Stewart, I.(2005). The H I Parkes Zone of Avoidance Survey: The Northern Extension. *Astronomical Journal*, **129**, 220-238.

Doroshkevich, A. G. (1973). The Origin of Rotation of Galaxies. *The Astrophysical Journal*, **14**, 11-13.

Doroshkevich, A. G., Shandarin, S.F. & Saar, E. (1978). Spatial structure of protoclusters and the formation of galaxies. *Monthly Notices of the Royal Astronomical Society*, **184**, 643-660.

Doroshkevich, A. G. & Shandarin, S. F. (1976). On the local anisotropy of expansion of the universe. *Monthly Notices of the Royal Astronomical Society*, **175**, 1976,

15P-18P.

Doroshkevich, A. G., Sunyaev, R. A. & Zeldovich, Ya.B. in: Longair M.S. (ed.) (1974). *The formation of galaxies in Friedmannian universes*. Confronta- tion of Cosmological Theories with Observational Data, Proc. IAU Symp. No. **63**. Reidel Dordrecht, 213-225

Einasto, M., Lietzen, H., Tempel, E., Gramann, M., Liivamägi, L. J. & Einasto, J., (2014), SDSS superclusters: morphology and galaxy content. *Astronomy & Astrophysics*, **562**, A87-95.

Einasto, M., Liivamägi1, L. J., Tago, E., Saar, E., Tempel, E., Einasto, J., Martínez, V. J. and Heinämäki, P. (2011). SDSS DR7 superclusters Morphology. *Astronomy & Astrophysics Journal*, **532**, 1-20.

Fall, S. Michael. (1980). Gravitational instability theory of galaxy formation and clustering - Some recent developments. *Annals of the New York Academy of Sciences*, **336**, 172-190.

Fall, S. Michael & Efstathiou, G. (1980). Formation and rotation of disc galaxies with haloes. *Monthly Notices of the Royal Astronomical Society*, **193**, 189-206.

Flin, P. (2001). The anisotropy of galaxy orientation in the Coma/A1367 supercluster. *Monthly Notices of the Royal Astronomical Society*, **325**, 49-58.

Flin, P., & Godlowski, W. (1986). The orientation of galaxies in the Local Supercluster. *Monthly Notices of the Royal Astronomical Society*, **222**, 535-533.

Flin, P. & Godlowski, W.(2009). Orientation of the galaxy groups in the Local Supercluster. eprint arXiv:0911.4392.

Gamow, G. (1946). Rotating Universe? *Nature* **158**, 549-564.

Gamow, G. (1952). The Role of Turbulence in the Evolution of the Universe. *Phys. Rev.*, **86**, 251-260.

Gamow, G. & Teller, E. (1939). On the Origin of Great Nebulae. *Phys. Rev.,* **55**, 654-665.

Godlowski, W.(1993). Galactic Orientation Within the Local Supercluster. *Monthly Notices of the Royal Astronomical Society*, **265**, 874-880.

Godlowski, W. (1994). Some aspects of the galactic orientation within the Local Supercluster. *Monthly Notices of the Royal Astronomical Society*, **271**, 19-30.

Godlowski, W. (2011), *Monthly Notices of the Royal Astronomical Society*, **442**, 856.

Godlowski, W. & Ostrowski, M., (1999). Investigation of galactic alignment in Local Supercluster galaxy clusters. *Monthly Notices of the Royal Astronomical Society*, **303**, 50-64.

Godlowski, W., Baier, F. W. & MacGillivray, H. T. (1998), Substructures and galaxy orientations in clusters. I. The cluster Abell 754, *Astronomy & Astrophysics Journal*, **339**, 709-716.

Gregory, S., Thompson, L., & Tifft, W. (1981). The Perseus Supercluster, *The Astrophysical Journal*, **243**, 411-426.

Gunn, J. E., Carr, M., Rockosi, C., Sekiguchi, M., Berry, K., Elms, B., de Haas, E., et al.(1998). The Sloan Digital Sky Survey Photometric Camera. *The Astronomical Journal*, **116**, 3040-3081.

Gunn, E. J., Siegmund, A. W., Mannery, J. E., Owen, E. R., Hull, L. C., Leger, R. F., Carey, N. L., Knapp, R. G., York, G. D., Boroski, N. W., Kent, M.S., Lupton, H.R. & 50 coauthors (2006). The 2.5 m Telescope of the Sloan Digital Sky Survey. *The*

Astrophysical Journal, **131**, 2332-2369.

Hawley, D. L. & Peebles, P. J. E. (1975). Distribution of observed orientations of galaxies. *The Astrophysical Journal*, **80**, 477-491.

Henning, P. A., Springob, C. M., Minchin, R. F., Momjian, E., Catinella, B., McIntyre, T., Day, F., Muller, E., Koribalski, B., Rosenberg, J. L., & 3 coauthors (2010). The Arecibo L-band Feed Array Zone of Avoidance Survey. I. Precursor Observations Through the Inner and Outer Galaxy. *Astronomical Journal*, **139**, 2130-2147.

Helou, G. (1984). Spin statistics in binary galaxies - Implications for formation and evolution. *The Astrophysical Journal*, **284**, 471-482.

Holmberg, E. (1946). On the Apparent Diameters and the Orientation in Space of Extragalactic Nebulae. *Meddelanden fran Lunds Astronomiska Observatorium Series II*, **117**, 3-82.

Hoyle, F., Burgers, J. M., van de Hulst, H.C., eds, (1949). *Problems of Cosmological Aerodyanamics*. Central Air Documents Office (Army-Navy-Air Force), Wright Patterson Air Force Base, Dayton, OH, 195-204.

Hu, F. X., Su, H. J., Wu,G. X. & Liu, Y. Z. (1995). Morphological dependence of the orientation of the spin vectors of disk galaxies in the Virgo cluster. *Astronomy & Astrophysics Journal*, **302**, 45-57.

Hu, F. X., Wu, G.X., Song, G. X., Yuan, Q. R. & S. Okamura, (2005). Orientation of Galaxies in the Local Supercluster: A Review. *astro-ph,* **669**, 01-31.

Hu, F. X., Yuan, Q. R., Su, H. J., Wu, G. X., & Liu, Y. Z. (1998). Orientation of Spin Vectors of Bright Field Disk Galaxies in the Local Supercluster and Its Implication. *The Astrophysical Journal*, **495**, 179-186.

Huchtmeier, W.K., Lercher, G., Seeberger, R., Saurer, W. & Weinberger R. (1995). Two new possible members of the IC342-Maffei 1/2 group of galaxies. *Astronomy & Astrophysics Journal*, **293**, L33-40.

Jaaniste, J. & Saar, E. (1978). Orientation of Spiral Galaxies as a Test of Theories of Galaxy Formation. The Large Scale Structure of the Universe; Proceedings of the Symposium, Tallin, Estonian SSR, September 12-16, 1977. Edited by M. S. Longair and J. Einasto. Symposium sponsored by IAU, Akademiia Nauk SSSR, and Akademiia Nauk Estonskoi SSR Dordrecht, D. Reidel Publishing Co. (IAU Symposium, No. 79), 1978., p.448

Jasche, J., Francisio, S. K., Li Cheng & A. E. Torsten., (2010). Bayesian non-linear large-scale structure inference of the Sloan Digital Sky Survey Data Release. *Monthly Notices of the Royal Astronomical Society*, **409**, 355-370.

Karachentsev, I. D. and Nasonova, O. G. (2010). Blueshifted Glaxies in the Virgo Cluster. *The Astrophysical Journal* , **53**, Issue 1, 32-41

Karttunen, H., Kroger, P., Oja, H., Poutanen, M. & Donner, K.J.(2006). *Fundamental of Astronomy*, Fifth Edition, Springer.

Kashikawa, N., & Okamura, S. (1992). Spatial orientation of spin vectors of galaxies in the Local Supercluster. *Publ. Astron. Soc. Japan, PASJ,* **44**, 493-507.

Kausch, W. (2004). *A Statistical Approach to a Possible Alignment of Galaxies in the Perseus Cluster*. M.Sc. (Astrophysics) Dissertation, Innsbruck University, Innsbruck, Austria.

Kerton, C.R. & Brunt, C.M. (2003). The association of IRAS sources and ^{12}CO emission in the outer Galaxy. *Astronomy & Astrophysics Journal*, **399**, 1083-1099.

Kitzbichler, M.G. & Saurer, W. (2003). Investigation of Galaxy Orientations in the

Coma Cluster.*Astronomische Nachrichten, Supplementary, ANS*, **324**, 23-28.

Liivamägi, L. J., Tempel, E.,& Saar, E., (2012). SDSS DR7 superclusters, The catalogues. *Astronomy & Astrophysics Journal*, **539**, A80-88

Li Xin Li. (1998). Effect of the Global Rotation of the Universe on the Formation of Galaxies. *General Relativity and Gravitation*. **30**, Issue 3, pp.497-507.

Maffei, P. (1968). Infrared Object in the Region of IC 1895. *Publications of the Astronomical Society of the Pacific, PASP*, **80**, 618-621.

MacGillivray, H. T. & Dodd, R. J. (1979a). Properties of faint galaxies in two fields near the South Galactic Pole. *Monthly Notices of the Royal Astronomical Society*, **186**, 69-84.

MacGillivray, H. T. & Dodd, R. J. (1979b). Studies of clusters of galaxies using measurements by COSMOS - 11. Static properties for galaxies in the rich cluster at 00^h47^m, - 29^0 46' (1950 coordinates). *Monthly Notices of the Royal Astronomical Society*, **186**, 743-754.

MacGillivray, H. T. & Dodd, R. J. (1985a). The anisotropy of the spatial orientations of galaxies in the Local Supercluster. *Astronomy & Astrophysics Journal*, **145**, 269-274

MacGillivray, H. T., Dodd, R. J. B., Binggeli, ed. (1985b). *An analysis of the geometrical properties for galaxies in the Virgo cluster core*. IN: ESO Workshop on the Virgo Cluster of Galaxies, Garching, West Germany, September 4-7, 1984,Proceedings (A86-37351 17-90). Garching, West Germany, European Southern Observatory, 1985, p. 217-225.

MacGillivray, H. T., Dodd, R. J., McNally, B. V. & Corwin H. G. (1982). Orientations of galaxies in the Local Supercluster. *Monthly Notices of the Royal Astronomical*

Society, **198**, 605-615.

Marchiotto, W., Wildauer, H.& Weinberger, R. (1999). Galaxies in the zone-of-avoidance: the region $20^0 \leq l \leq 80^0$, $-10^0 \leq b \leq +10^0$. Astronomische Gesellschaft Abstract Series. No. 15, P86-99.

Mo, H. J., Mao. S. & White, S. D. M. (1998). The formation of galactic discs. *Monthly Notices of the Royal Astronomical Society*, **295**, 319-336

Dadhich N. (2005). Derivation of the Raychaudhuri Equation., gr-qc (general relativity and quantum cosmology), **02**, 01-12

Dadhich N. & Peebles, P. J. E. (1975). Distribution of observed orientations of galaxies. *The Astrophysical Journal*, **80**, 477-486.

Obreschkow, D. and Glazebrook, K.(2014). Fundamental Mass-Spin-Morphology Relation Of Spiral Galaxies. *The Astrophysical Journal*, **784**, 1-18.

Ostriker, J. P. & Cowie, L. L. (1981). Galaxy formation in an intergalactic medium dominated by explosions. *The Astrophysical Journal*, **243**, L127-L131.

Ozernoy, L. M. (1971). Dynamical Parameters of Galaxy Clusters as a Consequence of Cosmological Turbulence. *Soviet Astronomy* **15**, 923-933.

Ozernoy, L. M. (1978). in Longair, M. S. Einasto, eds, Proc. IAU Symp. **79**, The Large Scale Structure of the Universe. Reidel, Dordrecht, 427-438

Paudel, A. (2012). *A Study of u-Magnitude Dependence in the Spatial Orientation of SDSS Galaxies*. M.Sc. (Physics) Dissertation. Central Department of Physics, Institute of Science and Technology, Tribhuvan University, Kathmandu, Nepal.

Padmanabhan, T. (2006). *An Introduction to Astrophysics, Text book*. Pune, India.

World Scientific Publishing Co. Pte. Ltd., Singapore.

Panko, E., Piwowarska, P., Godlowska, J., Godlowski, W., Flin, P. & Flin, P. (2013). *Astrophysics*, **56**, Issue 3, pp.322-331.

Peebles, P. J. E. (1993). The Mass Puzzle in Cosmology, *American Astronomical Society, AAS,* **182**, 896-905.

Peebles, P. J. E., (1969), Origin of the Angular Momentum of Galaxies. *The Astrophysical Journal*, **155**, 393-401.

Peebles, P. J. E., (1968), Dead Galaxies? *The Astrophysical Journal*, **154**, 121-129.

Peebles, P. J. E. (1967). The Gravitational Instability of the Universe. *The Astrophysical Journal*, **147**, 859-863.

Peebles, P. J. E. (1965). The Black-Body Radiation Content of the Universe and the Formation of Galaxies. *The Astrophysical Journal*, **142**, 1317-1326.

Phuyal, C. R. (2012). *A Study of r-Magnitude Dependence in the Spatial Orientation of SDSS Galaxies*, M.Sc. (Physics) Dissertation, St. Xaviers' College, Institute of Science and Technology, Tribhuvan University, Kathmandu, Nepal.

Reid, I. N., Brewer, C., . Brucato, R. J, McKinley, W. R., Maury, A., Mendenhall, D. Mould, J. R., Mueller, J., Neugebauer, G., Phinney, J., Sargent, W. L. W., Schombert, J., & Thicksten, R. (1991). The second Palomar Sky Survey. *PASP* (Astronomical Society of the Pacific, Publications (ISSN 0004-6280)), **103**, 661-674.

Reinhardt, M., & Roberts, M. S. (1972). Orientation of Galaxies and the Local Supercluster. *The Astrophysical Journal*, **12**, 201-206.

Ryan-Weber, E., Koribalski, B. S., Staveley-Smith, L., Jerjen, H., Kraan-Korteweg,

R. C., Ryder, S. D., Barnes, D. G., de Blok, W. J. G., Kilborn, V. A., Bhathal, R. & 29 coauthors (2002), The 1000 Brightest HIPASS Galaxies: Newly Cataloged Galaxies. *Astronomical Journal*, **124**, 1954-1974.

Seeberger, R. & Saurer, W. (1998). Penetrating the “zone of avoidance”. an optical survey for hidden galaxies in the region 90degr <= L <= 110degr , -10degr <= B <= +10degr, *Astrophysics & Space Science* **127**, 101-109.

Stein, R. (1974). Galaxy formation from primordial turbulence. *Astronomy & Astrophysics Journal*, **35**, 17-29.

Shandarin, S.F. (1974). Orientation of angular momenta of galaxies. *Astr. Zh,* **51**, 667-669 (in Russian), *Soviet Astron,* **18**, 392 (in English).

Strom, S. E. & Strom, K. M. (1978). Surface brightness and color distributions of elliptical and SO galaxies. II - E galaxies in the clusters Abell 426 /Perseus/ and Abell 1367. *Astronomical Journal*, **83**, 732-763.

Strom, S. E. & Strom, K. M. (1978). Surface brightness and color distributions of elliptical and S0 galaxies. I - The Coma cluster elliptical galaxies. *Astronomical Journal*, **83**, 73-91.

Thompson, L.A. (1976). The Angular Momentum Properties of Galaxies in Rich Clusters. *The Astrophysical Journal*, **209**, 22-34.

Trevese, D., Cirimele, G. & Flin, P. (1992). The orientation of galaxies in clusters. *Astronomical Journal*, **104**, 935-944

Weinberger, R., Saurer, W. & Seeberger, R. (1995). Penetrating the“zone of avoidance". A compilation of optically identified extragalactic objects within $|b|$<=5deg. *Astrophysics & Space Science*, **110**, 269.

White, S. D. M. & Rees, M. J. (1978). Core condensation in heavy halos - A two-stage theory for galaxy formation and clustering. *Monthly Notices of the Royal Astronomical Society*, **183**, 341-358.

Wiezsacker, C. F. (1951). The Evolution of Galaxies and Stars. *The Astrophysical Journal*, **114**, 165-186.

Wu, G. X., Hu, F. X., Su, H. J. & Liu, Y. Z. (1997). Orientation of the disk galaxies in the Coma cluster. *Astronomy & Astrophysics Journal*, **323**, 317-322.

Yadav, S. N., Aryal, B. and Saurer, W. Spatial Orientation of Spin Vectors of Blue-shifted Galaxies. *Astrophysics and Space Science* ,arXiv:1606.02881v1 [astro-ph.GA] 9 Jun 2016.

Yuan, Q. R., Hu, F. X., Su, H. J. & Huang, K. L. (1997). Orientation of the Field Galaxies in the Local Supercluster. *The Astrophysical Journal*, **114**, 1308-1313.

Zeldovich Ya. B., Astrofiz. (1970). Separation of uniform matter into parts under the action of gravitation. **6**, 319-328.

Zeldovich Ya. B. & Novikiv I.D.(1975). *Structure and Evolution of the Universe*, Text book, Nauka, Moscow.

Appendix A

Database of Low Redshift Galaxies

The database used in this work consists of galaxies, located within the survey regions of SDSS (7th data release, 2008 October) having redshift in the range 0.05 to 0.10. There are 242 904 galaxies in the region of interest. Among them, 89 galaxies were excluded due to very poor frequencies . Finally, we have 242 815 . The database consists redshift, right ascension, declination, position angle, major diameter, minor diameter and five different magnitudes. Here, we present a sample page of our database in Table 21.

Figure 74 shows the redshift (z), right ascension (RAJ2000), declination (DECJ2000) and position angle (PA) distribution respectively. Inhomogeneous distribution of positions (α and δ) can be seen. The redshift has nearly homogeneous nature. But position angle has homogeneous nature. It is because of the nature of the survey.

Figure 75 shows axial ratio (b/a), u, g, r, i and z magnitude respectively. The axial ratio distribution shows nearly cosine behavior. The u-magnitude shows a Gaussian like distribution where other distributions are found to be deviated from the Gaussian.

Table 21: A sample page of our database having redshift in the range 0.05 to 0.10. First column represent redshift. The second and the third column represent right ascension and declination respectively. The fourth, fifth and sixth column represent the position angle, major and minor diameters. The last five column represent u, g, r, i and z magnitude distribution.

z	α	δ	p	a	b	m_u	m_g	m_r	m_i	m_z
0.050000	240.3	26.9	116.1	26.2	22.0	18.86	17.21	16.43	16.05	15.76
0.050001	119.5	12.2	71.9	20.6	19.1	17.66	16.56	16.06	15.73	15.52
0.050001	144.7	34.5	146.0	34.8	30.7	18.00	16.26	15.51	15.15	14.88
0.050001	117.6	21.2	154.1	22.3	21.7	19.18	17.34	16.47	16.05	15.71
0.050001	143.3	23.7	53.2	36.1	5.5	19.31	18.29	17.82	17.60	17.62
0.050001	144.9	37.5	116.4	67.1	39.5	17.46	15.78	14.89	14.44	14.12
0.050001	192.8	6.6	114.5	23.0	20.3	18.02	17.00	16.71	16.50	16.62
0.050002	199.5	13.4	141.2	31.9	18.1	18.62	17.18	16.50	16.13	15.91
0.050002	34.8	0.4	156.7	18.8	18.1	18.96	17.24	16.39	16.02	15.72
0.050002	238.7	18.2	2.0	36.4	8.7	19.07	17.97	17.61	17.38	17.12
0.050002	230.2	2.4	50.0	30.7	20.4	18.70	17.48	17.08	17.06	16.88
0.050003	220.3	13.1	138.6	25.4	20.9	19.39	17.68	16.83	16.43	16.10
0.050003	240.9	21.2	171.8	17.3	13.9	19.26	17.93	17.30	16.93	16.65
0.050003	134.0	36.9	22.6	39.9	33.9	18.40	16.68	15.85	15.49	15.25
0.050003	168.0	56.2	99.6	27.2	16.5	19.26	17.94	17.77	17.49	17.85
0.050003	239.3	20.1	120.0	42.1	7.4	19.66	18.05	17.54	17.21	16.85
0.050003	169.4	59.4	59.2	16.0	15.0	18.15	17.28	16.99	16.73	16.62
0.050003	246.2	47.4	150.3	48.0	31.2	18.19	16.42	15.60	15.21	14.99
0.050004	140.4	25.5	33.8	47.6	36.6	18.00	16.10	15.21	14.79	14.48
0.050004	193.2	7.1	83.9	57.9	30.3	17.88	16.11	15.24	14.81	14.50
0.050005	30.6	-0.2	6.2	55.5	20.5	17.63	16.28	15.61	15.22	14.95
0.050005	168.0	57.1	179.0	29.8	18.9	18.62	16.90	16.09	15.71	15.43
0.050006	258.4	22.4	72.4	26.9	14.0	18.74	17.48	16.90	16.59	16.36
0.047932	246.6	25.8	98.1	45.1	40.0	17.64	16.04	15.22	14.80	14.51

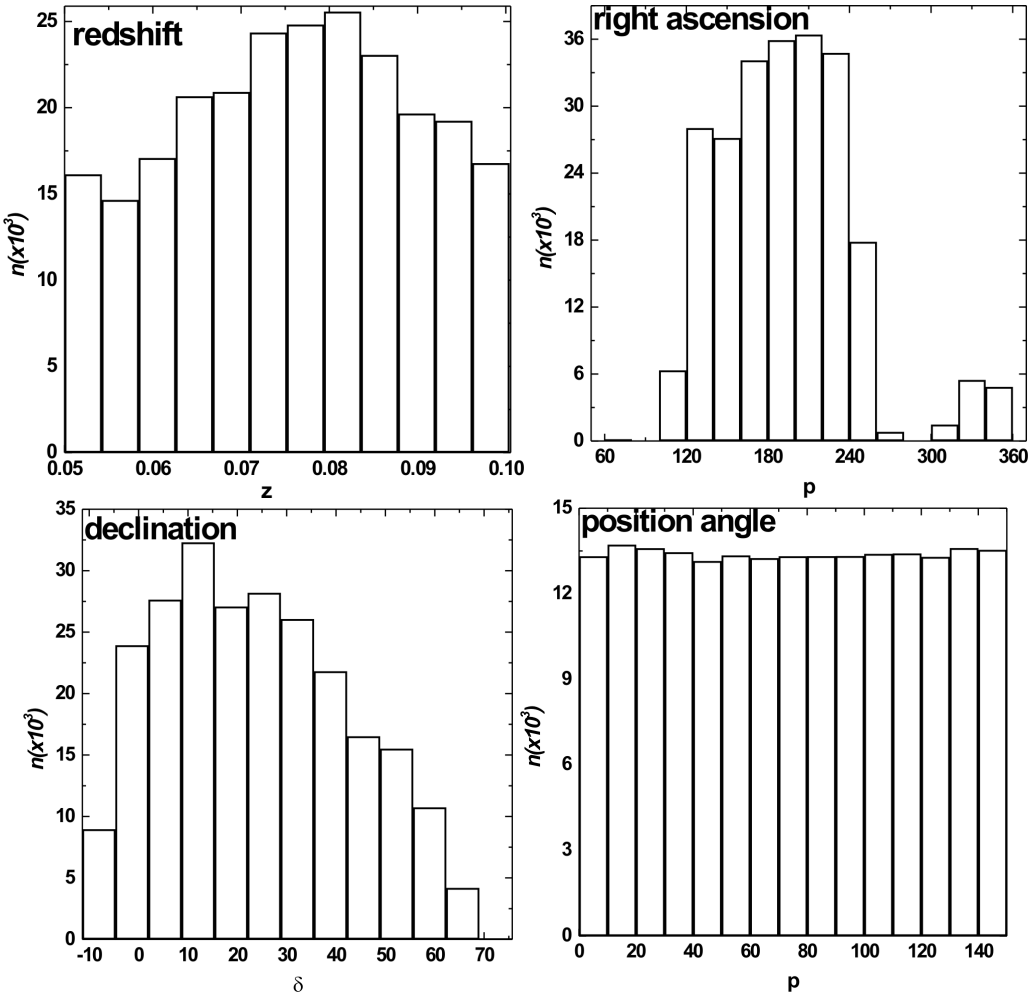

Figure 74: The distributions of redshift (z), right ascension (α), angle of declination (δ) and position angle (p) for the total sample.

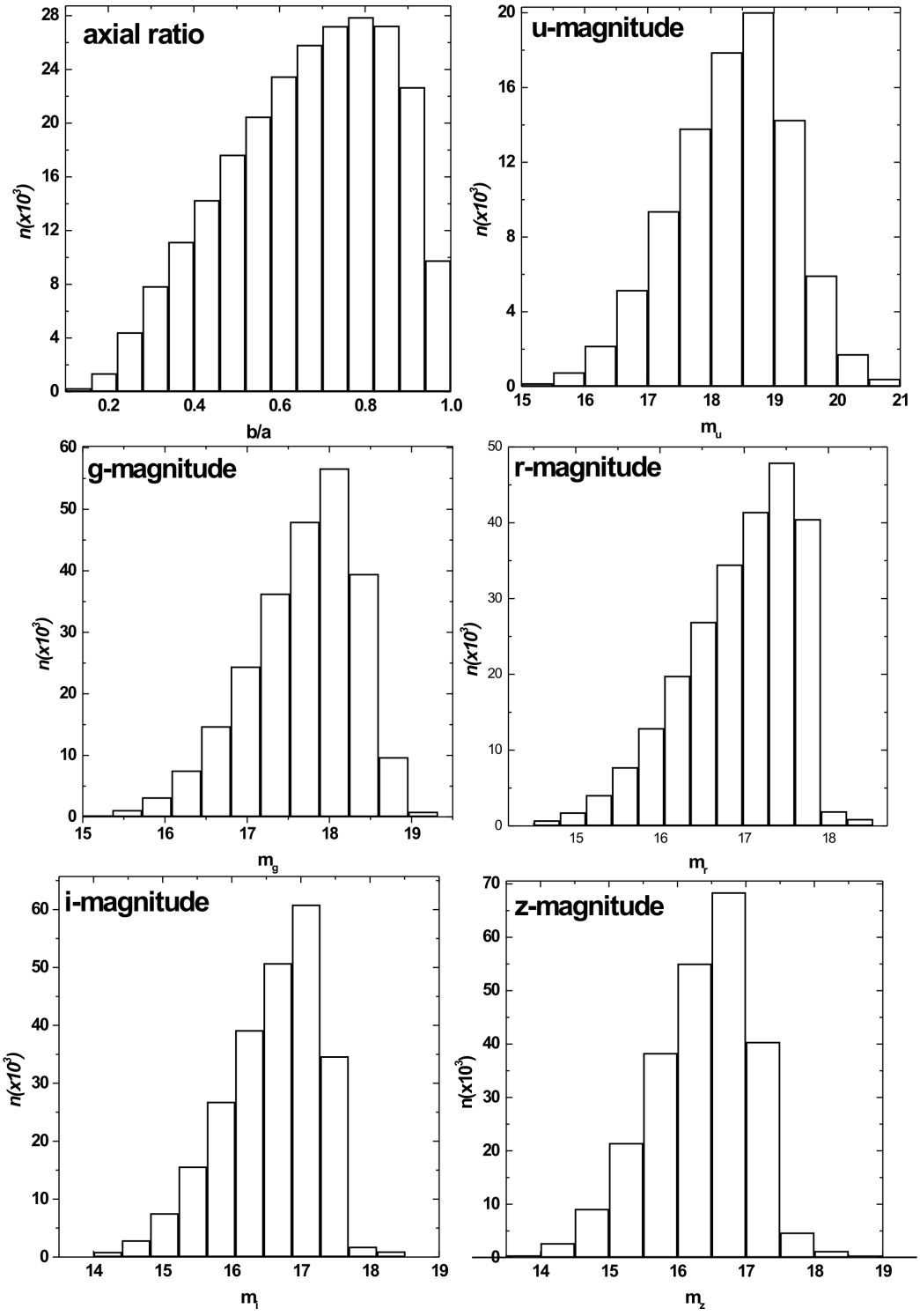

Figure 75: Axial ratio (b/a), u-magnitude(m_u), g-magnitude (m_g), r-magnitude (m_r), i-magnitude (m_i), z-magnitude(m_z) for the total sample.

Appendix B

Database of High Redshift Galaxies

The database used in this work consists of galaxies, located within the survey regions of SDSS (7th data release, 2008 October) having redshift in the range 0.40 to 0.50. There are 83 162 galaxies in the gegion of interest. The database consists redshift, right ascension, declination, position angle, major diameter, minor diameter and five different magnitudes. Here, we present a sample page of our database in Table 22.

Figure 76 shows the redshift(Z),right ascension (RAJ2000), declination (J2000) and position angle (PA) distribution respectively. Inhomogeneous distribution of positions (α and δ) can be seen. But position angle has homogeneous nature. It is because of the nature of the survey. The redshift has nearly gaussian nature.

Figure 77 shows axial ratio (b/a), u, g, r, i and z magnitude respectively. The axial ratio distribution shows nearly homogeneous behavior. The u-magnitude shows a Gaussian like distribution where other distributions are found to be deviated from the Gaussian. Axial ratio has homogeneous nature.

Table 22: A sample page of our database having redshift in the range 0.40 to 0.50. First column represent redshift. The second and the third column represent right ascension and declination. The fourth, fifth and sixth columns represent the position angle, major and minor diameters. The last five column represent u, g, r, i and z magnitude.

z	α	δ	p	a	b	m_u	m_g	m_r	m_i
0.400007993	158.2	58.8	1.3	15.5	11.7	20.54	20.56	18.65	18.07
0.400007993	129.4	35.5	86.6	10.3	7.2	19.94	20.43	18.65	19.12
0.400007993	191.2	17.8	165.0	13.0	10.7	19.98	20.86	18.83	18.17
0.400007993	172.0	51.4	171.1	15.7	11.4	21.34	21.34	19.89	18.05
0.400009006	144.7	17.7	52.8	15.2	11.9	20.46	20.41	18.83	18.10
0.40000999	186.8	9.1	91.4	19.9	14.1	26.10	20.17	18.45	17.79
0.400011986	120.0	18.6	107.5	11.0	8.9	24.53	20.80	19.24	18.50
0.400011986	113.0	46.5	110.5	12.6	11.1	20.54	21.13	19.14	18.45
0.400014013	208.8	18.7	166.7	14.8	9.1	27.60	20.97	19.23	18.49
0.40001601	199.6	34.3	162.2	11.1	10.3	21.47	20.64	19.02	18.30
0.400018007	250.7	45.7	10.2	22.1	18.2	20.62	19.88	17.93	17.24
0.400018007	126.3	39.1	57.5	14.1	10.6	20.62	20.50	18.81	18.16
0.400023013	118.2	22.8	22.1	13.8	9.5	21.34	21.08	19.17	18.40
0.400023997	117.7	21.0	24.0	10.5	8.1	18.93	21.09	19.11	18.54
0.400023997	163.3	7.2	133.3	12.5	9.7	19.48	20.89	19.29	18.43
0.40002501	184.6	-2.5	78.7	16.5	13.2	21.07	20.87	18.94	18.12
0.400029004	244.1	24.2	123.4	12.7	10.0	18.87	21.50	19.38	18.62
0.400041014	231.2	37.6	142.8	14.2	13.5	21.67	20.52	18.87	18.17
0.400049001	137.6	29.5	100.5	11.4	8.3	20.50	20.98	19.17	18.75
0.400050998	148.0	2.7	46.8	14.0	9.9	21.72	21.30	19.23	18.48
0.400052011	164.5	9.0	136.4	11.2	8.7	20.19	21.17	19.21	18.60
0.400052994	173.0	55.6	150.7	15.2	10.5	20.89	20.87	18.94	18.24
0.400059998	241.5	46.2	92.7	14.7	10.2	27.54	20.53	18.77	18.13
0.400070012	182.3	-1.3	127.6	13.7	9.7	21.40	20.43	18.95	18.33
0.400070012	169.9	33.3	146.3	17.8	11.2	22.49	20.47	18.90	18.16

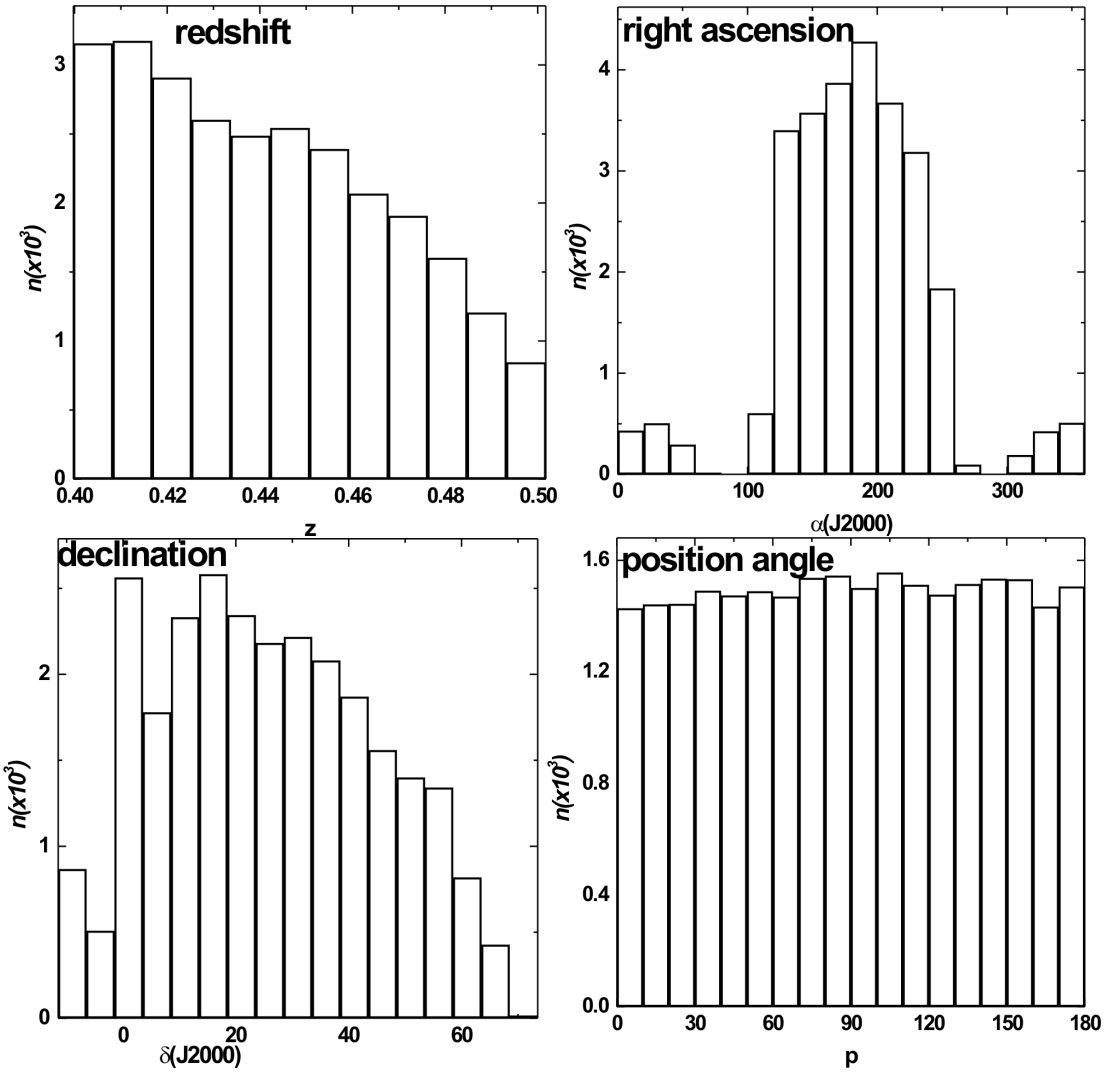

Figure 76: The distributions of redshift (z), right ascension (α), angle of declination (δ) and position angle (p) for the total sample having redshift 0.40 to 0.50.

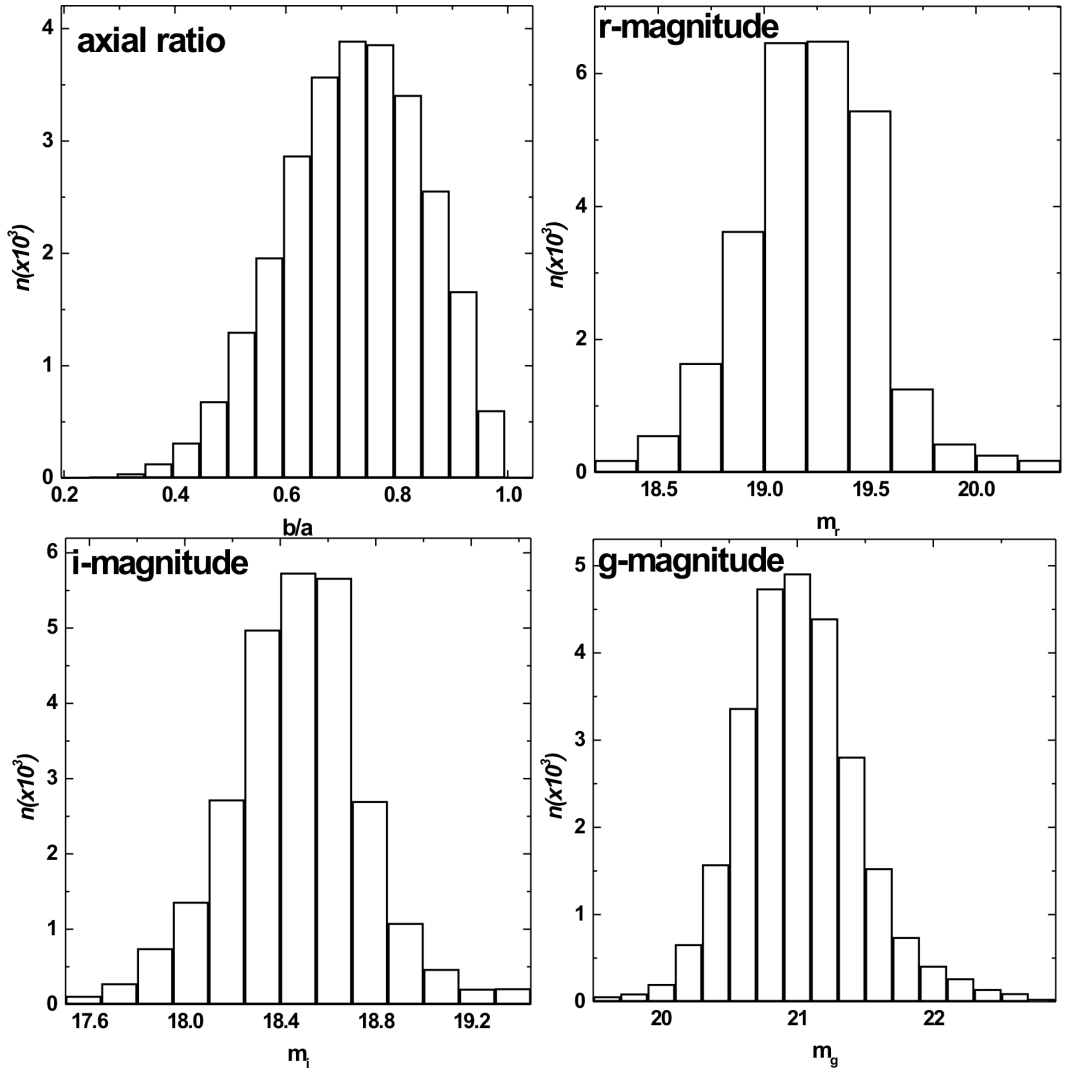

Figure 77: Axial ratio (b/a), r-magnitude (m_r), i-magnitude (m_i) and g-magnitude (m_g) for the total sample. The database of u-magnitude and z-magnitude are not complete.

Appendix C

Database: Blueshifted Galaxies

We obtained the data of 5 987 blue-shifted galaxies from The Sloan Digital Sky Survey (SDSS) Data Release 7 (DR7). We have retained only those galaxies that have redshift ($-z$) data at 95% level of significance. This removed 569 galaxies form our original data. After this removal we have 4 595 galaxies left in our database. Then the remaining galaxies were separated into three bins based upon their redshift values. We binned the data by taking the bin size of 1×10^{-4}, this resulted in three bins with number of galaxies roughly in the ratio of $3 : 2 : 1$ in the largest, medium and the smallest bins respectively. In binning process, galaxies that have very low and high redshift values were also removed.

We have compiled the database of diameters and position angle of galaxies using the database of near infrared ((i), 7 625 A°) and ultraviolet ((u), 3 543 A°) filters. These filters provide extreme limits for the isophotes.

Figure 78 shows redshift (z), right ascension (α), angle of declination (δ) and position angle (p) sample. Inhomogeneous distribution of positions (α and δ) can be seen. It is because of the nature of the survey. The redshift and position angle distribution are homogeneous.

Figure 79 shows axial ratio (b/a), u, g, r, i and z magnitude. The axial ratio distribution shows that there is heavy selection against nearly face on (b/a $\approx$1) galaxies and this distribution shows cosine behavior, as expected. The magnitude distribution is expected to show a Gaussian- like. The u-magnitude shows a Gaussian like distribution where other distributions are found to be deviated from the Gaussian.

Table 23: A sample page of database of blueshifted galaxies. First column represents blueshifts. The second and the third column represent right ascension and declination. The fourth and fifth column give the galactic longitude and galactic latitude. The sixth and seventh column represent position angle, ratio of minor and major diameters. The last five column represent u, g, r, i and z magnitude of negative blueshifted galaxies. A complete list of our database is added in a CD provided with this thesis.

z	(α)	(δ)	p	b/a	m_u	m_g	m_r	m_i	m_z
-0.0000133	207.47	24.64	0.08	0.84	20.91	18.48	17.08	16.09	15.55
-0.0000159	259.58	29.98	0.10	0.91	18.62	17.13	16.53	16.33	16.24
-0.000079	149.08	8.21	0.33	0.76	17.97	16.09	19.86	16.81	15.75
-0.000031	209.40	14.73	0.35	0.95	23.76	18.87	17.76	16.78	16.09
-0.0000297	226.86	48.48	0.69	0.89	19.08	16.98	16.13	15.85	15.69
-0.0000782	241.72	11.17	0.72	0.85	21.14	19.06	17.76	16.71	16.11
-0.0000702	172.58	-3.09	0.94	0.16	21.18	19.44	17.92	17.13	16.69
-0.0000638	153.19	27.86	0.97	0.79	20.78	18.83	17.85	17.84	17.50
-0.00000645	137.63	65.84	1.15	0.08	21.04	19.82	17.48	24.25	19.31
-0.0000466	233.34	-2.23	1.22	0.80	20.22	18.52	17.69	17.35	17.09
-0.0000628	120.51	10.74	1.27	0.74	20.28	17.75	16.66	16.29	16.08
-0.0000552	170.78	30.87	1.28	0.88	20.97	18.84	17.39	16.45	15.93
-0.0000015	213.34	39.08	1.36	0.94	20.13	17.99	17.37	17.91	18.10
-0.0000063	243.31	24.86	1.37	0.67	19.56	18.73	17.93	17.56	18.82
-0.0000656	120.52	35.02	1.47	0.95	19.01	16.79	15.70	15.24	14.97
-0.0000646	118.64	22.11	1.51	0.98	23.26	21.05	19.08	17.75	18.92
-0.0000409	168.86	17.88	1.84	0.74	20.40	18.20	17.19	16.13	16.21
-0.0000243	112.17	41.46	1.92	0.91	21.18	19.18	17.73	17.35	17.41
-0.0000386	246.01	14.55	1.95	0.86	21.39	19.95	18.52	17.79	17.44
-0.0000393	181.19	49.00	2.02	0.90	20.04	17.48	16.08	14.98	14.41
-0.0000743	220.56	51.82	2.04	0.56	23.12	21.95	20.57	18.90	17.88
-0.0000715	238.67	8.60	2.10	0.55	33.04	15.21	13.66	33.92	31.41
-0.0000358	153.80	8.33	2.19	0.82	22.08	19.94	18.42	17.56	17.05
-0.0000409	253.21	31.89	2.25	0.83	17.72	16.33	15.84	15.68	15.61

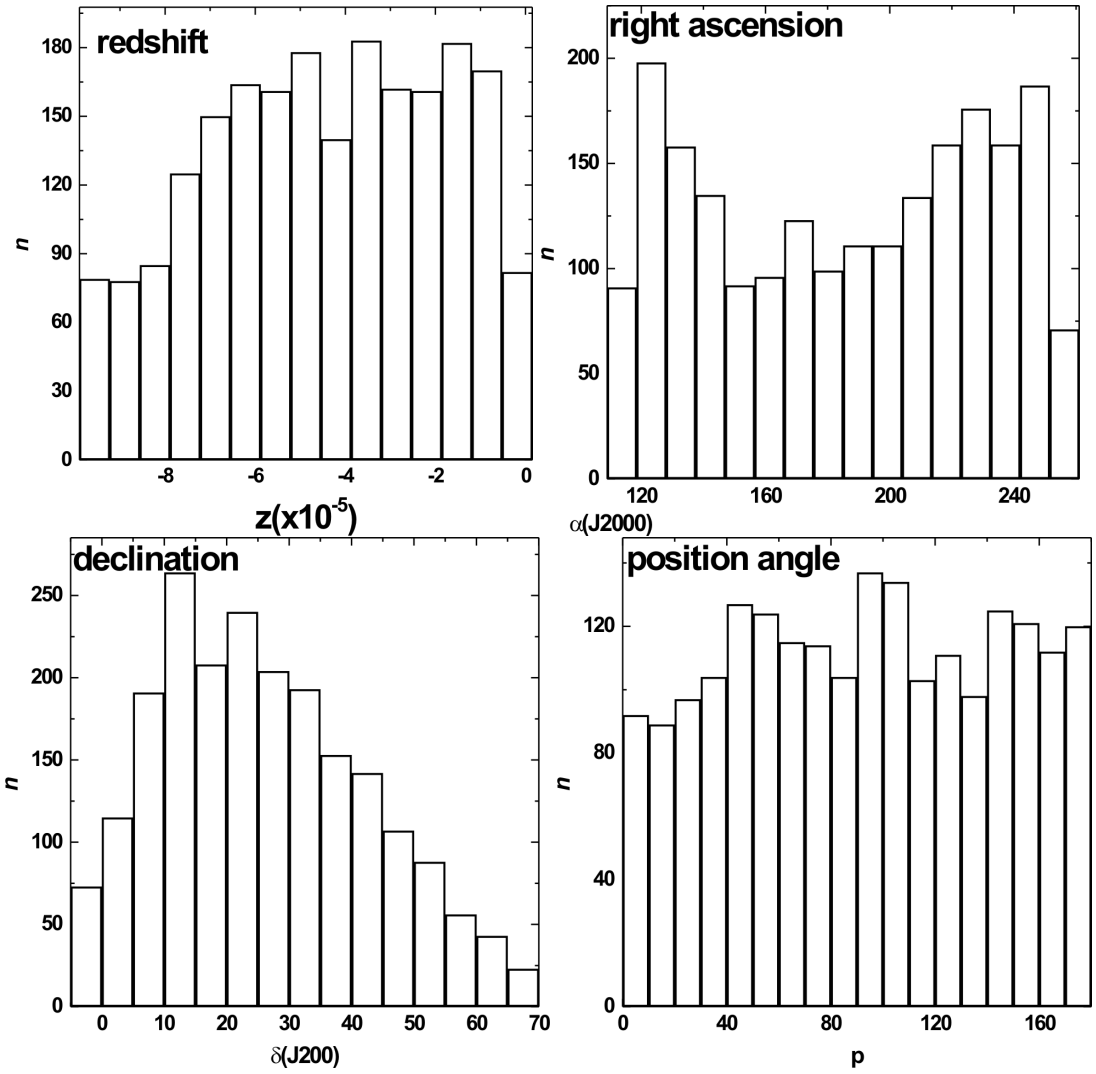

Figure 78: The distributions of redshift (z), right ascension (α), angle of declination (δ) and position angle (p) for the blue shifted galaxies.

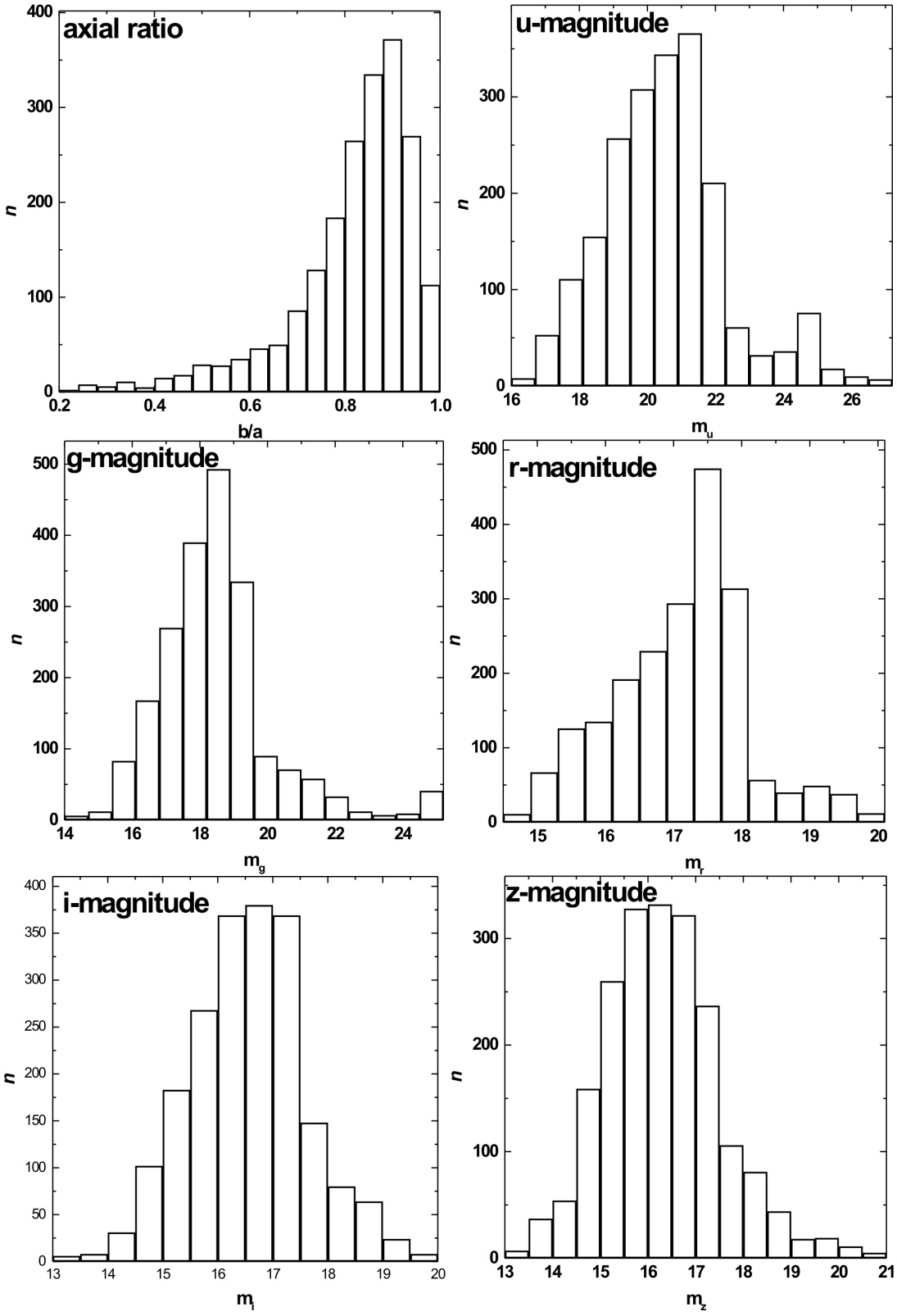

Figure 79: The distributions of axial ratio (b/a), u, g, r, i and z magnitude of blue shifted galaxies.

Appendix D

Database: Superclusters

D.1 Superclusters S[223+022+0117]

The database are taken from Sloan Digital Sky Survey (SDSS)of the Supercluster S[223+022+0117] consisting 1015 galaxies with redshift 0.11187 to 0.12282. The data base consisting redshift, right ascension, declination, position angle, axial ratio and five different magnitudes. Here, we present a sample page of our database in Table 24.

Figure 80 shows the redshift(Z), right ascension (RAJ2000), declination (DECJ2000) and position angle (PA) distribution respectively. Inhomogeneous distribution of positions (α and δ) can be seen. It is because of the nature of the survey. The redshift has nearly gaussian nature and position angle distribution are homogeneous.

Figure 81 shows axial ratio (b/a), u, g, r, i and z magnitude respectively. The axial ratio distribution shows that there is heavy selection against nearly edge on (b/a $\approx$0.1) galaxies and this distribution shows inhomogeneous behavior. The magnitude distribution is expected to show a Gaussian- like. The u-magnitude shows a Gaussian like distribution where other distributions are found to be deviated from the Gaussian.

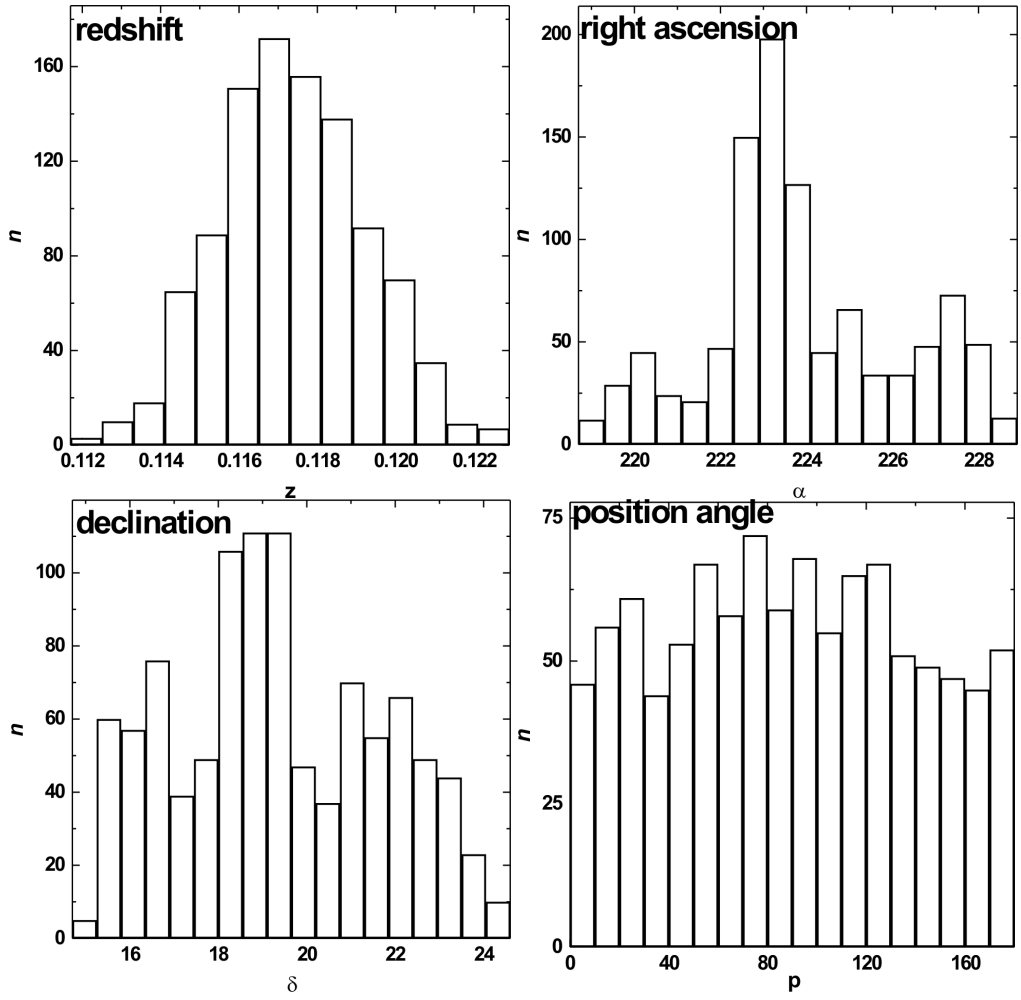

Figure 80: The distributions of redshift (z), right ascension (α), angle of declination (δ) and position angle (p) of the galaxies of the Superclusters S[223+022+0117]

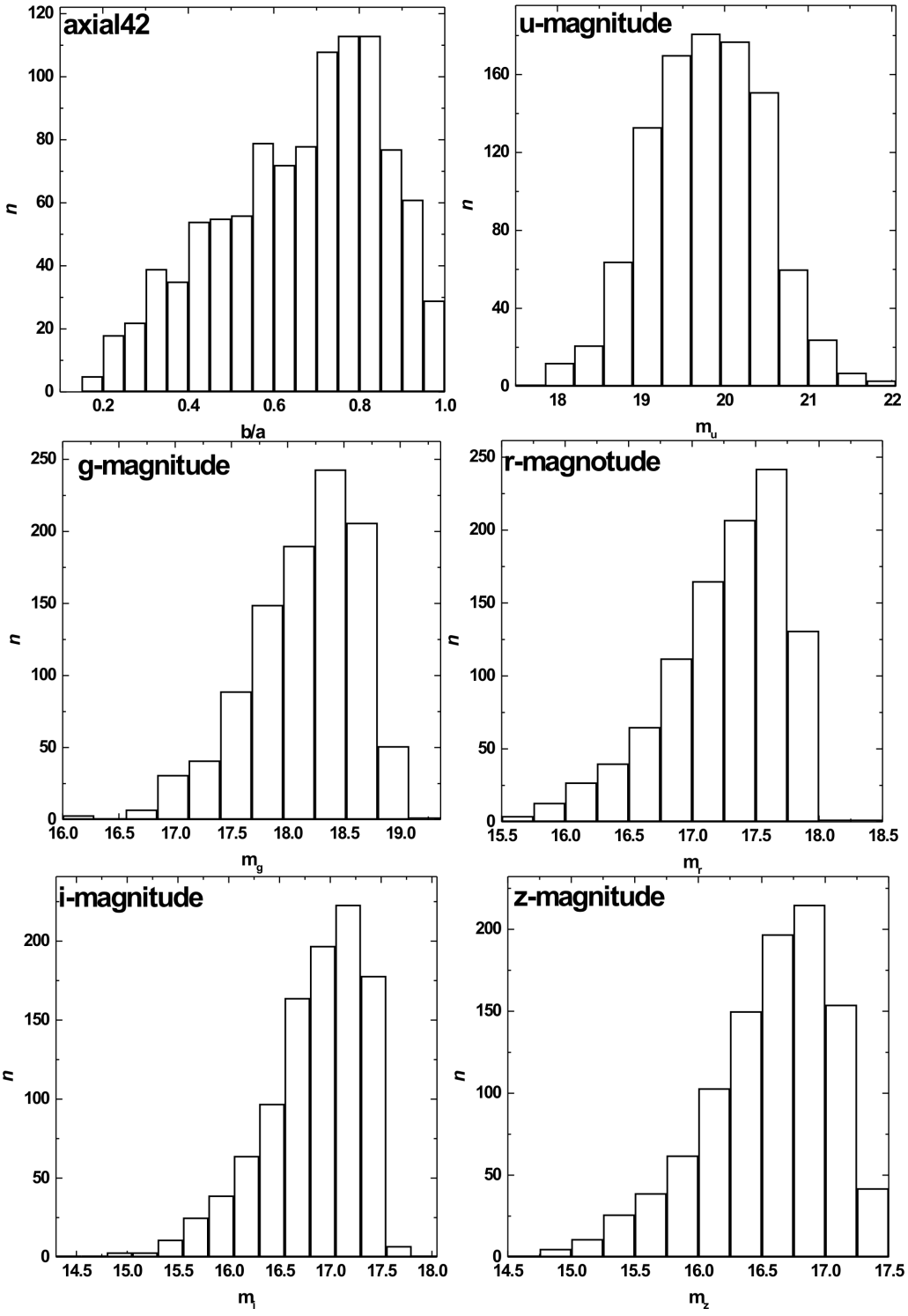

Figure 81: The distributions of axial ratio (b/a), u, g, r, i and z magnitudes of the galaxies of the Superclusters S[223+022+0117]

Table 24: A sample page of database of Superclusters S[223+022+0117]. First column represents redshift. The second and the third column represent right ascension and declination respectively. The fourth and fifth columns give the position angle, and ratio of major and minor diameters. The last five column represent u, g, r, i and z magnitude distributions respectively. A complete list of our database is added in a CD provided with this thesis.

z	(α)	(δ)	p	b/a	m_u	m_g	m_r	m_i	m_z
0.111871	222.45	20.91	102.09	0.37	20.36	18.42	17.44	17.02	16.71
0.112087	223.37	21.42	22.29	0.33	19.61	17.81	16.97	16.53	16.20
0.112455	219.23	18.93	57.08	0.88	19.97	17.80	16.80	16.35	15.95
0.112869	227.81	18.02	89.88	0.48	20.69	18.83	17.70	17.27	16.92
0.112921	223.11	22.01	85.08	0.41	20.31	18.49	17.49	17.04	16.70
0.112921	225.22	19.33	130.58	0.63	19.46	18.19	17.28	16.83	16.50
0.112925	223.33	21.45	120.99	0.47	19.35	17.50	16.50	16.06	15.74
0.11306	225.47	19.25	89.91	0.78	19.41	17.77	16.76	16.32	15.97
0.11313	223.46	21.80	117.34	0.69	19.99	18.30	17.34	16.93	16.64
0.113147	219.32	18.03	89.35	0.57	20.23	18.69	17.80	17.37	17.20
0.113147	219.32	18.10	181.26	0.73	19.82	18.06	17.14	16.72	16.39
0.113256	222.40	20.96	63.29	0.42	19.37	18.33	17.67	17.32	17.06
0.113291	222.70	21.22	90.96	0.78	20.79	18.74	17.76	17.38	17.01
0.113348	224.80	18.63	27.81	0.27	20.19	18.49	17.44	17.00	16.67
0.113487	227.76	18.07	100.67	0.34	20.25	18.46	17.38	16.94	16.57
0.113556	223.34	21.06	71.88	0.51	19.25	18.20	17.49	17.12	16.93
0.11362	223.59	21.74	140.94	0.67	19.50	17.97	17.32	16.94	16.57
0.113623	223.44	22.14	196.66	0.92	19.56	17.79	16.79	16.35	15.96
0.113714	223.31	21.44	59.50	0.78	19.76	17.92	16.88	16.41	16.13
0.113714	223.13	21.77	72.67	0.58	19.81	18.39	17.51	17.13	16.85
0.113798	219.16	18.93	75.69	0.34	20.79	18.56	17.47	17.03	16.62
0.113825	224.71	18.81	163.46	0.23	20.80	18.85	17.88	17.41	17.09
0.113843	223.35	22.00	58.84	0.63	19.60	17.86	16.86	16.44	16.12
0.113877	225.28	19.38	38.74	0.86	20.41	18.20	17.11	16.61	16.31
0.113918	227.74	18.09	80.23	0.88	20.56	18.89	17.82	17.42	17.04

D.2 Supercluster [239+016+0037]

The database are taken from Sloan Digital Sky Survey of seventh data released (SDSS DR7) of the Supercluster S[239+016+0037] consisting 1461 galaxies with redshift 0.029945 to 0.049101. The data base consisting redshift, right ascension, declination, position angle, axial ratio and five different magnitudes. Here, we present a sample page of our database in table 25.

Figure 82 shows the redshift(Z), right ascension (J2000), declination (J2000) and position angle (PA) distribution respectively. Inhomogeneous distribution of positions (α and δ) can be seen . It is because of the nature of the survey. The redshift has nearly gaussian nature and position angle distribution are homogeneous.

Figure 83 shows axial ratio (b/a),u, g, r, i and z magnitudes respectively. The axial ratio distribution shows nearly homogeneous behavior. The u-magnitude shows a Gaussian like distribution where other distributions are found to be deviated from the Gaussian.

Table 25: A sample page of our database of the Supercluster S[239+016+0037]. First column represents redshift. The second and the third column represent right ascension and declination. The fourth and fifth column represent the position angle and ratio of major and minor diameters. The last five column represent u, g, r, i and z magnitudes galaxies. A complete list of our database is added in a CD provided with this dissertation.

z	(α)	(δ)	p	b/a	m_u	m_g	m_r	m_i	m_z
0.029945	240.54	15.89	107.87	0.16	17.49	16.20	15.67	15.36	15.23
0.030182	240.47	15.83	119.88	0.62	18.37	17.11	16.31	15.94	15.68
0.03078	240.99	16.35	67.43	0.97	18.65	16.96	16.13	15.80	15.47
0.031049	240.76	15.99	153.86	0.82	19.10	17.37	16.48	16.13	15.87
0.031104	240.96	15.75	169.39	0.37	17.65	16.07	15.40	15.05	14.78
0.031118	240.62	15.63	51.42	0.55	19.42	17.96	17.29	17.00	16.95
0.031175	241.31	17.80	176.07	0.45	18.65	16.66	15.85	15.45	15.28
0.031414	241.28	16.31	140.55	0.22	19.10	17.39	16.49	16.02	15.77
0.031421	241.08	15.78	184.55	0.74	18.36	17.05	16.38	16.07	15.91
0.031457	241.29	17.76	168.95	0.30	19.56	17.46	16.63	16.26	16.02
0.031477	240.54	15.85	57.26	0.65	19.73	17.78	16.98	16.63	16.37
0.031562	241.29	17.72	167.66	0.91	20.00	18.02	17.17	16.79	16.54
0.03158	241.36	17.86	94.91	0.43	19.78	18.52	17.81	17.48	17.18
0.031634	241.18	17.76	162.98	0.43	18.95	17.59	17.07	16.80	16.66
0.031657	241.38	17.81	161.51	0.44	20.13	18.58	17.88	17.51	17.24
0.031675	241.24	16.34	67.04	0.64	19.28	18.05	17.57	17.33	17.17
0.031681	240.69	15.83	27.05	0.44	18.90	17.32	16.53	16.13	15.81
0.031731	241.03	17.24	129.54	0.94	19.13	17.48	16.88	16.64	16.51
0.031745	241.31	17.72	183.96	0.64	20.17	18.24	17.43	17.03	16.92
0.031810	240.37	15.61	122.86	0.51	19.29	17.89	17.18	16.83	16.60
0.031889	240.34	16.68	154.91	0.89	16.77	14.81	14.01	13.58	13.35
0.031895	240.38	16.76	185.67	0.61	17.02	15.51	14.81	14.40	14.17
0.031914	240.94	16.32	96.09	0.89	17.92	16.67	16.19	15.96	15.98
0.031962	240.79	16.63	162.50	0.49	19.21	18.46	17.72	17.63	21.19
0.031973	241.06	16.36	170.73	0.42	18.97	17.66	17.23	17.04	17.49

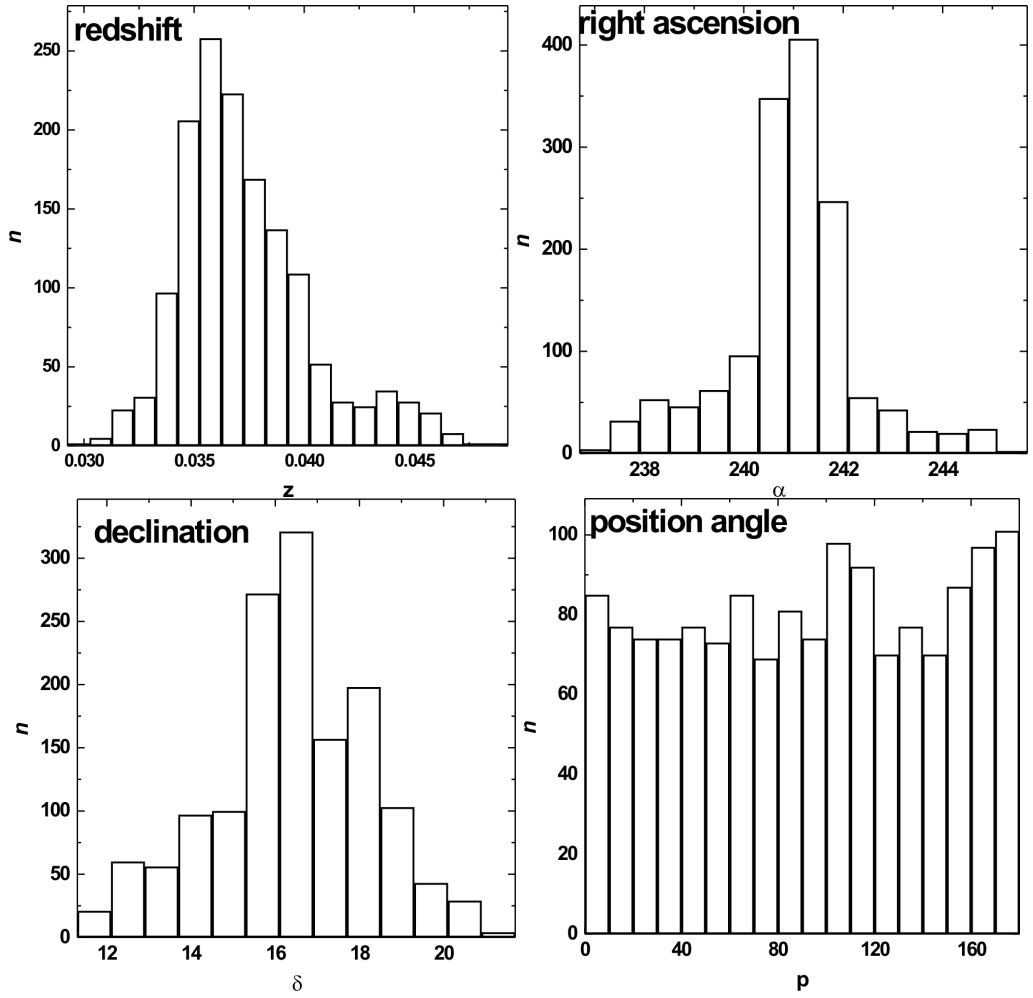

Figure 82: The distributions of redshift (z), right ascension (α), angle of declination (δ) and position angle (p) and inclination angle (i) for the total sample of the Supercluster [239+016+0037].

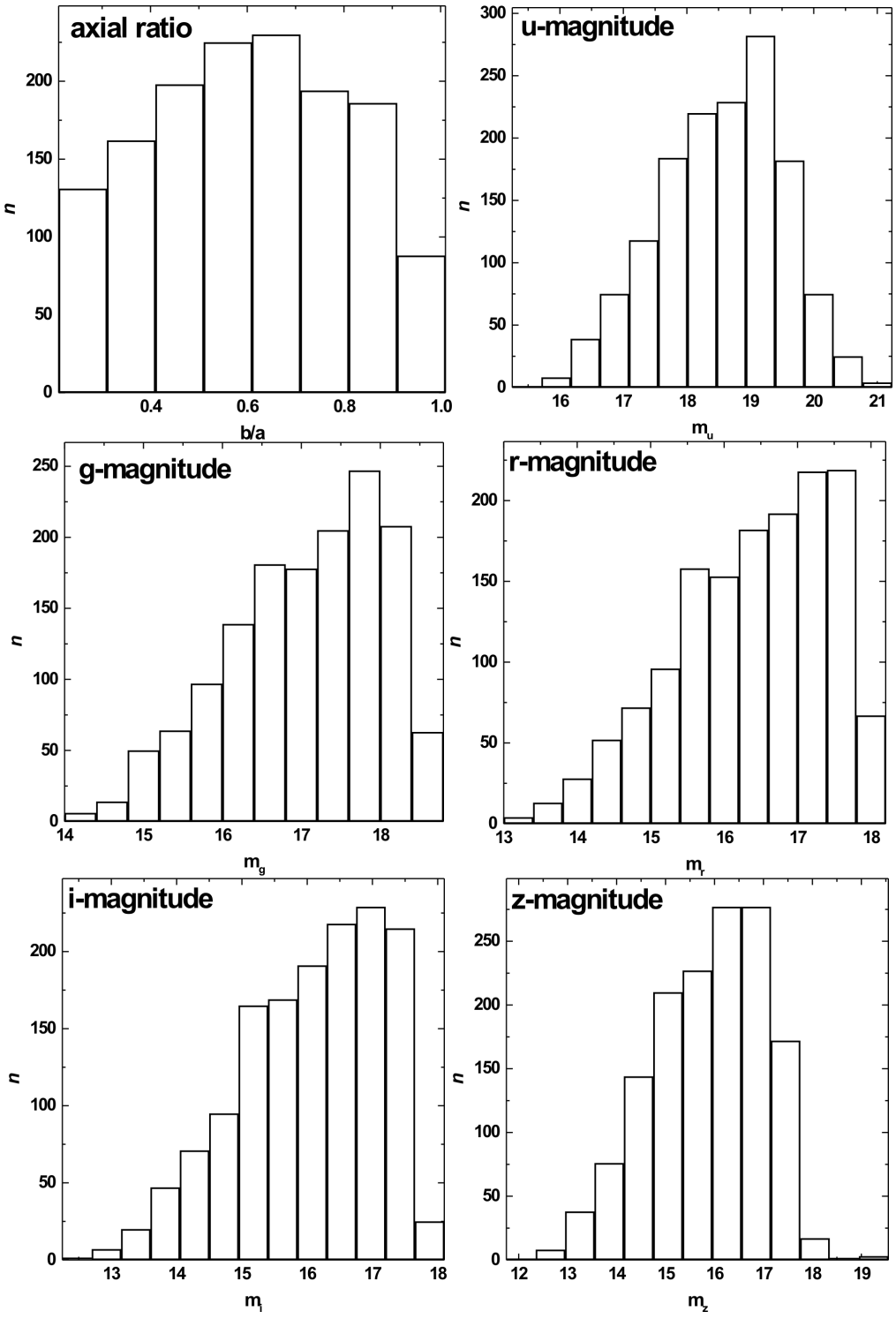

Figure 83: The distributions of axial ratio (b/a), u, g, r, i and z magnitude of the Supercluster [239+016+0037].

Appendix E

Database: Zone of Avoidance Galaxies

The database used in this work consists zone of avoidance galaxies located within regions $20^0 \leq l \leq 80^0$, $-10 \leq b \leq -5$ the survey in the first Palomar Observatory Sky Survey(POSS I). The database of these galaxies are taken from Marchitti (2001). The POSS I was carried out on the Oschin Schmit Telescope. Altogether 410 galaxy candidates are listed. The database consists right ascension, declination, galactic longitude, galactic latitude, position angle, semi major and semi minor diameters. Here, we present a sample page of our database in Table 26.

Figure 84, shows positions (α, δ), galactic longitude (l) and latitude (b), position angle and axial ratio of the galaxies. The right ascension, declination, axial ratio of galaxies are inhomogeneous while position angle is homogeneous. Also galactic longitude and latitude shows inhomogeneous nature.

Table 26: A sample page of the database of Zone of avoidance galaxies. First and second columns represent right ascension (α) and declination (δ). The next two columns represent galactic coordinates, longitude (l) and latitude (b), The last three columns shows position angle (p), major diameter (a) and minor diameter (b) respectively.

α	δ	l	b	p	a	b
283.36	-13.90	20.55	-6.81	175	2.0	1.5
284.96	-8.52	25.41	-6.16	100	3.0	2.0
285.28	-14.42	20.02	-9.13	85	2.0	1.5
285.76	-14.17	20.00	-9.65	135	2.5	1.5
285.81	-14.05	19.91	-9.75	45	1.5	1.0
285.97	-10.96	24.45	-7.74	85	2.0	1.0
286.64	-4.84	30.05	-5.71	95	1.5	0.6
286.82	-13.86	22.00	-9.85	175	1.5	1.0
286.88	-5.22	28.70	-6.65	85	6.0	1.5
288.49	-10.61	25.23	-10.11	95	1.5	1.0
288.53	-7.48	27.86	-8.89	160	1.5	1.0
288.64	-3.71	31.73	-7.09	95	3.0	1.0
288.64	-7.61	28.03	-8.93	150	5.0	2.0
288.70	-7.53	27.99	-9.01	170	2.0	1.0
289.14	-7.06	27.75	-9.62	95	2.0	1.0
289.40	-7.44	28.21	-9.68	35	2.5	1.0
289.57	-0.27	34.45	-6.76	150	3.0	1.0
290.04	-6.49	29.45	-9.78	50	2.0	1.5
290.52	-0.25	34.88	-7.62	155	2.0	1.5
290.57	-4.49	31.51	-9.37	15	3.0	1.0
290.58	-5.00	30.16	-10.03	0	2.0	1.5
290.61	-6.98	30.15	-10.07	35	1.5	1.0
290.78	-4.04	31.20	-9.75	170	9.0	1.5
290.81	-0.55	35.28	-7.74	160	1.5	1.0
290.84	-0.88	35.58	-7.61	0	2.0	1.0
291.15	0.42	36.36	-7.56	55	2.0	1.0
291.18	0.42	37.12	-7.21	95	3.5	2.0

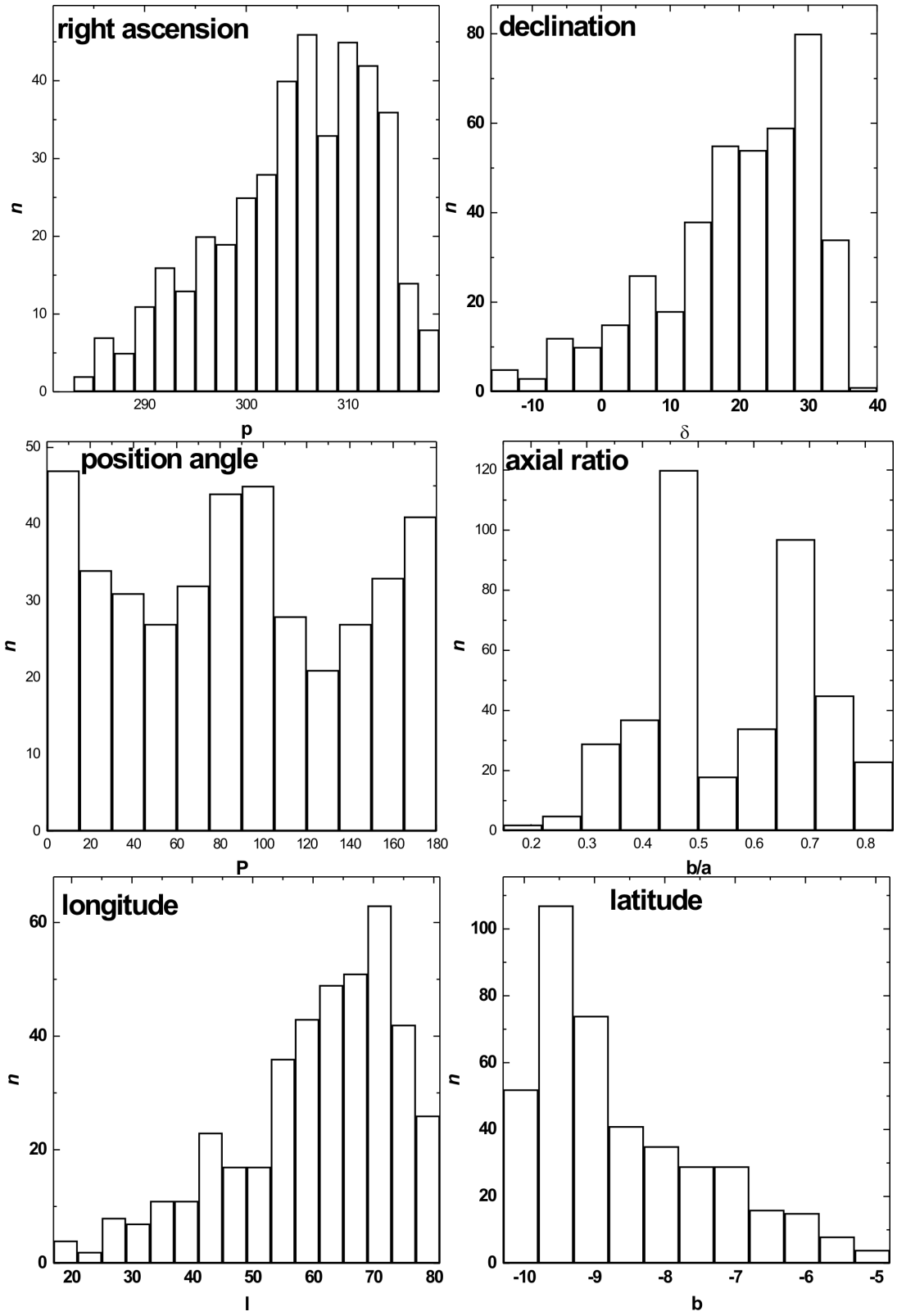

Figure 84: The distributions of right ascension (α), declination (δ), position angle (PA), axial ratio (b/a) for the sample, logitude (l) and latitude (b) of Zone-of-avoidance galaxies.

Appendix F

Database: SDSS DR7 Galaxies ($z = 0.10 - 0.11$)

The database used in this work consists galaxies located within the survey regions of Sloan Digital Sky Survey (SDSS) those have redshift in the range 0.10 to 0.11. Those database were searched and downloaded SDSS Data Release 7, which consists the table for the right assession, Declination, Major diameter, Minor diameter, Position Angle,five different magnitude and redshift values of those galaxies. There were 44 830 galaxies in the downloaded catalog. Among them, 81 galaxies were excluded due to the lack of the position angles. And, finally we have 44 741 galaxies in our sample, of which the positions (Right Ascension and Declination), major and minor diameters, position angles and redshifts are known. Here, we present a sample page of our database in Table 27.

Figure 85 shows the redshift(Z), right ascension (J2000), declination (J2000) and position angle (PA) distribution respectively. Inhomogeneous distribution of positions (α and δ) can be seen. It is because of the nature of the survey. The redshift and position angle distribution are homogeneous.

Figure 86 shows axial ratio (b/a), u, g and r magnitude respectively. The axial ratio distribution shows that there is heavy selection against nearly face on (b/a $\approx$1) galaxies and this distribution shows cosine behavior, as expected. The magnitude distribution is expected to show a Gaussian-like. The u-magnitude shows a Gaussian like distribution where other distributions are found to be deviated from the Gaussian.

Table 27: A sample page of the database of SDSS DR7 galaxies that have redshifts in the range 0.10 to 0.11. First column represent redshift. The second and the third columns represent right ascension and declination. The fourth, fifth and sixth columns represent the position angle ,major and minor diameters respectively. The last three column represent u, g and r magnitude distributions of galaxies respectively. List of our database is added in a CD provided with this thesis.

Redshift	α	δ	p	a	b	m_u	m_g	m_r
0.100000001	168.24	-0.01	155.08	30.59	14.23	20.02	18.17	17.13
0.100000001	168.97	18.10	179.33	32.35	20.18	18.69	17.21	16.45
0.100001000	122.65	40.34	100.96	30.40	25.68	19.66	17.71	16.72
0.100001000	160.98	4.83	126.97	20.12	16.98	20.14	18.30	17.42
0.100001000	173.90	4.71	32.33	18.12	16.21	20.46	18.66	17.70
0.100001000	203.42	57.83	147.58	19.37	18.53	19.76	18.01	17.10
0.100001000	203.48	40.05	107.50	20.43	15.77	19.65	18.22	17.41
0.100001000	229.30	4.59	82.51	27.06	11.36	20.02	17.93	16.93
0.100001000	255.76	33.92	11.46	34.28	15.66	19.21	17.37	16.43
0.100001998	121.64	16.19	151.27	19.76	17.95	19.98	18.41	17.50
0.100001998	123.76	12.22	150.94	40.63	24.18	19.46	17.34	16.40
0.100001998	137.83	62.32	22.24	26.55	18.96	19.71	17.90	16.92
0.100001998	147.11	28.17	42.24	18.32	8.01	20.04	18.75	17.84
0.100001998	155.53	47.96	2.82	17.66	12.73	19.73	18.17	17.27
0.100001998	182.59	42.20	9.16	21.60	18.16	19.31	18.36	17.80
0.100001998	228.77	4.51	18.89	38.62	27.03	19.58	17.14	16.18
0.100001998	248.10	37.63	152.02	23.05	11.44	20.04	18.46	17.53
0.100002997	124.20	6.52	78.35	18.37	17.27	19.17	18.01	17.27
0.100002997	133.19	15.84	61.35	34.14	13.56	20.02	17.77	16.92
0.100002997	138.69	13.85	32.86	24.41	15.15	19.46	18.00	17.36
0.100002997	175.15	14.03	165.91	23.36	18.26	19.15	17.70	16.91
0.100002997	184.75	28.22	77.00	16.13	11.85	20.40	18.51	17.69
0.100002997	187.41	2.61	104.47	21.61	17.39	19.27	17.64	17.03
0.100002997	209.37	13.57	152.83	22.83	9.80	19.65	18.41	17.56

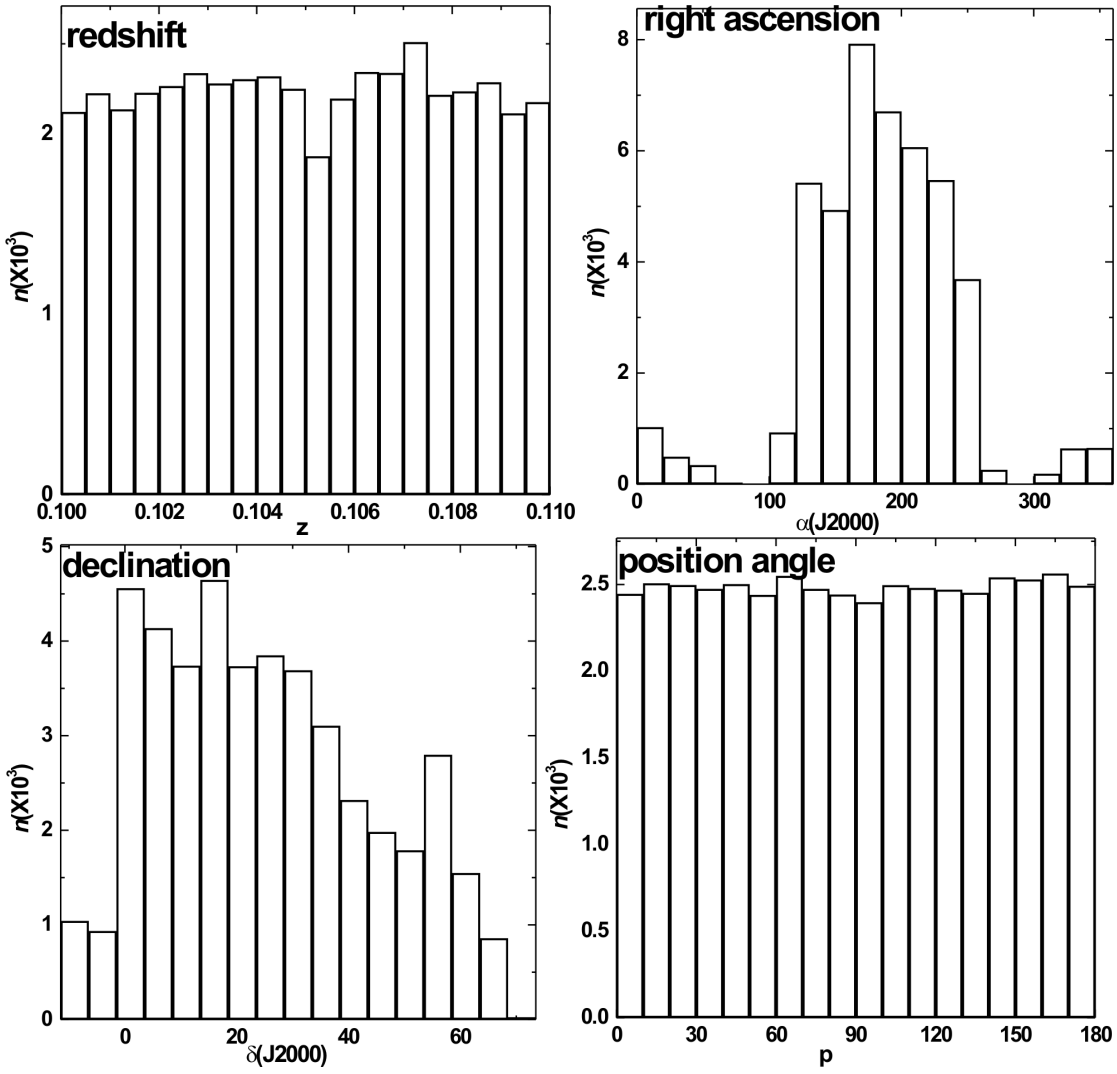

Figure 85: The distributions of redshift (z), right ascension (α), angle of declination (δ) and position angle (p) of the SDSS DR7 galaxies that have redshifts in the range 0.10 to 0.11.

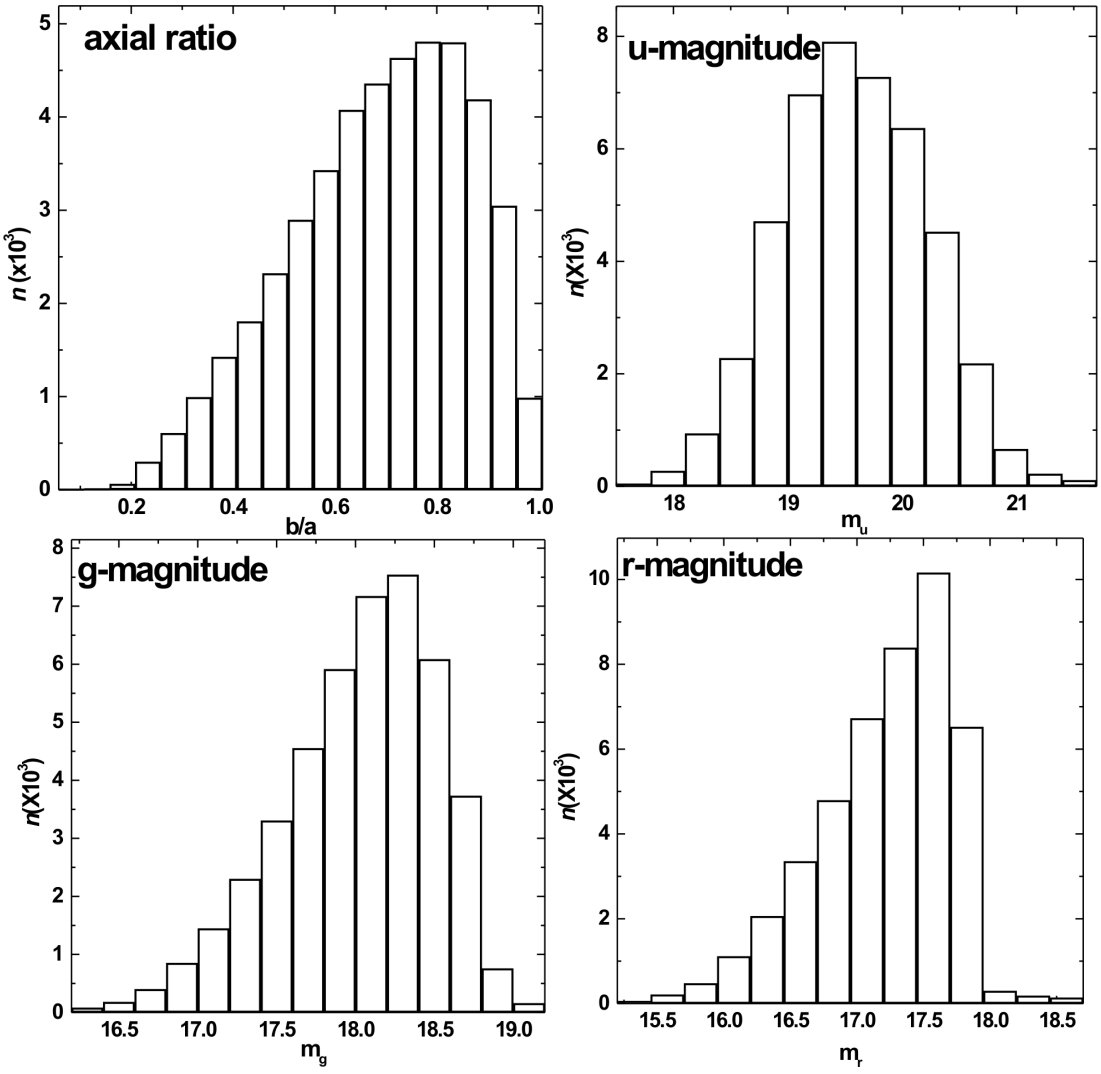

Figure 86: The axial ratio (b/a), u-magnitude (m_u), g-magnitude(m_g) and r-magnitude(m_r) distributions of SDSS DR7 galaxies that have redshifts in the range 0.10 to 0.11.

The result of all 200 samples are given below.

Table 28: Statistics of the polar angle (θ) and azimuthal angle (ϕ) distribution of galaxies that have redshifts in the range 0.10 to 0.11. The first column represents the samples. The second column represent angles. In the table, P($> \chi^2$) represents the chi-square probability (third column). Similarly, C/C(σ) represents the auto-correlation coefficient (forth column). The last two columns give the first order Fourier coefficient $\Delta_{11}/\sigma(\Delta_{11})$ and first order Fourier probability P($> \Delta_1$).

sample	angles	$P > \chi^2$	$C/C(\sigma)$	$\triangle_{11}/\sigma(\triangle_{11})$	$P > \triangle_1$
z1	polar	0.884	0.458	-0.632	0.797
Z1	azimuthal	0.917	0.208	0.265	0.289
Z2	polar	0.714	-0.824	-0.198	0.943
Z2	azimuthal	0.268	0.424	0.913	0.507
Z3	polar	0.268	0.319	-0.430	0.900
Z3	zimuthal	0.486	-0.322	-0.302	0.952
Z4	polar	0.495	-0.415	0.177	0.937
Z4	azimuthal	0.574	1.222	2.022	0.053
Z5	polar	0.671	0.071	-0.191	0.970
Z5	azimuthal	0.738	-0.987	-0.105	0.859
Z6	polar	0.640	-0.445	-1.057	0.524
Z6	azimuthal	0.179	-0.024	1.121	0.318
Z7	polar	0.553	0.038	-0.137	0.944
Z7	azimuthal	0.986	0.259	0.926	0.555
Z8	polar	0.988	0.188	0.448	0.879
Z8	azimuthal	0.745	-0.021	1.084	0.502
Z9	polar	0.745	-0.021	1.084	0.502
Z9	azimuthal	0.365	1.707	1.591	0.208
Z10	polar	0.643	-0.404	-0.141	0.954
Z10	azimuthal	0.960	-0.065	0.556	0.578

Continued on next page

Table 28 – continued from previous page

sample	angles	$P > \chi^2$	$C/C(\sigma)$	$\triangle_{11}/\sigma(\triangle_{11})$	$P > \triangle_1$
Z11	polar	0.188	-1.810	0.247	0.970
Z11	azimuthal	0.298	-0.784	0.930	0.347
Z12	polar	0.524	-1.657	-0.472	0.804
Z12	azimuthal	0.037	-2.452	0.368	0.895
Z13	polar	0.802	-0.825	-0.057	0.967
Z13	azimuthal	0.819	0.327	0.973	0.467
Z14	polar	0.939	0.033	-0.376	0.898
Z14	azimuthal	0.162	-0.689	0.382	-0.079
Z15	polar	0.493	-1.848	0.177	0.978
Z15	azimuthal	0.302	1.040	1.451	0.258
Z16	polar	0.908	0.258	-0.432	0.835
Z16	azimuthal	0.845	-0.715	0.323	0.908
Z17	polar	0.727	-0.199	-0.527	0.659
Z17	azimuthal	0.305	-1.108	1.762	0.142
Z18	polar	0.621	0.871	0.621	0.609
Z18	azimuthal	0.740	-0.006	-0.271	0.964
z19	polar	0.237	-2.158	-0.397	0.922
Z19	azimuthal	0.440	-0.287	0.491	0.681
Z20	polar	0.294	-0.238	0.498	0.698
Z20	azimuthal	0.314	-2.723	0.136	0.904
Z21	polar	0.372	-1.103	-0.404	0.910
Z21	azimuthal	0.705	-0.012	0.706	0.588
Z22	polar	0.416	0.354	0.380	0.915
Z22	azimuthal	0.859	-0.125	-0.095	0.995
Z23	polar	0.911	0.216	-0.926	0.598
Z23	azimuthal	0.900	0.165	-0.411	0.792
Z24	polar	0.930	-0.289	0.296	0.871
Z24	azimuthal	0.918	-0.331	-0.905	0.404
Z25	polar	0.903	-0.983	-0.178	0.982

Continued on next page

Table 28 – continued from previous page

sample	angles	$P > \chi^2$	$C/C(\sigma)$	$\triangle_{11}/\sigma(\triangle_{11})$	$P > \triangle_1$
Z25	azimuthal	0.832	-0.977	0.765	0.598
Z26	polar	0.575	-0.482	-0.264	0.761
Z26	azimuthal	0.691	0.348	-1.273	0.414
Z27	polar	0.995	-0.214	-0.320	0.947
Z27	azimuthal	0.935	0.585	0.467	0.739
Z28	polar	0.963	-0.370	-0.131	0.907
Z28	azimuthal	0.751	-0.129	0.023	0.969
Z29	polar	0.910	-0.364	0.162	0.983
Z29	azimuthal	0.862	-0.954	-0.435	0.907
Z30	polar	0.438	0.424	0.356	0.926
Z30	azimuthal	0.866	-0.187	-0.099	0.995
Z31	polar	0.494	0.615	-0.422	0.851
Z31	azimuthal	0.791	-1.138	-0.356	0.869
Z32	polar	0.745	-0.688	0.939	0.567
Z32	azimuthal	0.517	-0.355	-1.132	0.468
Z33	polar	0.703	0.551	-0.851	0.516
Z33	azimuthal	0.659	0.202	0.969	0.467
Z34	polar	0.921	-0.972	0.469	0.890
Z34	azimuthal	0.507	0.611	1.829	0.157
Z35	polar	0.928	-0.207	-0.133	0.983
Z35	azimuthal	0.538	-0.347	-0.016	1.000
Z36	polar	0.145	1.498	2.343	0.052
Z36	azimuthal	0.369	0.328	1.036	0.527
Z37	polar	0.960	-0.087	0.282	0.959
Z37	azimuthal	0.746	0.508	0.616	0.249
Z38	polar	0.855	-0.483	0.035	0.991
Z38	azimuthal	0.326	-1.296	-0.355	0.909
Z39	polar	0.759	-0.120	-0.475	0.889
Z39	azimuthal	0.811	0.647	0.557	0.644

Continued on next page

Table 28 – continued from previous page

sample	angles	$P > \chi^2$	$C/C(\sigma)$	$\triangle_{11}/\sigma(\triangle_{11})$	$P > \triangle_1$
Z40	polar	0.371	-0.229	0.309	0.832
Z40	azimuthal	0.513	-1.318	0.145	0.974
Z41	polar	0.271	0.360	-1.247	0.322
Z41	azimuthal	0.253	-0.957	0.301	0.412
Z42	polar	0.975	0.663	0.149	0.877
Z42	azimuthal	0.319	-0.938	0.987	0.611
Z43	polar	0.718	-1.223	0.389	0.802
Z43	azimuthal	0.628	-0.449	-1.385	0.322
Z44	polar	0.285	-0.607	-0.085	0.986
Z44	azimuthal	0.227	0.146	1.007	0.593
Z45	polar	0.991	0.036	0.930	0.644
Z45	azimuthal	0.363	-1.149	-0.042	0.977
Z46	polar	0.032	-1.560	0.069	0.953
Z46	azimuthal	0.868	-0.697	-0.680	0.778
Z47	polar	0.655	-0.140	0.426	0.809
Z47	azimuthal	0.071	-0.905	0.682	0.777
Z48	polar	0.876	0.018	0.149	0.988
Z48	azimuthal	0.986	-0.117	0.349	0.828
Z49	polar	0.525	-0.144	0.600	0.581
Z49	azimuthal	0.574	-0.682	-0.318	0.873
Z50	polar	0.359	-0.067	0.307	0.953
Z50	azimuthal	0.994	-0.069	0.744	0.674
Z51	polar	0.938	-0.343	-0.200	0.943
Z51	azimuthal	0.818	-0.482	-0.401	0.763
Z52	polar	0.241	-0.758	-0.456	0.850
Z52	azimuthal	0.987	-0.544	0.112	0.922
Z53	polar	0.038	-0.150	1.130	0.367
Z53	azimuthal	0.660	0.057	-0.302	0.876
Z54	polar	0.365	-1.115	-0.691	0.774

Continued on next page

Table 28 – continued from previous page

sample	angles	$P > \chi^2$	$C/C(\sigma)$	$\triangle_{11}/\sigma(\triangle_{11})$	$P > \triangle_1$
Z54	azimuthal	0.513	0.136	-0.038	0.574
Z55	polar	0.733	-0.411	-0.388	0.901
Z55	azimuthal	0.590	-0.466	0.134	0.816
Z56	polar	0.533	-1.239	-0.113	0.993
Z56	azimuthal	0.425	0.590	-1.139	0.386
Z57	polar	0.223	-1.412	0.422	0.908
Z57	azimuthal	0.121	-0.858	-1.075	0.313
Z58	polar	0.619	-0.136	-0.964	0.505
Z58	azimuthal	0.132	-2.051	1.284	0.434
Z59	polar	0.031	-2.003	-0.322	0.911
Z59	azimuthal	0.961	-0.025	-0.357	0.938
Z60	polar	0.317	-2.085	0.174	0.882
Z60	azimuthal	0.838	0.439	0.740	0.750
Z61	polar	0.927	-0.672	0.134	0.981
Z61	azimuthal	0.929	-0.152	0.707	0.609
Z62	polar	0.564	-1.316	-0.890	0.655
Z62	azimuthal	0.510	-1.471	0.382	0.914
Z63	polar	0.943	-0.156	-0.520	0.866
Z63	azimuthal	0.961	0.425	-0.246	0.376
Z64	polar	0.043	-2.291	0.030	0.945
Z64	azimuthal	0.856	0.435	0.789	0.711
Z65	polar	0.321	-0.831	0.042	0.978
Z65	azimuthal	0.649	-0.174	-0.408	0.774
Z66	polar	0.023	-1.212	0.473	0.661
Z66	azimuthal	0.283	2.253	1.974	0.097
Z67	polar	0.608	0.014	-0.013	0.963
Z67	azimuthal	0.396	-1.324	0.349	0.853
Z68	polar	0.435	0.558	-0.210	0.790
Z68	azimuthal	0.646	0.220	1.285	0.255

Continued on next page

Table 28 – continued from previous page

sample	angles	$P > \chi^2$	$C/C(\sigma)$	$\triangle_{11}/\sigma(\triangle_{11})$	$P > \triangle_1$
Z69	polar	0.106	-0.931	-0.880	0.579
Z69	azimuthal	0.948	-0.895	-0.193	0.982
Z70	polar	0.806	-0.729	0.599	0.786
Z70	azimuthal	0.754	-1.010	-0.370	0.717
Z71	polar	0.794	-0.114	0.358	0.887
Z71	azimuthal	0.263	-0.501	0.434	0.910
Z72	polar	0.566	0.275	-0.044	0.846
Z72	azimuthal	0.504	1.067	-1.907	0.121
Z73	polar	0.267	-1.616	0.434	0.885
Z73	azimuthal	0.921	-0.616	-0.449	0.878
Z74	polar	0.311	-1.040	-0.353	0.897
Z74	azimuthal	0.281	-0.732	0.571	0.653
Z75	polar	0.226	-0.821	0.239	0.852
Z75	azimuthal	0.408	-0.984	0.524	0.751
Z76	polar	0.435	-0.124	-0.775	0.720
Z76	azimuthal	0.894	-0.218	0.532	0.667
Z77	polar	0.972	0.856	0.472	0.830
Z77	azimuthal	0.116	0.893	0.086	0.799
Z78	polar	0.429	1.724	1.104	0.428
Z78	azimuthal	0.053	-2.200	1.030	0.416
Z79	polar	0.704	0.482	-0.759	0.512
Z79	azimuthal	0.240	-1.123	-0.056	0.606
Z80	polar	0.441	-1.513	0.712	0.753
Z80	azimuthal	0.677	0.381	1.855	0.126
Z81	polar	0.443	1.352	-1.399	0.279
Z81	azimuthal	0.304	-0.296	-1.595	0.229
Z82	polar	0.716	-1.363	-0.349	0.937
Z82	azimuthal	0.654	-1.018	0.185	0.760
Z83	polar	0.680	-1.309	-0.158	0.983

Continued on next page

Table 28 – continued from previous page

sample	angles	$P > \chi^2$	$C/C(\sigma)$	$\triangle_{11}/\sigma(\triangle_{11})$	$P > \triangle_1$
Z83	azimuthal	0.741	-0.370	0.532	0.525
Z84	polar	0.814	-0.409	-0.002	0.980
Z84	azimuthal	0.464	-0.551	-0.008	0.583
Z85	polar	0.445	-2.095	0.460	0.848
Z85	azimuthal	0.230	-1.820	1.086	0.498
Z86	polar	0.685	-0.491	-0.944	0.582
Z86	azimuthal	0.656	0.530	0.315	0.592
Z87	polar	0.680	-0.544	0.548	0.855
Z87	azimuthal	0.646	-0.412	0.032	0.722
Z88	polar	0.899	0.121	0.847	0.543
Z88	azimuthal	0.847	-0.026	0.858	0.657
Z89	polar	0.528	0.992	0.800	0.661
Z89	azimuthal	0.193	-1.203	1.233	0.467
Z90	polar	0.408	-1.738	-0.003	0.987
Z90	azimuthal	0.717	-0.868	-1.160	0.333
Z91	polar	0.013	0.995	0.222	0.788
Z91	azimuthal	0.882	0.056	1.657	0.250
Z92	polar	0.173	-0.006	-0.756	0.692
Z92	azimuthal	0.712	0.444	0.830	0.572
Z93	polar	0.348	-0.816	-0.789	0.594
Z93	azimuthal	0.243	-0.492	-0.089	0.722
Z94	polar	0.941	-0.172	-0.268	0.907
Z94	azimuthal	0.277	-0.710	0.319	0.799
Z95	polar	0.215	0.196	-0.502	0.865
Z95	azimuthal	0.225	-1.095	0.733	0.446
Z96	polar	0.576	-0.771	-0.729	0.709
Z96	azimuthal	0.237	-0.650	-0.444	0.856
Z97	polar	0.163	-2.149	-0.044	0.852
Z97	azimuthal	0.891	-0.305	-0.737	0.703

Continued on next page

Table 28 – continued from previous page

sample	angles	$P > \chi^2$	$C/C(\sigma)$	$\triangle_{11}/\sigma(\triangle_{11})$	$P > \triangle_1$
Z98	polar	0.208	-1.076	0.964	0.586
Z98	azimuthal	0.724	-0.465	-0.026	0.996
Z99	polar	0.978	-0.380	0.164	0.976
Z99	azimuthal	0.992	-0.410	-0.234	0.935
Z100	polar	0.577	0.115	-0.931	0.570
Z100	azimuthal	0.557	0.113	1.498	0.326
Z101	polar	0.470	0.136	0.256	0.928
Z101	azimuthal	0.332	-1.845	-0.645	0.812
Z102	polar	0.944	-0.055	0.551	0.852
Z102	azimuthal	0.820	-1.240	0.339	0.910
Z103	polar	0.418	-0.266	-1.042	0.554
Z103	azimuthal	0.214	-0.645	-1.793	0.172
Z104	polar	0.328	0.087	0.750	0.562
Z104	azimuthal	0.292	0.039	0.905	0.665
Z105	polar	0.787	0.214	0.128	0.948
Z105	azimuthal	0.722	-0.588	0.069	0.890
Z106	polar	0.635	-0.125	-1.100	0.518
Z106	azimuthal	0.272	-0.245	-0.770	0.534
Z107	polar	0.829	-0.638	0.136	0.917
Z107	azimuthal	0.286	-1.463	-0.301	0.600
Z108	polar	0.992	0.309	-0.322	0.946
Z108	azimuthal	0.445	0.072	-0.427	0.192
Z109	polar	0.238	-0.331	1.026	0.497
Z109	azimuthal	0.020	-2.173	-1.728	0.203
Z110	polar	0.242	-0.003	0.356	0.868
Z110	azimuthal	0.225	0.418	0.319	0.935
Z111	polar	0.344	-1.517	-0.132	0.931
Z111	azimuthal	0.781	1.471	-0.473	0.450
Z112	polar	0.864	-0.443	-0.188	0.981

Continued on next page

Table 28 – continued from previous page

sample	angles	$P > \chi^2$	$C/C(\sigma)$	$\triangle_{11}/\sigma(\triangle_{11})$	$P > \triangle_1$
Z112	azimuthal	0.833	-0.061	-0.211	0.944
Z113	polar	0.015	1.191	-0.683	0.453
Z113	azimuthal	0.113	-0.738	-0.370	0.368
Z114	polar	0.956	0.635	0.503	0.855
Z114	azimuthal	0.965	-0.228	0.320	0.923
Z115	polar	0.150	-1.149	0.130	0.975
Z115	azimuthal	0.771	1.310	0.525	0.396
Z116	polar	0.187	1.661	-1.400	0.324
Z116	azimuthal	0.016	1.250	0.932	0.294
Z117	polar	0.823	-0.294	-0.546	0.844
Z117	azimuthal	0.553	-0.235	-0.421	0.914
Z118	polar	0.272	-1.624	-0.262	0.960
Z118	azimuthal	0.719	-0.422	1.010	0.592
Z119	polar	0.739	0.102	0.560	0.811
Z119	azimuthal	0.109	-1.798	0.408	0.888
Z120	polar	0.018	0.592	-0.608	0.812
Z120	azimuthal	0.935	-0.076	1.330	0.399
Z121	polar	0.880	0.251	0.205	0.964
Z121	azimuthal	0.691	0.400	0.894	0.349
Z122	polar	0.949	-0.060	0.680	0.776
Z122	azimuthal	0.926	-0.587	-0.164	0.986
Z123	polar	0.210	-0.752	-0.070	0.997
Z123	azimuthal	0.162	-0.035	-0.135	0.437
Z124	polar	0.990	-0.385	-0.534	0.860
Z124	azimuthal	0.391	0.063	0.714	0.773
Z125	polar	0.034	-2.032	-1.076	0.552
Z125	azimuthal	0.857	-0.133	-0.197	0.539
Z126	polar	0.045	0.084	-0.687	0.623
Z126	azimuthal	0.154	-1.893	-0.166	0.699

Continued on next page

Table 28 – continued from previous page

sample	angles	$P > \chi^2$	$C/C(\sigma)$	$\triangle_{11}/\sigma(\triangle_{11})$	$P > \triangle_1$
Z127	polar	0.652	0.101	-0.307	0.897
Z127	azimuthal	0.337	0.673	-0.258	0.965
Z128	polar	0.088	0.644	0.273	0.778
Z128	azimuthal	0.827	-1.488	0.346	0.913
Z129	polar	0.694	-0.598	-0.900	0.584
Z129	azimuthal	0.281	-2.471	0.163	0.955
Z130	polar	0.550	-1.626	0.652	0.754
Z130	azimuthal	0.747	0.069	0.313	0.793
Z131	polar	0.338	-0.641	-0.913	0.642
Z131	azimuthal	0.703	-1.327	-1.021	0.532
Z132	polar	0.999	0.020	-0.525	0.808
Z132	azimuthal	0.851	0.499	0.040	0.565
Z133	polar	0.091	-1.584	-0.325	0.932
Z133	azimuthal	0.500	1.560	-1.674	0.139
Z134	polar	0.899	-0.558	-0.384	0.924
Z134	azimuthal	0.994	-0.659	-0.322	0.940
Z135	polar	0.332	-1.574	-0.198	0.975
Z135	azimuthal	0.657	-0.011	-0.439	0.886
Z136	polar	0.106	0.385	-1.061	0.507
Z136	azimuthal	0.488	-0.857	-0.592	0.662
Z137	polar	0.004	-0.294	-1.039	0.539
Z137	azimuthal	0.656	0.152	-1.990	0.126
Z138	polar	0.759	0.865	-0.978	0.599
Z138	azimuthal	0.879	0.038	-0.762	0.437
Z139	polar	0.773	-0.932	-0.174	0.939
Z139	azimuthal	0.493	-0.515	-1.867	0.179
Z140	polar	0.041	-0.235	-0.727	0.353
Z140	azimuthal	0.823	0.485	-0.137	0.954
Z141	polar	0.240	-0.854	-0.124	0.933

Continued on next page

Table 28 – continued from previous page

sample	angles	$P > \chi^2$	$C/C(\sigma)$	$\triangle_{11}/\sigma(\triangle_{11})$	$P > \triangle_1$
Z141	azimuthal	0.843	1.228	-1.896	0.087
Z142	polar	0.215	-0.548	-0.521	0.713
Z142	azimuthal	0.092	0.176	0.946	0.595
Z143	polar	0.769	0.429	0.118	0.873
Z143	azimuthal	0.849	-0.518	0.024	0.943
Z144	polar	0.012	-0.415	-0.301	0.731
Z144	azimuthal	0.534	-0.567	-0.335	0.920
Z145	polar	0.628	-0.890	0.596	0.816
Z145	azimuthal	0.855	-0.629	-0.051	0.948
Z146	polar	0.150	-1.303	-0.234	0.966
Z146	azimuthal	0.572	0.484	-0.626	0.287
Z147	polar	0.122	-1.311	0.643	0.698
Z147	azimuthal	0.909	-0.394	0.678	0.647
Z148	polar	0.399	-0.779	-0.027	0.949
Z148	azimuthal	0.183	-0.584	0.515	0.711
Z149	polar	0.700	0.493	-0.493	0.857
Z149	azimuthal	0.983	-0.128	-0.287	0.932
Z150	polar	0.473	-1.152	-0.464	0.832
Z150	azimuthal	0.717	-0.268	0.454	0.892
Z151	polar	0.243	-0.637	-0.770	0.687
Z151	azimuthal	0.825	-0.481	0.168	0.857
Z152	polar	0.882	0.230	0.415	0.845
Z152	azimuthal	0.808	0.039	0.617	0.649
Z153	polar	0.323	-1.325	0.491	0.832
Z153	azimuthal	0.674	0.353	-1.161	0.247
Z154	polar	0.674	0.459	-0.330	0.897
Z154	azimuthal	0.998	-0.309	0.261	0.945
Z155	polar	0.407	-0.026	-0.076	0.997
Z155	azimuthal	0.737	-0.554	1.778	0.206

Continued on next page

Table 28 – continued from previous page

sample	angles	$P > \chi^2$	$C/C(\sigma)$	$\triangle_{11}/\sigma(\triangle_{11})$	$P > \triangle_1$
Z156	polar	0.442	-2.196	0.262	0.962
Z156	azimuthal	0.368	-0.658	0.208	0.448
Z157	polar	0.223	-2.320	0.455	0.874
Z157	azimuthal	0.876	0.035	-0.756	0.753
Z158	polar	0.333	0.310	-0.121	0.990
Z158	azimuthal	0.213	-0.009	0.487	0.888
Z159	polar	0.294	0.137	0.592	0.779
Z159	azimuthal	0.658	-0.678	0.028	0.967
Z160	polar	0.414	0.230	-0.557	0.720
Z160	azimuthal	0.228	-1.652	0.485	0.857
Z161	polar	0.926	-0.376	-0.328	0.862
Z161	azimuthal	0.695	-1.246	0.680	0.684
Z162	polar	0.282	-0.858	-0.163	0.986
Z162	azimuthal	0.738	-0.098	0.673	0.785
Z163	polar	0.533	-0.143	-0.501	0.839
Z163	azimuthal	0.868	-0.515	0.941	0.624
Z164	polar	0.706	-1.145	-0.281	0.874
Z164	azimuthal	0.899	-0.858	0.397	0.560
Z165	polar	0.970	-0.484	0.132	0.990
Z165	azimuthal	0.458	-2.430	0.492	0.794
Z166	polar	0.919	-0.406	0.046	0.988
Z166	azimuthal	0.561	-0.731	-0.367	0.879
Z167	polar	0.434	0.590	-0.429	0.902
Z167	azimuthal	0.251	-0.789	-0.416	0.836
Z168	polar	0.259	-0.501	-0.415	0.779
Z168	azimuthal	0.661	-0.804	0.410	0.904
Z169	polar	0.030	0.552	-0.075	0.891
Z169	azimuthal	0.078	-0.168	-0.431	0.893
Z170	polar	0.945	0.263	-0.634	0.627

Continued on next page

Table 28 – continued from previous page

sample	angles	$P > \chi^2$	$C/C(\sigma)$	$\triangle_{11}/\sigma(\triangle_{11})$	$P > \triangle_1$
Z170	azimuthal	0.611	-0.694	0.130	0.670
Z171	polar	0.825	-0.012	-1.026	0.577
Z171	azimuthal	0.760	-0.110	-1.236	0.458
Z172	polar	0.056	-2.325	-0.550	0.822
Z172	azimuthal	0.897	-0.474	-0.348	0.863
Z173	polar	0.939	-0.224	-0.668	0.776
Z173	azimuthal	0.712	-0.800	0.370	0.530
Z174	polar	0.861	-0.309	0.062	0.986
Z174	azimuthal	0.740	-1.203	-0.445	0.798
Z175	polar	0.412	0.099	-0.165	0.984
Z175	azimuthal	0.936	0.482	0.080	0.996
Z176	polar	0.844	-0.113	-0.105	0.971
Z176	azimuthal	0.505	-0.035	0.610	0.814
Z177	polar	0.273	-0.266	0.472	0.871
Z177	azimuthal	0.976	-0.770	-0.153	0.989
Z178	polar	0.070	-1.680	-0.015	0.895
Z178	azimuthal	0.941	-0.866	0.658	0.710
Z179	polar	0.782	-0.220	-0.581	0.799
Z179	azimuthal	0.999	0.030	0.342	0.859
Z180	polar	0.956	-0.678	0.255	0.966
Z180	azimuthal	0.049	-1.918	-0.664	0.480
Z181	polar	0.943	-0.279	-0.103	0.854
Z181	azimuthal	0.161	-1.388	0.091	0.981
Z182	polar	0.167	0.016	0.043	0.990
Z182	azimuthal	0.732	0.507	0.988	0.619
Z183	polar	0.289	0.476	-0.255	0.771
Z183	azimuthal	0.719	-0.848	0.304	0.925
Z184	polar	0.496	-0.673	-0.638	0.797
Z184	azimuthal	0.720	-1.138	-1.100	0.474

Continued on next page

Table 28 – continued from previous page

sample	angles	$P > \chi^2$	$C/C(\sigma)$	$\triangle_{11}/\sigma(\triangle_{11})$	$P > \triangle_1$
Z185	polar	0.798	0.156	0.022	0.955
Z185	azimuthal	0.042	0.052	-0.968	0.293
Z186	polar	0.792	0.331	-0.716	0.733
Z186	azimuthal	0.856	-0.261	-0.974	0.499
Z187	polar	0.561	-1.258	-0.160	0.940
Z187	azimuthal	0.321	-1.205	-0.420	0.864
Z188	polar	0.415	-0.151	-0.004	1.000
Z188	azimuthal	0.453	-2.298	-0.127	0.773
Z189	polar	0.244	-1.086	0.785	0.594
Z189	azimuthal	0.924	-0.930	-0.258	0.967
Z190	polar	0.602	0.451	0.730	0.571
Z190	azimuthal	0.718	0.044	-0.281	0.764
Z191	polar	0.194	-2.222	0.675	0.691
Z191	azimuthal	0.527	0.231	0.042	0.957
Z192	polar	0.517	-0.851	0.018	0.954
Z192	azimuthal	0.064	-1.089	0.481	0.696
Z193	polar	0.903	-0.285	0.186	0.852
Z193	azimuthal	0.847	0.675	0.700	0.391
Z194	polar	0.503	-0.382	0.357	0.931
Z194	azimuthal	0.267	-0.706	0.431	0.473
Z195	polar	0.421	-0.554	-0.831	0.605
Z195	azimuthal	0.827	-0.322	0.950	0.623
Z196	polar	0.781	-1.013	0.150	0.988
Z196	azimuthal	0.641	-1.646	0.280	0.875
Z197	polar	0.608	0.523	0.829	0.678
Z197	azimuthal	0.651	-0.418	0.520	0.857
Z198	polar	0.296	-0.594	-0.080	0.976
Z198	azimuthal	0.206	0.323	-0.393	0.519
Z199	polar	0.076	-2.412	-0.445	0.903

Continued on next page

Table 28 – continued from previous page

sample	angles	$P > \chi^2$	$C/C(\sigma)$	$\triangle_{11}/\sigma(\triangle_{11})$	$P > \triangle_1$
Z199	azimuthal	0.386	-1.746	0.543	0.832
Z200	polar	0.594	-1.056	0.041	0.997
Z200	azimuthal	0.813	-1.324	-0.203	0.908

Appendix G

Simulation and Computation Programme

G.1 Origin Programme (ORIGIN 5.0)

ORIGIN 5.0 is used to calculate the following parameters: inclination angle(i), observed polar angle (θ) and observed azimuthal angle (ϕ).

G.1.1 Inclination Angle (i)

The formula used to calculate inclination angle in Origin 5.0 are as follows:

$$((col(C))^2 - 0.2^2)/(1 - 0.2^2) \tag{1}$$

The col(C) represents the axial ratio (b/a). The above equation gives the value of $\cos^2 i$ placed in the col(D). Then cos$i$ is calculated by the formula

$$(col(D))^{0.5} \tag{2}$$

Finally, i is obtained using formula

$$acos(col(cosi)) * 180/pi \tag{3}$$

Observed Polar Angle (θ) and Observed Azimuthal Angle (ϕ)

For the calculation of the observed polar angles, we go through the following steps: At first, sinθ_1 and sinθ_2 are calculated using formula

$$\begin{aligned} &-cos(pi/180 * col(I)) * sin(pi/180 * col(B)) + sin(pi/180 * col(I)) * \\ &sin(pi/180 * col(P)) * cos(pi/180 * col(B)) \end{aligned} \tag{4}$$

and

$$\begin{aligned} &-cos(pi/180 * col(I)) * sin(pi/180 * col(B)) - sin(pi/180 * col(I)) * \\ &sin(pi/180 * col(P)) * cos(pi/180 * col(B)) \end{aligned} \tag{5}$$

respectively. Here, col(B) and col(P) represent the declination and position angle respectively. Then, θ_1 and θ_2 are obtained by formula

$$asin(col(sinT1)) * 180/pi \tag{6}$$

and

$$asin(col(sinT2)) * 180/pi \tag{7}$$

respectively. Here, col(sinT1) and col(sinT2) represent sinθ_1 and sinθ_2 respectively.

For the calculation of the observed azimuthal angles, we go through the following steps: At first, we calculated three quantities using formula

$$cos(col(I) * pi/180) * cos(pi/180 * col(B)) * sin(pi/180 * col(L)) \tag{8}$$

$$sin(pi/180 * col(I)) * sin(pi/180 * col(P)) * sin(pi/180 * col(B)) * sin(pi/180 * col(L)) \tag{9}$$

and

$$sin(pi/180 * col(I)) * cos(pi/180 * col(P)) * cos(pi/180 * col(L)) \tag{10}$$

The col(L) and col(I) represent the right ascension and inclination angle, respectively. These quantities are placed in the col(u), col(v) and col(w), respectively. Then, sinϕ_1 and sinϕ_2 are calculated using formula

$$-(col(u) + col(v) + col(w))/cos(pi/180 * col(T1)) \tag{11}$$

and

$$(-col(u) + col(v) + col(w))/cos(pi/180 * col(T2)) \tag{12}$$

respectively.

Here, col(T1) and col(T2) represent θ_1 and θ_2 respectively. Finally, ϕ_1 and ϕ_2 are obtained by the formula

$$asin(col(sinP1)) * 180/pi \tag{13}$$

and

$$asin(col(sinP2)) * 180/pi \tag{14}$$

respectively. Here, col(sinP1) and col(sinP2) represent sinϕ_1 and sinϕ_2, respectively.

Microsoft Office Excel 2007

The statistical parameters chi-square probability (P $>\chi^2$), autocorrelation coefficient (C/C(σ)), first order Fourier coefficient ($\Delta_{11}/\sigma(\Delta_{11})$) and first order Fourier probability (P $>\Delta_1$) are calculated using MICROSOFT OFFICE EXCEL 2007.

G.3 Program and Input Files: An Example

Matlab 7.6.0 is used to write programme and input files for the simulation. As an example, we give program and input file for the galaxies of sample Z61 (a sample described in the chapter 4.6.8). The Program and Input Files is as follows

PROGRAM FILE

```
% Polar and Azimuthal angle for the galaxy rotation axes.

name of the program file: polar1

clear all;                                  % making the work place free of memory
t=cputime;

input(Type the name of your input file: );

theta1 = asin(-cos(i).*sin(B)+ sin(i).*sin(P).*cos(B));          %polar angle

theta2 = asin(-cos(i).*sin(B)- sin(i).*sin(P).*cos(B));          %polar angle

phi1 = asin ((-cos(i).*cos(B).*sin(L) + sin(i).*(-sin(P).*sin(B).*sin(L)-
cos(P).*cos(L))).*cos(theta1));          %azimuthal angle

phi2 = asin ((-cos(i).*cos(B).*sin(L) + sin(i).*(+sin(P).*sin(B).*sin(L)+
```

```
cos(P).*cos(L))./cos(theta2));          %azimuthal angle

theta1 = theta1.*180/pi;                %changing to degrees
theta2 = theta2.*180/pi;
phi1 = phi1.*180/pi;
phi2 = phi2.*180/pi;

theta=[theta1; theta2];                 %polar angle
phi=[phi1; phi2];                       %azimuthal angle
vec=[-87.5:5:87.5];                     %making 36 bins of 5° interval
(theta_n, dx) = hist(theta, vec);       %histogram showing polar angle distribution
(phi_n,dx) = hist(phi, vec);            %histogram showing azimuthal angle dis-
tributiion
theta_n = theta_n'                      %placing theta in column matrix
phi_n = phi_n'                          %placing phi in column matrix
```

INPUT FILE

```
% name of the input file: Z61
% 10^7 virtual galaxies are generated.
% generated parameters

% Right Ascension
 R1=rand(20306,1);
 R2=20;
 R3=R1*R2;
 R4=R3+0;

                R5=rand(10152,1);
                R2=20;
                R6=R5*R2;
                R7=R6+20;
```

```
                    R8=rand(15228,1);
                    R2=20;
                    R9=R8*R2;
                    R10=R9+100;

                              R11=rand(137056,1);
                              R2=20;
                              R12=R11*R2;
                              R13=R12+120;

                                        R14=rand(111675,1);
                                        R2=20;
                                        R15=R14*R2;
                                        R16=R15+140;

R17=rand(192893,1);
R2=20;
R18=R17*R2;
R19=R18+160;

          R20=rand(126904,1);
          R2=10;
          R21=R20*R2;
          R22=R21+180;

                    R23=rand(116751,1);
                    R2=20;
                    R24=R23*R2;
                    R25=R24+200;

                              R26=rand(111675,1);
                              R2=20;
                              R27=R26*R2;
                              R28=R27+220;
```

```
                                                    R29=rand(126904,1);
                                                    R2=20;
                                                    R30=R29*R2;
                                                    R31=R30+240;

 R32=rand(10152,1);
 R2=20;
 R33=R32*R2;
 R34=R33+260;

                R35=rand(5076,1);
                R2=20;
                R36=R35*R2;
                R37=R36+300;

                        R38=rand(10152,1);
                        R2=20;
                        R39=R38*R2;
                        R40=R39+320;

                                R41=rand(5076,1);
                                R2=20;
                                R42=R41*R2;
                                R43=R42+340;
L = [R4 R7 R10 R13 R16 R19 R22 R25 R28 R31 R34 R37 R40 R43];


L = L* pi/180;
j=randperm(max(size(L)));        % to make above matrix random again
theta2 = theta2.*180/pi;
LL=L(j(:));
L=LL;

% Declination
```

```
D1=rand(5075,1);
D2=5;
D3=D1*D2;
D4=D3-15;

        D5=rand(10152,1);
        D2=5;
        D6=D5*D2;
        D7=D6-10;

            D8=rand(40609,1);
            D2=5;
            D9=D8*D2;
            D10=D9-5;

                D11=rand(126904,1);
                D2=5;
                D12=D11*D2;
                D13=D12+0;

                    D14=rand(91371,1);
                    D2=5;
                    D15=D14*D2;
                    D16=D15+5;

D17=rand(65990,1);
D2=5;
D18=D17*D2;
D19=D18+10;

        D20=rand(101523,1);
        D2=5;
        D21=D20*D2;
        D22=D21+15;
```

```
                    D23=rand(86294,1);
                    D2=5;
                    D24=D23*D2;
                    D25=D24+20;

                              D26=rand(91371,1);
                              D2=5;
                              D27=D26*D2;
                              D28=D27+25;

                                        D29=rand(101523,1);
                                        D2=5;
                                        D30=D29*D2;
                                        D31=D30+30;

D32=rand(55838,1);
D2=5;
D33=D32*D2;
D34=D33+35;

          D35=rand(65990,1);
          D2=5;
          D36=D35*D2;
          D37=D36+40;

                    D38=rand(25381,1);
                    D2=5;
                    D39=D38*D2;
                    D40=D39+45;

                              D41=rand(45685,1);
                              D2=5;
                              D42=D41*D2;
                              D43=D42+50;
```

```
                                                    D44=rand(45685,1);
                                                    D2=5;
                                                    D45=D44*D2;
                                                    D46=D45+55;

 D47=rand(40609,1);
 D2=5;
 D48=D47*D2;
 D49=D48+60;
B=[D4 D7 D10 D13 D16 D19 D22 D25 D28 D31 D34 D37 D40 D43 D46 D49];
B = B* pi/180;
j=randperm(max(size(B)));          % to make above matrix random again
BB=B(j(:));
B=BB;

% Position angle

 P1=rand(35532,1);
 P2=10;
 P3=P1*P2;
 P4=P3+0;

                P5=rand(50761,1);
                P2=10;
                P6=P5*P2;
                P7=P6+10;

                                P8=rand(55838,1);
                                P2=10;
                                P9=P8*P2;
                                P10=P9+20;
```

```
                                        P11=rand(60914,1);
                                        P2=10;
                                        P12=P11*P2;
                                        P13=P12+30;

                                                P14=rand(76142,1);
                                                P2=10;
                                                P15=P14*P2;
                                                P16=P15+40;

P17=rand(101523,1);
P2=10;
P18=P17*P2;
P19=P18+50;

                P20=rand(55838,1);
                P2=10;
                P21=P20*P2;
                P22=P21+60;

                        P23=rand(25381,1);
                        P2=10;
                        P24=P23*P2;
                        P25=P24+70;

                                        P26=rand(25381,1);
                                        P2=10;
                                        P27=P26*P2;
                                        P28=P27+80;

                                                P29=rand(71066,1);
                                                P2=10;
                                                P30=P29*P2;
                                                P31=P30+90;
```

```
P32=rand(50761,1);
P2=10;
P33=P32*P2;
P34=P33+100;

                P35=rand(45685,1);
                P2=10;
                P36=P35*P2;
                P37=P36+110;

                                P38=rand(50761,1);
                                P2=10;
                                P39=P38*P2;
                                P40=P39+120;

                                                P41=rand(40609,1);
                                                P2=10;
                                                P42=P41*P2;
                                                P43=P42+130;

                                                                P44=rand(35533,1);
                                                                P2=10;
                                                                P45=P44*P2;
                                                                P46=P45+140;

P47=rand(101523,1);
P2=10;
P48=P47*P2;
P49=P48+150;

                P50=rand(55838,1);
                P2=10;
                P51=P50*P2;
                P52=P51+160;
```

```
                                P53=rand(60914,1);
                                P2=10;
                                P54=P53*P2;
                                P55=P54+170;
P=[P4 P7 P10 P13 P16 P19 P22 P25 P28 P31 P34 P37 P40 P43 P46 P49 P52 P55];
P = P* pi/180;
j=randperm(max(size(P)));          % to make above matrix random again
PP=P(j(:));
P=PP;

% Inclination angle
 I1=rand(5077,1);
 I2=5;
 I3=I1*I2;
 I4=I3+2.5;
                    I5=rand(5076,1);
                    I2=5;
                    I6=I5*I2;
                    I7=I6+7.5;
                                I8=rand(35533,1);
                                I2=5;
                                I9=I8*I2;
                                I10=I9+12.5;
                                            I11=rand(65990,1);
                                            I2=5;
                                            I12=I11*I2;
                                            I13=I12+17.5;
                                                        I14=rand(35533,1);
                                                        I2=5;
                                                        I15=I14*I2;
                                                        I16=I15+22.5;
```

```
I17=rand(86294,1);
I2=5;
I18=I17*I2;
I19=I18+27.5;

        I20=rand(65990,1);
        I2=5;
        I21=I20*I2;
        I22=I21+32.5;

                I23=rand(116751,1);
                I2=5;
                I24=I23*I2;
                I25=I24+37.5;

                        I26=rand(106599,1);
                        I2=5;
                        I27=I26*I2;
                        I28=I27+42.5;

                                I29=rand(101523,1);
                                I2=5;
                                I30=I29*I2;
                                I31=I30+47.5;

I32=rand(126904,1);
I2=5;
I33=I32*I2;
I34=I33+52.5;

        I35=rand(81218,1);
        I2=5;
        I36=I35*I2;
        I37=I36+57.5;
```

```
I38=rand(81218,1);
I2=5;
I39=I38*I2;
I40=I39+62.5;

I41=rand(40609,1);
I2=5;
I42=I41*I2;
I43=I42+67.5;

I44=rand(35533,1);
I2=5;
I45=I44*I2;
I46=I45+72.5;

I47=rand(10152,1);
I2=5;
I48=I47*I2;
I49=I48+77.5;
i = [I4 I7 I10 I13 I16 I19 I22 I25 I28 I31 I34 I37 I40 I43 I46 I49];
i = i* pi/180;
j=randperm(max(size(i)));          % to make above matrix random again
ii=i(j(:));
i=ii;
```

Similarly, other input files have been made. A list of tables giving input files with the range descriptions are given in appendix F

H Publications

H.1 International Journals

1. **Title of article: spatial orientation of galaxies in the zone of avoidance.**
   Bull.Astr.Scc.India **40**, 65(2012)

2. **Spatial Orientation of Spin Vectors of Blue-shifted Galaxies.**
   Astrophysics and Space Science, arXiv:1606.02881v1 [astro-ph.GA] 9 Jun 2016.

3. **Preferred alignments of angular momentum vectors of galaxies in six dynamically unstable Abell clusters**
   Submitted to Research in Astron. Astrophys.

H.2 National Journals

1. **A Study of co-existence between the Hubble flow and the random alignments of spin vectors of SDSS galaxies**.
   Bibechna, A Multidisciplinary Journal of Science, Technology and Mathematics, Biratnagar, **12**, 11787 (2014).

2. **Study of r- and u- Magnitude Dependence in the Spatial Orientation of Spin vectors of SDSS Galaxies having redshift 0.10 $\leq$ Z $\leq$ 0.11**
   The Himalayan Physics, P.N Campus Pokhara, **5**,01 (2014)

3. **Position Angle distribution of Galaxies in Clusters**
   The Himalayan Physics, P.N Campus Pokhara **4**, 01, (2013).

4. **Spatial Orientation of Angular Momentum Vectors of SDSS Galaxies having Redshift $1.000\times10^{-1}$to 1.005×10^{-1}**
   The Journal of University Grants Commission, **3**, 117 (2014).

5. **Spatial Orientation of Galaxies on the basis of Position Angle Distribution Method**
   Nepalese Journal of Integrated Sciences, Birgunj, **4**, 48 (2014).

6. **A Comparison Between Anisotropic Distribution of Spin Vectors of Galaxies Having Redshift 0.10 to 0.11 and 0.19 to 0.20**

   Pragyan Journal, Kathmandu, **1**, 25 (2014).

7. **A Study of Position angle Distribution of SDSS Galaxies.**

   Kathmandu Center For Research & Studies (KCRAS), **VI**, 65 (2014).

8. **Galaxy Evolution Models**

   Kathmandu Center For Research & Studies (KCRAS), **VI**, 72, (2014).

9. **Binary Stars**

   RevoScience, Scientific bulletin , Kathmandu, Nepal **II**, V, 7 (2013).

10. **Anisotropy in the spatial orientation of SDSS galaxies having redshift 0.100000 to 0.10125**

    RevoScience, Scientific bulletin, **II**, 27, (2013).

11. **Variation of Spatial Orientation of SDSS Galaxies with increase in value of redshift**

    RevoScience,Scientific bulletin, Kathmandu, Nepal, **III**, 32 (2013).

Bull. Astr. Soc. India (2012) **40**, 65–76

Spatial orientation of galaxies in the Zone of Avoidance

B. Aryal,[1,2*] S. N. Yadav[2] and W. Saurer[1]

[1]*Institute of Astro- and Particle Physics, Innsbruck University, Technikerstrasse 25 A-6020 Innsbruck, Austria*

[2]*Central Department of Physics, Tribhuvan University, Kirtipur, Kathmandu, Nepal*

Received 2011 September 22; accepted 2012 February 28

Abstract. We present spatial orientation of spin vectors of galaxies found in the region $20^\circ \leq \ell \leq 80^\circ$, $-10^\circ \leq b \leq -5^\circ$ in the first Palomar Observatory Sky Survey. The inclination angle and intrinsic flatness of a galaxy are used to determine the spin vector and spin vector projections of the galaxy. We studied the preferred alignments of spin vectors of galaxies with respect to equatorial, Galactic and supergalactic coordinate systems. We have carried out Kolmogorov-Smirnov (K-S), Kuiper-V and Fourier tests in order to examine non-random effects. It is found that the spin vectors of galaxies tend to lie in the equatorial plane whereas these vectors tend to be oriented perpendicular the Local Supercluster plane. A random alignment of spin vectors of galaxies is noticed with respect to the Galactic plane. Possible explanation of the results are discussed.

Keywords : catalogues – surveys – galaxies: evolution – galaxies: statistics

1. Introduction

The Zone of Avoidance (ZOA, hereafter) is the region of the sky that is obscured by the Galactic plane of the Milky Way. The dust and gas in the Milky Way cause extinction at optical wavelengths, and foreground stars can be confused with background galaxies, obstructing our view of around 20% of the extragalactic sky at visible wavelengths. Because of this, optical catalogues are usually incomplete close to the Galactic plane. In recent years, many projects (Weinberger et al. 1995; Huchtmeier et al. 1995; Seeberger & Saurer 1998; Marchiotto et al. 1999; Marchiotto 2000) have attempted to bridge the gap in our knowledge caused by the ZOA. The effect of extinction drops at longer wavelengths, such as the infrared, and the Milky Way is effectively transparent at radio wavelengths. Surveys in the infrared, such as the Infrared Astronomical

*e-mail:binil.aryal@uibk.ac.at

Satellite (IRAS) survey and and Two Micron All Sky Survey (2MASS), have given us a more complete picture of the extragalactic sky. Two very large nearby galaxies, Maffei 1 and Maffei 2, were discovered in the ZOA by Paolo Maffei by their infrared emission in 1968 (Maffei 1968). In spite of this, approximately 10% of the sky remains difficult to survey as extragalactic objects can be confused with stars in the Milky Way. Projects to survey the ZOA at radio wavelengths, particularly using the 21-cm emission line of neutral atomic hydrogen, have detected many galaxies (e.g., Dwingeloo Galaxy 1 and Dwingeloo Galaxy 2) that could not be detected in the infrared (Ryan-Weber et al. 2002 and the references therein).

Kerton & Brunt (2003) studied the association of CO emission with IRAS sources in the outer Galaxy using data from the FCRAO Outer Galaxy Survey (OGS). they found that ~ 25% of candidate ZOAGs are Galactic objects. They discovered two new far outer Galaxy star-forming regions, and six bright molecular clouds. Ryan-Weber et al. (2002) presented 138 HIPASS BGC (HI Parkes All-Sky Survey Bright Galaxy Catalog) galaxies that had no redshift measured prior to the Parkes multibeam HI surveys. The majority (57) of the newly catalogued galaxies lie within 10° of the Galactic plane and are missing from optical surveys as a result of confusion with stars or dust extinction. Zone of Avoidance survey finds new HI galaxies which lie hidden behind the Milky Way, and also provides redshifts for partially obscured galaxies known at other wavelengths. Donley et al. (2005) presented the results of the northern extension of the HI Parkes Zone of Avoidance Survey, a blind HI survey utilizing the multibeam receiver on the Parkes 64 m telescope and detected 77 HI galaxies, 20 of which have been previously detected in HI. In addition, they found several filaments crossing the Galactic plane, one of which appears to be the continuation of a sine-wave-like feature that can be traced across the whole southern sky. Henning et al. (2010) observed two low-latitude precursor regions, totaling 138 deg^2, with 72 HI galaxies.

In order to understand the evolution of galaxies it is essential to know when and how they have formed and how their structures and constituents have been changing with time. Our aim is to examine non-random effects in the galaxy alignments, in the framework of three different scenarios: 'pancake model' (Doroshkevich 1973; Shandarin 1974), the 'hierarchy model' (Peebles 1969) and the 'primordial vorticity theory' (Ozernoy 1978). The 'pancake model' predicts that the rotation axes of galaxies tend to lie within the cluster plane. According to the 'hierarchy model' the directions of the rotation axes should be distributed randomly. The 'primordial vorticity theory' predicts that the rotation axes of galaxies are primarily distributed perpendicular to the cluster plane. In this work, we intend to study the spin vector orientations in order to understand the evolution of galaxies in the ZOA.

2. The sample: Zone of Avoidance galaxies

As the final part of the extensive Innsbruck ZOA galaxy project (e.g. Weinberger et al. 1995; Seeberger & Saurer 1998; Marchiotto et al. 1999), Marchiotto (2000) presented the galaxy searches for the region $20° \leq \ell \leq 80°$, $-10° \leq b \leq -5°$ on first Palomar Observatory Sky Survey (hereafter POSS I) with the aid of a microscope having 16× magnification. The POSS I was carried out

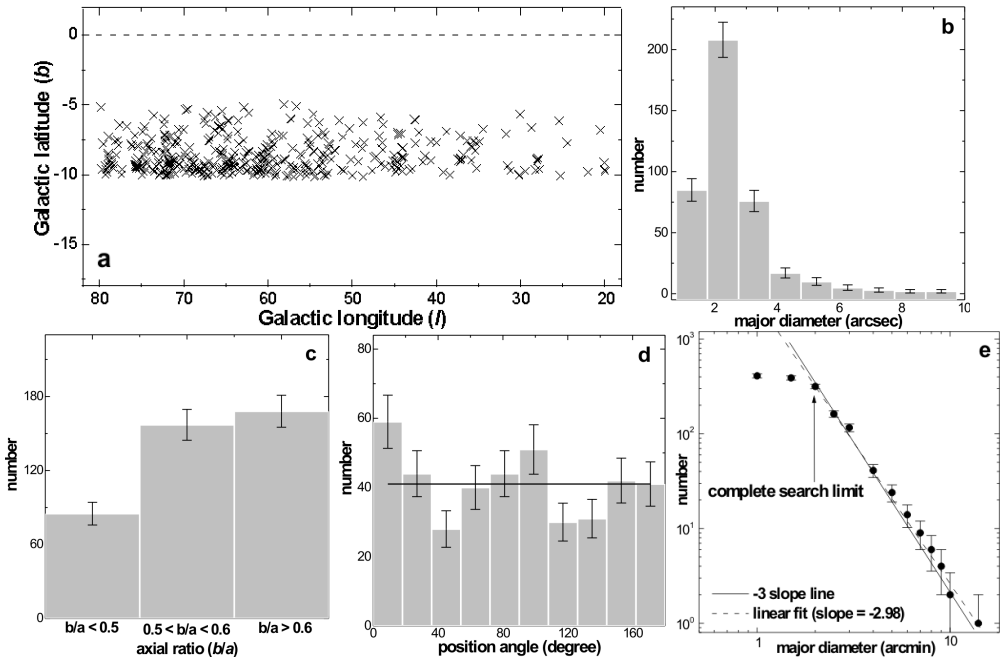

Figure 1. All sky distribution of 410 Zone of Avoidance galaxies in the region $20° \le \ell \le 80°$, $-10° \le b \le -5°$ (a). The major diameter (b), axial ratio (c) and equatorial position angle (PA) distributions (d) of galaxies. The solid line represents the expected distribution. (e) The distribution of the major diameter (in arcmin) of galaxies in the ZOA. The axes are in logarithm scale. The solid and dashed lines represent the theoretical line having slope '−3' and the best fit line, respectively. The statistical $\pm 1\sigma$ error bars are shown.

on the Oschin Schmidt Telescope in 1950-57 using 103aO and 103aF plates. POSS I continues to be one of the most frequently used astronomical resources; paper or glass copies of the plates are to be found in most of the world's observatories and a digitized version is available on line from the Space Telescope Science Institute. Altogether 410 galaxy candidates are listed; about 5% have counterparts in the IRAS PSC. The position angle (PA) and diameters of the galaxies are available on-line[1]. All-sky distribution of these ZOA galaxies are shown in Fig. 1a. Inhomogeneous distribution of galaxies can be seen. The major diameter (a), axial ratios (b/a) and equatorial PA distributions of these galaxies are shown in Figs. 1b,c,d. Marchiotto et al. (1999) concluded that the distribution is approximated by an exponential falling off in number density between $b = -5°$ to $-10°$ and a roughly linear falling off between $\ell = +80°$ to $+20°$. No obvious clustering of galaxies, pointing to a possible rich galaxy cluster, is evident in the region surveyed. The chi-square and Fourier probability is found to be less than 5% in the PA-distribution, suggesting anisotropy. This result motivates us to study the spin vector orientation of these 410 ZOA galaxies with respect to suitable reference coordinate system.

[1]http://www.ncra.tifr.res.in/ basi/toc12March.htm

The distribution of the apparent diameters of the galaxies can give information about the completeness of the optical catalogue. Aryal, Bachchan & Saurer (2010) discuss a 'toy model' by assuming a homogeneous distribution of galaxies in space having equal linear diameter. They ignored the effect of clustering in the model. Due to this assumption one expect to get large deviations from the −3 slope line in the diameter distribution of cluster galaxies. Fig. 1e shows the distribution of the apparent diameters of ZOA galaxies. In the figure, the solid and dashed lines represent the −3 slope and the best fit lines, respectively. The slope of the best fit line is found to be −2.98. The observed distribution is found to deviate from these lines. The point at which the diameter starts to deviate from the solid line (−3 slope line) is taken as the 'limit' up to which the optical catalog is assumed to be complete. In the ZOA, this limit is found to be 2.0 arcmin. So, the catalog of galaxies in ZOA that have apparent major diameter ≥2.0 arcmin is complete. In other words, the diameter distribution of 316 galaxies (about 77%) is found to be fit with the model. This value rules out the existence of heavy clustering phenomena in the ZOA. However, the existence of groups and subclusters in the region of interest cannot be denied.

The Great Attractor is situated at a distance 45−50 Mpc from the Milky Way, in the direction of the constellations Hydra and Centaurus (Mieske, Hilker & Infante 2005). The objects in that direction lie in the ZOA and are thus difficult to study at visible wavelengths. X-ray observations have revealed that the region of space is dominated by the Norma cluster (Abell 3627), containing a large number of old galaxies, many of which are colliding with their neighbors, and/or radiating large amounts of radio waves. X-ray survey of ZOA reported that the Great Attractor was actually only one tenth the mass that scientists had originally estimated. The survey also confirmed earlier theories that the Milky Way galaxy was in fact being pulled towards a much more massive cluster of galaxies near the Shapley Supercluster which lies beyond the Great Attractor (Tonry et al. 2000).

3. Method

We adopt 'PA-inclination' method originally proposed by Öpik (1970), applied by Jaaniste & Saar (1978) and significantly modified by Flin & Godłowski (1986) and Godłowski (1993, 1994) in order to convert two dimensional given parameters (i.e., PA) into three dimensional parameters (i.e., spin vectors and spin vector projections of galaxies). The selection effects in the database are removed and the expected isotropic distribution for spin vectors (SVs hereafter) and spin vector projections of galaxies are determined using the method proposed by Aryal & Saurer (2000). The observed and expected distributions are compared with the help of appropriate statistical tests.

3.1 Observed distribution: spin vectors of galaxies

We convert two-dimensional given parameters (R.A., Dec. and equatorial PA) into three-dimensional (spin vectors or polar/azimuthal angles) parameters using axial ratios and intrinsic flatness of galaxies. For this, we adopt the method described by Flin & Godłowski (1986) and calculate

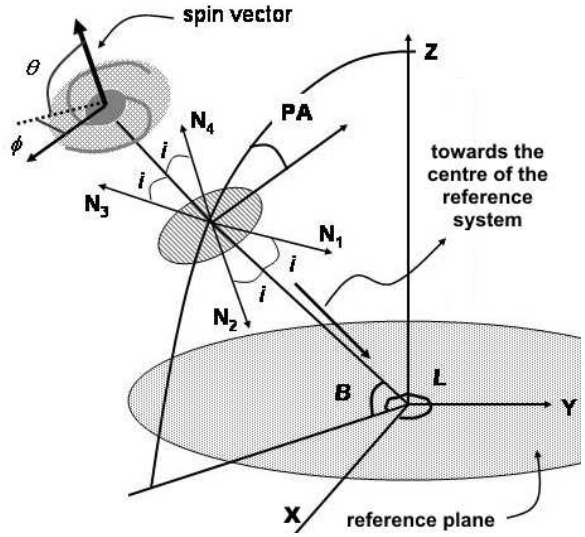

Figure 2. Schematic illustration of θ (polar angle between the galaxy SV and the LSC plane) and ϕ (azimuthal angle between the projection on the LSC plane of the galaxy SV and the supergalactic X-axis), whose distribution we examined. L and B are the supergalactic longitude and latitude. The four possible normals are denoted by N_1, N_2, N_3 and N_4. See text for the explanation.

the polar (θ) and azimuthal (ϕ) angles of galaxies. In their method, the three dimensional orientation of the SV of a galaxy is characterized by polar and azimuthal angles. The polar angle (θ) represents the angle between the galactic SV and a reference plane (Fig. 2). The angle between the projection of a galactic SV on to this reference plane is the azimuthal angle (ϕ). The formulae to obtain θ and ϕ in SCS are as follows (Flin & Godłowski, 1986):

$$\sin\theta = -\cos i \sin B \pm \sin i \sin P \cos B \tag{1}$$

$$\sin\phi = (\cos\theta)^{-1}[-\cos i \cos B \sin L + \sin i(\mp \sin P \sin B \sin L \mp \cos P \cos L) \tag{2}$$

where L, B and P are the supergalactic longitude, latitude and position angle, respectively. The angle i is the inclination angle, estimated with Holmberg's (1946) formula: $\cos^2 i = [(b/a)^2 – q^2]/(1–q^2)$ where b/a is the measured axial ratio and q is the intrinsic flatness of disk galaxies. The method of determination of intrinsic flatness of galaxies is the same as in Aryal et al. (2007).

There is no information from which we can define a physically-based reference frame for the ZOA galaxies. The reference plane might be complex because of large number of HI galaxies investigated in the past few years (Henning et al. 2010 and the references therein). There is no information from which we can define a physically based reference frame for ZOA galaxies. In this situation, we study the spatial orientation of SVs of ZOA galaxies with respect to three well

known coordinate systems: equatorial (ECS hereafter), Galactic (GCS hereafter) and supergalactic (SCS hereafter). In the Galactic coordinate system, the principal axis is the Galactic equator (the intersection of the plane of the Milky Way with the celestial sphere) and the reference points are the north Galactic pole and the zero point on the Galactic equator; the coordinates of a celestial body are its Galactic longitude and latitude. In this system, the zero point on the Galactic equator has the equatorial coordinates R.A. (J2000) = $17^h39.3^m$ and Dec. (J2000) = $-28°55^m$; this lies in the direction of the center of our Galaxy, the Milky Way. We adopt the SCS as defined by Tammann & Sandage (1976).

The above formulae show that there are two possible solutions for a given galaxy. Because the normals (N_1, N_2, N_3, N_4) shown in Fig. 2 cannot be determined unambiguously, because we do not know the side of the galaxy which is nearer/farther from us, and the direction of rotation. Thus, there are four solutions of the SV orientation for a galaxy. We count all four possibilities independently in our analysis.

3.2 Expected distribution: numerical simulations

Godłowski (1993) noted that if some galaxies were excluded from the sample, the theoretical isotropic distribution must be obtained from random simulations. Aryal & Saurer (2000) were the first who discussed this problem in detail. Aryal & Saurer (2000) noticed that any selections on the data may cause severe changes in the shapes of the expected isotropic distribution curves in galaxy orientation study. They found that the isotropic θ distribution is independent of positions only when the range of i is full. The isotropic ϕ distribution is independent of latitude (B) provided the range of i and longitude (L) is full. Their method has been applied by several authors in galaxy orientation studies (Hu et al. 2006; Aryal et al. 2008, 2012 and references therein). Three kinds of selection effects are noticed in our database: (1) inhomogeneous distribution of positions of galaxies (see Fig. 1a), (2) lack of knowledge of PAs of nearly face-on galaxies and (3) lack of edge-on galaxies (see Fig. 1c). These selection effects are removed and the expected isotropic distribution curves (θ and ϕ) are determined using the numerical simulation method as proposed by Aryal & Saurer (2000). Because our galaxy samples are from a limited region of the sky it is of importance to remove both the positional and the inclination effects. This problem is crucial in the ZOA because of shape of the survey (Fig 1a). This lack could even be real if the alignment is connected with galaxy plane. At present, this problem is very difficult to solve. We will address this problem in the future. For simplicity, a true spatial distribution of the galaxy rotation axis is assumed to be isotropic. Then, due to the projection effects, i can be distributed $\propto sin\ i$, latitude can be distributed $\propto cos\ B$, the variables longitude (L) and PA can be distributed randomly, and formulae (1) and (2) can be used to simulate (numerically) the corresponding distribution of θ and ϕ. The isotropic distribution curves are based on simulations including 10^6 virtual galaxies. The simulation procedure is described in Aryal & Saurer (2004). We perform numerical simulations with respect to all three reference systems (ECS, GCS and SCS). Fig. 3 shows the expected isotropic distribution of ZOA galaxies for polar (a) and azimuthal (b) angles with respect to ECS (solid line), GCS (dash line) and SCS (dash-dot line), respectively. For a comparison, cosine distribution (dot line) is shown. The expected isotropic distribution is cosine in θ and average

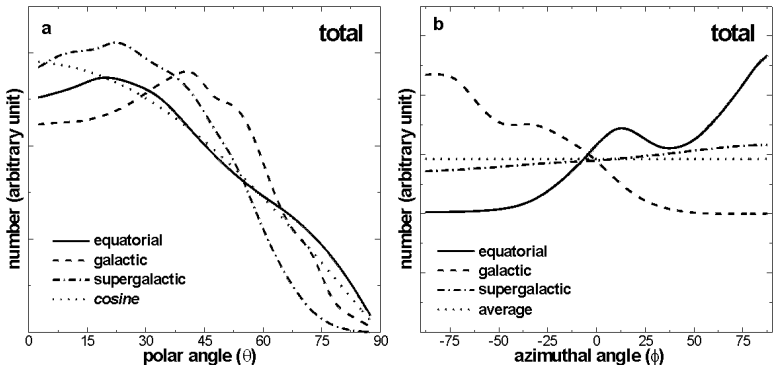

Figure 3. The expected polar (θ) (a) and azimuthal angle (ϕ) distribution (b) of ZOA galaxies with respect to equatorial, Galactic and supergalactic coordinate systems, respectively. The dotted line represents expected distribution when there are no selections on inclination angle and positions.

in ϕ when there are no selections on inclination angles and positions. We use these expected isotropic distributions for the comparison with the observed distribution.

3.3 Statistical tests

Our observed distributions are compared with expected isotropic distribution curves in θ and ϕ. For this comparison we applied Fourier (Hawley & Peebles 1975; Godłowski 1993, 1994; Godłowski & Ostrowski 1999; Aryal 2011; Godłowski 2011), Kolmogorov-Smirnov (K-S) (Stephens 1970; Press et al. 1992; Kanji 1995) and Kuiper-V (Kuiper 1962; Stephens 1970) tests. We do not describe these statistical tests here. These tests are described in the appendix of Aryal et al. (2007). These tests are a proper method in our case, because θ and ϕ are independent data. The significance level is chosen to be 95%, the null hypothesis is established to be an equidistribution for the θ and ϕ. As null hypothesis a spatial isotropy of the angular momentum vector was chosen. In cases of too small sample size only the K-S and Kuiper-V tests are meaningful. The conditions for anisotropy are the following: K-S = 1, Kuiper-V = 1, first order Fourier coefficient $\Delta_{11}/\sigma(\Delta_{11})>1$ and the first order Fourier probability $P(>\Delta_1)<0.150$.

4. Results

The ranges for the angles θ and ϕ are 0° to 90° and –90° to +90°, respectively. The bin size was chosen to be 10° for polar angle (θ) and 20° for azimuthal (ϕ) angle distributions in the Fourier test. Table 1 lists the values of the statistical parameters for θ and ϕ distributions of ZOA galaxies with respect to ECS, GCS and SCS. Fig. 4 shows the polar (θ) and azimuthal (ϕ) angle distributions of the SVs of galaxies with respect to ECS, GCS and SCS, respectively. We assume weak anisotropy if K-S and Kuiper-V tests do not agree and $1<\Delta_{11}/\sigma(\Delta_{11})\leq 1.5$.

Table 1. Statistics of the θ and ϕ distributions. The first column shows the reference systems: equatorial (ECS), Galactic (GCS) and supergalactic (SCS). The next two columns lists the results of Kolmogorov-Smirnov (K-S) and Kuiper-V (KV) tests. In these tests, "0" denotes that the null hypothesis (isotropy) can not be rejected at the chosen significance level, "1" designates that the null hypothesis can be rejected (anisotropy). The last two columns give the first order Fourier coefficient $\Delta_{11}/\sigma(\Delta_{11})$ and first order Fourier probability P($> \Delta_1$). The next four columns repeats the columns 2-5.

	θ				ϕ			
Abell	K-S	KV	Δ_{11}/σ	P($> \Delta_1$)	K-S	KV	Δ_{11}/σ	P($> \Delta_1$)
ECS	1	1	+2.0	0.115	0	0	+0.9	0.736
GCS	1	0	+1.0	0.260	1	1	+2.4	0.150
SCS	1	1	−3.2	0.045	1	1	−1.6	0.136

Fig 4a shows polar angle distribution of ZOA galaxies with respect to the ECS. All three statistical tests suggest anisotropy. The value of first order Fourier probability (P($> \Delta_1$)) is found to be less than <15%, suggesting anisotropy. The symbol "1" in K-S and Kuiper-V tests indicates that the null hypothesis (isotropy and homogeneous) can be rejected. The value of $\Delta_{11}/\sigma(\Delta_{11})$ is found to be positive at 2σ level, suggesting that the SVs of galaxies tend to lie in the equatorial plane. Two humps at 5° (1.5σ) and 15° (1.5σ) support this result. With respect to GCS, we found a mixed result: isotropy in the Fourier and Kuiper-V tests whereas anisotropy in the K-S test. In the histogram, humps at the middle (25°-45°) can be seen (Fig. 4b). These humps are compensated by the dip at smaller and larger angles, suggesting isotropy. Thus, no preferred alignments of SVs of galaxies in the ZOA is found when analyzed with respect to the GCS. We found anisotropy when analyzing with respect to the SCS. Humps at larger angles (55°, 65° and 75°) at 1.5σ level can be seen (Fig. 4c). Because of these humps, the value of $\Delta_{11}/\sigma(\Delta_{11})$ is found to be negative at $> 3\sigma$ level, suggesting that the SVs of galaxies tend to be oriented perpendicular to the Local Supercluster plane. Other statistical tests support this result. Thus, it is interesting that the SV orientation of ZOA galaxies support hierarchy model when analysing with respect to GCS whereas it supports pancake model (primordial vorticity model) when analyzing with respect to SCS (ECS). These inconsistencies in the preferred alignments strongly suggest the need of true physical reference system for ZOA galaxies.

In the ϕ distribution, value of $\Delta_{11}/\sigma(\Delta_{11})$ is found to be less than 1σ limit when analyzing with respect to the ECS. No significant humps or dips can be seen (Fig. 4d). All three statistical tests suggest isotropy (Table 1). Thus, no preferred alignments of the SV projections of ZOA galaxies with respect to ECS is noticed. Two humps (–20°, 0°) at the middle of the histogram can be seen in Fig. 4e. Humps in the region −50° to +50° and the dips at −90° to −50° (first 2 bins) and at 50° to 90° (last 2 bins) turn the Δ_{11} value positive in the ϕ distribution. A positive Δ_{11} suggests that the projections of SVs of galaxies tend to point towards the Galactic center. All three statistical tests support this result. In SCS, anisotropy is found in all three statistical tests (Table 1). The Δ_{11} value is found to be $> 1.5\sigma$ error limit, suggesting a preferred alignment. The

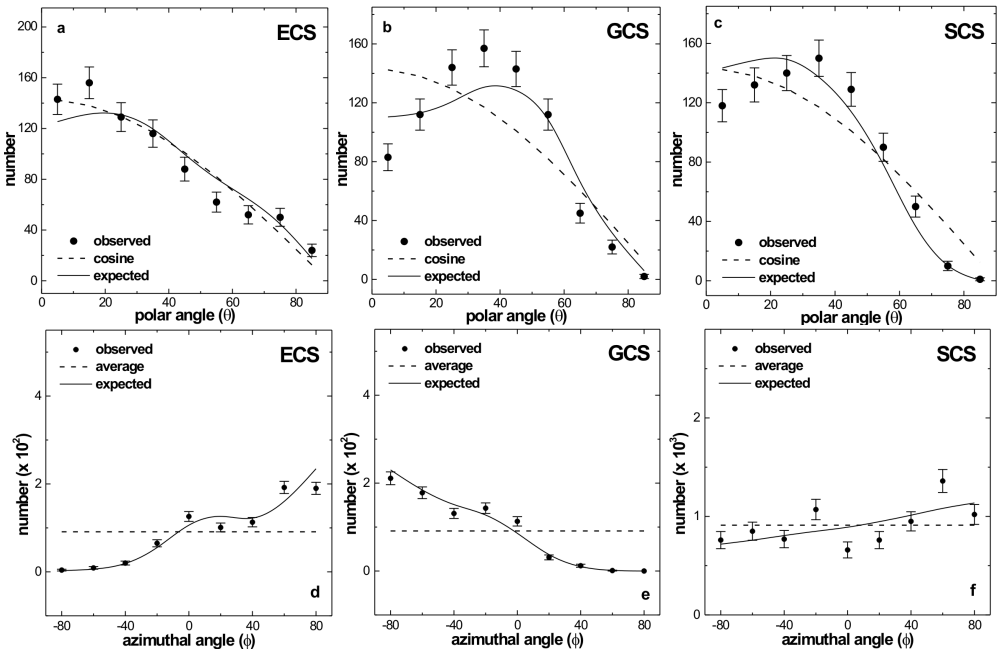

Figure 4. The polar (θ) and azimuthal (ϕ) angle distributions of ZOA galaxies with respect to equatorial (ECS), Galactic (GCS) and supergalactic (SCS) coordinate system. The solid line represents the expected isotropic distributions. The cosine distribution (dashed) is shown for the comparison. The statistical error ($\pm 1\sigma$) bars are shown for the observed counts. $\theta = 0^\circ$ (90°) corresponds to the galactic angular momentum vector tends to lie parallel (perpendicular) the reference plane. $\phi = 0^\circ$ means the direction to the centre of the reference coordinate system.

SV projections of ZOA galaxies is found to be oriented perpendicular with respect to the LSC center. A significant hump at $+60^\circ$ (2σ) supports this result (Fig. 4f).

The ZOA galaxies showed anisotropy in both θ and ϕ distributions when analyzing with respect to the SCS. In other two systems (ECS and GCS), either θ or ϕ distribution showed isotropy. It is difficult to explain the situation where SV orientation of galaxies showed isotropy and the distribution of their projections turned anisotropy or vice versa.

Aryal & Saurer (2005) studied the orientations of 1 433 galaxies found in the region $15^{\rm h}48^{\rm m} \leq \alpha(2000) \leq 19^{\rm h}28^{\rm m}$, $-68^\circ \leq \delta(2000) \leq -62^\circ$ with respect to equatorial coordinate system and noticed a random orientation of spin vectors of galaxies. Aryal, Kandel & Saurer (2006) reported orientations of 323 galaxies in the core of the Shapley concentration with respect to Galactic coordinate system. They noticed isotropy in both the two- and three-dimensional study when analyzing with respect to the Galactic coordinate system. Thus, these results support the hierarchy model (Peebles 1969), which predicts that the directions of the spin vectors are entirely random.

Aryal et al. (2007) noticed a systematic change in the galaxy alignments from early-type (BM I) to late-type (BM III) clusters. The spin vectors (SVs) of galaxies in the high radial velocity (RV) clusters are found to be oriented parallel with respect to the Local Supercluster (LCC) plane. The SV projections of galaxies showed a significant anisotropy in the high RV clusters. They studied 4 clusters (A0042, A1227, A1920, and A2142) that have RV > 30 000 km s^{-1}. All 4 clusters showed anisotropy in both the θ and ϕ distributions. The high RV cluster galaxies showed anisotropy in such a way that their SV orientations tend to lie parallel to the LSC plane. In the past and the present work, the common point is the reference coordinate system, i.e., supergalactic system. Therefore a relation between the orientation of cluster galaxies, LSC galaxies and the galaxies in the ZOA can be suspected. Probably, this could be connected with the fact that LSC plane roughly coincides with a plane with a larger concentration of galaxies at much more larger scales.

Aryal, Kafle & Saurer (2008) studied the RV dependence in 10 subsamples of 10 562 galaxies that have RV less than 5 000 km s^{-1}. They used supergalactic coordinate system as a physical reference system. The RV dependence is found to be significant for high RV galaxies than that of low RV galaxies in both the θ and ϕ distributions. Thus, the distant galaxies showed a significant preferred alignment.

5. Conclusions

We studied the spatial orientations of spin vector (SV) orientation of 410 Zone of Avoidance (ZOA) galaxies found in the region $20° \leq \ell \leq 80°$, $-10° \leq b \leq -5°$ on the first Palomar Observatory Sky Survey. We used the position angle - inclination method to find the three-dimensional rotation axes of galaxies. A spatially isotropic distribution is assumed to examine non-random effects. To check for anisotropy or isotropy we have carried out three statistical tests: Kolmogorov-Smirnov, Kuiper-V and the Fourier.

Interestingly, all three possible scenarios (pancake-, primordial vorticity- and hierarchy model) are observed when we studied preferred alignments with respect to equatorial, Galactic and supergalactic systems. The 'pancake model' predicts that SVs of galaxies tend to lie within the reference plane. According to the 'hierarchy model' the directions of the SVs should be distributed randomly. The 'primordial vorticity theory' advocates that the SVs of galaxies are distributed primarily perpendicular to the reference plane. We noticed that the SV orientation of ZOA galaxies tend to lie in the equatorial plane. These vectors are found to be oriented perpendicular to the Local Supercluster plane. A random alignment of SVs of galaxies is noticed with respect to the Galactic plane. The projections of SVs showed a mixed picture: tend to point towards the Galactic centre and tend to be oriented perpendicular towards the LSC centre. This result clearly hints the need of suitable reference system for the ZOA galaxies. The supergalactic coordinate system is found to be most suitable among three systems because we noticed anisotropy in both the SV distributions and the distribution of SV projections of galaxies. The issue of suitable physical reference system is critical while studying spatial orientation of galaxies

in a cluster or supercluster. We intend to work on this issue using the Sloan Digital Sky Survey (seventh data release) and Galaxy Zoo project data in the future.

Acknowledgments

We have great pleasure to thank the anonymous referee for his/her constructive criticisms and useful comments. We are thankful to W. Marchiotto, Innsbruck University, Austria for providing the data. B. Aryal is grateful to the University of Innsbruck for financial support for a research stay during October to December 2009. We acknowledge Mr. Dirgh Raj Shahi for the help during data reduction. This research has made use of the NASA/IPAC Extragalactic Database (NED), which is operated by the Jet Propulsion Laboratory, California Institute of Technology, under contract with the National Aeronautics and Space Administration.

References

Aryal B., 2011, RAA, 11, 293
Aryal B., Saurer W., 2000, A&A, 364, L97
Aryal B., Saurer W., 2005, MNRAS, 360, 125
Aryal B., Kandel S.M., Saurer W., 2006, A&A, 458, 357
Aryal B., Paudel S., Saurer W., 2007, MNRAS, 379, 1011
Aryal B., Kafle P., Saurer W., 2008, MNRAS, 389, 741
Aryal B., Bachchan R. K., Saurer W., 2010, BASI, 38, 165
Aryal B., Paudel R. R., Saurer W., 2012, Ap&SS, 337, 313
Donley J.L., et al., 2005, AJ, 129, 220
Doroshkevich A.G., 1973, AJ, 14, L11
Flin P., Godłowski W., 1986, MNRAS, 222, 525
Godłowski W., 1993, MNRAS, 265, 874
Godłowski W., 1994, MNRAS, 271, 19
Godłowski W., 2011, arXiv 1110.2245
Godłowski W., Ostrowski M., 1999, MNRAS, 303, 50
Hawley D.L., Peebles P.J.E. 1975, AJ, 80, 477
Henning P.A., et al., 2010, AJ, 139, 2130
Holmberg E., 1946, Medd. Lund. Astron. Obs., Ser VI, No. 117
Hu F.X., Wu G.X., Song G.X., Yuan Q.R., Okamura S., 2006, Ap&SS, 302, 43
Huchtmeier W.K., Lercher G., Seeberger R., Saurer W., Weinberger R., 1995, A&A, 293, L33
Jaaniste J., Saar E., 1978, in Longair M.S., Einasto J., eds., Proc. IAU Symp. No. 79, The Large Scale Structure of the Universe, Reidel, Dordrecht, p. 448
Kanji G.K., 1995, 100 Statistical tests, Sage Publication
Kerton C.R., Brunt C.M., 2003, A&A, 399, 1083
Kuiper N.A., 1962, Proceedings of the Kononklijke Nederlandse Akademie Van Wetenschappen, Ser. A, 63, 38
Maffei P., 1968, PASP, 80, 618

Marchiotto W., 2000, M.Sc. Thesis, Institute of astrophysics, Innsbruck University, Innsbruck, Austria
Marchiotto W., Wildauer H., Weinberger R., 1999, AG Abstract Services, 15, 34
Mieske S., Hilker M., Infante L., 2005, A&A, 438, 103
Öpik E.J., 1970, Irish AJ, 9, 211
Ozernoy L.M., 1978, in Longair M.S., Einasto J., eds, Proc. IAU Symp. 79, The Large Scale Structure of the Universe, Reidel, Dordrecht, p. 427
Peebles P.J.E., 1969, ApJ, 155, 393
Press W.H., Teukolsky S.A., Vetterlin W.T., Flannery B.P., 1992, Numerical Recipes in C, 2nd ed., Cambridge University Press
Ryan-Weber E., et al., 2002, AJ, 124, 1954
Seeberger R., Saurer W., 1998, A&AS, 127, 101
Shandarin S.F., 1974, Astr. Zh, 51, 667 (in Russian), Soviet Astron, 18, 392 (in English)
Stephens, M.A., 1970, Journ. Royal Statistical Society, Ser. B, 32, 115
Tammann G.A., Sandage A., 1976, ApJ, 207, L1
Tonry J.L., Blakeslee, J.P., Ajhar E.A., Dressler A., 2000, ApJ, 530, 625
Weinberger R., Saurer W., Seeberger R., 1995, A&AS, 110, 269

Astrophysics and Space Science manuscript No.
(will be inserted by the editor)

S. N. Yadav[1], · **B. Aryal**[1] · **W. Saurer**[2]

Spatial Orientation of Spin Vectors of Blue-shifted Galaxies

Received: 12 Dec 2015 / Accepted: .....

Abstract We present the analysis of the spin vector orientation of 5 987 SDSS galaxies having negative redshift from -87.6 to -0.3 km s^{-1}. Two dimensional observed parameters are used to compute three dimensional galaxy rotation axes by applying 'position angle–inclination' method. We aim to examine the non-random effects in the spatial orientation of blue-shifted galaxies. We generate $5{\times}10^6$ virtual galaxies to find expected isotropic distributions by performing numerical simulations. We have written MATLAB program to facilitate the simulation process and eliminate the manual errors in the process. Chi-square, auto-correlation, and the Fourier tests are used to examine non-random effects in the polar and azimuthal angle distributions of the galaxy rotation axes. In general, blue-shifted galaxies show no preferred alignments of galaxy rotation axes. Our results support Hierarchy model, which suggests a random orientation of angular momentum vectors of galaxies. However, local effects are noted suggesting gravitational tidal interaction between neighboring galaxies.

Keywords galaxies: evolution – galaxies: formation – galaxies: statistics – galaxies: blue shift

1 Introduction

It is commonly believed that the blue-shifted galaxies are relatively nearby ones whose peculiar motion overcomes the Hubble flow. All of the most distant galaxies (and indeed the overwhelming majority of all galaxies) are red-shifted. According to the conventional definition, the redshift of galaxies is the sum of two terms: the isotropic cosmic expansion velocity and the peculiar velocity owning to gravitational attraction by the surrounding matter. In practice, determining the peculiar velocity of a galaxy requires knowledge of both its observable radial velocity relative to some reference system and the distance to the galaxy determined independently of the radial velocity. According to the linear theory of gravitational instability, the peculiar velocities of galaxies are related to fluctuations in the mass (Peebles 1980).

Burbidge & Demoulin (1969) first observed IC 3258 with a blueshift of -490 km s^{-1}. They give three possible interpretations of their observations. First, IC 3258 is a member of the Virgo cluster and has a very high velocity relative to the average for the cluster. Second, IC 3258 is a field galaxy closer to the Virgo cluster and its large velocity is just a random motion. Third, IC 3258 has velocity because it has been ejected in an outburst involving one of the radio galaxies in the Virgo cluster. Several other blue-shifted galaxies appear in the direction of the Virgo cluster.

By measuring the distance d of a galaxy, one can obtain the peculiar velocity of a galaxy $V_{pec} = V_{obs} - H_o\, d$, here $H_o\, d$ is Hubble expansion velocity, V_{obs} is observed velocity of the galaxy. Since the Hubble expansion velocity is small for nearby galaxies, the peculiar velocity could be negative. Negative peculiar velocities are seen all over the region around the Virgo cluster and this have long been seen as a reflex of the pull of the cluster on us (Aaronson et al. 1982). We live in the Local Supercluster, which is overdense part of the Universe. So there is possibly the a local retardation of the cosmic expansion or a net infall within this region. In another example, an observer living on the outskirts of a large concentration is also pulled towards the overdense part of the clusters.

When the radiation propagates inside the collapsing body it is blue-shifted. If this blueshift is greater than the redshift caused by the propagation of the radiation through expanding universe, distant observer can detect the gravitational blueshift from the collapsing object.

First Author: S. N. Yadav
[1]Central Department of Physics, Tribhuvan University, Nepal
E-mail: ysibnarayan@yahoo.com

B. Aryal
[1]Central Department of Physics, Tribhuvan University, Nepal
E-mail: binil.aryal@uibk.ac.at

W. Saurer
[2]Institute of Astro- and Particle physics, Innsbruck University, Technikstrasse 25/8, A-6020 Innsbruck, Austria
E-mail: water.saurer@uibk.ac.at

Also the AGNs have blue-shifted spectrum. Bian et al. (2005) studied the radial velocity difference between the narrow emission-line components and of [O III] λ and Hβ in a sample of 150 SDSS narrow-line Seyfert 1 galaxies. They found seven 'blue outliers' with [O III] blueshifted by more than 250 km s^{-1}. They interpreted the blueshift as possible result of the outflowing gas from the nucleus and the obscuration of the receding part of the flow by an optically thick accretion disk and on the viewing angle.

Spatial orientation of angular momentum of blue-shifted galaxies (SDSS) has not been studied, so we are interested to carry out the spatial orientation of blue-shifted galaxies. An idea of the origin of angular momentum of galaxies is very important to understand the evolution of large scale structures of the universe. This paper is organized as follows: in Sect. 2 we describe the sample used and the method of data reduction. In Sect. 3 we describe the methods, statistical tools and the selection effects. Finally, a discussion of the statistical results and the conclusions are presented in Sects. 4 and 5.

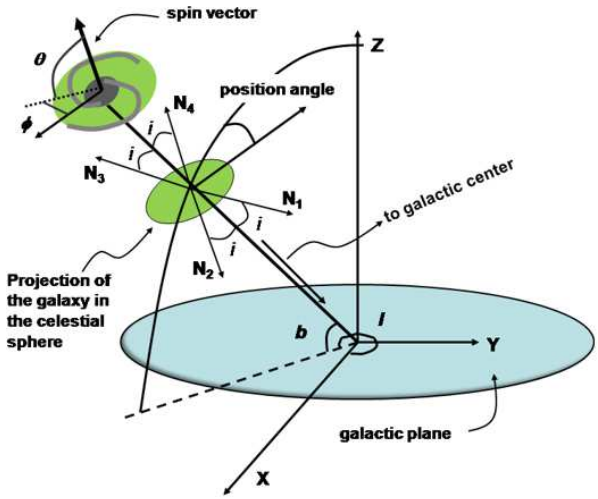

Fig. 2 Schematic illustration of θ (polar angle between the SV of the galaxy and the reference plane) and ϕ (azimuthal angle between the projection of SV and the X-axis of the reference plane). The galactic longitude (l) and latitude (b) are shown. For details: Flin & Godlowski (1986) and Aryal et al. (2008).

2 Blue-shifted SDSS Galaxies

We compiled a database of 5 987 blue-shifted galaxies from The Sloan Digital Sky Survey seventh Data Release (SDSS DR7). All sky distribution of blue-shifted galaxies is shown in Fig. 1a. The inhomogeneous distribution of galaxies is because of the nature of the survey. The distribution of blue-shifted galaxies is shown in Fig. 1b. We found a linear relationship between the blue-shift and logarithm of the number of galaxies ($-z \propto \log(N)$). We have retained only those galaxies that have blue-shift ($-z$) data at 95% level of significance. This removed 569 galaxies form the original data. Since blue-shift is found to be decreases lineally with number (Fig. 1b), the remaining 4 595 galaxies were classified into three bins by considering the bin size of 1×10^{-4}. This resulted in three bins with number of galaxies roughly in the ratio of 3 : 2 : 1 in the largest, medium and the smallest bins respectively. In the binning process, galaxies that have very low and high blue-shift values were also removed.

Since our galaxies are blue-shifted, their apparent magnitude increases with time. In order to check the effect of blue-shift on preferred alignments, we have chosen two extreme filters: infrared (i) and ultraviolet (u). The wavelengths of SDSS i and u filters are 7 625 $\mathring{A}$ and 3 543 $\mathring{A}$, respectively. The true magnitudes of i filter lies in the far-infrared and u in the visual bands. The study of far-infrared and optical activity in the galaxy gives information regarding the early star formation activity and the HII region, respectively. Fig. 1c,d shows the magnitude distribution of near infrared and ultraviolet galaxies. For both, Gaussian distribution fits well with the observed distribution.

In order to find angular momentum vectors (or spin vectors, SV hereafter), the diameters, position angles and positions of galaxies should be known. We have compiled the database of diameters and position angle of galaxies using SDSS survey.

3 Method of analysis

We follow the method suggested by Flin & Godlowski (1986) to convert two dimensional parameters (positions, diameters, position angles of the DR7 SDSS blue shifted galaxies) into three dimensional parameters (galaxy rotation axes in spherical polar coordinates). The expected isotropic distribution for angular momentum vectors or SVs of galaxies are determined by using the method proposed by Aryal & Saurer (2000). The observed and expected distributions are compared with the help of three statistical tests namely chi-square, auto-correlation and the Fourier.

3.1 Observed distribution: SVs of galaxies

The two-dimensional SDSS parameters (positions, position angles and diameters) are converted into polar (θ) and azimuthal (ϕ) angles of galaxies using Flin & Godlowski (1986). Our blue-shifted galaxies have negative radial velocities probably due to their larger peculiar velocity. These galaxies are mostly nearby galaxies. Thus, it is convenient to use galactic coordinate system as a physical reference plane. The formulae to obtain θ and ϕ in are as follows (Flin & Godlowski, 1986):

$$\sin\theta = -\cos i \sin b \pm \sin i \sin p \cos b \qquad (1)$$

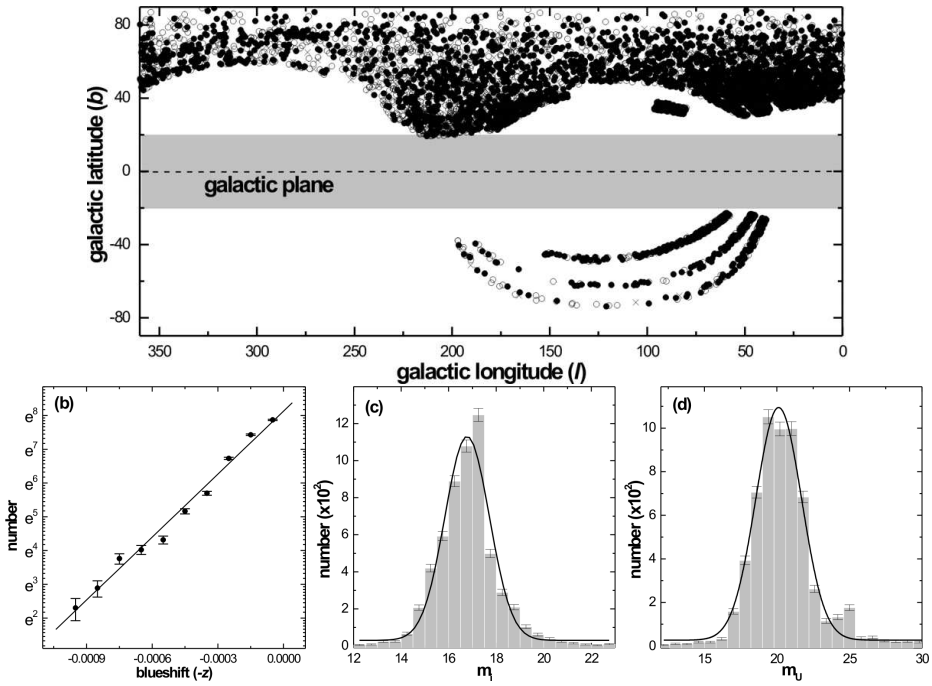

Fig. 1 (a) All sky distribution of blue-shifted galaxies in the galactic coordinate system. The grey-shaded region represents plane of the Milky Way. The symbols solid circle, hollow circle and cross represent small, moderate and strongly blue-shifted galaxies (description in the text) (b) Blue-shift (c) i-magnitude and (d) u-magnitude distribution of galaxies. The solid line in (b) is the linear fit. The Gaussian fits are shown by solid curves in (c) and (d).

$$\sin\phi = (\cos\theta)^{-1}[-\cos i\cos b\sin l + \sin i(\mp\sin p\sin b\sin l \mp \cos p\cos l) \quad (2)$$

where l, b and p are the galactic longitude, latitude and position angle, respectively. The i represents the inclination angle, obtained using Holmberg's (1946) formula: $\cos^2 i = [(b/a)^2 – q^2]/(1 – q^2)$ where b/a is the measured axial ratio and q is the intrinsic flatness of disk galaxies. The method of determination of intrinsic flatness of galaxies is the same as in Aryal et al. (2013).

The above formulae show that there are two possible solutions for a given galaxy. The normals (N_1, N_2, N_3, N_4) shown in Fig. 2 can not be determined unambiguously, because we do not know the side of the galaxy which is nearer/far to us, and the direction of rotation. Thus, there are four solutions of the SV orientation for a galaxy. We count all four possibilities independently in our analysis.

3.2 Expected distribution: numerical simulation

Aryal & Saurer (2000) studied the effects of various types of selections in the database and concluded that such selections may cause severe changes in the shapes of the expected isotropic distribution curves in the galaxy orientation study. Their method has been applied by several authors in galaxy orientation studies (Hu et al. 2006, Aryal et al. 2013 and the references therein). Two kinds of selection effects are noticed in our database: (1) inhomogeneous distribution of positions of galaxies, and (3) less number of high inclination (edge-on) galaxies. These selection effects are removed and the expected isotropic distribution curves (θ and ϕ) are determined using the numerical simulation method as proposed by Aryal & Saurer (2000). For this, a true spatial distribution of S of galaxies is assumed to be isotropic. Then, due to the projection effects, i can be distributed $\propto sin\ i$, latitude can be distributed $\propto cos\ b$, the variables longitude (l) and PA can be distributed randomly, and formulae (1) and (2) can be used to simulate (numerically) the corresponding distribution of θ and ϕ. The isotropic distribution curves are based on simulations including 10^7 virtual galaxies. The simulation procedure is described in Aryal & Saurer (2004). We perform numerical simulation with respect to galactic coordinate system systems. These expected isotropic distribution curves are compared with the observed distribution.

3.3 Statistical tests

Our observed θ and ϕ-distributions are compared with expected isotropic distribution curves. For this comparison we applied chi-square, autocorrelation and the Fourier (Godlowski 1993) tests. These tests are described in the appendix of Aryal et al. (2007). These statistical tests are a proper method in our case, because θ and ϕ are

independent data. The significance level is chosen to be 95%, the null hypothesis is established to be an equidistribution for the θ and ϕ.

4 Results

We have classified our database into six subsamples on the basis of their redshift values and u & i-magnitudes. Here we discuss the distribution of the polar (θ) and azimuthal (ϕ) angles of galaxy rotation axes in each subsamples. We study the spatial orientation of SVs of galaxies with respect to the galactic coordinate system. Any deviation from the expected isotropic distribution will be tested using four statistical parameters, namely the chi-square probability ((P$> \chi^2$)), auto-correlation coefficient ((C/C(σ))), first order Fourier coefficient (Δ_{11} /$\sigma(\Delta_{11})$), and first order Fourier probability ((P$> \Delta_1$)). The conditions for anisotropy are the following: P($> \chi^2$) < 0.050, C/C(σ) and $\Delta_{11}/\sigma(\Delta_{11}) > 1$, and P($> \Delta_1$) < 0.150. These statistical limits were proposed by Godlowski (1993, 1994). In the θ-distribution, a positive (negative) Δ_{11} suggests that the SVs of galaxies tend to orient parallel (perpendicular) with respect to plane of the Milky Way. In the ϕ-distribution, a positive (negative) Δ_{11} suggests that the SV projections of galaxies tend to point radially (tangentially) with respect to center of the Milky Way. Any 'humps' or 'dips' in the histogram will be discussed. Here 'hump' and 'dip' are defined as having more or less observed solutions than expected respectively.

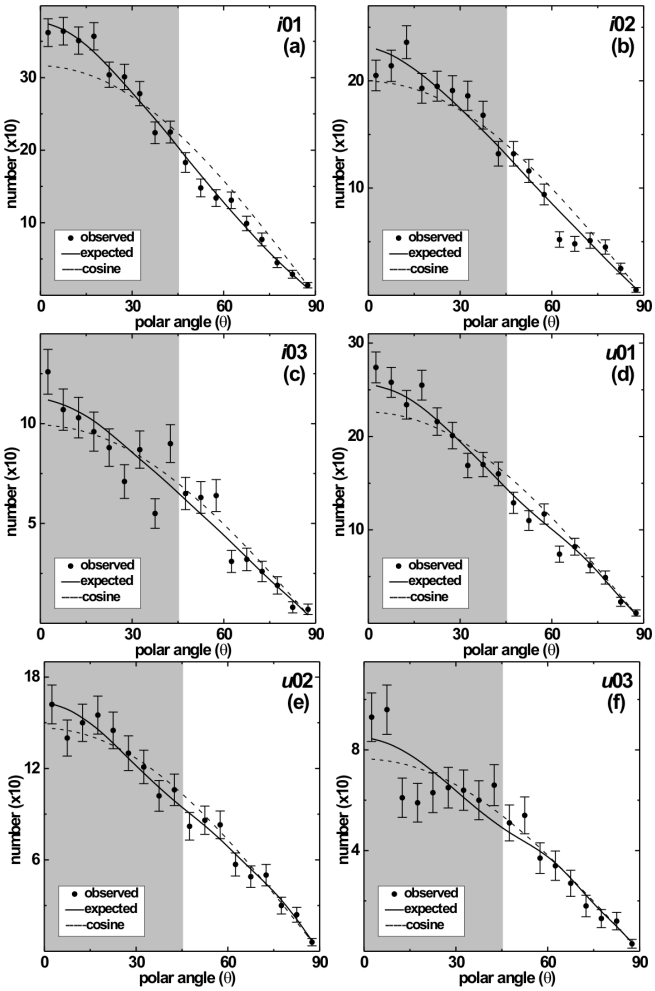

Fig. 3 The polar (θ) angle distributions of blue shifted SDSS galaxies in 6 subsamples. The solid circles with $\pm$ 1σ error bars represent the observed distribution. The solid line represents the expected isotropic distributions. The cosine distributions (dashed) are shown for the comparison.

4.1 Polar angle distribution

All three statistical tests suggest isotropy in the θ distribution of subsample $i01$ (Table 1). The galaxies in this subsample are nearby blue-shifted (RV < -28.5 km s^{-1}) having i-magnitude in the range 12.45 and 32.08. In the histogram, no significant humps or dips can be seen (Fig. 3a). Thus, a random orientation of angular momentum vectors of galaxies is found, suggesting hierarchy model of the structure formation as suggested by Peebles (1969).

The galaxies in the subsample $i02$ are moderately blue shifted (RV: 28.5-58.5 km s^{-1} and m$_i$: 10.46 - 36.10). The chi-square and the correlation tests show anisotropy (Table 1). However, the first order Fourier probability and the first order Fourier coefficient suggest isotropy. Since the observed distribution follow the expected, we regard the Fourier test as more reliable. There are small dips at 5°, $\sim$ 65°, and a hump at 15° (Fig.3b). These are possibly due to the binning effect.

Strong blue-shifted (RV: $\geq$58.5 km s^{-1}) SDSS galaxies (m$_i$: 10.82 - 42.23) are grouped in the subsample $i03$. In the histogram, a very good agreement between the observed and expected distributions can be seen. Similar to the subsample $i03$, chi-square probability and correlation coefficient show anisotropy, whereas first-order Fourier probability and the first-order Fourier coefficient suggests isotropy (Table 1). Several humps (0°, 45°, 60°) and dips (30°, 35°, 60°) suggests the local effect. Thus, the strong blue-shifted infrared galaxies are in the process of grouping or subclustering because of the tidal or gravitational shearing effect.

All three statistical tests support isotropy in θ distribution of u-magnitude low blue-shifted (RV < 58.5 km s^{-1}) galaxies. In Fig. 3d, no significant humps or dips are found. A small hump at 20° and a dip at 60° are because of the binning effects. These effects do not change the statistics of the subsample $u01$. Hence, no preferred alignments of SVs of galaxies in subsample $u01$ is noticed.

Table 1 Statistics of the polar (θ) and azimuthal angle (ϕ) distributions of galaxies in the six subsamples. The first column lists the subsamples. The second and third columns give the number of galaxies (N) in the subsample and their blue-shift (-z, in km s^{-1}). The fourth and fifth columns list the values of chi-square probability (P($>\chi^2$)) and auto-correlation coefficient (C/C(σ)). The last three columns gives the first order Fourier coefficient ($\Delta_{11}/\sigma(\Delta_{11})$), the first order Fourier probability (P($>\Delta_1$)), and standard deviation of Fourier amplitude ($\sigma(\Delta_1)$) respectively.

subsample	N	$-z$	P($>\chi^2$)	C/C(σ)	$\Delta_{11}/\sigma(\Delta_{11})$	P($>\Delta_1$)	$\sigma(\Delta_1)$
polar angle							
$i01$	1813	<28.5	0.781	−0.1	−0.4	0.939	0.023
$i02$	1144	28.5-58.5	0.025	+1.9	−0.1	0.849	0.030
$i03$	569	≥58.5	0.023	−1.7	−0.7	0.773	0.042
$u01$	1297	<28.5	0.644	−1.0	+1.2	0.404	0.028
$u02$	839	28.5-58.5	0.896	−0.5	−0.2	0.931	0.035
$u03$	438	≥58.5	0.146	+1.8	−0.4	0.879	0.048
azimuthal angle							
$i01$	1813	<28.5	0.657	+0.1	−1.1	0.432	0.023
$i02$	1144	28.5-58.5	0.107	−1.4	−2.1	0.090	0.030
$i03$	569	≥58.5	0.449	+1.5	−2.0	0.093	0.042
$u01$	1297	<28.5	0.039	+0.2	−2.2	0.098	0.028
$u02$	839	28.5-58.5	0.433	+0.5	−1.7	0.116	0.035
$u03$	438	≥58.5	0.860	+0.3	+0.1	0.747	0.048

In subsample $u02$, all three statistics show isotropy in polar angle (θ) distribution. A small dip at 10° is because of the binning effect (Fig. 3e). A random orientation of SVs of galaxies is noticed in this subsample.

All statistics except correlation coefficient showed isotropy in the polar angle distribution of high blue-shifted (RV ≥ 58.5 km s^{-1}) u-magnitude galaxies (subsample $u03$). The correlation coefficient is found to be 1.8 (>1.5σ level). This is because of the humps at 10°, 45°, 55° and dips at 15°, 20°. These humps and dips suggests the possibility of grouping or subclustering because of the tidal or gravitational shearing effects between comoving galaxies.

To sum up, the spatial orientation of blue-shifted galaxies is found to be random, supporting hierarchy model (Peebles 1969) of structure formation. It is found that the rapidly moving blue shifted galaxies are in the process of large structure (galaxy groups, subclusters, clusters, etc) formation. In addition, magnitude is found to be independent of the preferred alignments.

4.2 Azimuthal angle distribution

All three statistics support isotropy in the azimuthal angle distribution of low blue-shifted high magnitude infrared (subsample $i01$) galaxies (Table 2). There is a hump at +65° and dips at −5° and −55° (Fig.4a). These are due to the binning effect and hence do not change the statistics. Thus, no preference is noticed for spin vector projections of low blue-shifted infrared galaxies.

All statistics except χ^2-test suggest anisotropy in the ϕ distribution of the subsample $i02$. In the histograms for the ϕ-distribution of the subsample $i02$ (Fig.4b), humps at −60°, +30° and +90°, and dips at −50° to +20° can be seen. These humps and dips lead this subsample to show anisotropy. The spin vector projection of $i02$ galaxies is found to be directed tangentially outwards with respect to the center of the Milky Way. Fig. 4c shows the distribution of the spin vector projections of high blue-shifted galaxies (subsample $i03$). Similar to the subsample $i02$, all statistical parameters except P($>\chi^2$) show anisotropy. There is a significant hump at +90° and dips at −10° and 0°. The SV projections of high blue-shifted galaxies is found to be oriented tangentially with respect to the center of the Milky Way.

All statistics except C/C(σ) show anisotropy in the ϕ-distribution for subsample $u01$. In the histogram, several humps and dips can be seen: humps at −90° and +80°, and dips in the region from −50° to +50° (Fig. 4d). This subsample showed isotropy in the polar and anisotropy in the azimuthal angle distribution. This inconsistency is because of the inappropriate reference coordinate system. A physical reference system should be identified in the future.

Fourier test suggests isotropy in the subsample $u02$. There are dips at −40°, +20° and a hump at +90° (Fig.4e). We observe weak anisotropy in the spin vector projection of $u02$ galaxies with respect to galactic coordinate system.

Interestingly, all statistics show isotropy in the distribution of SV projections of high blue-shifted galaxies ($u03$). There are small dips at 70° and 40°, not significant to alter the statistics of the subsample. There is a very good agreement between the observed and expected distributions (Fig. 4f) Thus, a random orientation of spin vector projections is found.

4.3 Discussion

In the numerous past literatures authors have studied the spatial orientation of red-shifted galaxies in the field, clusters and Superclusters and found mixed result: (1) noticed anisotropy supporting either 'pancake model' (Flin & Godlowski 1986; Godlowski 1993, 1994; Godlowski, Baier & MacGillivray 1998, Flin 2001) as suggested by

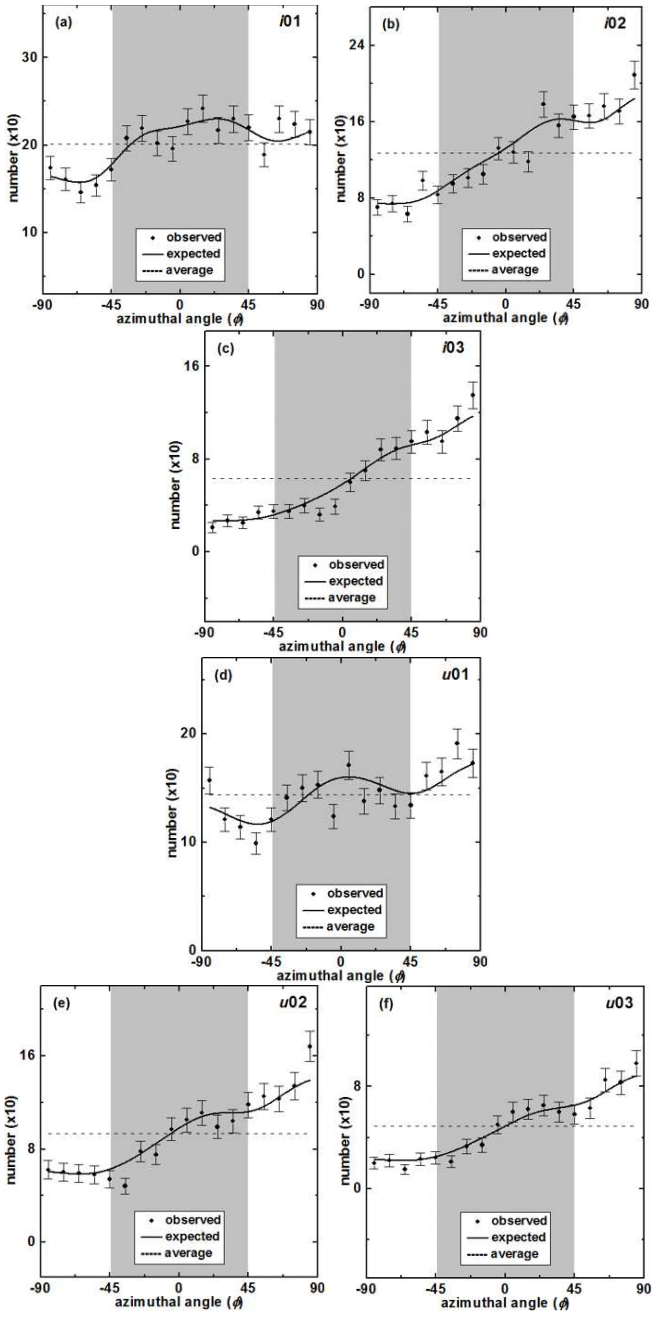

Fig. 4 The azimuthal (ϕ) angle distributions of blue shifted SDSS galaxies in 6 subsamples. The solid circles with $\pm$ 1σ error bars represent the observed distribution. The solid line represents the expected isotropic distributions. The average distributions (dashed) are shown for the comparison.

Doroshkevich (1973) or 'primordial vorticity model' (Baier, Godlowski & MacGillivray 2003) as proposed by Ozernoy (1978)(2) found isotropy suggesting a random orientation of spin vectors of galaxies supporting 'hierarchy model' (Bukhari & Cram 2003; Aryal & Saurer 2005a, Aryal et al. 2006, 2012, 2013) as recommended by Peebles (1969).

In addition to these scenarios a bimodal tendency (Kashikawa & Okamura 1992), local anisotropy (Flin 1995, Djorgovski 1983, Aryal & Saurer 2004, 2005b), global anisotropy (Parnovsky, Karachentsev & Karachentseva 1994) are noticed. Godlowski & Ostrowski (1999) noticed a strong systematic effect, generated by the process of deprojection of a galactic axis from its optical image. In isolated Abell clusters, only brightest galaxies are preferentially aligned (Trevese, Cirimele & Flin 1992). Panko et al. (2013), Godlowski (2012) and Godlowski et al. (2010) noticed a dependence of alignment with respect to cluster richness.

The anisotropy is found mostly for those samples which is taken from a limited region of the sky (e.g., clusters, sub-clusters, groups, etc). For the field galaxies and superclusters, i.e., the database taken from the large scale structure, authors notice a random orientation supporting hierarchy model. In both the cases (isotropy or anisotropy), a local effect is noticed. This effect might arises due to the tidal connections between the neighboring galaxies or because of the gravitational shearing effect. Interestingly, blue-shifted galaxies support hierarchy model. Thus, it can be concluded that the blue-shift is not different cosmological effect, it is because of the peculiar velocity as suggested by Aaronson et al. (1982).

5 Conclusion

We studied the spatial orientation of spin vectors of 5 987 blue-shifted galaxies (-87.6 to -0.3 km s^{-1}) observed through i- and u-filter. These database were taken by SDSS (7^{th} data release). We classified our data into 6 subsamples based upon their blue-shift. We have used the 'PA-inclination' method proposed by Flin & Godlowski (1986) to convert two dimensional observed parameters to three dimensional galaxy rotation axes (polar and azimuthal angles) and carried out random simulation by creating 5×10^6 virtual galaxies in order to remove selection effects from the database (Aryal & Saurer 2000). To check for anisotropy or isotropy, we have carried out three statistical tests: chi-square, auto-correlation and the Fourier.

Since our observed distributions do not vary significantly from the expected distribution, we have regarded the Fourier test as more reliable. The local effects are examined by the correlation test. We have taken χ^2 test in order to check the binning effect. In general, we found isotropic distribution of the spin vector of galaxies in all six subsamples with respect to the galactic coordinate system. There are humps and dips in the polar angle distributions, and these humps and dips alter the correlation test showing anisotropy in subsamples $i02$, $i03$, and $u03$. Hence, local effect was observed in these subsamples suggesting a local tidal connection between the rotation axes of neighboring galaxies or the gravitational shearing effect. However, in the rest of the subsamples

($i01$, $u01$, and $u02$) small humps and dips do not alter the statistics of the total subsample, so we suppose these as binning effects. In general, we observe that there is no preferred alignment of spin vectors of galaxies. Our results of θ-distribution support the hierarchical clustering scenario (Peebles 1969), which predicts the random orientation of the directions of the spin vectors of galaxies.

On the other hand, we found interesting results for the ϕ-distribution. As mentioned above, we have regarded the Fourier test as more reliable. Out of six subsamples only two subsamples ($i01$ and $u03$) show isotropy in all tests. Rest of the subsamples ($i02$, $i03$, $u01$, and $u02$) show anisotropic distribution of the spin vector projections of galaxies. Also, all subsamples (except $u03$) have negative value of the first order Fourier coefficient Δ_{11}. Therefore, in general the spin vector projection of the galaxies tend to be orientated perpendicular to the equatorial plane. However, this result needs to be examined by using other reference system such as Supergalactic coordinate system in the future.

Acknowledgements This research has made use of the Sloan Digital Sky Survey (SDSS) database (www.sdss.org) which is funded by Alfred P. Sloan Foundation and the Participating Institutions. We acknowledge Dr. Rajendra Parajuli, Amrit Campus, Kathmandu for his fruitful comments on the manuscript. We thank Mr. R. K. Bachchan for helping in the data compilation and Mr. S. Dangi for the data reduction. One of the authors (SNY) acknowledges Central Department of Physics, Tribhuvan University, Nepal for all kinds of support for his Ph.D. work.

References

1. Aaronson, M., Huchra J., Mould, J., Schechter P. L., Tully R. B.: *Astrophys. J.* **258**, 64 (1982)
2. Bian, W., Yuan, Q., Zhao, Y., *Monthly Notices Royal Astron. Soc.* **364** 187 (2005)
3. Aryal, B., Bhattarai, H., Dhakal, S., Rajbahak, C., Saurer, W.: *Monthly Notices Royal Astron. Soc.* **434**, 1939 (2013)
4. Aryal, B., Paudel, R. R.; Saurer, W.: *Astrophys. Space Sci.* **337**, 313 (2012)
5. Aryal, B., Kafle, P., Saurer, W.: *Monthly Notices Royal Astron. Soc.* **389**, 741 (2008)
6. Aryal, B., Paudel, S., Saurer, W.: *Monthly Notices Royal Astron. Soc.* **379**, 1011 (2007)
7. Aryal, B., Saurer, W.: *Monthly Notices Royal Astron. Soc.* **366**, 438 (2006)
8. Aryal, B., Saurer, W.: *Astronom. Astrophys.* **432**, 841 (2005b)
9. Aryal, B., Saurer, W.: *Astronom. Astrophys.* **432**, 431 (2005a)
10. Aryal, B., Saurer, W.: *Astronom. Astrophys.* **425**, 871 (2004)
11. Aryal, B., Saurer, W.: *Astronom. Astrophys. lett.* **364**, L97 (2000)
12. Baier, F.W., Godlowski, W., MacGillivray, H.T.: *Astroph. Space Sci.* **403**, 847 (2003)
13. Burbidge, E. M., Demoulin, M. H.: *Astrophys. J.* **157**, 155 (1969)
14. Bukhari, F.A., Cram, L.E.: *Astrophys. Space Sci.* **283**, 173 (2003)
15. Doroshkevich, A.G.: *Astrophys. J.* **14**, L11 (1973)
16. Flin, P.: *Comments Astrophys.* Overseas Publishers Association, Amsterdam B.V., Vol. **18**, No. 2, p.81 (1995)
17. Flin, P., Godlowski, W.: *Monthly Notices Royal Astron. Soc.* **222**, 525 (1986)
18. Flin, P.: *Monthly Notices Royal Astron. Soc.* **325**, 49 (2001)
19. Godlowski, W.: *Astrophys. J.* **747**, 1, 7 (2012)
20. Godlowski, W., Piwowarska, P., Panko, E., Flin, P.: *Astrophys. J.* **723**, 985 (2010)
21. Godlowski, W., Ostrowski, M.: *Monthly Notices Royal Astron. Soc.*, **303**, 50 (1999)
22. Godlowski, W., Baier, F.W., MacGillivray, H.T.: *Astronom. Astrophys.* **339**, 709 (1998)
23. Godlowski, W.: *Monthly Notices Royal Astron. Soc.* **271**, 19 (1994)
24. Godlowski, W.: *Monthly Notices Royal Astron. Soc.* **265**, 874 (1993)
25. Holmberg, E.: *Medd. Lund. Astron. Obs.*, Ser VI, No. 117 (1946)
26. Kashikawa, N., Okamura, S.: *pasj*, **44**, 493 (1992)
27. Ozernoy, L.M.: in: Longair M.S., Einasto J., eds, Proc. IAU Symp. 79, *The Large Scale Structure of the Universe.* Reidel, Dordrecht, p.427 (1978)
28. Panko, E., Piwowarska, P., Godlowska, J., Godlowski, W., Flin, P.: *Astrophysics* **56**, 3, 322 (2013)
29. Parnovsky, S.L., Karachentsev, I.D., Karachentseva, V.E.: *Monthly Notices Royal Astron. Soc.* **268**, 665 (1994)
30. Peebles, P.J.E.: *Astrophys. J.* **155**, 393 (1969)
31. Trevese, D., Cirimele, G., Flin, P.: *Astronom. J.* **104**, 935 (1992)

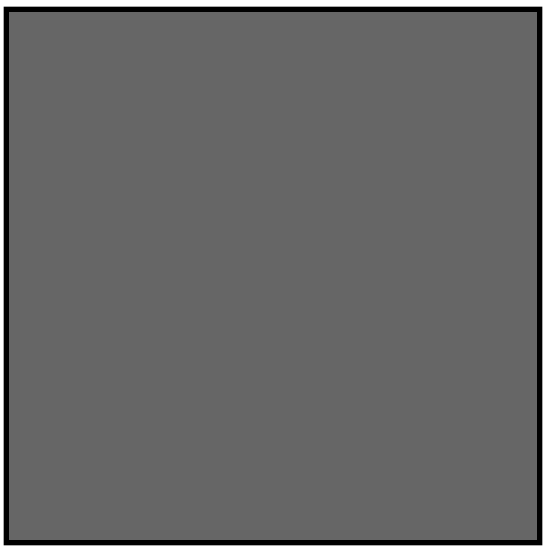

Research in Astron. Astrophys. Vol. 000 No.0, 000–000
http://www.raa-journal.org *http://www.iop.org/journals/raa*

***R**esearch in*
***A**stronomy and*
***A**strophysics*

Preferred alignments of angular momentum vectors of galaxies in six dynamically unstable Abell clusters

S. N. Yadav[1], B. Aryal[1] and W. Saurer[2]

[1] Central Department of Physics, Tribhuvan University, Kirtipur, Nepal *ysibnarayan@yahoo.com*
[2] Central Department of Physics, Tribhuvan University, Kirtipur, Nepal
[3] Institute of Astro-particle Physics, Innsbruck University, A-6020 Innsbruck, Austria

Received 2017 January 13; accepted 2017 February 22

Abstract A spatial orientation of angular momentum vectors of galaxies in six dynamically unstable Abell clusters (S1171, S0001, A1035, A1373, A1474 and A4053) is studied. For this, two-dimensional observed parameters (e.g., positions, diameters, position angles) are converted into three-dimensional rotation axes of the galaxy using 'position angle - inclination' method. The expected isotropic distribution curves for angular momentum vectors are obtained by performing random simulations. The observed and expected distributions are compared using several statistical tests. No preferred alignments of angular momentum vectors of galaxies are noticed in all six dynamically unstable clusters supporting hierarchy model of galaxy formation. These clusters have a larger value of velocity dispersion. However, local effects are noticed in the clusters that have substructures in the 1D-3D number density maps.

Key words: galaxies: evolution – galaxies: clusters: general – astronomical databases: miscellaneous.

1 INTRODUCTION

The formation of galaxy cluster is one of the major unsolved problems of modern astrophysics. The process by which larger structures (e.g., clusters, superclusters) are formed through the continuous merging of smaller structures (e.g., galaxy, galaxy groups) is called hierarchical clustering, which is supported by concordance model (ΛCDM). The study of preferred alignment of angular momentum vectors of galaxies in the clusters is one of the most effective ways of testing the concordance model. Godlowski et al. (2003) described Li (1988) model and showed the relation between the angular momenta and the masses of the large scale structures. This relationship was observationally tested by several authors (Godlowski et al. 2005, Hu et al. 2006, Aryal & Saurer 2006, Aryal et al. 2007, 2008, Godlowski et al. 2010, Godlowski 2012) and found the vanishing angular momenta for less massive structures and non-vanishing for larger structures.

Aryal et al. (2013) studied preferred alignments of angular momentum vectors of galaxies in six rotating clusters (A954, A1139, A1399, A2162, A2169, and A2366) that are dynamically stable and have a single peak in 1D-3D number density maps. These clusters have no substructures. They found a random orientation of angular momentum vectors of galaxies in all six clusters, supporting hierarchy model (Peebles 1969).

In the present work we intend to study preferred alignments of angular momentum vectors of galaxies in six Abell clusters namely S1171, S0001, A1035, A1373, A1474 and A4053 that have multiple

Table 1 Database of six clusters that have multiple number-density peaks in 1D-3D maps (HL). The first column lists the Abell name followed by their positions (Abell et al. 1989). The fourth-eighth columns give BM type cluster morphology (Bautz & Morgan 1970), mean radial velocity ($\overline{cz}$), velocity dispersion ($\sigma_{\rm v}$), number (N) of galaxies in the cluster and its morphology, as given in HL.

Abell	R.A. (J2000)	Dec. (J2000)	BM-type	$\overline{cz}$ (km s^{-1})	$\sigma_{\rm v}$ (km s^{-1})	N	morphology
S1171	$00^{\rm h}01^{\rm m}21.70^{\rm s}$	$27^\circ32'18.0''$	II	8377	646	42	Spherical
S0001	$00^{\rm h}02^{\rm m}33.93^{\rm s}$	$30^\circ44'06.2''$	I	8815	577	51	Elongated
A1035	$10^{\rm h}32^{\rm m}14.16^{\rm s}$	$40^\circ14'49.2''$	II-III	21753	1825	97	Spherical
A1373	$11^{\rm h}45^{\rm m}30.95^{\rm s}$	$02^\circ27'12.9''$	III	37595	1768	48	Elongated
A1474	$12^{\rm h}07^{\rm m}57.20^{\rm s}$	$14^\circ57'18.0''$	III	24151	714	60	Elongated
A4053	$23^{\rm h}54^{\rm m}45.39^{\rm s}$	$27^\circ40'52.8''$	III	20691	1366	76	Elongated

peaks in 1D-3D number density maps with a larger value of velocity dispersion. These clusters have substructures. We intend to find out the answer of the following: (1) does the orientation of angular momentum vectors of galaxies that have substructures favor hierarchical clustering? (2) do the clusters with large velocity dispersion prefer a random orientation of angular momentum vectors of galaxies? and finally (3) does the substructure formation cause large velocity dispersion in the cluster? Our aim is to compare results with concordance model. The database and the methods are described in sections 2 and 3. Our results and conclusions are presented in sections 4 and 5.

2 DATABASE

Hwang & Lee (2007, HL hereafter) proposed six rotating clusters (A954, A1139, A1399, A2162, A2169, and A2366) that are in dynamical equilibrium and show a single peak in 1D-3D number density maps. In addition, six dynamically unstable clusters (S1171, S0001, A1035, A1373, A1474 and A4053) that have multiple number-density peaks in 1D-3D maps with a large velocity dispersion are presented. After investigating substructure using Dressler-Scectman, HL classified rotating clusters into two category: (1) clusters with single number density peak and hence are in dynamical equilibrium and (2) clusters with multiple number-density peak and are dynamically unstable. In both cases, clusters have a very large value of velocity dispersion. In this paper we study the preferred alignments of angular momentum vectors of galaxies in the Abell clusters S1171, S0001, A1035, A1373, A1474 and A4053. Table 1 lists the the database (positions, BM type classification, mean redshift, velocity dispersion, number of galaxies in the cluster and its morphology) of six clusters (HL, Hwang 2011) used for this study.

3 METHOD

The PA-inclination method is used to convert two dimensional given parameters (positions, diameters, position angles) into three dimensional (galaxy rotation axes: angular momentum vectors and its projections) (Flin & Godlowski 1986). The expected isotropic distribution curves for angular momentum vectors and its projections are determined by performing a random simulation (Aryal & Saurer 2000). The observed distributions are compared with the expected using various statistical tests.

3.1 Observed distribution: angular momentum vectors of galaxies

The angular momentum vectors (θ) of galaxies and its projections (ϕ) to the galactic (G) and supergalactic (S) planes are obtained by using the method described by Flin & Godlowski (1986). For this, SDSS/2dFGRS database (positions, position angles and diameters) provided by Hwang (2011) are used. In the previous works (Godlowski 1994, Baier et al. 2003, Hu et al. 2006, and the references therein),

authors have studied the preferred alignments of galaxies in clusters with respect to galactic or supergalactic (or both) system. The formulae to obtain angular momentum vectors (θ) and its projection (ϕ) in S-system are as follows (Flin & Godlowski, 1986):

$$\sin\theta = -\cos i \sin B \pm \sin i \sin P \cos B \tag{1}$$

$$\sin\phi = (\cos\theta)^{-1}[-\cos i \cos B \sin L + \sin i(\mp \sin P \sin B \sin L \mp \cos P \cos L). \tag{2}$$

The inclination angle (i) is the angle between line-of-sight and the normal to the plane of the galaxy. This angle can be calculated using Holmberg's (1946) formula: $\cos^2 i = [(b/a)^2 – q^2]/(1 – q^2)$ where b/a is the measured axial ratio and q is the intrinsic flatness of disk galaxies. Since the morphological information of galaxies are not known, therefore the value of intrinsic flatness (q) is assumed to be 0.2 (Aryal et al. 2007, Godlowski 2011a). The parameters L, B and P are the supergalactic longitude, latitude and position angle, respectively.

The formulae (1) and (2) give two solutions for a galaxy. The reason for this is the approaching and receding sides of a galaxy, which can not be identified in our database. Therefore, there are four solutions for the preferred alignments of a galaxy: two each for angular momentum vectors and its projections. We count all these possibilities independently in the analysis.

3.2 Expected distribution: numerical simulation

Aryal & Saurer (2000) performed random simulations imposing various types of selections in the database and concluded that any selections can cause the changes in the expected isotropic distribution curves for both angular momentum vectors (polar angles) and its projections (azimuthal angles). We noticed following selection effects in our database: (1) the positions of galaxies in the clusters are inhomogeneous. (2) the PAs of face-on ($i\sim 0^\circ$) are mostly unknown and (3) the deficiency of high inclination ($i\sim 0^\circ$) galaxies. We perform random simulation method proposed by Aryal & Saurer (2000) in order to find expected isotropic distribution curves (θ and ϕ) by removing above mentioned selection effects. We apply cosmological principle by assuming isotropic distribution of angular momentum vectors of 10^7 virtual galaxies and use the formulae (1) and (2) in the random simulation. Therefore, the inclination angle (i) and latitude (B) are distributed as $\propto sin\ i$ and $\propto cos\ B$, respectively and the variables longitude (L) and position angle (PA) are distributed randomly (Aryal & Saurer 2000).

3.3 Statistical tests

We perform chi-square, autocorrelation, Fourier (Godlowski 1993), Kolmogorov-Smirnov (K-S) (Press et al. 1992, Kanji 1995) and Kuiper-V (Kuiper 1962) tests in order in the observed and expected distributions to discriminate anisotropy from isotropy. The details about these statistical tests are given in the appendix of Aryal et al. (2007). The limits for anisotropy are as follows:

- chi-square probability (P($> \chi^2$)) < 0.050,
- auto-correlation coefficient (C/C(σ)) > 1,
- first order Fourier coefficient ($\Delta_{11}/\sigma(\Delta_{11})$) > 1,
- Fourier probability (P($> \Delta_1$)) < 0.150,
- K-S = 1
- Kuiper-V = 1.

In last two statistical tests, null hypothesis (isotropy) is represented by "0" that can not be rejected at the chosen significance level whereas the value "1" designates that the null hypothesis can be rejected (anisotropy).

The first order Fourier coefficient (Δ_{11}) provides information regarding preferred alignments. A positive (negative) value of first order Fourier coefficient (Δ_{11}) in the θ-distribution suggests that the angular momentum vectors of galaxies tend to orient parallel (perpendicular) with respect to the reference coordinate system. Similarly, a positive (negative) Δ_{11} in the ϕ-distribution indicates that the

Table 2 Statistical values for both θ and ϕ distributions. The Abell number of the cluster, values of chi-square probability (P($> \chi^2$)) and auto-correlation coefficients (C/C(σ)) are given in first three columns. The fourth-seventh columns list the values of first order Fourier coefficient $\Delta_{11}/\sigma(\Delta_{11})$, first order Fourier probability P($> \Delta_1$), results of Kolmogorov-Smirnov (K-S) and Kuiper-V (KV) tests, respectively.

Abell	P($>\chi^2$) G/S	C/C(σ) G/S	$\Delta_{11}/\sigma(\Delta_{11})$ G/S	P($>\Delta_1$) G/S	K-S G/S	Kuiper-V G/S
polar angle						
S1171	$0.959/0.820$	$-0.5/+0.1$	$+0.0/-0.6$	$0.999/0.805$	$0/0$	$0/0$
S0001	$0.554/0.779$	$-0.4/+0.7$	$-0.6/+1.2$	$0.798/0.435$	$0/0$	$0/0$
1035	$0.721/0.795$	$+0.1/-1.0$	$+0.4/-0.5$	$0.864/0.868$	$0/0$	$0/0$
1373	$0.495/0.553$	$+0.7/-0.9$	$-0.2/-0.2$	$0.796/0.964$	$0/0$	$0/0$
1474	$0.012/0.610$	$-1.8/+0.2$	$+1.1/-0.9$	$0.380/0.501$	$0/0$	$0/0$
4053	$0.718/0.937$	$-1.3/+0.1$	$-0.4/-0.6$	$0.900/0.825$	$0/0$	$0/0$
azimuthal angle						
S1171	$0.264/0.759$	$+0.1/-0.2$	$+2.0/-0.4$	$0.141/0.903$	$0/0$	$0/0$
S0001	$0.267/0.914$	$-0.8/-0.1$	$-1.8/+0.3$	$0.185/0.928$	$0/0$	$0/0$
1035	$0.851/0.154$	$+0.4/-1.7$	$-1.5/-0.2$	$0.296/0.883$	$0/0$	$0/0$
1373	$0.041/0.964$	$+0.7/0.1$	$-2.0/+0.1$	$0.019/0.980$	$0/0$	$0/0$
1474	$0.000/0.271$	$-0.7/-0.2$	$+0.9/+0.6$	$0.118/0.646$	$0/0$	$0/0$
4053	$0.064/0.104$	$-0.6/-0.7$	$-2.2/-1.2$	$0.095/0.333$	$0/0$	$0/0$

projections of angular momentum vectors of galaxies in the galactic (G) or supergalactic (S) planes tend to point radially (tangentially) towards the center of the reference coordinate system.

4 RESULTS

Table 2 shows the values of statistical parameters with respect to galactic (G) and supergalactic (S) coordinate systems. In this section we discuss polar (θ) and azimuthal (ϕ) angle distributions of galaxies in each clusters separately.

4.1 Abell S1171

Abell S1171 is the spherically shaped nearby ($\overline{cz}$ = 8 377 km s^{-1}) cluster in our database (Table 1). HL noticed that a few galaxies have a large velocity deviations (cz – $\overline{cz}$ ∼1 400 km s^{-1}) from the cluster main body (cz ∼8 400 km s^{-1}). The position and radial velocity (cz) distributions of member galaxies show a bimodal velocity distribution (Fig. 1a). A large number of substructures with central condensation can be seen in the number density map (Fig. 2b).

Figure 1c,d shows the polar (θ) and azimuthal angle (ϕ) distributions of member galaxies in S1171. The solid and dashed curves represent the expected isotropic distribution curves obtained from random simulation. The polar angle, θ = 0° (90°) corresponds to the angular momentum vector tends to lie parallel (perpendicular) to the galactic/Supergalactic plane. All six statistical parameters suggest isotropy in the θ-distribution (see Table 2). No preferred alignment of angular momentum vectors of galaxies is observed with respect to the G- and S-coordinate systems. Therefore, a random orientation of angular momentum vectors of galaxies is noticed in the cluster.

In the ϕ-distribution, 0° corresponds to the projections of angular momentum vectors tend to point radially towards centre of the reference coordinate system (centre of the Milky way in G-system and Virgo cluster center in S-system). No humps and dips are observed in Fig. 1d, suggesting no preferred alignments. It can be concluded that the galaxies with a large velocity dispersion cause the cluster dynamically unstable as discussed by Godlowski (2011b).

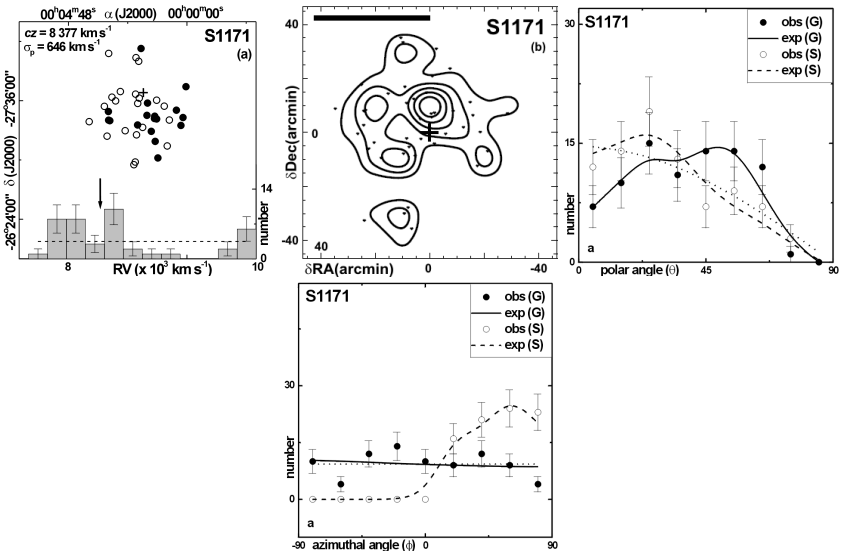

Fig. 1 (a) Distribution of galaxies in Abell S1171. The galaxies having radial velocity $(cz) < (>) \overline{cz}$ of the cluster is represented by solid (hollow) circle. The dashed line and an arrow represent the average distribution of cz of galaxies and the cluster $\overline{cz}$. (b) Number density map: the member galaxies are represented by dots and the number density contours are overlaid. The cross and the thick horizontal bar indicate the cluster center and the the physical size of 1 Mpc. The polar (θ) (c) and azimuthal (ϕ) angle (d) distributions of galaxies with respect to the G- (solid line) and S- (dashed line) co-ordinate systems. The cosine and average distributions (dotted line) are shown for the comparison. The statistical $\pm 1\sigma$ error bars are shown for the observed counts.

4.2 Abell S0001

HL noticed substructures in 2D and 3D number density maps. A low-velocity tail at $cz \sim 7\,800$ km s^{-1} which is far from the mean radial velocity of the cluster can be seen in Fig. 2a. Fig. 2b shows two widely separated local minima, strongly suggests that the cluster might not be in the dynamical equilibrium. All six statistical parameters show isotropy in both the θ- and ϕ-distributions (Table 2). A very good correlation between the expected and observed distribution can be seen in the histograms (Fig. 2c,d), suggesting a random orientation of angular momentum vectors of galaxies. No preferred alignments of angular momentum vectors of galaxies in the cluster Abell S0001 is found.

4.3 Abell 1035

This cluster has the largest velocity dispersion with two subclusterings along north and south (Fig. 3a,b). HL found substructures in all maps (1D, 2D and 3D), suggesting a large but unequal velocity dispersion causing dynamically unstable. Using photometric database (Lauberts 1982), Aryal and Saurer (2006) studied the preferred alignments in this cluster and found that the angular momentum vector of galaxies tend to lie in the Local Supercluster (LSC) plane, supporting pancake model (Doroshkevich 1973) of galaxy formation. HL found that the angle between the rotation axes and the LSC plane is about 56°, suggesting a bimodal distribution. In the present study we used spectroscopic database (SDSS and 2dFGRS) and verified the prediction made by HL by observing a significant hump at 35° ($>1\sigma$) in the θ-distribution (Fig. 3c), supporting bimodal distribution: angular momentum vectors of galaxies tend to lie both parallel and perpendicular with respect to the plane of the Milky way. In the ϕ-distribution, isotropy is noticed (Fig. 3d), suggesting that the choice of co-ordinate system is independent of preferred alignments.

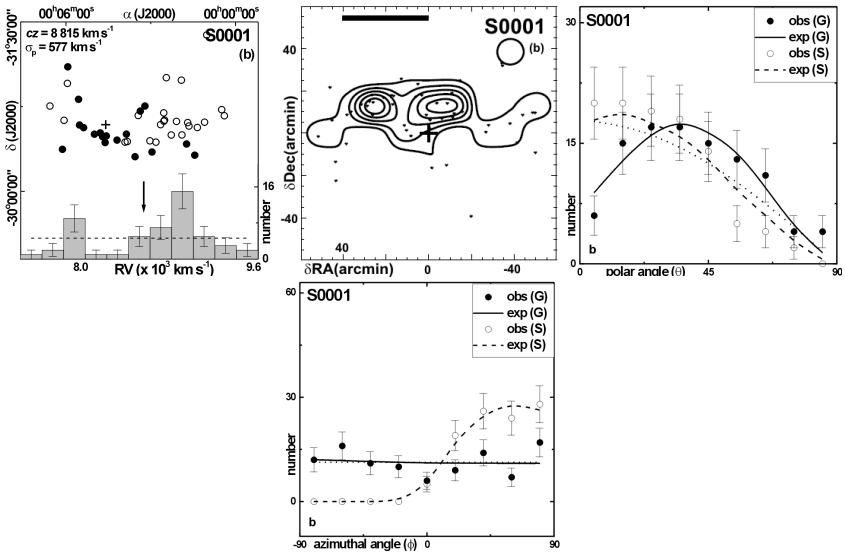

Fig. 2 The cluster Abell S0001: the scatter plot (a), number density map (b), θ and (c) ϕ (d) distributions of galaxies. Symbols and explanations as in Fig. 1.

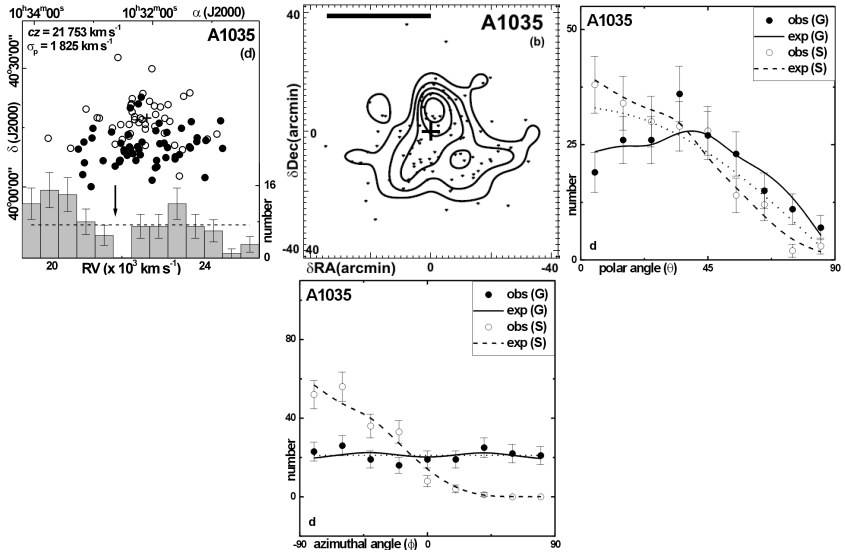

Fig. 3 The cluster Abell A1035: the scatter plot (a), number density map (b), θ and (c) ϕ (d) distributions of galaxies. Symbols and explanations as in Fig. 1.

4.4 Abell 1373

This cluster is the most distant ($\overline{cz}$ = 37 595 km s^{-1}) with bimodal velocity distribution spatially separated by the rotation axes (Fig. 4a). The number density map is similar to that of the cluster Abell 1035, i.e., substructure is seen in 1D-3D (HL). All statistical tests suggest isotropy in both the θ- and ϕ-distributions, advocating hierarchy model (Peebles 1969) of galaxy evolution. In the θ-distribution,

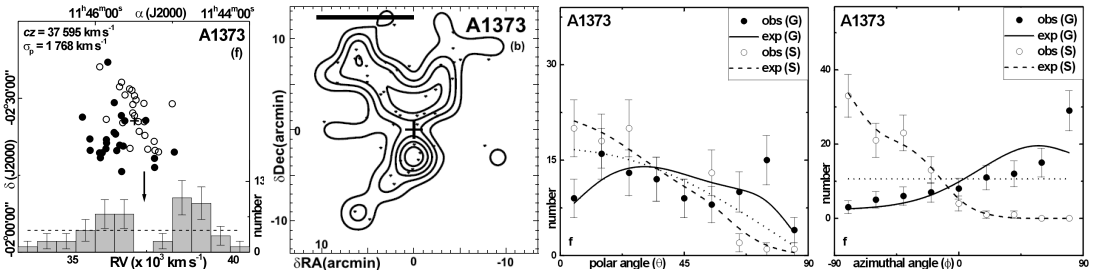

Fig. 4 The cluster Abell A1373: the scatter plot (a), number density map (b), θ and (c) ϕ (d) distributions of galaxies. Symbols and explanations as in Fig. 1.

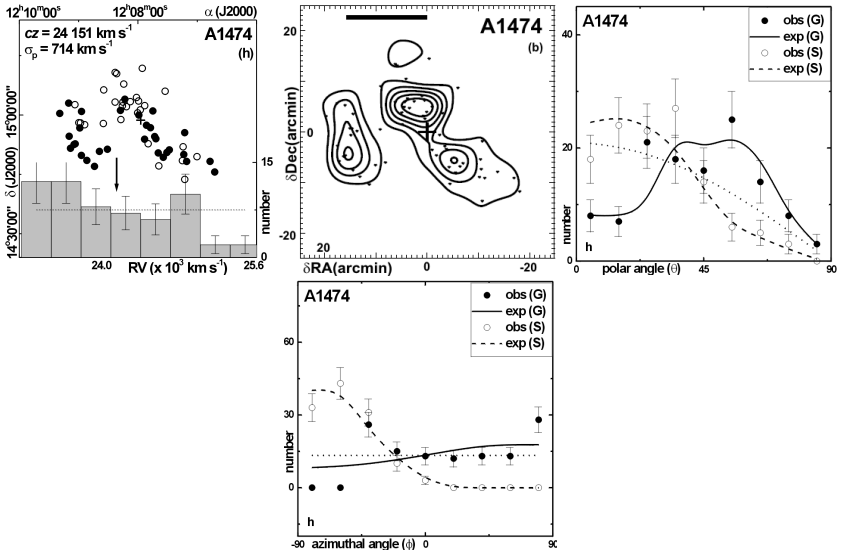

Fig. 5 The cluster Abell A1474: the scatter plot (a), number density map (b), θ and (c) ϕ (d) distributions of galaxies. Symbols and explanations as in Fig. 1.

a significant hump at 75° (>1.5σ) can be seen (Fig. 4c). In addition, a dip at 45° (∼1.5σ) is followed by the hump. Therefore, a local tidal effect, probably due to the substructure formation, is noticed. In the ϕ-distribution, a hump at 85° ((>2σ) and dips at 65° (∼1.5σ) and 75° (∼1.5σ) supports local effect (Fig. 4d).

4.5 Abell 1474

Einasto et al. (2001) studied Virgo-Coma supercluster and concluded that Abell 1474 is the member cluster of of that supercluster. HL noticed three substructures in the number density map (Fig. 5b), suggesting dynamically unstable rotating cluster which is not in the dynamical equilibrium because of large value of $\overline{cz}$–σ_v. The chi-square and autocorrelation tests show anisotropy in the θ-distribution, whereas isotropy is noticed in the Fourier, KS and Kuiper V tests. A hump at 25° (∼2σ) and a dip at 45° (1σ) suggest a local tidal effect because of the subsclustering (Fig. 5c). In the ϕ-distribution, significant humps at $-45°$ (2σ) and 90° (1.5σ) supports it (Fig. 5d). Therefore, the spatial orientation of galaxies in the cluster Abell 1474 shows a weak preference in the alignments.

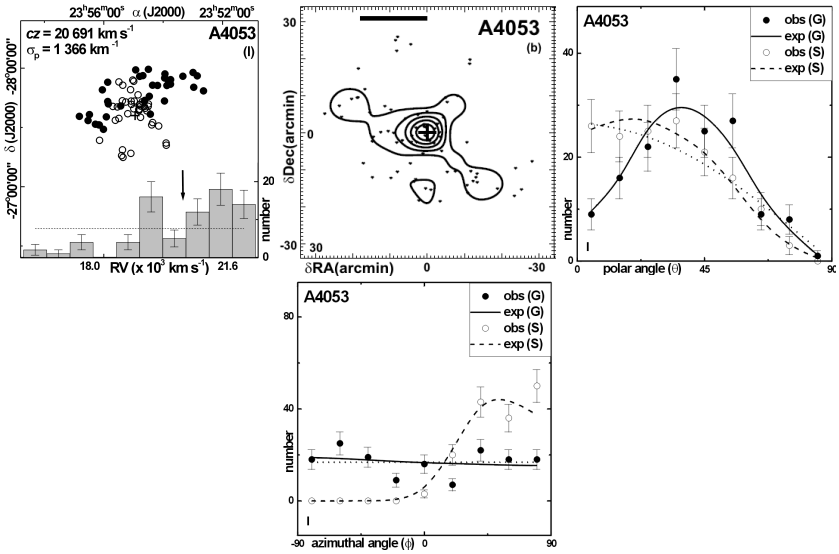

Fig. 6 The cluster Abell A4053: the scatter plot (a), number density map (b), θ and (c) ϕ (d) distributions of galaxies. Symbols and explanations as in Fig. 1.

4.6 Abell 4053

Porter & Raychaudhury (2005) reported that the cluster A4053 is a member clusters of Pisces-Cetus supercluster. HL found that the cluster shows substructures in 1D and 3D maps. The number density map (Fig. 6b) shows elongation along north-east and south-west direction. In the histogram of polar (θ) angle distribution, a good agreement between the expected and observed distribution is noticed, suggesting no preferred alignments (Fig. 6c). All statistical tests support this. In the ϕ-distribution, humps ($-70°$, $50°$) and dips ($-20°$, $20°$) at 1.5σ level are significant (Fig. 6d), suggesting anisotropy. Statistical tests support this result. Therefore, projections of angular momentum vectors of galaxies in A4053 tend to be oriented perpendicular towards the plane of the Milky way, whereas no preference is noticed with respect to Virgo cluster centre. Therefore a local effect can not be ruled out in the cluster which has a multiple number-density peaks and large value of velocity dispersion.

5 CONCLUSION

The preferred alignments of angular momentum vectors of galaxies in six clusters having multiple number-density peaks with a spatial segregation of high- and low-velocity galaxies are studied. We adopted 'position angle - inclination' method (Flin & Godlowski 1986) to compute three dimensional parameters (polar and azimuthal angles of the galaxy rotation axes) using two-dimensional observed parameters (e.g., positions, diameters, position angles). To remove selection effects from the database, a numerical simulation is performed, as proposed by Aryal & Saurer (2000). The observed and expected isotropic distributions are compared using five statistical tests namely, chi-square, auto-correlation, Fourier, K-S and Kuiper V.

In general, no preferred alignments is noticed for all six clusters supporting hierarchy model as predicted by Peeples (1969). However, local effects are noticed in the clusters that have substructures in 1D, 2D and 3D analysis (HL). Therefore, a large value of velocity dispersion with substructures in the clusters do not lead their galaxies to support pancake (Doroshkevich 1973) and primordial vorticity theory (Ozernoy 1978). A very good correlation between the hierarchy (Peebles 1969) and Li model (1998) is found, as in our previous work (Aryal et al. 2013). Therefore, vanishing angular momenta

favor the formation of substructures in the clusters that have large velocity dispersion. The preferred alignment is found to increase with the cluster richness. Therefore it can be interpreted as an effect of tidal forces mechanism (Heavens & Peacock 1988, Catela & Theuns 1996, Stephanovich & Godlowski, 2015), but also is in agreement with Li's (1998) model in which galaxies form in the rotating universe.

The tidal torque naturally arises in the hierarchical clustering scenario and hence the distribution of angular momentum vectors of galaxies becomes random. However, a tidal torque shear tensor (due to gravitational effect) can cause a local preference on angular momentum vectors as predicted by Lee (2004) and Trujillo et al. (2006).

Acknowledgements The authors thank the anonymous referee whose remarks contributed to improve the paper. We acknowledge Dr. Ho Seong Hwang of Department of Physics and Astronomy, Seoul National University, Korea, for providing database. One of the authors (SNY) acknowledges Central Department of Physics, Tribhuvan University, Nepal for all kinds of support for his Ph.D. work.

References

Abell G.O., Corwin H.G., Olowin R.P., 1989, ApJS, 70, 1

Aryal B., Bhattarai H., Dhakal S., Rajbahak C., Saurer W., 2013, MNRAS, 434, 1939

Aryal B., Kafle P., Saurer W., 2008, MNRAS, 389, 741

Aryal B., Paudel S., Saurer W., 2007, MNRAS, 379, 1011

Aryal B., Saurer W., 2006, MNRAS, 366, 438

Aryal B., Saurer W., 2000, A&A, 364, L97

Baier F.W., Godlowski W., MacGillivray H.T., 2003, A&A, 403, 847

Bautz L.P., Morgan W.W., 1970, ApJ, 162, L149

Catelan, P., Theuns, T., 1996, MNRAS, 282, 2, 436

Colless M., Dalton G., Maddox S., Sutherland W., Norberg P., Cole S., Bland-Hawthorn J., et al., 2001, MNRAS, 328, 1039

Doroshkevich A.G., 1973, ApJ, 14, L11

Einasto M., Einasto J., Tago E., Mueller V., Andernach, H., 2001, AJ, 122, 2222

Flin P., Godlowski W., 1986, MNRAS, 222, 525

Godlowski W., 2012, ApJ, 747, 1, 7

Godlowski W., 2011a, Acta Physica Polonica B, 42, 2323

Godlowski W., 2011b, IJMDP, 20, 9, 1643

Godlowski W., 1993, MNRAS, 265, 874

Godlowski W., Piwowarska, P., Panko, E., Flin, P., 2010, ApJ, 723, 2, 985

Godlowski W., Szydlowski, M., Flin, P., Biernacka, M., 2003, General Relativity and Gravitation, 35, 907

Godlowski W., Szydlowski, M., Flin, P., 2005, General Relativity and Gravitation, 37, 615

Heavens, A., Peacock, J., 1988, MNRAS, 232, 339

Holmberg E., 1946, Medd. Lund. Astron. Obs., Ser. VI, No. 117

Hu F.X., Wu G.X., Song G.X., Yuan Q.R., Okamura S., 2006, Ap&SS, 302, 43

Hwang H.S., 2011, private communication

Hwang H.S., Lee, M.G., 2007, ApJ, 662, 236 (HL)

Kuiper N.A., 1962, in Proc. Kononklijke Ned. Akad.Wetenschappen, A 63, 38

Lauberts, A. 1982, ESO/Uppsala Survey of the ESO B Atlas. ESO, Garching bei Muenchen

Lee J, 2004, ApJ, 614, L1

Li, L.-X. 1998, General Relativity and Gravitation, 30, 497

Ozernoy L.M., 1978, In: Longair M.S., Einasto J., eds, Proc. IAU Symp. 79, The Large Scale Structure of the Universe. Reidel, Dordrecht, p.427

Peebles P.J.E., 1969, ApJ, 155, 393
Porter S.C., Raychaudhuary S., 2005, MNRAS, 364, 1387
Press W.H., Teukolsky, S.A., Vetterlin, W.T., Flannery, B.P., 1992, in Numerical Recipes in C, 2nd ed. Cambridge University Press, Cambridge
Stephanovich, V., Godlowski, W., 2015, ApJ, 810, 2, 14
Trujillo I., Carretero C., Patiri S.G., 2006, ApJ, 640, L111

This paper was prepared with the RAA LaTeX macro v1.2.